



**NOVEL DOMESTIC DESIGN AND MANUFACTURING OF PELTON
TURBINE BUCKET: A KEY TO MANAGE AND ENHANCE SUB-SAHARAN
AFRICA'S HYDRO ENERGY POTENTIAL**

Submitted by

Ebhota, Williams Saturday (*B.Eng, M.Eng*)


213573556

Supervisor: Prof. Freddie L. Inambao

In fulfilment for the requirements for the degree of Doctor of Philosophy in
Mechanical Engineering at the College of Agriculture, Engineering and Science,
University of KwaZulu-Natal.

2017

As the candidate's supervisor, I have approved this thesis for submission.

Signed..........Date.....*25th Jan 2017*.....

Name: Prof. Freddie L. Inambao

Declaration 1 - Plagiarism

I, **Ebhota, Williams Saturday**, declare that:

1. The research reported in this thesis, except where otherwise indicated is my original research.
2. This thesis has not been submitted for any degree or examination at any other university.
3. This thesis does not contain other persons' data, pictures, graphs or other information, unless specifically acknowledged as being sourced from other persons.
4. This thesis does not contain other persons' writing, unless specifically acknowledged as being sourced from other researchers. Where other written sources have been quoted, then:
 - a) Their words have been re-written but the general information attributed to them has been referenced.
 - b) Where their exact words have been used, then their writing has been placed in italics and inside quotation marks, and referenced.
5. This thesis does not contain text, graphics or tables copied and pasted from the internet, unless specifically acknowledged, and the source being detailed in the thesis and in the References sections.

Signed.....



25th January, 2017

Declaration 2 - Publications

This section presents the articles that form part and/or include the research presented in this thesis. The following papers have been published or under review:

ISI/SCOPUS/DoHET Accredited Journals

1. W. S. Ebhota and F. L. Inambao, "Electricity insufficiency in Africa: a product of inadequate manufacturing capacity," *African Journal of Science, Technology, Innovation and Development*, vol. 8, no. 2, pp. 197-204, 2016. DOI: 10.1080/20421338.2016 (*published*).
2. W. S. Ebhota and F. L. Inambao, "Facilitating greater energy access in rural and remote areas of sub-Saharan Africa: small hydropower," *Energy & Environment*, 2016. DOI: 10.1177/0958305X16686448 (*Published Onlinefirst*)
3. W. S. Ebhota and F. L. Inambao, "Sub-Saharan Africa power sustainability: a function of a domestic small hydropower (SHP) design and manufacturing," *Journal of Energy in Southern Africa*, 2016. (*Under review.*)
4. W. S. Ebhota and F. L. Inambao, "Design basics of a small hydro turbine plant for capacity building in sub-Saharan Africa," *African Journal of Science, Technology, Innovation and Development*, vol. 8, no. 1, pp. 111-120, 2016. DOI: 10.1080/20421338.2015.1128039 (*Published*).
5. W. S. Ebhota, A. S. Karun and F. L. Inambao, "Principles and baseline knowledge of functionally graded aluminium matrix materials (FGAMMs): fabrication techniques and applications," *International Journal of Engineering Research in Africa* Vol. 26, pp 47-67. DOI:10.4028/www.scientific.net/JERA.26.47 (*Published*).
6. W. S. Ebhota, A. S. Karun and F. L. Inambao, "Centrifugal casting technique baseline knowledge, applications, and processing parameters: overview," *International Journal of Materials Research*, 04 August, 2016. DOI: 10.3139/146.111423 (*Published*).
7. W. S. Ebhota and F. L. Inambao, "Functionally graded metal matrix composite by centrifugal casting technique mathematical correlation," *African Journal of Science, Technology, Innovation and Development*, 2016. (*Under review*)

8. W. S. Ebhota and F. L. Inambao, "Smart design and development of small hydropower system and exploiting of locally sourced material for Pelton turbine bucket production," *Iranian Journal of Science and Technology, Transactions of Mechanical Engineering*, 2016. (*Under review*).
9. W. S. Ebhota, A. S. Karun and F. L. Inambao, "Investigation of functionally graded aluminium A356 Alloy and A356-10%SiCp composite for hydro turbine bucket application," *International Journal of Engineering Research in Africa*, 2016. Vol. 26, pp 30-46. DOI:10.4028/www.scientific.net/JERA.26.30 (*Published*).
10. W. S. Ebhota and F. L. Inambao, "Enhancing the wear and corrosion resistance of a Pelton turbine bucket surface by centrifugal casting technique and heat treatment," *Journal of the Southern African Institute of Mining and Metallurgy*, 2016. (*Under review*.)

International and DHET accredited conferences

1. W. S. Ebhota and F. L. Inambao, "Domestic turbine design, simulation and manufacturing for sub-Saharan Africa energy sustainability," presented at 14th International Conference on Sustainable Energy Technologies (SET), Nottingham, UK, 25-27 August, 2015. (Appendix 1)
2. W. S. Ebhota and F. L. Inambao, "Examining the effects of production method on Aluminium A356 alloy and A356-10%SiCp composite for hydro turbine bucket application," in *Proceedings of 18th International Conference on Mechanical and Materials Engineering (ICMME)*, *International Journal of Chemical, Molecular, Nuclear, Materials and Metallurgical Engineering* Vol:10 No: 10, 2016, Paris, France, 24-25 October, 2016. (Appendix 2)
3. W. S. Ebhota and F. L. Inambao, "Novel domestic manufacturing of Pelton turbine bucket: a key to enhance sub-Sahara Africa energy potential," in *Proceedings of the Industrial and Commercial Use of Energy*, Vineyard Hotel, Cape Town, South Africa, 15-17 August, 2016.
4. W. S. Ebhota and F. L. Inambao, "Functionally graded materials and aluminum alloys investigation for small hydro turbine blade application," presented at 9th International Conference on Researches in Engineering, Technology and Sciences (ICRETS), Imperial College London, London, September 17-18, 2015.

5. W. S. Ebhota and F. L. Inambao, "Functionally graded materials (FGMs) fabrication techniques, processing parameters and applications: baseline knowledge and overview," presented at 9th International Conference on Researches in Engineering, Technology and Sciences Imperial College London, UK, September 17-18, 2015.

The candidate is the main and corresponding author respectively for all the publications while Prof. Freddie L. Inambao is the supervisor.

Dedication

This thesis is dedicated to my late father, John Aighayighan Ebhota, for his passion for education, he passed away in 2007. May his gentle soul rest in the bosom of the lord, amen. To my mother, wife, son, brothers, sisters, colleagues and friends for their love, encouragement and support.

Acknowledgements

To God, the author and finisher of my faith, goes my first appreciation and acknowledgement who made this programme possible. My second acknowledgement goes to my lovely and caring wife, friend, and reading mate, Chika, my son, Peculiar and Prof. Freddie L. Inambao for his supervision and understanding. To my mum, brothers and sisters: Janet, Thomas, Catherine, Lucky, Mary, Victor, Florence, Fr. Jacob-Neri, and Faith for their love, encouragement and support.

To my childhood friends, Okoromi, Jude, Enojiela and Parker and to my Nnewi, NEDDI and NASENI friends Ademola and family, Michael and family, Iduma and family, Godstime and family, Cajethan, Amos, Nnalue, Yusuf, Ugochukwu, Mgbemena, Iboi, Sunday, Makinde and family, Victoria, Mr. Pawa, Engr. Ajulu, Charity, Anamasonye's family, and Okeke's family.

To my friends in the University of KwaZulu-Natal Andrew (Bomboo) and Victoria, Samuel and family, Chiemela, Adefemi, Segun, Gloria, Getihun (my best academic friend), Yuwa, Young, Taty, Emmanuel, Ebeanizer, Usy, Kazeem, Shaun (my invaluable research tool provider) and others too numerous to mention, I salute you all.

Table of Contents

Declaration 1 - Plagiarism	iii
Declaration 2 - Publications	iv
Dedication.....	vii
Acknowledgements	viii
Table of Contents	ix
Nomenclature.....	xviii
Acronyms	xxiii
Abstract.....	xxiv
CHAPTER 1: INTRODUCTION.....	1
1.1 Introduction	1
1.2 Research rationale.....	1
1.3 Problem statement	1
1.4 Background to the study	2
1.4.1 Energy, human existence and national growth.....	2
1.4.2 Generation of electricity by hydro.....	3
1.4.3 Basic principles of small hydropower	4
1.4.4 Turbine materials.....	5
1.5 Aim of the study	5
1.6 Objectives of the study	5
1.7 Significance of the study	6
1.8 Scope of the study	7
1.9 Thesis layout.....	7
Bibliography.....	9
CHAPTER 2: ANALYSIS OF ENERGY ISSUES IN SUB-SAHARAN AFRICA	12
Part 1: Electricity Insufficiency in Africa: A Product of Inadequate Manufacturing Capacity	13
Part 2: Facilitating Greater Energy Access in Rural and Remote Areas of Sub-Saharan Africa: Small Hydropower	15
2.2.1 Introduction	16

2.2.1.1 Problem statement: gross inadequate access to electricity in sub-Saharan Africa despite the abundance of small hydropower resources	17
2.2.2 Regional electricity situation	17
2.2.3 Small hydropower energy conversion principle	19
2.2.4 Small hydropower (SHP) system and access to energy in SSA	20
2.2.5 Small hydropower development barriers in sub-Saharan Africa	21
2.2.5.1 Cost of power projects	22
2.2.5.2 Power generation and distribution policies	22
2.2.5.3 Inadequate SHP design and manufacturing infrastructure	23
2.2.6 Way forward	24
2.2.6.1 Domestication of SHP in SSA	24
2.2.6.2 Design and fabrication of hydro turbine components in SSA	24
2.2.6.3 Turbine blade material selection	25
2.2.6.4 Policy and implementation	26
2.2.7 Conclusion	27
Bibliography	29
Part 3: Sub-Saharan Africa Power Sustainability: A Function of a Domestic Small Hydropower (SHP) Design and Manufacturing	33
2.3.1 Introduction	34
2.3.2 Hydro potential in Africa and benefits of small hydropower	36
2.3.2.1 Large scale hydropower projects	37
2.3.2.2 Small hydropower (SHP)	37
2.3.3 Hydro turbine design and manufacturing procedures	38
2.3.3.1 Sustaining power through domestic participation	39
2.3.3.2 Hydropower plant operation principle	39
2.3.3.3 Hydro turbine main components	40
2.3.3.4 Selection of turbine and design of turbine	40
2.3.3.5 The Kaplan/Propeller turbine	41
2.3.3.6 The Pelton turbine: Main elements of a Pelton turbine system	42
2.3.4 Methodology	43
2.3.4.1 Propeller turbine design for low head	43
2.3.5 Design calculation and simulation of a Pelton bucket high head	44
2.3.5.1 Pelton design parameters	44

2.3.6 Material selection for Pelton bucket.....	45
2.3.6.1 Evaluation of 6061-T6 Aluminium Alloy	46
2.3.7 Conclusion.....	48
Bibliography.....	49
CHAPTER 3: DESIGN BASICS OF A SMALL HYDRO TURBINE PLANT FOR CAPACITY BUILDING IN SUB-SAHARAN AFRICA	52
CHAPTER 4: PRINCIPLES AND BASELINE KNOWLEDGE OF FUNCTIONALLY GRADED ALUMINIUM MATRIX MATERIALS (FGAMMS): FABRICATION AND APPLICATIONS.....	54
CHAPTER 5: CENTRIFUGAL CASTING TECHNIQUE BASELINE KNOWLEDGE, APPLICATIONS, AND PROCESSING PARAMETERS: OVERVIEW.....	55
CHAPTER 6: FUNCTIONALLY GRADED METAL MATRIX COMPOSITE BY CENTRIFUGAL CASTING TECHNIQUE MATHEMATICAL CORRELATION.....	57
6.1 Introduction	58
6.2 Mathematical expressions	63
6.2.1 Particle and solid/liquid interface	63
6.2.1.1 The discussion on Stokes' flotation velocity.....	64
6.2.1.2 Evaluation of solid/liquid interface shape in particle vicinity.....	64
6.2.2 Forces acting on particle in a melt.....	66
6.2.2.1 Gravitational force.....	66
6.2.2.2 Drag force	66
6.2.2.3 Repulsive/Van der Waals force	67
6.2.2.4 Force balance equation, F_{net}	69
6.2.3 Significant conditions for pushing/engulfment transition	69
6.2.4 Volume fraction resolution.....	71
6.2.5 Particle matrix field temperature configuration 153.....	71
6.2.6 Boundary conditions.....	72
6.2.7 Heat conduction expression.....	73
6.2.8 Governing expression	73
6.2.9 Composites thermophysical properties.....	73
6.2.10 Centrifugal casting system initial conditions.....	74
6.2.11 Boundary conditions.....	74

6.2.12 Formulation of heat-transfer coefficient.....	75
6.2.13 Composite thermal conductivity, K.....	76
6.3 Conclusion.....	76
Bibliography.....	77

CHAPTER 7: SMART DESIGN AND DEVELOPMENT OF A SMALL HYDROPOWER SYSTEM AND EXPLOITATION OF LOCALLY SOURCED MATERIAL FOR PELTON TURBINE BUCKET PRODUCTION 80

7.1 Introduction	81
7.2 Review	82
7.3 Theoretical framework and design considerations	83
7.3.1 SHP system and principle of operation	83
7.3.2 Designing and development of key components of a SHP system	84
7.3.3 Civil design.....	85
7.3.3.1 Weir and intake.....	85
7.3.3.2 Headrace canal/open channel	86
7.3.3.3 Spillway and settling basin.....	88
7.3.3.4 Trash rack design.....	89
7.3.3.5 Forebay and penstock design.....	90
7.3.4 Hydro Pelton turbine mechanical design.....	94
7.3.4.1 Main categories of turbine and their applications	95
7.3.4.2 Euler equation.....	95
7.3.4.3 For Pelton turbine	96
7.3.4.4 The real Pelton runner	97
7.3.4.5 Turbine shaft diameter.....	99
7.4 Pelton turbine bucket production.....	99
7.4.1 Selection of material.....	99
7.4.2 Manufacturing of a Pelton turbine bucket	99
7.5 SHP system design results.....	100
7.5.1 Civil works design charts for SHP	101
7.5.2 Pelton turbine bucket design charts	104
7.6 Prototype design parameters.....	107
7.7 Pelton bucket simulation results	107
7.8 Conclusion.....	109

Bibliography	110
CHAPTER 8: INVESTIGATION OF FUNCTIONALLY GRADED ALUMINIUM A356 ALLOY AND A356-10%SiC _p COMPOSITE FOR HYDRO TURBINE BUCKET APPLICATION.....	114
CHAPTER 9: ENHANCING THE WEAR AND CORROSION RESISTANCE OF A PELTON TURBINE BUCKET SURFACE BY CENTRIFUGAL CASTING TECHNIQUE AND HEAT TREATMENT.....	115
9.1 Introduction	116
9.1.1 Pelton turbine material and fabrication	118
9.2 Experimental method.....	119
9.2.1 Fabrication of a permanent mould for a Pelton turbine bucket	119
9.2.2 Production of the mould	119
9.2.3 Mould material	120
9.2.4 A390-aluminium alloy formation.....	121
9.2.5 A390-5%Mg aluminium alloy formation.....	121
9.2.6 Electrochemical corrosion test.....	123
9.2.7 Specimen preparation	124
9.2.8 Hardness test.....	125
9.2.9 Heat treatment.....	125
9.3 Theoretical background	126
9.4 Result and discussion	127
9.4.1 Microstructure	127
9.4.2 Effect of centrifuge and heat treatment on hardness	130
9.4.3 Electrochemical corrosion	132
9.5 Protective coating of Pelton bucket.....	133
9.6 Conclusion.....	133
Bibliography	135
CHAPTER 10: CONCLUSION AND FUTURE WORK.....	138
10.1 Conclusion.....	138
10.2 Future work	139
10.2.1 Materials and manufacturing process	139
10.2.2 Optimisation of domestic design and production.....	140

APPENDIXES..... 141

List of Tables

Table 1.1: Classification of hydropower	3
Table 1.2: Classification of SHP by countries	4
Table 2.2.1: Categories of hydro turbine based on output size propagation	20
Table 2.2.2: SHP Barriers peculiar to the different regions of Africa	21
Table 2.3.1: Various size classification of SHP	38
Table 2.3.2: Types of hydro turbine and their applications	41
Table 2.3.3: Nominal conditions for Kaplan/Propeller turbine design	43
Table 2.3.4: Nominal conditions for Pelton turbine design	44
Table 2.3.5: Material (6061-T6 Aluminum) properties	46
Table 2.3.6: Mesh information	46
Table 2.3.7: Study results for stress, displacement and strain	46
Table 7.1: Common types of weir and intake flow rate	86
Table 7.2: Headrace canal/channel design equations	87
Table 7.3: Headrace canal/channel velocity and roughness coefficient	88
Table 7.4: Calculation of settling basin	89
Table 7.5: Penstock flow velocity	90
Table 7.6: Expressions for forebay and penstock design	92
Table 7.7: Manning's roughness coefficients, n_p , for common channel materials	92
Table 7.8: Relations to calculate the internal diameter of a penstock	93
Table 7.9: Types of hydro turbine and their applications	95
Table 7.10: The calculation details of a turbine design	98
Table 7.11: Main turbine design parameters and constants	107
Table 7.12: Mechanical properties of the bucket material	107
Table 7.13: Study properties	108
Table 7.14: Von Mises stress, displacement, and strain results	109
Table 9.1: OHNS material chemical composition	120
Table 9.2: Elemental compositions of A390 and A390-5%Mg	121
Table 9.3: A390 and A390-5%Mg alloys in 3.5 % NaCl solution	132

List of Figures

Figure 2.2.1: Variation of electricity at different scenario	18
Figure 2.2.2: No power for 7 days for the different kind of workers	18
Figure 2.2.3: SHP potential in regions of Africa	19
Figure 2.2.4. Energy conversion in turbine	20
Figure 2.2.5: The development process of a SHP	21
Figure 2.2.6: SSA major sources of machinery imports	24
Figure 2.2.7. Production layout model of a pico hydro turbine system	25
Figure 2.2.8. Components of the design system	25
Figure 2.3.1: Regional access to electricity in 2015	34
Figure 2.3.2: World TPES	35
Figure 2.3.3: Global primary energy supply and CO ₂ emissions	35
Figure 2.3.4: Change in CO ₂ emissions by region (2011-2012)	35
Figure 2.3.4: CO ₂ emission by sector	36
Figure 2.3.6: Electricity generation by fuel	36
Figure 2.3.7: Hydropower potential and installed capacity in Africa	37
Figure 2.3.8: Correlation between material selection and manufacturing process.	39
Figure 2.3.9: Production layout model of a pico hydro turbine system	39
Figure 2.3.10: Schematic diagram of a hydro turbine system	40
Figure 2.3.11: Head-flow range of small hydro turbines	41
Figure 2.3.12: Kaplan/Propeller runner blade parameters and parts	41
Figure 2.3.13: Pelton turbine arrangement	42
Figure 2.3.14: The general layout of a Pelton hydro turbine plant	42
Figure 2.3.15: Runner and bucket parameters	44
Figure 2.3.16: Turbine velocity diagrams	44
Figure 2.3.17: Nodal stress distribution	47
Figure 2.3.18: Nodal fatigue distribution	47
Figure 2.3.19: Factor of Safety distribution	48
Figure 6.1: Schematic of Gao and Wang experimental setup	61
Figure 6.2: Representation of a particle near solid/liquid interface and the forces acting on the particle	64
Figure 6.3: Depiction of solid/liquid interface shapes for various conditions	65
Figure 6.4: Depiction of solid/liquid interface shapes for various conditions	65
Figure 6.5: Representation of forces acting on a particle moving in molten metal	66
Figure 6.6: Effects of thermal conductivity ratio	73
Figure 6.7: Direction of heat flows in a centrifugal casting system	73
Figure 6.8: Schematic depiction of centrifugal cast system of metal matrix composites	74
Figure 7.1: Schematic of a hydropower system and the direction of flow	84
Figure 7.2: SHP development stages	84
Figure 7.3: SHP design and development layout	85
Figure 7.4: Schematic of a weir	85
Figure 7.5: Schematic of a submerged intake	86
Figure 7.6: Common channel cross sections	86
Figure 7.7: A normal spillway in a SHP system	88
Figure 7.8: (a) Side view and (b) Top view of a settling basin	89
Figure 7.9: Schematic showing normal forebay in SHP system	90
Figure 7.10: Components of the penstock assembly	91
Figure 7.11: penstock and powerhouse arrangement	94
Figure 7.12: Stemming jet impinges on splitter of a bucket	94
Figure 7.13: The different types of turbine	95
Figure 7.14: The Pelton wheel velocities triangle, showing the relative and absolute velocities of the flow.	95
Figure 7.15: Theoretical variation of runner efficiency for a Pelton wheel with blade speed to jet speed ratio for several values of friction factor k	96
Figure 7.16: The arrangement of a runner	97
Figure 7.17: Assembly of buckets on runner	97
Figure 7.18: An offset of section X-X of a Pelton bucket	100
Figure 7.19: Intake discharge vs sectional area	101
Figure 7.20: Canal discharge vs sectional area	101
Figure 7.21: Canal area vs depth and radius	102

Figure 7.22: Notch discharge vs weir depth	102
Figure 7.23: Canal sectional area vs perimeter wet	102
Figure 7.24: Length vs volume of settling basin	103
Figure 7.25: Discharge vs penstock internal diameter	103
Figure 7.26: Discharge vs penstock vent diameter	103
Figure 7.27: Discharge vs power of turbine	104
Figure 7.28: Discharge vs jet diameter	104
Figure 7.29: Velocity vs runner diameter of a turbine	105
Figure 7.30: Bucket design parameters	105
Figure 7.31: Rotational speed vs specific speed	105
Figure 7.32: Turbine power vs turbine efficiency	106
Figure 7.33: Graph of torque against reaction force	106
Figure 7.34: Graph of turbine shaft against power	106
Figure 7.35: The designed bucket prototype	107
Figure 7.36: Diagrammatic representation of simulation process and von Mises result	108
Figure 9.1: The design parameters of a bucket	119
Figure 9.2a: Exploded view of Pelton bucket mould assembly as designed	119
Figure 9.2b: Exploded view of Pelton bucket mould assembly as fabricated	120
Figure 9.3: The manufactured mould components for Pelton bucket	120
Figure 9.4: Degassing of the molten metal with RID machine	121
Figure 9.5: Vertical centrifugal casting machine	122
Figure 9.6: The arrangement of the buckets in the mould	122
Figure 9.7: Castings from different casting techniques	123
Figure 9.8: The setup of the electrochemical corrosion laboratory workstation	123
Figure 9.9: Preparing microstructural and hardness specimens	124
Figure 9.10: Schematic of how the specimens were cut from the cylindrical casting	124
Figure 9.11: Specimens for electrochemical test	124
Figure 9.12: Bucket test samples	125
Figure 9.13: Schematic of T6 heat treatment profile of A390 and A390-5%Mg	125
Figure 9.14: Micrographs of centrifugally cast aluminium A390 alloy	127
Figure 9.15: Optical micrographs of A390-5%Mg by gravity casting method	128
Figure 9.15b-g: Optical micrographs of A390-5%Mg by centrifugal casting method	128
Figure 9.16: Optical micrograph of A390-5%Mg bucket fabricated by the centrifugal cast process	128
Figure 9.17: The particles acceleration and centrifugal-gravity ratio curve	130
Figure 9.18: Hardness of A390-5%Mg as-cast by centrifugal casting in relation to the microstructure	131
Figure 9.19: Optical micrographs of A390 and A390-6T as-cast by gravity casting	131
Figure 9.20: Graphs of hardness variation of A390 and A390-5%Mg fabricated by centrifugal casting technique	132
Figure 9.21 a: Tafel of A390 and A390-5%Mg	133
Figure 9.21b: Tafel of Specimens E ₁ , E ₂ , and E ₃	133

Nomenclature

<u>Symbol</u>	<u>Description</u>	<u>Unit</u>
Δh_1	Total head loss	m
ΔW	Work done	kW
a	Cavity width	m
A	Sectional flow area	m ²
A_{ch}	Open channel cross-sectional area	m ²
A_j	Jet/nozzle cross sectional area	m ²
A_{or}	Area of the orifice	m ²
B_d	Bucket depth	m
B_1	Bucket radial length	m
B_w	Bucket axial width	m
C	Discharge coefficient	m ³ /s
C_1	Jet velocity	m/s
C_2	The absolute velocity at the exit	m/s
C_c	Chezy's C	
C_n	Nozzle discharge coefficient	
C_{silt}	Silt concentration of incoming flow	
C_w	Spillway profile coefficient	
C_{w1}	Input velocity of the whirl	m/s
C_{w2}	Exit velocity of the whirl	m/s
D_h	Hub diameter	m
D_j	Jet/nozzle diameter	m
D_p	Penstock diameter	mm
D_r	Runner diameter	m
D_t	Blade diameter	m

E	Young's modulus for the penstock	N/m^2
f	Darcy-Weisbach friction factor	
F	Safety factor	
F_A	Force acting on the runner	N
F_d	The deflector required force	N
g	Acceleration due to gravity	m/s^2
G	Gravity acceleration	
h_1	Cavity length	m
h_2	Length to impact point	m
h_{fld}	Flood level height in the canal	m
H_g	Gross head	m
h_h	Downstream orifice water level	m
H_n	Net head	m
h_r	Upstream orifice water level	m
h_{sp}	Spillway crest height	m
k	Offset of bucket	m
K_{ben}	Loss of head through bend	mm
K_{con}	Loss of head through contraction	mm
K_{ent}	Loss of head through entrance	mm
k_u	Coefficient after impact	
K_{ug} ,	the tip-to-head velocity ratio	
K_{val}	Loss of head through valves	mm
L_{ab}	Length of bucket moment arm	m
L_p	Penstock length	m
N	Runner speed	rpm
n_a	Number of bucket	

n_{ch}	Roughness coefficient	
n_p	Manning's coefficient	
N_s	Specific speed	
n_z	Number of nozzle	
p	Internal pressure	kg/m ²
P_{factor}	Water packing factor	
P_{ti}	The input power to the turbine	kW
P_{to}	The output power to the turbine	kW
P_w	Wetted perimeter	m
Q	Flow rate	m ³ /s
Q_{ch}	Headrace canal	m ³ /s
Q_d	Set design discharge	m ³ /s
Q_{din}	Intake design discharge	m ³ /s
Q_{fld}	Flood flow through the intake	m ³ /s
Q_n	Nozzle flow rate	m ³ /s
Q_p	Water flow rate	m ³ /s
R_{br}	Radius of bucket centre of mass to runner centre	m
R_{ch}	Hydraulic radius of the section area	m
r_h	Hub radius	m
r_h	hub radius	m
r_t	Blade radius	m
r_t	Blade radius	m
S_{ch}	Canal sides slope	
T	Blade torque	N-m
t_{ef}	Effective penstock wall thickness at upper end	mm
t_{extr}	Extra thickness for corrosion	mm

t_p	Minimum penstock thickness	mm
T_{silt}	Silt emptying frequency	s
T_t	The torque produced by the turbine	N-m
u	Velocity	m/s
U_1	Bucket speed	m/s
U_1	Bucket speed	m/s
U_2	Bucket speed vector	m/s
U_2	Speed vector at the exit	m/s
V_{axial}	Axial velocity	m/s
V_b	Volume of bucket	m ³
V_{ch}	Normal open channel velocity	m/s
V_{chc}	Chezy open channel velocity	m/s
V_{chd}	Darcy-Weisbach velocity	m/s
V_{chm}	Manning's velocity	m/s
V_{chw}	Hazen-Williams velocity equation	m/s
V_j	Absolute velocity of water jet	m/s
V_p	Penstock velocity	m/s
V_{tr}	Tangential velocity of the runner	m/s
V_{vert}	Fall velocity	m ³ /s
W	Suitable basin width	m
w_1	Relative velocity at the inlet	m/s
w_2	Relative velocity at the exit	m/s
x_{nb}	Distance between bucket and nozzle	m
β_2	Jet inclined angle to the horizontal plane	°
η	Efficiency	%
η_t	Efficiency of the wheel	

ρ_{silt}	Density of silt	Kg/m^3
ω	Turbine speed	rad/s.

Greek Symbols

<u>Symbol</u>	<u>Description</u>	<u>Unit</u>
η_{th}	Turbine hydraulic efficiency	
η_{tl}	total efficiency.	
ρ	Density of water	Kg/m^3
σ	Tensile stress	N/m^2
Φ	Flow coefficient	
Ω_s	Specific speed	
Ω_{sp}	Power specific speed	
Γ	Power coefficient	rad/s

Acronyms

A- HT	Alloy heat treated
AC	As-cast
AC-C	As-cast composite;
CCT	Centrifugal casting technique
C-HT	Composite heat treated
FGAAMCs	Functional graded aluminium alloy matrix composites
FGMs	Functionally graded materials
GDP	Gross domestic product
GHG	Greenhouse gases
IEA	International Energy Agency
PM	Powder metallurgy
PPP	Public-private partnership
SHP	Small hydropower
SSA	Sub-Saharan Africa

Abstract

This study, seeks to identify and discuss barriers responsible for the perennial power challenges in the region. The identified limiting factors include insufficient fund in the power sector; high cost of power projects; lack of adequate manufacturing infrastructure; lack of adequate power generation and distribution policies; insufficient human and power infrastructure capacities; insufficient public-private partnership (PPP); over reliance on foreign power technology; and, inadequate domestic and regional participation in the design and manufacturing of power devices and systems. Further, the study has singled out small hydropower (SHP) schemes as the best power system for rural and remote areas and stand-alone electrification in the region. This is due to the technology simplicity, environmental friendliness, cost effectiveness, and the abundance of SHP potentials especially pico- and micro-hydropower systems in the region. Additionally, hydro is a renewable energy source with minimal emission of greenhouse gases (GHG).

The study opines that adequate power supply impediments in the region will best be tackled through domestic participation in the design and manufacturing of SHP components and their production technologies. However, the study revealed that the present dwindling manufacturing sector in the region cannot adequately support the production of hydro turbine blades, the most critical component in a hydropower system. The conventional materials for hydro turbine blades are stainless based. The study further found that locally sourced materials that their properties could be enhanced through manufacturing and heat treatment processes should be promoted. Aluminium alloys and their composites are naturally suitable for aerodynamic applications and corrosion resistance and should be exploited further for turbine blade application. The study concluded with an investigation of locally sourced aluminium based materials and manufacturing techniques in the production of a hydro Pelton turbine bucket.

CHAPTER 1: INTRODUCTION

1.1 Introduction

Africa has enormous hydropower potential of about 4,000,000 GWh/year spread throughout the continent. The distribution of the hydro resources in the region has been described as technically good for Small Hydropower (SHP) for rural and standalone electrification [1]. Of this huge potential, which is enough for the power requirements of Africa, only 76,000 GW/year is being generated from a total of 20.3 GW installed capacity. This means that only 6 % of the feasible hydro energy available in Africa has been tapped as against 18 % in Asia, 18 % in South and Central America, 22 % in Oceania, 55 % in North America and 65 % in Europe [2-4]. Generation of electricity from hydropower is least on the African continent despite the perennial power problems and the huge SHP potential in the region. In sub-Saharan Africa (SSA), the rate of average electrification is about 35 %. This situation is severe in the rural areas where it is below 20 %. Over half of the population has no access to electricity in 41 countries of Sub-Sahara Africa. Consequently, the region is faced with high transaction costs, low productivity and efficiency, struggling small and medium enterprises and sluggish economic growth [5, 6]. Other fallout from this insufficient and erratic power generation and supply in the region are high rates of unemployment, abject poverty, and insecurity.

1.2 Research rationale

In 2014 the International Energy Agency (IEA) reported that of the 620 million people of SSA, about two-thirds have no access to electricity and other modern energy services [7]. It was also reported that in the region, four out of five people depend on firewood (traditional biomass) for cooking [8, 9]. The power sector is characterised by gross inadequacies of generation, transmission and distribution facilities, erratic power supply, and emission of greenhouse gases (GHG) from fossil fuel power plants. These challenges are coupled with high cost of power project execution and generation.

1.3 Problem statement

Inadequate manufacturing capacity for small hydropower components and systems in sub-Saharan Africa.

Inadequacies in manufacturing infrastructure has grossly affected the power sector in SSA. Manufacturing and power are intertwined in such a way that deficiency of one directly affects the other. Manufacturing is a product of power that needs to give back to the source in a diversified manner. In this context, energy challenges will exist in the region if domestic manufacturing is not able to deliver adequate, quality, affordable, and sustainable power supply. Sub-Saharan Africa is lagging behind in technological advancement. The average share manufacturing contributed to the gross domestic product (GDP) in 2013 was 11 % which is equal that of 1990s [10]. Takahiro described the development of manufacturing in SSA in 2004 as stagnant and that the process of industrialisation has not begun in most countries [11]. Takahiro stated that manufacturing as a proportion of GDP of SSA in 2004 was about 13 % when South Africa is excluded. South Africa accounts for about 60 % of the manufacturing in SSA. The World Bank Development indicator shows that manufacturing in SSA GDP dropped from 17.16 % in 1975 to 11.32 % in 2014 [12]. South Africa is the only country in SSA that generates and distributes fairly adequate, quality and affordable power.

The low level of manufacturing in SSA is the prime power limiting factor in a region that is chronically short of electricity. The technical aspects of power production include design, manufacturing, installation, operation, maintenance and repair of power devices and systems. Failure of the region to tenaciously develop engineering design and manufacturing of power equipment, has left the region with gross inadequate and erratic power supply along with dependence on foreign power equipment, expertise, technology and exorbitantly high costs of power project execution [5].

1.4 Background to the study

1.4.1 Energy, human existence and national growth

Energy is an indispensable component of human survival, national economic growth, and promotion of health, manufacturing, security, research and development and transportation. Adequate access to reliable, quality and affordable energy is a prerequisite and critical to national security, employment, and acceptable standard of living. Social evolution relies on energy conversion for human use and energy is a cornerstone to civilisation. Many people still hold on to the belief that advancement and standard of living are proportional to the quantity, quality and sustainable energy a society possesses. This pushes many people to accept this correlation: energy = progress = civilization [13]. The earliest tools such as tools for hunting animal, catching fish, plant harvesting, processing and moving foodstuffs to where they are

needed were products of energy. Subsequently, human existence has been grappling with the age-old challenge of energy as it is needed to carry out virtually all daily activities.

In the same way that humans cannot do without energy, so it is with a country; no country can develop without quality, adequate and sustainable energy. From the foregoing, it is clear that energy is an essential input to all aspects of modern life. The United Nations Millennium Development Goals (MDGs) recognised that the provision of modern energy services are vital to the eradication of extreme poverty. To better comprehend the importance of energy in human and national growth, the IEA recently developed an energy development index which measures a country’s progress in its transition to modern fuels as well as the degree of maturity of its energy end-use. After incorporating energy into the production function, the IEA studies point to energy use as a contributing factor in development, rather than simply an outcome [14]. In some cases, access to energy is a dividing line between the poor/undeveloped countries and the rich/developed countries. For any nation to tackle the problem of poverty, the country needs to provide adequate, quality, affordable and sustainable energy for its citizens [15]. This explains the wide margin of energy per capita between developed countries and the undeveloped countries.

1.4.2 Generation of electricity by hydro

The generation of electricity by hydro requires water to be in motion to possess kinetic energy which strikes and turns the turbine blade. The blade is linked to the generator (alternator) via a shaft that transmits the rotary motion of the blade to the generator. The generator then converts the available mechanical energy into electricity. Hydro turbines are broadly categorised into two types, namely, reaction and impulse turbines [16, 17]. Hydropower is mainly categorised based on the head, capacity, and source of water, as presented in Table 1.1.

Table 1.1: Classification of hydropower

Capacity (output)	Type of flow source	Head
Large hydropower (>100 MW)	Run-of-river	High head (>300 m)
Medium hydropower (20–100 MW)	Storage	Medium head (30–300 m)
Small hydropower (1–20 Mw)	Pumped storage	Low head less than (<30 m)
Mini hydropower (100 kW–1 MW)	In-stream	
Micro hydropower (5–100 kW)		
Pico hydropower (≤5 kW)		

There is no international standard of classification, but Table 1.2 presents some countries' specific classification of small hydropower (SHP) in terms of power output. In this study, SHP will be used for any small scale hydropower equal to or less than 20 MW, which means that small, mini, micro and pico hydropower are grouped as SHP.

Table 1.2: Classification of SHP by country

Country	SHP (MW)
United States	5-100
Sweden	≤ 15
Norway	≤ 10
India	≤ 25
Europe	≤ 20
China	≤ 50
Canada	< 50
Brazil	≤ 30

Small hydropower has been identified as a non-polluting, cost effective and environmentally benign renewable energy source suitable for rural electrification [18, 19]. The use of SHP schemes for rural electrification can increase access to reliable and adequate energy in the region. Small hydropower is essential to industrialisation, improving the living standards of the people, enhancing safety and security, and preserving a healthy environment. To boost energy accessibility and sustainability sufficiently in SSA requires the region's active participation in the manufacture of SHP equipment. This step has positive multiplying effects on power as this will ensure a reduction in the cost of power projects execution compared to the present cost situation. Further, the ability to design and manufacture will improve operation, maintenance and parts availability problems and jobs will be created. Adequate access to power in the region will provoke commercial and industrial activities and consequently, raise the productivity and standard of living of the people [20, 21]. This can be achieved through the popularisation and use of SHP technology for rural areas, industrial estates and standalone electrification rather than the national grid [22].

1.4.3 Basic principles of small hydropower

Small hydropower is associated with the combining of head and flow of a river or any other water source to produce energy that powers a turbine (hydro machine). The water must flow to possess energy as still water has no energy and the amount of power that can be generated is defined by head and the rate of flow. The flowing water is diverted away from the river through an intake, channelled past a settling basing for desilting and flows to the forebay.

From there the water is directed through the penstock to drive the turbine, which subsequently turns the generator to produce electricity. There are different types of turbines for different applications. The selection of turbine type to be used is governed by the hydraulic properties of the water source. Hydro turbines are broadly categorised into two types, namely, reaction and impulse turbines [16, 17]. The blade is the most vulnerable turbine component because of the pressure put on it by the striking water.

1.4.4 Turbine materials

The blade converts kinetic energy in a moving water or the linear momentum of a water jet into rotational motion that turns the alternator for transformation into electrical energy [23]. As a result, blades are constantly under dynamic load, coupled with the aggressive and notorious environment in which they work. The blades are prone to corrosion and erosion wear caused by the flowing or impinging jet water that may contain sand and chemically aggressive elements. Blades are sometimes used in seawater which is the most corrosive of natural mediums containing corrosive halide reagents such as NaCl and MgCl₂. The compositional content of seawater depends on geographical location and varies over a wide range, however, the salt content of the world's oceans is approximately constant, about 3.1 % [5, 6]. To satisfy both rigidity and environment requirements, stainless steel has been the common material for buckets coated with epoxy or polyurethane based resins materials [24, 25]. The production of stainless based materials is complex, expensive and huge energy is required for casting and welding. Production of stainless steels is not adequately supported by the dwindling manufacturing infrastructure in sub-Saharan Africa (SSA).

1.5 Aim of the study

To analyse key barriers to adequate power supply in SSA, proffer solutions and to exploit locally sourced materials and production facilities to domesticate SHP technology.

1.6 Objectives of the study

The objectives of the study are summarised as follows:

- i. To present the power situation, limitations to adequate, reliable, affordability and quality power and to discuss the correlation between manufacturing infrastructure and rate of power accessibility in SSA.

- ii. To examine and identify simple renewable energy technology schemes to supply adequate, reliable, affordability and quality power to rural areas and standalone electrification.
- iii. To examine simple renewable energy technology schemes to enhance greater access to greener energy and energy sustainability that could to be developed domestically to reduce reliance on foreign technologies in SSA.
- iv. To present a simplified and basic design process of SHPs, to accelerate local fabrication of SHP components and plants in SSA.
- v. To advance smart design and development of SHPs and exploitation of locally sourced material for Pelton turbine bucket production.
- vi. To research bulk fabrication technologies for functionally graded materials (FGMs) that can enhance the mechanical properties of locally sourced aluminium alloys and composites.
- vii. To examine the mathematical correlation that exists between reinforcement particle and metal matrix of composites produced by means of the centrifugal casting technique.
- viii. To investigate functionally graded aluminium A356 alloy and A356-10%SiC_p composites for hydro turbine bucket production.
- ix. To enhance the wear and corrosion resistance of a Pelton turbine bucket surface by using the centrifugal casting technique and heat treatment.
- x. To submit the findings of this study to Department of Higher Education and Training (DHET) recognised journals and conferences as required by the University of KwaZulu-Natal for thesis by publication.

1.7 Significance of the study

The significance of the study is as follows:

- i. Promotion of domestic design and manufacturing of small hydropower components, systems and their production technologies in sub-Saharan Africa.
- ii. Empowerment of rural dwellers through domestic design and fabrication of SHP components and systems capacity building in SSA countries.

- iii. Promotion of the use of locally sourced materials and technology for turbine blade production.
- iv. Promotion and sensitisation of the use of SHP schemes which are simple and cost effective renewable energy source in SSA for rural and industrial estate electrification.
- v. Use of centrifugal casting technique to fabricate and enhance the mechanical properties of a non-cylindrical part, Pelton turbine bucket.
- vi. Development of SHP design charts for smart design of SHP components and systems.
- vii. Development of a novel manufacturing technique for Pelton turbine bucket production.

1.8 Scope of the study

The scope of the study includes:

- i. The analysis of the power situation and barriers to adequate, reliable and affordable power supply in SSA.
- ii. Simplification of SHP components and system design processes and development of design charts.
- iii. Development of a production system for Pelton turbine buckets.
- iv. Comprehensive literature review of bulk manufacturing techniques for FGMs.
- v. Design and fabrication of a Pelton bucket prototype.
- vi. Investigation of locally sourced materials and manufacturing processes for blade production.

1.9 Thesis layout

Chapter 1 is the introductory part of this study, it provides the rationale, problem statement, and highlights of the background of the study. It also presents the aim, overall objectives, significance, scope, and highlights of the study contribution. This thesis is a product of research publications and conference papers as required by the University of KwaZulu-Natal for awarding of a doctoral degree. Altogether there are nine publications and/or conference papers distributed through Chapters 2-9.

Chapters 2 deals with the analysis of power issues in sub-Saharan Africa and is divided into three sections. Part 1 delves into the main barriers to adequate, quality and affordable power

in Africa and explores the relationship between power and level of manufacturing on the continent. Part 2 discusses domestic participation in SHP design and manufacturing as a key to overcoming the power challenges in the region. Part 3 advocates SHP as a suitable power scheme for rural areas and standalone electrification.

Chapter 3 presents a simplified design process of a propeller hydro-turbine.

Chapter 4, deals with functionally graded materials (FGMs) bulk fabrication techniques, their principles and applications.

Chapter 5, discusses baseline knowledge, applications, and processing parameters of the centrifugal casting technique.

Chapter 6 discusses the mathematical correlation of functionally graded metal matrix composite and the centrifugal casting technique.

Chapter 7 deals with the coding of SHP system design and the development of design parameter charts and modelling and simulation of the Pelton bucket prototype.

Chapters 8 examines functionally graded aluminium A356 alloy and A356-10%SiC_p composite for the production of Pelton buckets.

Chapter 9 presents functionally graded aluminium A390 and A390-5%Mg alloys produced by the centrifugal casting method and characterised for hydro turbine bucket production.

Chapter 10 draws conclusions and makes recommendations for future works.

Bibliography

- [1] GSMA, "Tower power Africa: energy challenges and opportunities for the mobile industry in Africa," GSMA Green Power for Mobile Programme, GSMA, London, September 2014.
- [2] M. C. Lokolo, "Enlightening a continent in the dark – prospects for hydropower development in Africa," presented at the United Nations Symposium on Hydropower and Sustainable Development, Beijing, 2004.
- [3] T. J. Hammons, N. Pathmanathan and M. Lawrence, "Run of river bulk hydroelectric generation from the Congo River without a conventional dam," *Natural Resources*, vol. 2, pp. 18-21, 2011.
- [4] T. J. Hammons, "Harnessing untapped hydropower," in *Electricity Infrastructures in the Global Marketplace*, Chapter 2, InTech, 2011.
- [5] International Renewable Energy Agency (IRENA). (2012, 19/03/2015). Prospects for the African power sector: scenarios and strategies for Africa project. Available: https://www.irena.org/DocumentDownloads/Publications/Prospects_for_the_African_PowerSector.pdf
- [6] L. Habtamu, "Challenges to entrepreneurial success in Sub-Saharan Africa: a comparative perspective," *European Journal of Business and Management*, vol. 7, pp. 22-35, 2015.
- [7] International Energy Agency (IEA), "2014 FACTSHEET Energy in Sub-Saharan Africa today," *World Energy Outlook*, Paris, 2014.
- [8] C. Z. M. Kimambo, "Regional cooperation in academic capacity building – added value or added challenges?" presented at NUFU-NOMA conference, Dar Es Salaam, 2011.
- [9] International Energy Agency (IEA), "World Energy Outlook special report: a focus on energy prospects in Sub-Saharan Africa," *World Energy Outlook*, Paris, 2014.
- [10] C. Guangzhe, G. Michael and F. Minghui, "Manufacturing FDI in Sub-Saharan Africa: trends, determinants, and impact," World Bank Group, Washington, 2015.

- [11] F. Takahiro, "International competitiveness of manufacturing firms in sub-Saharan Africa: why has the manufacturing sector remained small?" Discussion Paper No. 2, *Institute of Developing Economies*, JETRO, Japan, 2004.
- [12] WDI, (2016, 24/06/2016). World Development Indicators (WDI), September 2015. Available: <https://knoema.com/WBWDIGDF2015Aug/world-development-indicators-wdi-september-2015?tsId=2794260>.
- [13] W. C. James, (2006, 20/01/2013). History of Energy. Available: <http://www.fi.edu/learn/case-files/energy.html>
- [14] F. Christopher and H. A. Molly, "The potential role of renewable energy in meeting the Millennium Development Goals," REN21 Network, Worldwatch Institute, 2005.
- [15] U. Etiosa, A. Matthew, E. Agharese, O. G. Ogbemudia, P. U. Osazee and G. O. Ose, "Energy efficiency survey in Nigeria: a guide for developing policy and legislation," Community Research and Development Centre, Benin City, Edo State, Nigeria, 2009.
- [16] D. Ugyen and G. Reza, "Hydro turbine failure mechanisms: an overview," *Engineering Failure Analysis*, vol. 44, pp. 136-147, 2014.
- [17] Tokyo Electric Power Company (TEPCO), "Micro-Hydro designing," Workshop on Renewable Energies, Nadi, Republic of the Fiji Islands: Tokyo Electric Power Co., 2005.
- [18] H. Ramos and A. B. de Almeida. (2016, 30/08/2016). *Small Hydropower Schemes as an Important Renewable Energy Source*. Available: <http://www.civil.ist.utl.pt/~hr/hidroenergia.pdf>.
- [19] US. (2006). Wind and hydropower technologies program: advantages and disadvantages of hydropower. Available: <http://www.envirothonpa.org/documents/19bHydropowerAdvantagesandDisadvantages.pdf>
- [20] W. S. Ebhota and F. L. Inambao, "Electricity insufficiency in Africa: a product of inadequate manufacturing capacity," *African Journal of Science, Technology, Innovation and Development*, vol. 8, pp. 197-204, 2016.
- [21] W. S. Ebhota and F. L. Inambao, "Design basics of a small hydro turbine plant for capacity building in sub-Saharan Africa " *African Journal of Science, Technology, Innovation and Development*, vol. 8, pp. 111-120, 2016.

- [22] O. Paish, "Small hydropower: technology and current status. renewable and sustainable," *Energy Reviews*, vol. 6 pp. 537-556, 2002.
- [23] A. Priyabrata, K. R. Pankaj and M. Asis, "Selection of hydro-turbine blade material: application of fuzzy logic (MCDA)," *International Journal of Engineering Research and Applications*, vol. 3, pp. 426-430, 2013.
- [24] Hydropower Advancement Project (HAP), (2012). Best Practice Catalog: Pelton Turbine. Available:
http://hydropower.ornl.gov/docs/HAP/MechPeltonTurbineBestPracticeRev2_1.pdf.
- [25] International Energy Agency (IEC), "Field acceptance tests to determine the hydraulic performance of hydraulic turbines, storage pumps and pump-turbines," IEC International standard 60041, 3rd Ed, 1991.

CHAPTER 2: ANALYSIS OF ENERGY ISSUES IN SUB-SAHARAN AFRICA

This chapter is divided into three parts

Part 1: Electricity Insufficiency in Africa: A Product of Inadequate Manufacturing Capacity

Part 2: Facilitating Greater Energy Access in Rural and Remote Areas of Sub-Saharan Africa:
Small Hydropower

Part 3: Sub-Saharan Africa Power Sustainability: A Function of a Domestic Small
Hydropower (SHP) Design and Manufacturing

Part 1: Electricity Insufficiency in Africa: A Product of Inadequate Manufacturing Capacity

W. S. Ebhota and F. L. Inambao, "Electricity insufficiency in Africa: a product of inadequate manufacturing capacity," *African Journal of Science, Technology, Innovation and Development*, vol. 8, no. 2, pp. 197-204, 2016. DOI: 10.1080/20421338.2016 (published).



Electricity insufficiency in Africa: A product of inadequate manufacturing capacity

Williams S. Ebhota & Freddie L. Inambao

To cite this article: Williams S. Ebhota & Freddie L. Inambao (2016) Electricity insufficiency in Africa: A product of inadequate manufacturing capacity, African Journal of Science, Technology, Innovation and Development, 8:2, 197-204

To link to this article: <http://dx.doi.org/10.1080/20421338.2016.1147206>



Published online: 22 Jun 2016.



Submit your article to this journal [↗](#)



View related articles [↗](#)



View Crossmark data [↗](#)

Electricity insufficiency in Africa: A product of inadequate manufacturing capacity

Williams S. Ebhota* and Freddie L. Inambao

Discipline of Mechanical Engineering, Howard College, University of KwaZulu-Natal, Durban, South Africa

**Corresponding author email: willymoon2001@yahoo.com*

Energy availability is fundamental and crucial for human survival and for national economic development. Energy consumption per capita of a country or region is a measure of quality of life and industrialisation of a country or region. This to certain extent explains why energy consumption is higher in technologically developed countries than the developing ones. Africa is faced with chronic power problems and this stalls her economic growth, in spite of availability of vast natural resources in the region. The number of Africans without access to modern energy is over 600 million and the projected year of adequate power accessibility in Africa is 2080. This study shows that the main hindrances to access to power in Africa are insufficient continental collective effort, inadequate application of academic based research findings, inadequate manufacturing infrastructure and overdependence on foreign technology, insufficient human capacity development and the high cost of power projects in the region. The study went further to identify small hydropower plant (SHP) technology capacity building to facilitate domestication, establishment of regional energy research institutions, transformation of research findings into real products, and adoption of Asian developing countries' energy development approach as formidable ways of tackling power problems and power sustainability in Africa.

Keywords: consumption, development, energy, manufacturing, power, research, R&D

JEL classification: L94, N67, N77, O55

Introduction

Energy is a basic requirement for every human activity and for forming and reshaping human conditions and is vital for human survival and national economic growth. But the developing countries of Africa have been bedevilled with inadequate access to reliable energy supply and this has led to underdevelopment, poor standards of living, poor health systems and inadequate safety and security. The figure of Africans without access to modern energy is over 600 million and the projected year of adequate power accessibility in Africa is 2080 (Ebhota, Eloka-Eboka, and Inambao 2014, APP 2015). Human existence may no longer be possible without energy because virtually every activity that makes it possible needs energy. Some of these activities are shown in Table 1. The same way as energy is to man (no energy, no existence), so also it is to national growth (no energy, no industrialisation).

A scientific finding of different ways for goods and services delivery in industries, homes, and businesses, and investing in better paths to improving existing products, services and production processes is termed research and development (R&D) (Encarta 2009). R&D could also be defined as a methodical process of data and information collection for the purpose of closer study for advancement of knowledge in a particular field. It attempts to logically look for answers to intellectual and technical questions through the use of systematic methods. R&D products are basic discoveries and new principles or facts yet unknown or unrecognised, which in most cases, are targeted to improving and safeguarding human existence.

Energy availability and cost are significant parameters for industries' profits, and innovation is the engine that drives growth. Access to all forms of clean and reliable energy, especially electricity, is key to the economic and social development of a country. Energy coupled with

human capital, land, natural resources and machinery are critical to human welfare and a productive economy. It is pertinent to realise that Africa's economic relevance and wellbeing tomorrow depend and are anchored on today's energy R&D. This is because the socioeconomic strength of a nation thrives on R&D. The economic future of Africa dims without massive and strategic energy R&D to lift it from where it is today (Winkler et al. 2011, Mohammed et al. 2015, Ocampo 2005).

Methodology

The methodology of this article is to draw on quantitative Africa energy situation studies, highlight the fundamental issues of access to affordability and quality energy and discuss possible remedies to the key issues. The article considers and discusses the following as instruments to tackle inadequate access to electricity in Africa: building capacity for small hydropower (SHP) infrastructure; the establishment of regional energy research institutions;

Table 1: Energy needs for human activities (Ebhota, Eloka-Eboka, and Inambao 2014)

Energy need category	Activities
Industrial/commercial	Small to medium, industries, business, establishments (shops, offices, banks, restaurants, bakeries etc.).
Domestic	Cooking, lighting, domestic water pumping and distribution, television and radio powering, water heating, refrigeration, etc.
Agriculture	Water pumping and distribution for irrigation, drying, operation of various agricultural equipment, etc.
R&D	Power laboratories, research institutions, etc.
Community	Hospitals, clinics, schools, barracks, prison houses, etc.

adopting Asian developing countries’ energy development approach; and transformation of research findings into real products.

Africa and energy potential

The presence of untapped energy resources, from fossil-based to renewable, for the generation of affordable electricity in Africa is vast. Table 2 presents untapped renewable energy sources in Africa with about 1 526 785 GWh hydro potential in Congo River and the Upper Nile. The hydro energy potential on the continent, which is the least costly of renewable energy solutions today, is enormous. Other renewable energy sources that are in reasonable commercial quantities in Africa are solar, onshore wind, biomass and geothermal energy (IRENA 2012).

This paper will focus more on hydropower because of its advantages over other renewable and non-renewable sources of energy. The main advantages include the following:

- The technology is mature and reliable
- It is a clean energy source
- Its construction, maintenance and operation costs are comparatively low.

Only 6% of the feasible hydro energy available in Africa that has been tapped as against 18% in Asia, South and Central America 18%, Oceania 22%, North America 55% and Europe 65% (Hammons 2011, Lokolo 2004). This means that hydro power development is the least in Africa and this gives viable opportunities to hydro power developers to invest in Africa.

Energy generation and power infrastructure performance in Africa

Sub-Saharan Africa’s installed electricity generation capacity is approximately 70 000 MW, of which 44 000 MW is installed in South Africa (KPMG 2014). The effective power generation has dropped drastically below the installed capacity as a result of aging power infrastructure, however. Table 3 shows power infrastructure in the different regions of Africa and its performance. Most of the present infrastructure was installed in the 90s and is currently bedevilled with increasing costs of maintenance and frequent outages. According to the World Bank report on Africa’s infrastructure, short-term Africa power need is put within the range of 70 000 MW (KPMG 2014).

In sub-Saharan Africa, the average rate of electrification is about 35%. This situation is severe in the rural areas and is below 20%. Over half of the population has no access to electricity in 41 countries of sub-Saharan Africa. Consequently, the region is faced with high transaction costs, low productivity and efficiency, struggling small and medium enterprises and dwindling sustainable growth (IRENA 2012, Habtamu 2015).

Comparison of energy situations in Africa

The total amount of power generated in the 49 countries of sub-Saharan Africa with a population of about 1 billion is approximately the same amount of power generated by Spain with a population of 45 million (KPMG 2014). The power consumption in the region is barely 100 W per person, 3 hours a day.

Southern Africa has the highest power generation per capita and experiences least power outages, as presented in Figure 1. In 2007–2008, power outages were very high in Congo Democratic Republic and Angola.

Over half of the population has no access to electricity in 41 countries of sub-Saharan Africa (IRENA 2012). The scenario of power accessibility is almost the same in the countries of Sub Sahara Africa. Figure 2 shows selected countries in the region and it presents Togo, Gabon and Zimbabwe leading the chart of countries with a very low rate of access to power.

The amount of electricity generated in the different regions is shown in Table 4. It is crystal clear from the

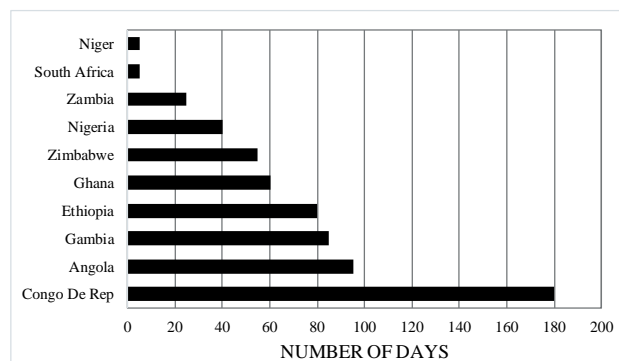


Figure 1: Days of power outages per year 2007–2008 (Dayo 2008)

Table 2: Some of untapped renewable energy in Africa (IRENA 2012; IEA 2010; Hammons 2011)

Untapped renewable energies in Africa	Quantity (GWh)	Where they are predominantly found
Hydro	1 526 785	Congo River and the Upper Nile
Wind (onshore)	1 750	North-West Atlantic coast, the Red Sea, the Horn of Africa, South Africa and Namibia
Geothermal	7–15	East African Rift Valley (Kenya and Ethiopia)

Table 3: Power infrastructure performance in the different regions of Africa (AFDB 2013)

Region	ECOWAS	CEMAC	COMESA	EAC	SADC
Installed generation capacity (MW)	3 912	583	1 085	774	9 855
Net generation per capita (kWh/capita/year)	171	147	114	82	1 214
Outages number annually (day/year)	165	152	119	132	91
Outages value lost annually (% of sales)	7	5	7	8	2
Firms with own generator (%)	54	51	43	56	19
Collection rate of electricity (% of billing)	71	93	93	94	89

ECOWAS: Economic Community of West African States; CEMAC: Economic and Monetary; Community of Central Africa; COMESA: Common Market for Eastern and Southern Africa; EAC: East African Community; SADC: Southern African Development Community

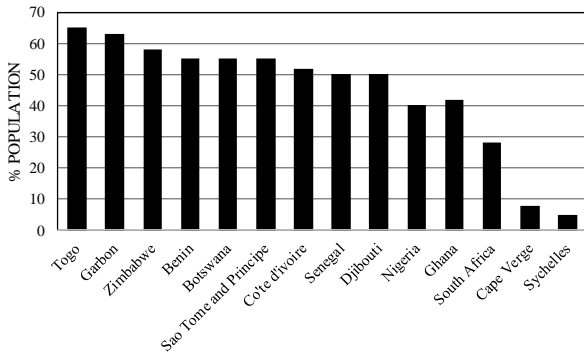


Figure 2: Population without electricity access in sub-Saharan Africa (IRENA 2012)

figures that over the last three decades, not much has been achieved in power generation in Africa.

In 2009, the per capita rate of energy consumption in sub-Saharan Africa excluding South Africa was 153 kWh, against India's 640 kWh and the world's 2 730 kWh. The different values of per capita rates from 2007 to 2008 of countries in the different regions is shown in Figure 3. Sub-Saharan Africa has the world's lowest electricity access rate, at only 26%. The rural electricity access rate is only 8%, with 85% of the population relying on biomass for energy (UNEP 2012).

Table 4: Regional shares of electricity generation (1973 & 2010) (IEA 2012)

Region	1973 (%)	2010 (%)	Increase (%)
Non-OECD Europe and Eurasia	16.7	7.9	-8.8
China	2.8	19.8	17.0
Asia	2.6	9.7	7.1
Non-OECD America	2.5	5	2.5
Africa	1.8	3.1	1.3
OECD	73.1	50.7	-22.4
Middle East	0.5	3.8	3.3

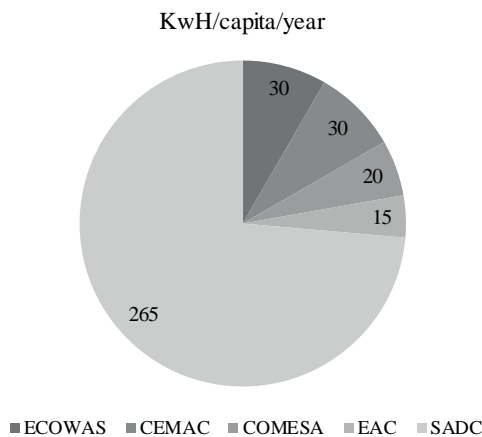


Figure 3: Net generation per capita in Africa

Table 5: Selected country profiles, 2014 (KPMG 2014)

Country	Population (million)	Installed capacity (MW)	Power produced (TWh)	Annual kWh per capita
Kenya	45.5	2,326.70	9.302	178.2
Mozambique	25.8	4,110	23.715	527.7
Nigeria	178.5	11,542.20	31.723	162.3
South Africa	53.1	49,578.90	251.328	4,241.30
Zambia	15	2,130	12.742	708.8

The pie chart in Figure 3 represents the net energy generation per capita in the different regions of Africa and Figure 4 shows the electrical energy production and consumption per capita of selected world countries.

In 2014, it was reported by KPMG (Table 5) that South Africa annual energy per capita was 4 241.30 kWh (KPMG 2014).

Comparison between population growth and electricity production

As it stands today, power accessibility in Africa is in a pitiable state. The situation does not correspond with the interventions, both domestic and international, that have been made to stabilise the power sector. Table 6, shows a steady growth in population and unsteady growth in electricity consumption per capita. In 2004, the electricity consumption per capita was 531 as against 735×10^6 total population and dropped to 525 as against 855×10^6 total population in 2010.

The difference in the degree of growth between population and electricity is shown in Figure 5. For

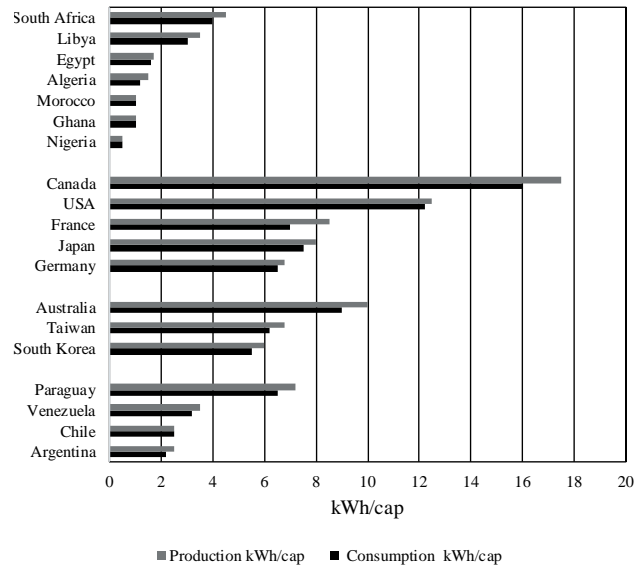


Figure 4: Electrical energy production and consumption per capita of selected world countries (Dayo 2008)

Table 6: Population and electricity growth in sub-Saharan (Economics 2015a, 2015b)

Year	Total population	Electricity production (kWh)	Electric power consumption (kWh/capita)
2004	735×10^6	395×10^9	531
2005	750×10^6	400×10^9	533
2006	775×10^6	415×10^9	535
2007	795×10^6	418×10^9	526
2008	810×10^6	429×10^9	530
2009	830×10^6	427×10^9	517
2010	855×10^6	449×10^9	525

Downloaded by [UNIVERSITY OF KWAZULU-NATAL], [Williams Ebhota] at 01:12 23 June 2016

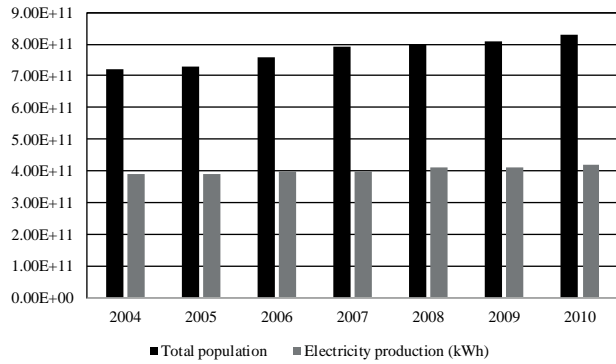


Figure 5: Population growth versus electricity production (kWh) in sub-Saharan Africa (Economics 2015; 1a, 2015; 1b)

adequate power accessibility, the growth between the two must be simultaneous in a direct proportion pattern. Figure 5 compares the growth in population and electricity generated from 2004 to 2010.

Population greatly influences the amount of energy needed and is one the main factors responsible for the unsteady electricity consumption per capita. Figure 6 shows the unsteady nature of electricity consumption per capita.

Factors responsible for power problems in Africa

It is heartbreaking knowing that the power problems in Africa are much as they were two decades ago. The challenges are conspicuously present; in some areas the problem has deepened despite the efforts and resources that have been expended trying to fix the sector. The challenges are numerous and peculiar to different countries, but this article addresses the challenges peculiar to African countries. Some of the causative elements are (Mohammed et al. 2015, KPMG 2014):

- Population growth without corresponding power growth
- Insufficient national and continental collective effort
- Research results are not being used appropriately
- Inadequate in manufacturing infrastructure and over dependence on foreign technology
- Insufficient human capacity development
- High cost of power projects in region
- Under-utilisation of installed generation facilities due to low and inadequate maintenance
- High cost of primary energy to fuel present and new build assets

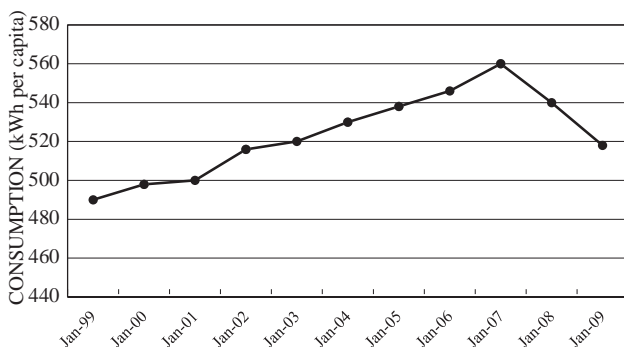


Figure 6: Electric power consumption (kWh per capita) in sub-Saharan Africa (Economics 2015b)

- High loss caused due to lack of operational competence and low revenue generation
- Power losses (about 25%) caused by ineffective infrastructure of transmission and distribution
- Politically motivated tariffs
- Power industry unfavourable policies and regulations to private sector investment
- Additional funding required to meet international environmental emission legislation and standards
- Inadequate funding to take care of development expenses of viable projects
- Inadequate expertise to develop and execute projects
- Population growth influences, etc.

Population growth without corresponding power infrastructure growth

Energy requirements are proportional to the size of the population of a given country. It has been reported that the population of Africa will increase by 1.3 billion between 2013 and 2050 – the highest compared to other regions of the world (Carl and Toshiko 2013). Figure 7 shows the different regions of the world’s population projection. This will have a lot of implications for power demand. To ensure that Africans have adequate access to power, power infrastructure needs to be improved correspondingly.

Inadequate manufacturing infrastructure and over dependence on foreign technology

Overdependence on foreign expatriates, power generation and distribution equipment are responsible for the high cost of power projects. The cost of power equipment is higher in Africa; on average it is put at twice the cost in China (IRENA 2012).

The region’s inability to manufacture has caused real problem in the sector. The technical (engineering and technology) jobs in the power sector can be broadly classified into:

- (1) Design
- (2) Manufacturing
- (3) Installation
- (4) Operation
- (5) Maintenance.

Inadequacies in design and manufacturing affect (3–5) negatively. However, the ability to do (1) and (2) guarantees (3–5) capability. It is obvious that the region has failed to develop engineering design and manufacturing to the level

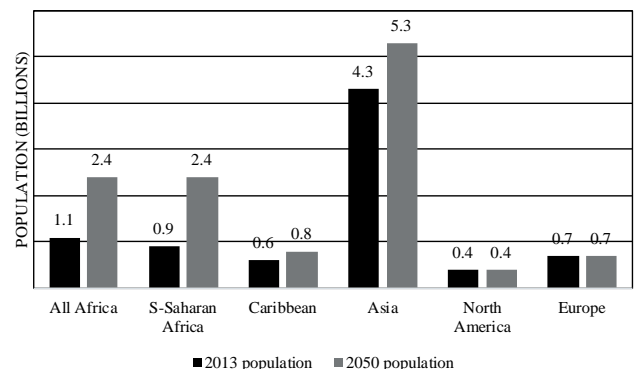


Figure 7: Regions of the world population projection (Carl and Toshiko 2013)

Downloaded by [UNIVERSITY OF KWAZULU-NATAL], [Williams Ebhota] at 01:12 23 June 2016

where manufacturing of power equipment can be supported adequately. This study tried to establish the number of manufacturing firms in the region without success. It therefore, concludes that power generating equipment manufacturing firms in the region are grossly inadequate.

Insufficient and incoherent regional collective effort

There seems to be no purposeful and well driven energy development strategy among countries in the region in practical terms. Though the leaders in the region have had several joint power development programmes, there was no commitment to the implementation. This is evident from the amount of electricity produced in Africa between 1973 and 2010 as presented in Table 7.

Disconnection between researchers and the government

The assemblage of energy intellectuals in energy conferences, workshops and seminars in the region over the years has not significantly addressed the power problem. These exercises, including journal publications of energy research results and postgraduate and undergraduate research seem to be mere academic exercises for individual and institutional academic growth. This happens because most governments in the region have not adequately partnered with academic researchers in proffering lasting solutions to these problems. Quite a number of these researchers fund their research and this has caused disconnection and ultimately they affect development of the research results into real solutions. The results are lying and piling up in the archives. What are the results doing in the archives? This is one of the many factors responsible for persistent energy issues in Africa.

The region has not been able to fuse research and development properly and it has been difficult for the region to action power policies that are knowledge-based to the letter, unlike European countries that jointly fund energy R&D and implement policies that will advance the region. They show adequate financial commitment and political will to the course.

In Europe and America there are regional institutions with different energy research mandates that are heavily funded. For example in 2006, the Seventh European

Table 7: Regional shares of hydro production (1973 & 2010) (IEA 2012)

Region	1973 (%)	2010 (%)	Increase (%)
Non-OECD Europe and Eurasia	11.6	8.9	-2.7
China	2.9	20.5	17.6
Asia	4.3	7.5	3.2
Non-OECD America	6.8	19.1	12.3
Africa	2.2	3.1	0.9
OECD	71.9	40.5	-31.4
Middle East	0.3	0.5	0.2

Research Framework Programme was proposed with the mandate of paying attention to specified research needs of range of energy options that will be economically viable in short, medium and long terms basis (Commission 2006).

The missing link

Over the years, solutions to the power challenges in Africa have been propagated, evaluated and re-evaluated without significant implementation. The identified problems and suggested research-based solutions are not linked sufficiently. Until they are linked adequately, the problems will not only remain, but will increase in magnitude.

Reflecting the achievements in power production made by Asian countries, the missing link can easily be identified. In China, the success was attributed to self-construction, self-management and value added tax on electricity; 6% for SHP and 17% for large hydropower. There were heavy investments in the manufacture of a solar module in Malaysia. In other words, the research results were developed into physical solutions and developmental energy policies were implemented. For the case of developing countries in Asia, Figure 8 shows the relation between problem and solution.

The developing countries in Africa have a different scenario. Figure 9 represents the African scenario. The development and policy implementation in Africa involves massive purchase of foreign technologies and hiring of expatriates for every aspect of the process (installation, operation and maintenance).

Energy R&D activities and power intervention programmes in Africa

Conferences and journal papers

Energy R&D activities in Africa seem to have only the R (research) and the D (development) is in oblivion, or missing, or the level of its activity makes it insignificant. The research is massive across Africa and energy conferences (refer to Table 8), workshops and seminars are held annually in different parts of Africa. This has been occurring for over two decades and has availed Africans the opportunity to discuss energy problems and solutions and cross-pollinate ideas explicitly. Accordingly, many energy studies have been published in high profile journals and a high number of unpublished undergraduate and postgraduate dissertations are centred on energy studies. Despite these efforts and attempts to eradicate or ameliorate energy challenges in Africa to an acceptable level, the issues still persist, and in some areas have deepened.

Government efforts

Power production is a priority for governments of Africa and a very huge part of the annual budget is

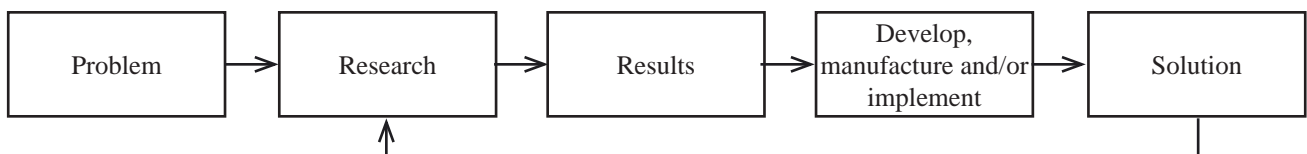


Figure 8: Relation of problem and solution in Asia

Downloaded by [UNIVERSITY OF KWAZULU-NATAL], [Williams Ebhota] at 01:12 23 June 2016

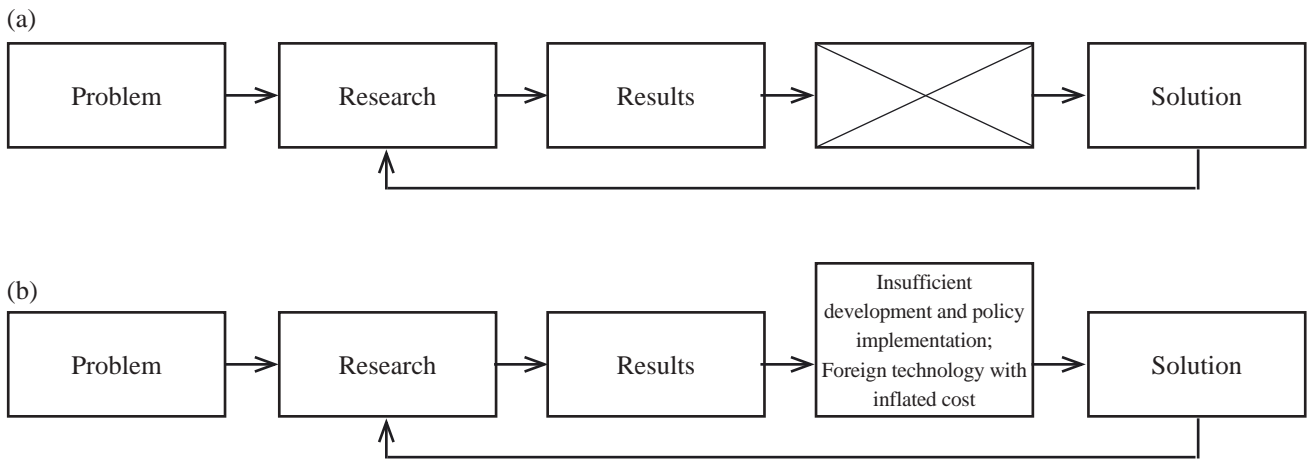


Figure 9: Relation of problem and solution in the African scenario

always appropriate for it. But it seems that the delivery is not commensurate with the funding. Apart from giving power a priority in the annual budget, some power sector restructuring has equally been carried out. This is part of repositioning the sector for better delivery in terms quantity and quality.

The activities of government in the power sector in most countries of Africa have been discretised for the purpose of simplicity and quick response. In some countries, a ministry of power coordinates the activities while agencies and parastatal are created and saddled with specific mandates.

International aid for power

The western world has been supporting Africa with different types of power development aid for a very long time. One such is the Oversea Development Assistance (ODA) targeted at pro-poor programmes in sub-Saharan

Africa (Ogunlade and Stanford 2004). In the mid-1990s, public and private sources of aid to Africa for power development was put at US\$600 million annually. China, India and the Arab States have recently joined significant donor countries to Africa for power development.

The World Bank has 48 power-related projects going on presently in Africa and these include increased access to power and rehabilitating war-torn grids. Despite this aid, it has been reported that for Africa to increase access to power significantly by 2030, the aid needs to be doubled (World Bank 2015). Additional international assistance on power projects in Africa are presented in Table 9.

Campaign promises

The power issue in Africa is one of the areas that the political class pick on to make promises during campaigns. They will always give high hopes of fixing the mess in the sector and very often it has turned out to be a mere political promise.

Table 8: Some Africa-based energy related conferences for 2015 (Altenergymag 2015, Conal 2015).

S/N	Conference	Place	Date
1.	Powering East Africa	Nairobi, Kenya	March 25–27, 2015
2.	CSP Today South Africa 2015	Cape Town, South Africa	April 21–22, 2015
3.	Solar & Off-Grid Renewables West Africa Conference	Accra, Ghana	April 21–22, 2015
4.	4th Power & Energy Africa 2015	Nairobi, Kenya	April 27–29, 2015
5.	Powering Africa: Mozambique 2015	Maputo, Mozambique	May 7–8, 2015
6.	African Utility Week 2015	Cape Town, South Africa	May 12–14, 2015
7.	Clean Power Africa 2015	Cape Town, South Africa	May 12–14, 2015
8.	Energex Africa 2015	Johannesburg, South Africa	May 20–22, 2015
9.	Africa Future Energy Forum	Nairobi, Kenya	May 27–28, 2015
10.	Africa Energy Forum 2015	Dubai, UAE	June 8–11, 2015
11.	2nd Annual Wind Energy Summit	Cape Town, South Africa	March 16, 2015
12.	SASEC 2015: 3rd Southern African Solar Energy Conference	Skukuza, South Africa	May 11, 2015
13.	Solar PACES 2015 – Concentrating Solar Power and Chemical Energy Systems	Cape Town, South Africa	October 13, 2015
14.	26th ICDE World Conference	Sun City, South Africa	October 13, 2015

Table 9: Additional International Assistance on Power (Fortune and Collins 2014, KPMG 2011, OPEC 2010)

International Donors	Project	Amount
World Bank/IDA	Ugandan Energy for Rural Transformation Project II	US\$75 million
IBRD, CTFM, AfDB and Agense Francaise de Development	Sere 100 MW wind farm project in South Africa	US\$350 million
World Bank, DEG, AfDB and other partners	Bujagali 250 MW hydro power plant in Uganda	US\$250 million
Chinese Bank and DBSA	Kariba North Expansion Project (KNBEP) in Zambia	US\$430 million
World Bank and OPEC	Energy Development and Access Project (EDAP APL-2) in Mozambique	US\$118 million
German Investment Corporation, European Development Finance Institutions and smaller donors	OLKARIA III geothermal project in Kenya	US\$119.7 million

Downloaded by [UNIVERSITY OF KWAZULU-NATAL], [Williams Ebhota] at 01:12 23 June 2016

Factors that guarantee energy sustainability

Provision of adequate, affordable, reliable and quality energy services that satisfy social, economic and environmental requirements defines energy sustainability (Fortune and Collins 2014). The success of energy sustainability in Africa depends on several factors and some of the steps favourable to energy sustainability are discussed below (WEC 2005).

Building capacity for small hydropower (SHP) in Africa

“Infrastructure plays critical and positive role in economic development and it interacts with the economy through multiple and complex processes” (Ebhotu, Eloka-Eboka, and Inambao 2014). One of the ways to overcome the electricity problem in sub-Saharan Africa is through technology domestication approach. Massive indigenous capacities in SHP technologies should be built to facilitate rapid local manufacture of SHP facilities.

Building local design and manufacturing capabilities in power generation and distribution technologies (especially SHP), will provoke an increase in local content of power generation, transmission and distribution projects. This will lead to project cost reduction, availability of parts, adequate operation and maintenance personnel, more job creation and make power sustainability a reality. Sub-Saharan Africa needs to build capacity in SHP design, production, and development of local materials for renewable energy devices applications for her own economic growth (Sambo 2005).

Although, some African countries have started promoting domestic manufacturing of power equipment, the rate is not close to the enormous problems in the power sector. There is a wind turbine producer in Egypt, Senegal is strengthening the operations of her power organisation to be able to satisfy the demands of neighbouring countries (like Mali, Guinea and Niger), NASENI in Nigeria is manufacturing solar PV, and Algeria is in partnership with a German company to produce solar PV equipment as well. A lot of effort and resources need to be put into this because local content development is crucial component for fast growth of power infrastructure and sustainability in Africa.

Establishment of regional energy research institutions

Like the western world, the countries of Africa should employ the advantages of synergy and jointly establish energy research institutions with specific mandates. The framework of this programme should cover the present and future of the region’s entire energy system. The programme should be technologically driven with set indicators that will better use human and infrastructure resources in both public and private investments in the member states.

The programme’s responsibility will include the provision of adequate fund for researchers, data harmonisation and transfer of research results to the industries, market and decision-makers for implementation considerations.

The complexity of modern technology requires synergy and combination of the different innovations of dissimilar disciplines (Ebhotu, Eloka-Eboka, and Inambao

2014). Exchange energy technology programmes should be encouraged and strengthened among member states.

**Adopting the approach of Asian developing countries
Small hydropower (SHP)**

In the case of China’s 20 years commitment to SHP for rural electrification, in 2004 the total of SHP installed was put at 34 GW and this amount was increased to 38 GW in 2005. The percentage generation growth from 2000 (25 GW) to 2005 (38 GW) was reported to be 52%. This achievement reflects the determination and strong political will of the government, acceptance and level of adoption of the technology. The success was equally attributed to self-construction, self-management and the value added tax on electricity, 6% for SHP and 17% for large hydropower (Oparaku 2007, Altinbilek, Seelos, and Taylor 2005).

Solar photovoltaics (PV)

China’s policy and implementation on PV were similar to that of SHP. In Malaysia, favourable conditions were created for the development through a rural electrification programme. This prompted the partnership between BP solar and an indigenous company to set up a module manufacturing plant of 5 MWh/year in the country. Again, Malaysia in 2005 invested in the Building of Integrated Photovoltaics (BPV) with the United Nation Development Programme (UNDP) and Global Environmental Facility providing 80% of the cost (Oparaku 2007).

Transformation of research findings into real products

The relevance of academic research work is a function of the problem the research is directed to and it becomes effective if the application of its findings leads to expected end. The research finding needs to be developed to a level before it can be applied to real life situation, otherwise it becomes ineffective. The development could be in form of manufacturing or policy implementation or both. But it is a mere academics exercise when the research results are kept in the archives without development. All the renewable energy academic research work should coordinated and re-evaluated to find feasible lasting solutions to the power perennial problems in Africa. Funds should be provided and monitored to move researches from mere academic exercises to industries for transformation into real products (solutions) and to the market for wealth creation.

The roles of assemblage of energy research intellectuals in energy sustainability

The coming together of energy researchers and experts in form conferences, seminars and workshops in the region should include:

- (1) Harmonising energy technologies, across ideas and policies suggested by authors in their research
- (2) Identifying feasible and marketable energy technologies
- (3) Evaluating the growth using the set key performance indicators by the regional leadership
- (4) Reviewing regional position on energy development
- (5) The energy experts should have a harmonised energy position and push it to the regional governments for implementation.

Conclusion

Energy is fundamental in shaping human and economic conditions and is crucial for human survival and national economic growth. The magnitude of energy consumption per capita of a country or region reflects directly on the quality of life and industrialisation of that country or region. Access to energy separates the underdeveloped countries from the developed ones. This explains why energy consumption is higher in technologically developed countries than the developing ones.

In most countries of Africa, power (electricity) demand by far outstrips the supply and this same undersupply is equally erratic. The continent is faced with a chronic power problem and this has deterred her economic development programmes, notwithstanding the availability of enormous natural resources in the region. Some of the hindering factors are insufficient national and continental collective efforts, research results not being used appropriately, inadequate manufacturing infrastructure and over-dependence on foreign technology, insufficient human capacity development and the high cost of power projects in the region. In tackling these power problems and for sustainability, the continent needs to build capacity for small hydropower (SHP), establish regional energy research institutions, transform research findings into real products, and adopt Asian developing countries' energy development approach.

Acknowledgement

The authors hereby acknowledge the Centre for Engineering Postgraduate Studies (CEPS)/HVDC/Smart Grid Centre of the University of KwaZulu-Natal.

References

- AFDB. 2013. *State of Infrastructure in East Africa*. Tunisia: Statistics Department Africa Infrastructure Knowledge Program.
- Altenergymag. 2015. "Alternative Energy Event Calendar: Alternative Energy Africa." Accessed 21/03/2015. <http://www.altenergymag.com/events.php>.
- Altinbilek, Dogan, Karin Seelos, and Richard Taylor. 2005. "Hydropower's Role in Delivering Sustainability." *Energy & Environment* 16 (5): 815–24. doi:10.1260/095830505774478503.
- APP, Africa Progress Panel. 2015. *Power People Planet: Seizing Africa's Energy and Climate Opportunities*. In *Africa Progress Report* Geneva, Switzerland.
- World Bank. 2015. Fact Sheet: The World Bank and Energy in Africa.
- European Commission. 2006. *Energy Futures: The Role of Research and Technological Development*. Brussels: Directorate-General for Research, Information and Communication Unit.
- Conal. 2015. "Conferences in South Africa." <http://www.conferencealerts.com/>
- Ebhota, W.S., A.C. Eloka-Eboka, and F. I. Inambao. 2014. "Energy Sustainability through Domestication of Energy Technologies in Third World Countries in Africa." Industrial and Commercial Use of Energy (ICUE), 2014 International Conference on the Energy efficiency in buildings, Cape Town. 10.1109/ICUE.2014.6904197.
- Economics. 2015a. Electric power consumption (kWh per capita) in sub-Saharan Africa. <http://www.tradingeconomics.com/sub-saharan-africa/electricity-production-kwh-wb-data.html>
- Economics. 2015b. Total Population in sub-Saharan Africa. <http://www.tradingeconomics.com/sub-saharan-africa/population-total-wb-data.html>
- Encarta. 2009. Research and Development. In *Encarta Premium Encyclopedia* Microsoft
- Dayo, Felix B. 2008. *Clean Energy Investment in Nigeria*. International Institute for Sustainable Development. Manitoba: IISD.
- Fortune, Ganda, and C. Ngwakwe Collins. 2014. "Problems of Sustainable Energy in sub-Saharan Africa and Possible Solutions." *Mediterranean Journal of Social Sciences* 5 (6): 453–463.
- Habtamu, Legas. 2015. "Challenges to entrepreneurial success in sub-Saharan Africa: A comparative perspective." *European Journal of Business and Management* 7 (11): 22–35.
- Hammons, T. J. 2011. "Harnessing untapped hydropower." In T. J. Hammons (ed.), *Electricity infrastructures in the global marketplace*, 79–139. Rijeka, Croatia: InTech.
- Haub, Carl, and Kaneda Toshiko. 2013. *World Population Data Sheet* Population Reference Bureau, Washington, DC, USA.
- IEA. 2010. "Renewable Energy Essentials: Hydropower." http://www.iea.org/publications/freepublications/publication/hydropower_essentials.pdf.
- IEA. 2012. "Key World Energy Statistics." The International Energy Agency. https://www.iea.org/publications/freepublications/publication/KeyWorld_Statistics_2015.pdf
- IRENA. 2012. *Prospects for the African Power Sector*. Masdar City, Abu Dhabi, United Arab Emirates: IRENA. https://www.irena.org/DocumentDownloads/Publications/Prospects_for_the_African_PowerSector.pdf
- KPMG. 2014. "Sub-Saharan Africa Power Outlook 2014." Africa Infrastructure & Major Projects Group. <http://www.kpmg.com/ZA/en/IssuesAndInsights/ArticlesPublications/General-Industries-Publications/Documents/2014%20Sub-Saharan%20Africa%20Power%20Outlook.pdf>.
- Lokolo, Michel Claude 2004. "Enlightening a Continent in the Dark – Prospects for Hydropower Development in Africa." United Nations Symposium on Hydropower and Sustainable Development Beijing, 27-29 October.
- Mohammed, Modu Aji, Gutti Babagana, K. Highina Bitrus, and A. Hussaini ustapha. 2015. "Challenges to Energy Sustainability in Nigeria as a Developing Nation and the Way Forward." *Applied Research Journal* 1 (2): 46–50.
- Ocampo, José Antonio. 2005. "The Path to Sustainability: Improving Access to Energy." *Energy & Environment* 16 (5): 737–42. doi:10.1260/095830505774478585.
- Ogunlade, Davidson, and A. Mwakasonda Stanford. 2004. *Electricity Access to the Poor: A study of South Africa and Zimbabwe*. Cape Town: Energy and Development Research Centre, University of Cape Town.
- Oparaku, O. U. 2007. *Decentralised Power Generation in Nigeria: Role of Renewable Energy Resources*. Proceedings of the 1st International Workshop on Renewable Energy for Sustainable Development in Africa (IWRESDA), University of Nigeria, Nsukka, Nigeria.
- OPEC. 2010. *World Oil Outlook*. Vienna: Organization of the Petroleum Exporting Countries.
- Sambo, A. S. 2005. "Renewable Energy for Rural Development: The Nigerian Perspective." *ISESCO Science and Technology Vision* 1.
- UNEP. 2012. *Financing renewable energy in developing countries*. Geneva: UNEP.
- WEC, World Energy Council. 2005. "Delivering Sustainability: Challenges and Opportunities for the Energy Industry." *Energy & Environment* 16 (5): 722–728.
- Winkler, Harald, André Felipe Simões, Emilio Lèbre la Rovere, Mozaharul Alam, Atiq Rahman, and Stanford Mwakasonda. 2011. "Access and Affordability of Electricity in Developing Countries." *World Development* 39 (6): 1037–1050. doi:10.1016/j.worlddev.2010.02.021.

Part 2: Facilitating Greater Energy Access in Rural and Remote Areas of Sub-Saharan Africa: Small Hydropower

W. S. Ebhota and F. L. Inambao, "Facilitating greater energy access in rural and remote areas of sub-Saharan Africa: small hydropower," *Energy & Environment*, p. 0958305X16686448, 2017. ([Onlinefirst](#)).

Facilitating Greater Energy Access in Rural and Remote Areas of Sub-Saharan Africa: Small Hydropower

Williams S. Ebhota¹ and Freddie L. Inambao²

¹ Discipline of Mechanical Engineering, Howard College, University of KwaZulu-Natal, Durban, South Africa; wilymoon2001@yahoo.com

² Discipline of Mechanical Engineering, Howard College, University of KwaZulu-Natal, Durban, South Africa; inambaof@ukzn.ac.za

Correspondence: wilymoon2001@yahoo.com

Abstract—Flowing water has hydraulic energy that can be transformed into electrical energy. Sub-Saharan Africa (SSA) has an abundance of hydro resources that are untapped. In this study, various barriers limiting the use of small hydropower to tap the abundant hydro potentials for power generation are discussed. These barriers include insufficient fund; lack of adequate manufacturing infrastructure; lack of adequate power generation and distribution policies; inaccurate hydrological data; insufficient human and power infrastructure capacities; and, inadequate domestic and regional participation in design and manufacture of SHP component devices and systems. This study sees hydro as a cleaner energy source and SHP as the best power system for rural and remote areas and for stand-alone electrification. For power sustainability in the region, public-private partnership (PPP), domestication of SHP technologies, and less reliance on foreign technologies and international support are key factors.

Index Terms: Sub-Saharan Africa; Characterisation; Crossflow; Hydropower, Manufacturing processes; Turbine blade; Small hydropower barriers; Small hydropower policies

2.2.1 Introduction

In a 2014 factsheet the International Energy Agency (IEA) reported that two-thirds of SSA's population of around 620 million people has no access to electricity and other modern energy services [1]. And in the region, four out of five people depend on firewood (traditional biomass) for cooking [2, 3]. The power sector is typified by gross inadequacies of generation, transmission and distribution infrastructure, poor quality power supply, and emission of greenhouse gases (GHG) from fossil fuel power plants. These challenges are coupled with high the cost of power projects and generation.

Africa is blessed with enormous hydropower potentials, put at about 4,000,000 GWh/year. The distribution of hydro resources in the region can be described as technically good for SHP for rural and standalone electrification [4]. Of this huge potential, which is enough for the power requirements of Africa, only 76,000 GW/year is being generated from a total of 20.3 GW installed capacity. The countries of SSA did not recognise the importance of small hydropower (SHP) in a growing economy early. Asia, Europe and America have provided reasonable power for domestic use, agriculture, industry, etc. through SHP schemes. Although SHP has been accepted in SSA as a reliable option for the provision of electricity for rural and remote areas in the region, the installed capacity is very low. This occurrence is attributed to several factors including financial, technical and environmental issues.

2.2.1.1 Problem statement: gross inadequate access to electricity in sub-Saharan Africa despite the abundance of small hydropower resources

This study examines power accessibility limitation factors in SSA and discusses possible ways of using SHP to enhance the energy available in the region. There is a correlation between energy consumption, economic activities and level of poverty. Access to modern, adequate, affordable, green and sustainable energies will provoke productivity and consequently, reduction of poverty.

2.2.2 Regional electricity situation

The power sector performance in SSA (excluding South Africa) is wrecked by inadequate generation and leakages caused by poor and sub-standard transmission and distribution facilities. The average access rate of electricity is less than 31% in sub-Saharan Africa countries excluding South Africa. The total annual power generation in sub-Saharan Africa is about 145 TWh which is almost what Spain generates. Out of this total, South Africa alone generates 35 GW, meaning that the rest put together generates 28 GW [5]. Globally, Africa has the weakest power per capita of 620 kWh/year which drops to 153 kWh/year when SSA is considered without South Africa. The consumption in India is equal to four times the consumption in SSA (excluding South Africa). Presently, the capacity of the power installed in Africa is 147 GW which is equivalent to the amount China installed in two years [4]. Research carried out by Bob and Magali in 2010 is represented in Figure 2.2.1 and shows the electricity available in various scenarios [6].

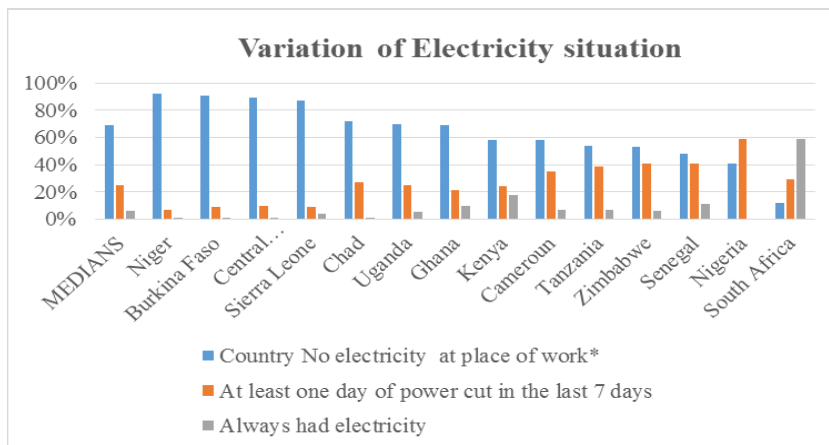


Figure 2.2.1: Variation of electricity in various scenarios [6]

The rural areas of SSA are worst affected by inadequate power supply despite the fact that the inhabitants of the rural areas are engaged with agriculture which is a key economic sector of the region. The study of Bob and Magali found that 62 % of the working class in the rural area has no access to the grid. A median of 62 % of the rural adult population in surveyed countries have some type of work, compared with a median of 52 % among urban adults. But the lack of access to the power grid is especially acute for rural workers. This is noteworthy as agriculture is a key economic sector in many countries across the sub-continent and many farmers live at subsistence levels. A scenario of power received for 7 days between urban and rural shows 34 % and 72 % respectively. No power for 7 days for various types of workers is depicted in the pie chart in Figure 2.2.2.

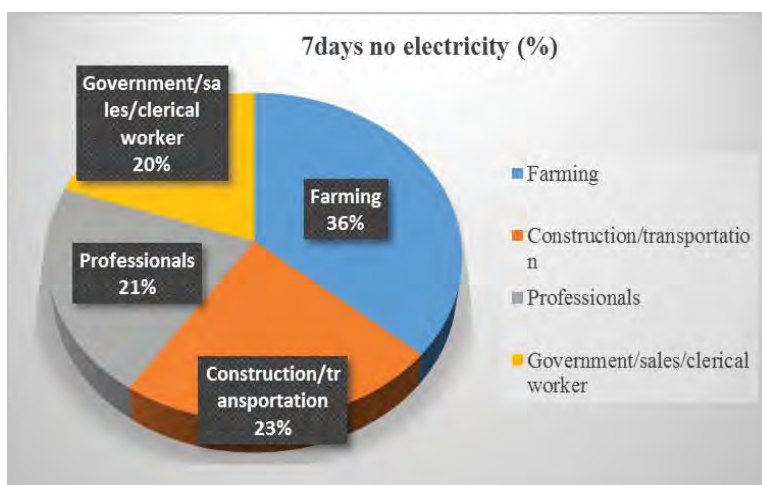


Figure 2.2.2: No power for 7 days for various types of workers

The countries where Bob and Magali's survey was conducted are Nigeria, Uganda, Liberia, Senegal, Tanzania, South Africa, Botswana, Mali, Niger, Zimbabwe, Chad, Ghana, Central African Republic, Burkina Faso, Sierra Leone, Kenya and Cameroon.

The perennial inadequacy of electricity supply has become a way of life in most countries of SSA. In these countries, electricity is provided by costly diesel and petrol generators with a cost rate from 3-6 times higher than the average grid system price across the world. The consequences of this are slow employment growth, uncompetitive Africa-based manufacturing sectors and reduction of annual GDP growth by from one to three percentage points [7]. Sub-Saharan Africa has abundant SHP potential as shown in Figure 2.2.3 that is not sufficiently tapped [8]. The amount of SHP potential present in the region is enough to solve the chronic power problem in the region if harnessed optimally. Many of the SHP sites are yet to be developed and this has been attributed to several reasons [9-11]. The reasons can be classified into policy for rural electrification; insufficient fund for SHP; nature of electricity market; inadequate synergy among the stakeholders; non-implementation of energy research outputs in the region; inadequate human and manufacturing facility development.

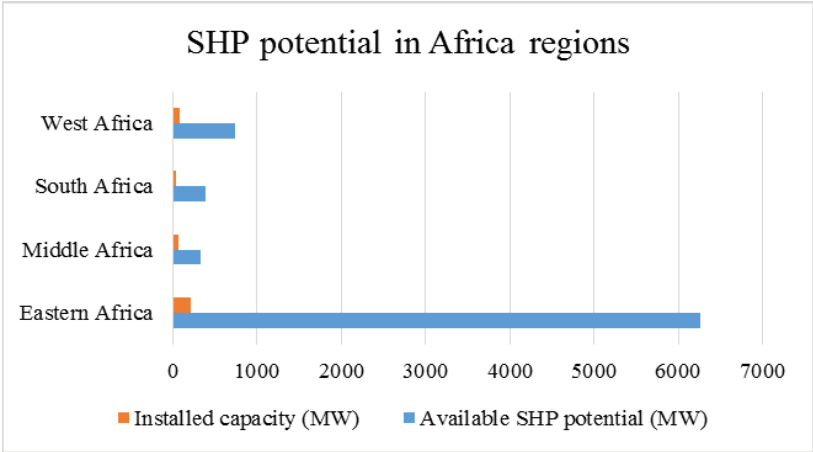


Figure 2.2.3: SHP potential in regions of Africa [8, 12]

2.2.3 Small hydropower energy conversion principle

Moving water possesses hydraulic energy which the turbine blade converts into circular motion via the shaft to turn the generator that subsequently converts the mechanical energy into electrical energy. The sources of this moving water could river, ocean, stream, waterfall, storage tank, etc. [13, 14]. Hydro turbine plants are rotating machines that convert the hydraulic energy in flowing water into torque to turn the alternator for electricity production. Turbines are classified into two types, impulse and reaction turbines and their application depends on the method of water energy transfer [15-19]. The energy conversion in the process is represented in Figure 2.2.3:

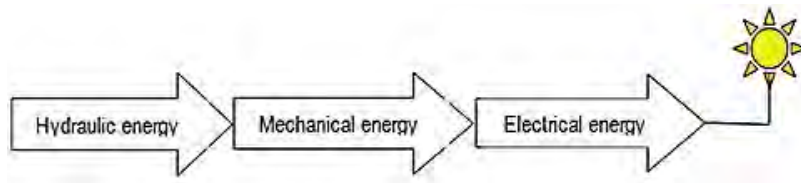


Figure 2.2.4. Energy conversion in turbine

Hydro turbine classification can be based on capacity as shown Table 2.2.1, although internationally there is no standardised classification [12]. Europe and some countries accept the classification according to Table 2.2.1 and which has 10 MW as the SHP upper limit [9, 20]. In this study, SHP is taken as being equal or less than or equal to 20 MW ($SHP \leq 10MW$).

Table 2.2.1: Categories of hydro turbine based on output size propagation

Category	Capacity	Storage source
Pico	≤ 10 kW	Run-of-river
Micro	≤ 100 kW	Run-of-river
Mini	≤ 500 kW	Run-of-river
Small	≤ 10 MW	Run-of-river
Medium	≤ 100 MW	Dam and reservoir
Large	> 100 MW	Dam and reservoir

2.2.4 Small hydropower (SHP) system and access to energy in SSA

Small hydropower systems have been portrayed as a suitable power scheme for SSA due to their merits compared to large hydropower systems and the other power sources. Application of SHP systems in the region is favoured by the abundance of SHP potential in the region; simplicity, especially pico- and micro-hydropower systems; the possibility of being designed, manufactured and installed locally; and, environmentally friendly. Additionally, hydro is a renewable energy source with minimal emission of greenhouse gases (GHG). The best power system for rural and stand-alone electrification is SHP. In 2004, the Intergovernmental Panel on Climate Change (IPCC), reported that energy production contributed highest to world GHG emissions (26 %), with forestry (17 %), transport (13 %) and agriculture (13 %) the main consumers [21]. The majority of emissions in the power sector was due to the use of fossil fuel for power generation [22]. Though SSA region is not known for significant production of GHG, it is imperative that the region participates in global GHG reduction initiatives.

Other benefits of SHP are [12, 23]: A renewable energy generation system that produces the lowest cost of electricity of between 0.02/kWh and 0.05/kWh USD; suitable for rural, remote and standalone electrification that produces an average level cost of energy (LCOE) of

0.05/kWh USD; hydropower is already supplying the largest proportion of renewable power generation; SHP schemes have environmental benefits compared to large scale schemes; and, SHP can be domesticated. From the aforementioned, SHP schemes can fast track adequate reliable, affordable and sustainable power for the promotion of the socio-economic development of SSA rural and remote hinterlands.

2.2.5 Small hydropower development barriers in sub-Saharan Africa

The development of SHP may be broadly divided into five processes as shown in Figure 2.2.4. They are hydrological study, design, manufacturing, installation and post-installation operations. The process usually starts with the hydrological evaluation of the hydro resource to establish if it is technically feasible.



Figure 2.2.5. The development process of a SHP

Although, the development of SHP looks conventional, the design transformation is generally limited in SSA by: insufficient funds; lack of adequate manufacturing infrastructure; lack of appropriate power generation and distribution policies; inaccurate hydrological data of some of the identified sites; inadequate domestic and regional participation in the design and manufacture of SHP component devices, installation, operation and maintenance. However, there are barriers that are peculiar to different regions are presented in Table 2.2.2.

Table 2.2.2: Barriers peculiar to the different regions of Africa hindering SHP development

Regions of Africa	SHP Barriers in SSA
Eastern	Lack of hydrological and up to date data Insufficient awareness of SHP Lack of road infrastructure to access sites in the in remote areas Lack of public-private partnership with both domestic and foreign investors Inadequate human capacity Power distribution cost
Middle	Lack of clear cut renewable energy policy
North	Lack of motivation and suitable SHP site Lack of SHP merits awareness by the public Lack of support policies and technical capacity
South	Lack of SHP components and system, insufficient human capacity on SHP Unfavourable climatic condition
West	Lack of reliable and up to date hydrological data Inadequate SHP project financing and no incentive to attract domestic and foreign SHP investors

	Various degrees of insufficient technical expertise for equipment design, manufacturing, civil construction, operation and maintenance
	Effect of climate change on water bodies like river
Other common barriers	Long distance between potential sites and consumption points
	Low electricity demands due to low population density
	Long distance between consumers (scattered settlement)
	Low utilisation factor
	Prohibitive high capital costs

2.2.5.1 Cost of power projects

Funds are always scarce when it comes to infrastructure provision, though the region has heavily depended on central governments and development partners. The region needs a huge capital injection to increase access to power adequately, considering the high cost of power projects. Over dependence on foreign power equipment, technology and human resource is responsible for the high cost of SSA power projects. It has been observed that the cost of a power project in the region is two times higher than in China [24]. The difference in the project costs is due to the cost of consultation, equipment transportation and hiring of foreign expertise for installation and in some cases for operation and maintenance. In addition to these costs, is the cost of facility monitoring and protection in the region.

2.2.5.2 Power generation and distribution policies

In many countries in SSA it is not possible for individuals or organisations to generate and sell electricity directly to customers (consumers). In many cases, the state government is not allowed to independently generate electricity without connecting to the national grid. However, in an attempt to increase access to electricity, the Nigerian government in 2003 approved a national energy policy that encourages the use of all effective energy sources. The policy advances the use of viable sources of energy for national economic sustainability through joint efforts between the government and active private participation. The policy states that special attention will be given to SHP for development in line with emerging technology [25, 26].

In some cases, insufficient or absence of SHP policy and regulatory structure to monitor the development and implementation of the system discourages SHP project developers from investing in SHP. The lack of cooperation between stakeholders in SHP development involves agriculture, power utilities, water resources and environmental management, national and local authorities, and fund providers.

2.2.5.3 Inadequate SHP design and manufacturing infrastructure

This study identifies inadequate infrastructure for designing and manufacturing of SHP components and devices as the strongest element mitigating against the development of SHP in the region. This factor is as a result of insufficient human and manufacturing infrastructure capacity building. A study by UNESCO of some regions revealed that from 2008-2010, engineering, manufacturing and construction in undergraduate studies was lowest in SSA [27].

Presently, manufacturing plays an insignificant role in the economies of most countries in SSA compared to the role it plays in other developing regions. The power problems in the region are a reflection of the weak manufacturing performance over the years, associated with weak productive abilities and insufficient enabling logistics and policies. Further, there are shortages of the necessary skills and new productive capabilities [28]. These factors often yield low product quality and standards, insufficient volume, high cost of production and low rate of production. The result is insufficient locally manufactured product to meet domestic need or for export and consequently, the region is forced to heavily depend on foreign products and technologies. Su-Saharan Africa’s sources of power, transport equipment and other machinery mainly come from Japan, South Korea, Germany, the United Kingdom, China, and the United States as shown in Figure 2.2.5 [29].

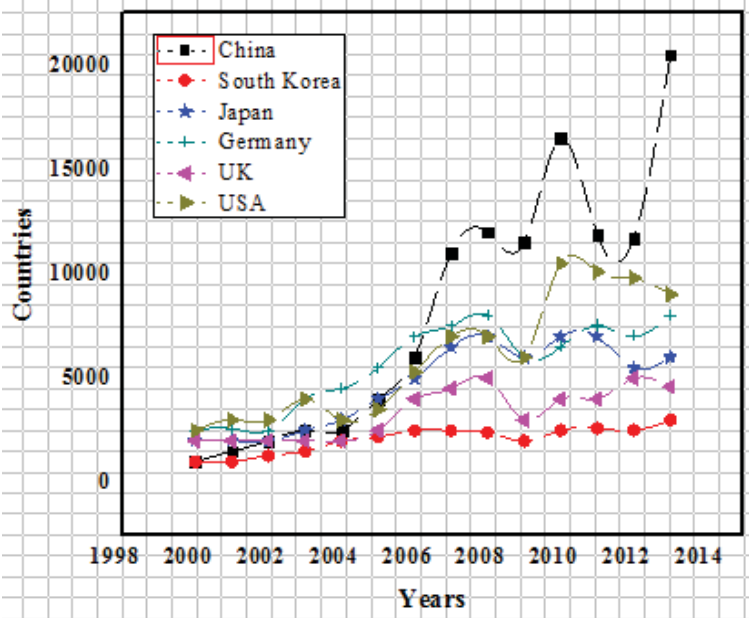


Figure 2.2.6: SSA major sources of machinery imports

2.2.6 Way forward

2.2.6.1 Domestication of SHP in SSA

The power problems in SSA will continue as long as the region heavily depends on foreign power equipment and technologies. Over dependence has severe consequences on power projects, installation, maintenance and repair costs and downtime duration. Power sustainability in the region will only be feasible if human resource capacity is increased and power equipment manufacturing infrastructure is enhanced to meet the present challenges. For sustainability reasons, which means being less dependent on donors, there is a need for the region to strategise on how to fund power projects. This could be achieved through active public-private partnership and lending from financial institutions.

Many governments in SSA have realised the inadequacy in human capacity and the importance of human development for the realisation of SHP benefits [30]. To address this situation and to remove the limiting barriers, some international agencies have agreed to support the region to develop SHP and these include: United Nations Development Program (UNDP); United Nations Industrial Development Organisation (UNIDO); Japan International Cooperation Agency (JICA); United Nations Environment Programme (UNEP); and, Practical Action [9]. In 2006, UNIDO established regional SHP training and support centres in Nigeria to provide technical support within Economic Community of West African States (ECOWAS) [31]. The UNIDO also built demonstration SHPs in Tanzania, Mali, Rwanda and Kenya [32]. However, these interventions are not sufficient and the impact is yet to be felt adequately in the sector. For wider local participation, the hydrological study, design and fabrication methodology should be as simple as possible and the use of computer-aided design (CAD) should be encouraged.

2.2.6.2 Design and fabrication of hydro turbine components in SSA

There is an urgent need for power capacity building for personnel and manufacturing facilities as existing ones are outdated and unable to support present needs. The capacity building should include simple design and manufacturing processes of SHP components, using locally sourced material and facilities. This should follow the conventional production layout as shown in Figure 2.2.6.

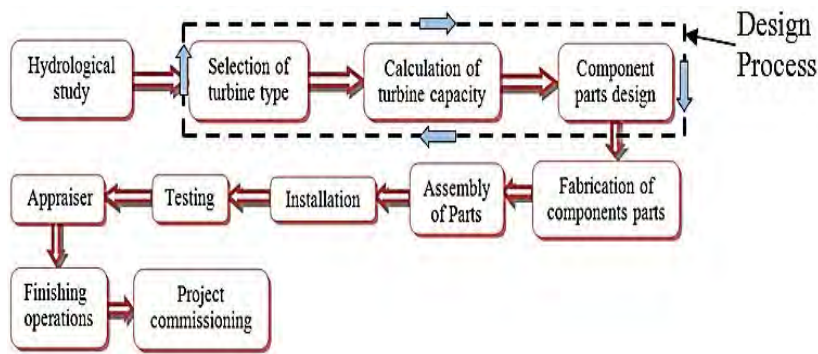


Figure 2.2.7. Production layout model of a pico hydro turbine system

Sub-Saharan Africa comprises low-income countries, therefore industrial development is fundamental and a priority area for human development and to meet the Sustainable Development Goals (SDGs) in the region. The design of SHP systems includes civil work, mechanical design and electrical design as shown in Figure 2.2.7. Design and fabrication of the civil aspect is domestically done while major mechanical components especially the blade and bearings are imported. The electrical components are also sourced outside the region.

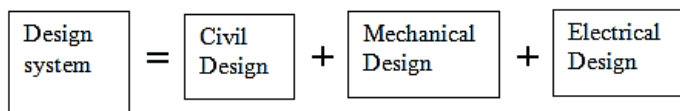


Figure 2.2.8. Components of the design system

2.2.6.3 Turbine blade material selection

The generation of electricity by hydro requires water to be in motion to possess kinetic energy which strikes and turns the turbine blade. The blades are in different kinds and number, and the river or stream flow characteristics define the choice of the turbine to apply [33, 34]. The turbine names are derived from turbine arrangement and their relationship with the flow of water. Hydro turbines are categorised into two types, namely, reaction and impulse turbines [35, 36]. The blade is the most vulnerable turbine component because of the pressure put on it by the strike water. The blade experiences erosion wear and corrosion caused by silt and the flowing water.

Stainless steel materials are the most common materials for hydro turbine blades [37]. The materials are complex to produce, need huge energy for casting and welding and are very expensive. Stainless steels production is not adequately supported by the dwindling manufacturing infrastructure in the developing countries of SSA. However, good hydro turbine products can still come out of the region if material and manufacturing inadequacies are considered early in the design process. Most times projects fail when the design process in

not anchored in the available transforming elements. The choice of material should not be controlled by only operational requirements but also by availability, cost and the manufacturing processes obtainable in the region. In designing for manufacturing, a relation exists between the material and the production processes. For successful turbine project execution, this relationship should be factored into the design process from an early stage.

If the desirable is not available, the available becomes desirable. In the modern world, the relevance and economic vibrancy of a country are tied to its manufacturing strength which is a cornerstone of a healthy economy. The use of locally sourced materials and the beneficiation of their properties through manufacturing and heat treatment processes should be promoted. Aluminium alloys and their composites are naturally good for aerodynamic applications and corrosion resistance and should be exploited further for turbine blade applications.

2.2.6.4 Policy and implementation

There are several policies that have been put in place by individual countries in SSA to promote SHP. If these are strenuously implemented a lot of progress will be made in increasing power accessibility in the rural areas in the region. In Kenya for instance, the Electric Power Act of 1997 was amended and the new Act allows the following: the use of SHP integrated mini-grid systems for rural electrification; a licence is not required only a permit for generation capacity from 100 kW to 300 kW; licence or permit is not required for generation capacity if less than 100 kW [12, 38]. In 2010, Nigeria inaugurated a standing committee through the Federal Ministry of Power to develop hydropower capacity for the country. The government of Mali formulated the following key energy policy papers in 2006: National Energy Policy (2006), and the National Strategy for the Development of Renewable Energies (2006). These strategies were targeted at 25 % renewable energy penetration by 2015 [39].

Other countries in the region have similar policies which are focused on general renewable energy development. It is sad to note that most of the renewable energy policies formulated by these countries have not yielded the expected results. This might not be unconnected to the fact that the policies have no clear cut on specific renewable energy type. Kenya tends to have well-focused SHP policies compared to Nigeria and Mali as cited. In the case of Nigeria and Mali, the policies are in a general framework on renewable energies without being specific. With the level of inadequate power accessibility in the region, one would have expected SHP policies to incorporate key performance indicators.

This study identifies insufficient policy support for SHP technology domestication and inadequate implementation. China managed to increase electricity generation from 25 GW in 2000 to 38 GW in 2005, about a 52 % increase. This can be attributed to self-management, self-construction, and a value added tax on electricity of 6 % for SHP and 17 % for large hydropower [40, 41]. There is a cyclic correlation between supporting policies, technology enhancement and cost reductions in SHP. For realisable, affordable and sustainable SHP schemes in SSA, policies should be centred on technology domestication. The region's SHP policy, therefore, should support the following:

- i. Strict implementation of SHP rural electrification projects with key performance indicators.
- ii. Periodic updating of hydrological data of the SHP potentials in the region.
- iii. Encouragement of public-private partnership in SHP schemes.
- iv. The sale of energy generated by individuals to the grid and directly to consumers.
- v. Promotion of research and development of domestic SHP materials and technologies in higher education institutions through research grants.
- vi. Encouragement of SHP component manufacturers to establish manufacturing companies in the region through tax incentives for SHP foreign investors and waivers on SHP production machines.
- vii. Promotion of local participation in design, manufacture, operation, maintenance and repair.
- viii. SHP Standards and codes formulation for best practices and to safeguard the right of customers.
- ix. Provision of incentives to financial institutions that give loans to SHP scheme developers.
- x. Active synergy of the stakeholders for better delivery of SHP projects.

2.2.7 Conclusion

The most suitable and sustainable electrification scheme for provoking developments and economic activities in the rural and remote areas is SHP. It is regarded as a matured power technology that has low operation and maintenance cost and provides the lowest power generation prices of all off-grid technologies. Small hydropower schemes have been tested globally and certified as a formidable scheme for power production in developing countries.

Sub-Saharan Africa as a region is blessed with abundant SHP potential and should no longer accept the situation of gross inadequate access to power with these resources being untapped. The paradigm of the total importation of power generation and distribution devices should change. Reliable data dissemination regarding the potential of SHP is key to policy development, energy planning and as a guide to investors in participating in the hydropower energy market. Human and infrastructural capacities should be built in the design and manufacturing of SHP components and system centred on domestic participation and sustainability. Power policies and infrastructure for manufacturing should be enhanced in the region to accommodate SHP equipment and plant production.

Bibliography

- [1] International Renewable Energy Agency (IEA), "2014 FACTSHEET Energy in Sub-Saharan Africa today", *World Energy Outlook*, Paris 2014.
- [2] C. Z. M. Kimambo, "Regional cooperation in academic capacity building – added value or added challenges?" presented at NUFU-NOMA conference, Dar es Salaam, 2011.
- [3] International Renewable Energy Agency (IEA), "World Energy Outlook special report: a focus on energy prospects in Sub-Saharan Africa," IEA, Paris, 2014.
- [4] GSMA, "Tower Power Africa: energy challenges and opportunities for the mobile industry in Africa," GSMA Green Power for Mobile Programme, London, 2014.
- [5] United Nations Environment Programme (UNEP), "Regional report on efficient lighting in Sub-Saharan African countries," UNEP, Nairobi, 2012
- [6] T. Bob and R. Magali. (2012, 21/05/2016). In sub-Saharan Africa, most workers are without electricity. Available: <http://www.gallup.com/poll/151889/sub-saharan-africa-workers-without-electricity.aspx>.
- [7] A. Castellano, A. Kendall, M. Mikomarov and T. Swemmer, "Brighter Africa: the growth potential of the Sub-Saharan electricity sector," Mckinsey & Company, New York, 2015.
- [8] H. Liu, D. Masera and L. Esser, "World small hydropower development report 2013." United Nation Industrial Development Organization (UNIDO) and International Centre on Small Hydropower (ICSHP), 2013.
- [9] C. S. Kaunda, C. Z. Kimambo and T. K. Nielsen, "Potential of small-scale hydropower for electricity generation in Sub-Saharan Africa," *International Scholarly Research Network*, vol. 2012, pp. 1-15, 2012.
- [10] F. Mtalo, R. Wakati, A. Towo, S. Makanu, O. Munanyeza and B. Abate, "Design and fabrication of crossflow turbine," Nile Basin Capacity Building Network (NBCBN): Hydraulic Research institute Cairo, Egypt, 2010.
- [11] W. J. Klunne, "Small hydro a potential bridge for Africa's energy divide," *World Rivers Review* vol. 28, pp. 6-7, 2012.

- [12] H. Liu, D. Masera and L. Esser, "World small hydropower development report 2013." United Nation Industrial Development Organization (UNIDO) and International Centre on Small Hydropower (ICSHP), 2013.
- [13] M. J. Khan, M. T. Iqbal and J. E. Quaiocoe, "River current energy conversion systems: progress, prospects and challenges," *Renewable and Sustainable Energy Reviews*, vol 12, no. 8, pp. 2177-2193, 2007.
- [14] J. B. Johnson and D. J. Pride. "River, Tidal, and Ocean Current Hydrokinetic Energy Technologies: Status and Future Opportunities in Alaska." Alaska Center for Energy and Power, 2010. Prepared for the Alaska Energy Authority.
- [15] B. A. Nasir, "Design of high-efficiency Pelton turbine for micro hydropower plant," *International Journal of Electrical Engineering and Technology (IJEET)* vol. 4, no. 1, pp. 171-183, 2013.
- [16] L. Gudukeya and I. Madanhire, "Efficiency improvement of Pelton wheel and crossflow turbines in micro-hydropower plants: Case Study," *International Journal of Engineering and Computer Science*, vol. 2, pp. 416-432, 2013.
- [17] L. Barelli, L. Liucci, A. Ottaviano and D. Valigi, "Mini-Hydro: a design approach in case of torrential rivers," *Energy*, vol. 58, pp. 695-706, 2013.
- [18] J. F. Claydon. (2015, 18/05/2015) Turbines. Available: <http://www.jfccivilengineer.com/turbines.htm>.
- [19] Energypedia (2014, 02/06/2013). Hydropower Basic https://energypedia.info/wiki/Hydro_Power_Basics#Classification_of_Hydro_Power
- [20] European Small Hydropower Association (ESHA), "Guide on how to develop a small hydropower plant." ESHA, Brussels, Belgium, 2004.
- [21] S. Singal, "Planning and implementation of small hydropower (SHP) projects," *Hydro Nepal*, vol. 5, July 2009.
- [22] Spatial Plans and Local Arrangement for Small Hydro (SPLASH), "Guidelines for micro hydropower development," Spatial Plans and Local Arrangement for Small Hydro, SPLASH Project, European Commission, Brussels, 2005.
- [23] International Renewable Energy Agency (IRENA), "Renewable power generation costs in 2014," IRENA, 2014.

- [24] International Renewable Energy Agency (IRENA). (2012, 19/03/2015). Prospects for the African power sector: scenarios and strategies for Africa Project. Available: https://www.irena.org/DocumentDownloads/Publications/Prospects_for_the_African_PowerSector.pdf.
- [25] L. L. Ladokun, K. R. Ajao and B. F. Sule, "Hydrokinetic energy conversion systems: prospects and challenges in Nigerian hydrological setting," *Nigerian Journal of Technology (NIJOTECH)*, vol. 32, no. 3, pp. 538-549, 2013.
- [26] A. S. Sambo, "Policy and plans on renewable energy in Nigeria," presented at the Keynote Presentation made at the two day Workshop on Impact of Hydropower on Host Communities, Ilorin. Kwara State, Nigeria, 2012.
- [27] Deloitte, "Sub-Saharan Africa power trends: power disruption in Africa," Johannesburg, 2015.
- [28] [N. Balchin](#), [S. Gelb](#), [J. Kennan](#), H. Martin, [D. W. te Velde](#) and [C. Williams](#), "Developing export-based manufacturing in Sub-Saharan Africa," Overseas Development Institute, London, 2016.
- [29] R. Atta-Ankomah, "Chinese technologies and pro-poor industrialisation in Sub-Saharan Africa: the case of furniture manufacturing in Kenya," *The European Journal of Development Research*, vol 28, no. 3, 397-413, 2015.
- [30] M. Gaul, F. Kolling and M. Schroder. (2012). Policy and regulatory framework conditions for small hydropower in Sub-Saharan Africa. Available: <http://kerea.org/media/2012/12/Policy-and-regulatory-framework-conditions-for-small-hydro-power-in-Sub-Saharan-Africa.pdf>.
- [31] A. Esan, "UNIDO Regional Centre and small hydropower development in Africa— Abuja, International Centre for Science and Technology," in *Proceedings of the Instruments and Potential for the Use of Renewable Energies for Regional Development Conference*, International Centre for Science and Technology and UNIDO (United Nations Industrial Development Organization), Trieste, Italy, Trieste, Italy, May 2011.
- [32] United Nations Industrial Organization (UNIDO), "UNIDO projects for the promotion of small hydropower for productive use: independent thematic review," UNIDO, Vienna, Austria, 2010.

- [33] J. Goodell, J. Lange, T. Newville and F. Semmler, "Grand Rapids public utilities commission's hydro turbine generator," Final Technical Report, Iron Range Engineering Fall 2012.
- [34] W. S. Ebhota and F. L Inambao, "Design basics of a small hydro turbine plant for capacity building in sub-Saharan Africa," *African Journal of Science, Technology, Innovation and Development*, vol. 8, pp. 111-120, 2016.
- [35] U. Dorji and R. Ghomashchi, "Hydro turbine failure mechanisms: an overview," *Engineering Failure Analysis*, vol. 44, pp. 136-147, 2014.
- [36] Tokyo Electric Power Company (TEPCO), "Micro-Hydro designing," Workshop on Renewable Energies, Nadi, Republic of the Fiji Islands: Tokyo Electric Power Co, 2005.
- [37] P. Adhikary, P. K. Roy and A. Mazumdar, "Selection of hydro-turbine blade material: application of fuzzy logic (MCDA)," *International Journal of Engineering Research and Applications*, vol. 3, pp. 426-430, 2013.
- [38] J. Muriithi, "Developing small hydropower infrastructure in Kenya," presented at the 2nd Small Hydropower for Today Conference INSHP, Hangzhou, 2006.
- [39] African Development Bank Group (AfDB), "Renewable energy in Africa: Mali country profile," AfDB, Côte d'Ivoire, 2015.
- [40] O. U. Oparaku, "Decentralised power generation in Nigeria: role of renewable energy resources," In *Proceedings of the 1st International Workshop on Renewable Energy for Sustainable Development in Africa (IWRESDA)*, University of Nigeria, Nsukka, Nigeria, 2007.
- [41] D. Altinbilek, K. Seelos and R. Taylor, "Hydropower's role in delivering sustainability," *Energy & Environment*, vol. 16, no. 5, pp. 815-824, 2005.

Part 3: Sub-Saharan Africa Power Sustainability: A Function of a Domestic Small Hydropower (SHP) Design and Manufacturing

W. S. Ebhota and F. L. Inambao, “Sub-Saharan Africa power sustainability: a function of a domestic small hydropower (SHP) design and manufacturing,” *Journal of Energy in Southern Africa*, 2016. (*Under review.*)

Sub-Saharan Africa Power Sustainability: A Function of Domestic Small Hydropower (SHP) Design and Manufacturing

Williams S. Ebhota¹ and Freddie L. Inambao²

^{1,2}Discipline of Mechanical Engineering, University of KwaZulu-Natal, South Africa

Correspondence email: willymoon2001@yahoo.com

Abstract–The quest for alternative energy sources is on the increase in Sub-Saharan Africa due to gross power inadequacy coupled with a global trend of greenhouse gas emission. This study identifies solar, geothermal, wind and hydro which are renewable energy sources as options. Small hydropower (SHP) has been singled out as the best alternative power system in the region. But there is insufficient local content in terms of design and manufacturing of SHP devices and systems in the region. To boost local participation, the study simplified the design process for low (3 m) and high (60 m) heads for Kaplan/propeller and Pelton pico hydro turbines respectively. The design of a propeller turbine started with a river hydrological data; flow rate (Q) 0.2 m³/s and head (H_n) 3 m using rotational speed (N) of 1500 rpm. In the case of the Pelton turbine, given flow rate (0.02 m³/s), net head (60 m) and rotational speed (1500 rpm) were used to design 8.2 kW output power P_{to} with specific speed N_s of 26.16. CAD modelling and simulation software was used to evaluate the mechanical properties of aluminium alloy (6061-T6) for Pelton bucket application. The study concludes that adaptive design, domestic manufacturing and regional joint SHP research are factors that promote sustainable power development.

Key words: Power; Turbine Design; Pelton turbine; Propeller turbine; Sub-Saharan Africa; Small hydropower

2.3.1 Introduction

The power situation in sub-Saharan Africa (SSA) is in a pathetic state despite several intervention measures [1]. The problems and challenges that trail the power sector in the region seem as fresh as they were two decades ago and even deepened in some areas. Truly, this is heart breaking considering the resources and efforts that have been put in to fix it. The International Renewable Energy Agency (IRENA) reported in 2012 that the average rate of electrification in SSA is about 35 %. It added that the situation is worse in the rural areas which was below 20 %. Further, over 50 % of the population in 41 countries in the region had no access to electricity [2]. One billion sub-Saharan Africans have been projected to have access to electricity in 2040 with 530 million people without access especially in the remote areas [3]. Internationally the regional access to electricity in 2015 is shown in Figure 2.3.1. Some of the factors responsible for this ugly situation are under developed manufacturing infrastructure, over reliance on foreign power technologies, exorbitant cost of power projects and under developed human capacity in the power sector [4].

The search for ways of increasing access to power and alternatives to conventional energy sources (fossil fuel) to supply power to remote and rural areas in the region is massive. This has led to several power schemes. The identified options include solar, geothermal, wind and hydro and they are generally called renewable energies. However, hydropower has been singled out as the most abundant alternative renewable energy source with the potential of increasing access to power in the region. The World Bank has stated that only 8 percent of the hydropower potential in SSA has been developed [5].



Figure 2.3.1: Regional access to electricity in 2015 [6]

The Framework Convention on Climate Change (UNFCCC) of United Nations has recognised the challenge of Greenhouse Gases (GHG). The goal of the Convention is to stabilise GHG concentrations to a level that would prevent hazardous anthropogenic meddling with the climatic condition of the atmosphere [7]. The use of energy was reported to be the highest source of GHG due to CO₂ being a by-product of carbon oxidation during fossil fuel

combustion. Global total primary energy supply (TPES) demand which depends mainly on fossil fuels more than double from 1971-2012 as depicted in Figure 2.3.2 [8].

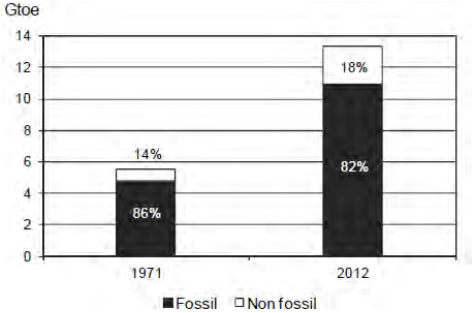


Figure 2.3.2: World TPES [7]

Coal accounts for 29 % of the global TPES but represents 44 % of the world CO₂ emissions while carbon-neutral fuels represent 18 % of TPES [9] (Figure 2.3.3).

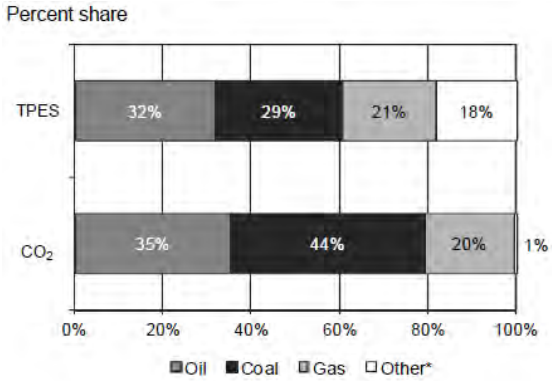


Figure 2.3.3: Global primary energy supply and CO₂ emissions [7]

Greenhouse gas emissions in 2012 decreased in North America (-3.7 %), Annex II Europe (-0.5 %) and Annex I EIT (-0.8 %), but increased was in China (3.1 %), Africa (5.6 %), Asia excluding China (4.9 %) and the Middle East (4.5 %) as represented by Figure 2.3.4.

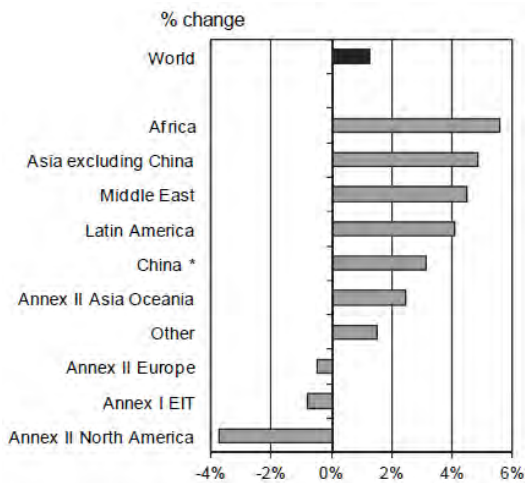


Figure 2.3.4: Change in CO₂ emissions by region (2011-2012)

In 2012, electricity and heat generation emitted about two-thirds of global CO₂ emission which is about 42 %, while transport accounted for 23 % as illustrated by Figure 2.3.5. Although use of renewable energies has gained ground in the region, SSA still relies heavily on coal and fossil fuels for electricity and heat generation.

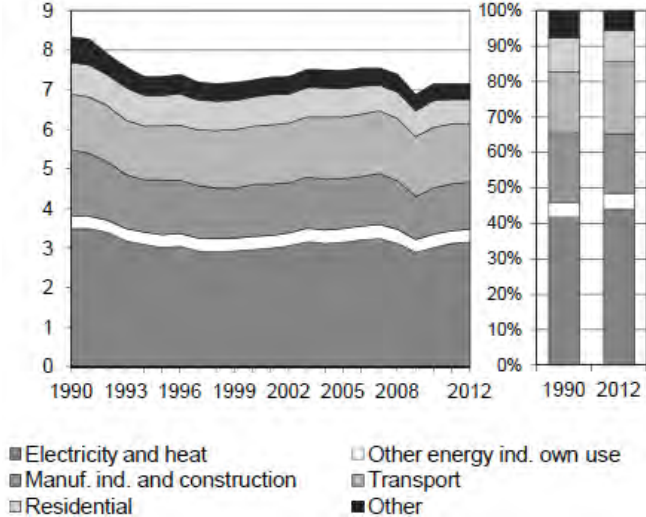


Figure 2.3.5: CO₂ emissions by sector [7]

Amongst the major forms of fuel for power generation, coal emits the highest GHG while hydro produces the least as represented in Figure 2.3.6.

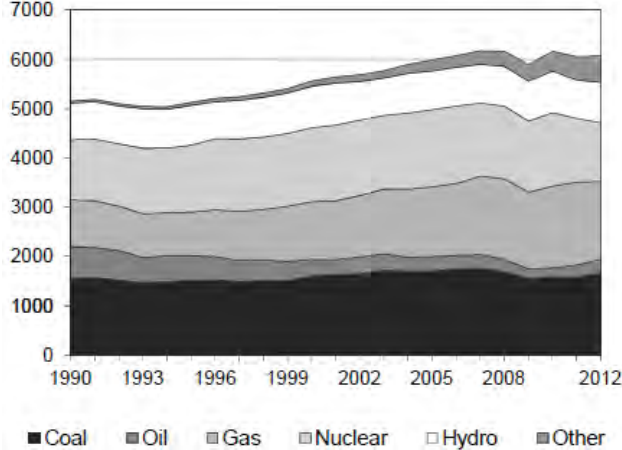


Figure 2.3.6: Electricity generation by fuel

2.3.2 Hydro potential in Africa and benefits of small hydropower

Hydropower is the most used renewable energy in the region due to its large scale potential development and the cost of electricity generated is lower than other technologies both renewable and non-renewable. The effective hydropower potential available in Africa is put at 283 GW which is more than 300 % the current electricity consumption in SSA [1]. Over 50 % of this potential is in Central and East Africa (Cameroon, Congo, DR Congo, Ethiopia and

Mozambique). Reasonable amounts also exist in Southern Africa (Angola, Madagascar, Mozambique and South Africa) and West Africa (Guinea, Nigeria and Senegal). DR Congo has the largest hydropower potential as proposed by the 44 GW Grand Inga project which when actualised will transform African power supply tremendously. Despite gross inequalities in access to electricity and hydro abundance in the region, only 20 GW of hydropower capacity is installed as depicted by Figure 2.3.7. This is less than 10 % of the effective available hydro potential.

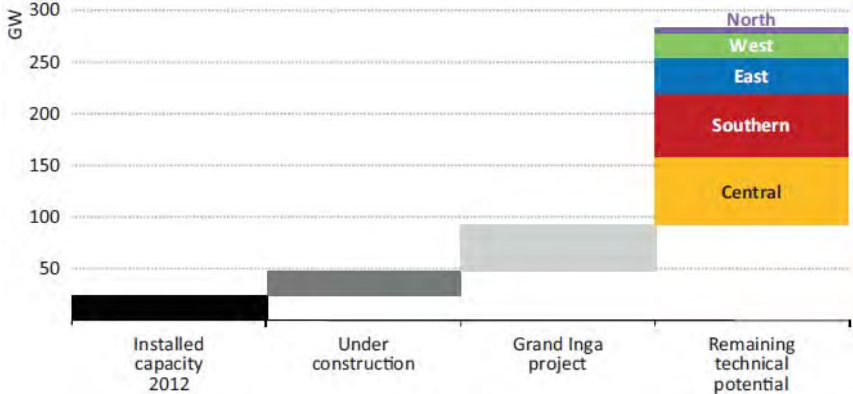


Figure 2.3.7: Hydropower potential and installed capacity in Africa

2.3.2.1 Large scale hydropower projects

Exploration of large hydropower projects are associated with the following challenges:

- i. Large sums of upfront capital.
- ii. Exportation of large amounts of generated electricity is limited due to low levels of interconnection in the region – domestic markets are generally too small to absorb all the power generated by large scale hydropower projects.
- iii. Supply is a function of seasonal and annual variations.
- iv. Hydro dams pose environmental concerns such as displacing communities and may adversely affect water availability for other uses.
- v. Inadequate technical expertise in hydropower development in some countries, etc.

2.3.2.2 Small hydropower (SHP)

Small hydropower refers to the generation of electrical power from a water source on a small scale, usually with a capacity of not more than 10 MW. However, there is still no internationally agreed upon definition of small hydropower as capacity classification varies from country to country as shown in Table 2.3.1 [10, 11]. For rural and electrification of remote areas in developing countries, SHP or micro-hydropower has been described as the

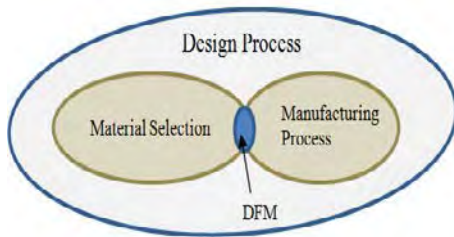
most effective energy scheme [12]. The technology is environmentally benign, extremely robust and long lasting – lasting for 50 years or more with little maintenance [13]. Other striking benefits include [14]: minimal vandalisation of power facility; reduction in transmission losses; reduction in network problems (especially during raining season); reduction in illegal electricity connections to the national grid; the resource is in abundance and largely untapped; it emit low GHG (CO₂) and is regarded as a clean renewable energy source; it can create jobs; and it encourages energy diversification of systems thereby enhancing energy supply reliability in the region, etc. The global quest for cleaner energy to replace or minimise the use of fossil fuels which are the bulk of electricity generation in SSA favours the use of SHP. This will consequently reduce GHG emission [15]. Aggressive use of renewable energy in SSA will reduce CO₂ emissions by 27 % in the region [1].

Table 2.3.1: Various size classifications of SHP

Country	Micro (KW)	Mini (KW)	Small (MW)
United States	< 100	100-1000	1-30
China	-	< 500	0.5-25
USSR	< 100	-	0.1-30
France	5-500	-	-
India	< 100	101-1000	1-15
Brazil	< 100	100-1000	1-30
Norway	< 100	100-1000	1-10
Nepal	< 100	100-1000	1-10
Various	< 100	< 1000	< 10

2.3.3 Hydro turbine design and manufacturing procedures

There is a strong correlation between material selection and manufacturing processes. They could be said to be elements of the universal set called the Design Process. Figure 2.3.8 represents the relation that exists between material selection and manufacturing processes. For successful product design, the design process should provide an interphase between material selection and manufacturing process. This interphase is subjected to material and manufacturing facility availability. The manufacturing system in SSA is not as advanced and adequate compare to what is obtainable in Europe and America or even in Asia. However, good hydro turbine products can still come out of the region if material and manufacturing inadequacies are factored into the design process early.



DFM – Design for manufacturing

Figure 2.3.8: Correlation between material selection and manufacturing process

2.3.3.1 Sustaining power through domestic participation

Domestic participation in the design and manufacturing of SHP devices and systems in SSA will promote access to electricity in the region and the creation of jobs. Power sustainability in the region will always be threatened by overdependence on foreign technology due to high cost of power project execution, inadequate skilled personnel for installation, operation, maintenance and repair challenges. This participation can be activated through regional joint capacity building for SHP technology in the following areas: foundry technology; mechatronics; fluid mechanics; manufacturing processes; and material development engineering.

A simplified hydro turbine production procedure can be categorised into twelve sequential steps as shown in Figure 2.3.9.

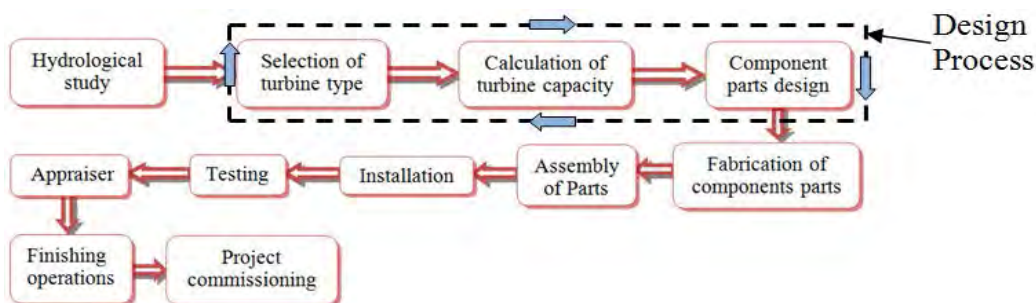


Figure 2.3.9: Production layout model of a pico hydro turbine system

2.3.3.2 Hydropower plant operation principle

Hydro turbine plants are rotating machines that transform the mechanical energy in flowing water into torque to turn the generator for the purpose of electricity production. Turbine can be categorised into two types, namely, impulse and reaction turbines [16-18]. This classification depends on the water energy transfer method.

For impulse turbines, water is projected from the nozzle as a jet and strikes on the buckets that are arranged on the circular edge of the runner. The buckets are made up double hemispherical cups. The nozzle is at the end of penstock while the buckets discharges used

water into the tailrace. A schematic diagram of a Pelton turbine is shown in Figure 2.3.10. In a reaction turbine, the runner or spinning wheel (blade) is completely immersed in the flow and uses water pressure and kinetic energy of the flow. They are appropriate for low to medium head applications. The two main types of reaction turbine are the propeller (with Kaplan variant) and Francis turbines.

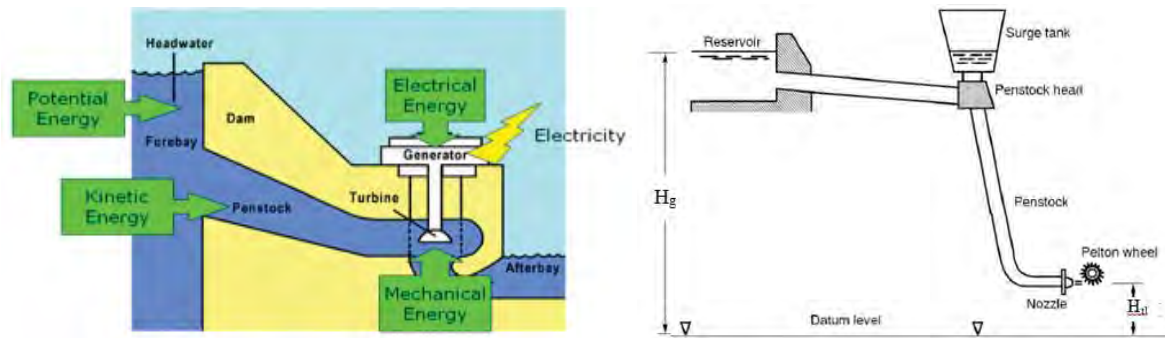


Figure 2.3.10: Schematic diagram of a hydro turbine system [19]

2.3.3.3 Hydro turbine main components

The hydro turbine is composed of the following main components as shown in Figure 2.3.10:

- Dam/Weir – is a wall across the river or flow channel to store water.
- Headrace – The reservoir created by the dam/weir.
- Penstock – the pipe that connects the headrace to the turbine runner.
- Runner – the aspect of the layout that converts the energy of the flowing water into torque that drives the generator via a shaft. The runner of a turbine has a wheel and buckets or cups for Pelton turbine, or blade and hub for Kaplan, Turgo and Francis turbines.
- Shaft – this connects the blade and the generator.
- Generator – this is the device that receives the mechanical energy through the shaft and converts this energy into electrical energy.
- Tailrace – the used water flows out of the turbine through this channel.

2.3.3.4 Selection of turbine and design of turbine

There are two factors that determine the kind of turbine to be used. These factors are products of hydrological study of the hydro potential like river or water falls. The parameters are head (H) and the volumetric discharge (Q) of the river (Figure 2.3.11).

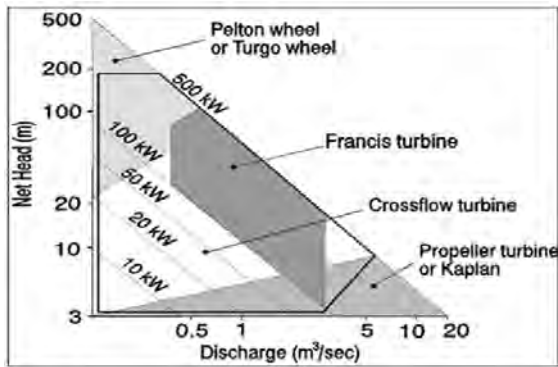


Figure 2.3.11: Head-flow range of small hydro turbines [13]

The type of turbine to be used according to head classification; the head is classified into low (> 10 m), medium (10 m to 50 m) and high head (above 50 m). Table 2.3.2 shows type of turbines and the various head domains where they are applied.

Table 2.3.2: Types of hydro turbine and their applications [19, 20]

Turbine	Head Classification		
	High (> 50 m)	Medium (10-50 m)	Low (< 10 m)
Impulse	Pelton, Turgo, Multi-jet Pelton	crossflow, Pelton, Turgo, multi-jet Pelton	Crossflow
Reaction		Francis (spiral case)	Francis (open-flume), Propeller, Kaplan, Darius

2.3.3.5 The Kaplan/Propeller turbine

The Kaplan or propeller turbines are appropriate for low head and large discharge operations. Figure 2.3.12 shows a schematic diagram of a Kaplan/Propeller turbine blade. The Kaplan is an adjustable runner blade with high, almost constant efficiency over a wide range of load. The range of Kaplan turbine applications has been greatly improved, which has favoured the improvement of numerous undeveloped hydro sources previously discarded for economic or environmental reasons. The Kaplan Turbine generation efficiency is sometimes over 90% at low heads and high flows [21].

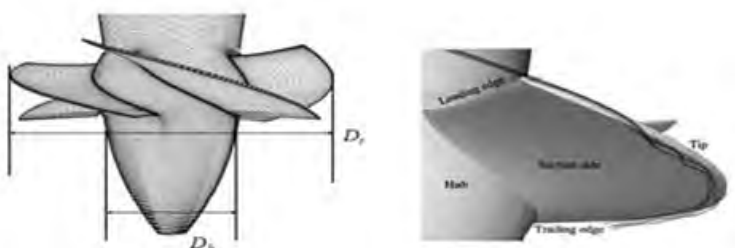


Figure 2.3.12: Kaplan/Propeller runner blade parameters and parts

2.3.3.6 The Pelton turbine: Main elements of a Pelton turbine system

This turbine is typically used in small-scale micro-hydro systems (with power of up to about 100 kW) and a head ranging from 10 m to 200 m. It consists of a wheel (or runner) with a number of buckets attached around its edge, which are shaped like two cups joined together with a sharp ridge between them as shown in Figure 2.3.13. In addition, a notch is cut out of the bucket at the outside end of the ridge. Water is directed to the turbine through a pipe and nozzle to this ridge. Its shape allows for the production of a lot of power from such a small unit and it is easy to manufacture.

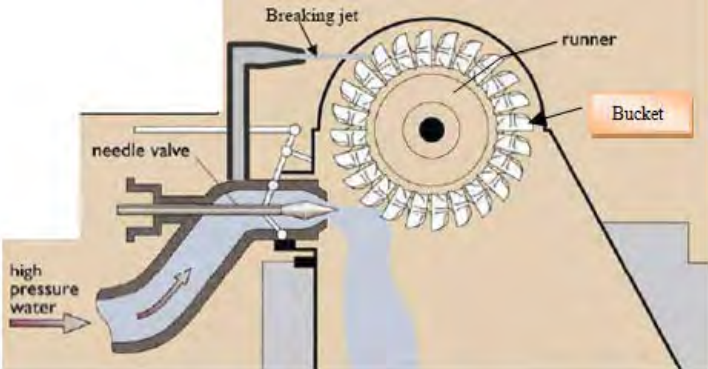


Figure 2.3.13: Pelton turbine arrangement

As the water strikes at the symmetrical line it then distributes into the two halves of the bucket while some water is reflected back to the nozzle. The angle of jet deflection theoretically for a perfect hemispherical bucket is 180° . This is not possible to obtain practically so the angular deflection of 165° is used in practice [16]. The main parts of Pelton turbine are penstock, spear, nozzle, wheel and buckets, shaft, generator, valves and powerhouse (Figure 2.3.14). Water flows from the headrace through the penstock to runner. The penstock has a nozzle at its exit before the runner.

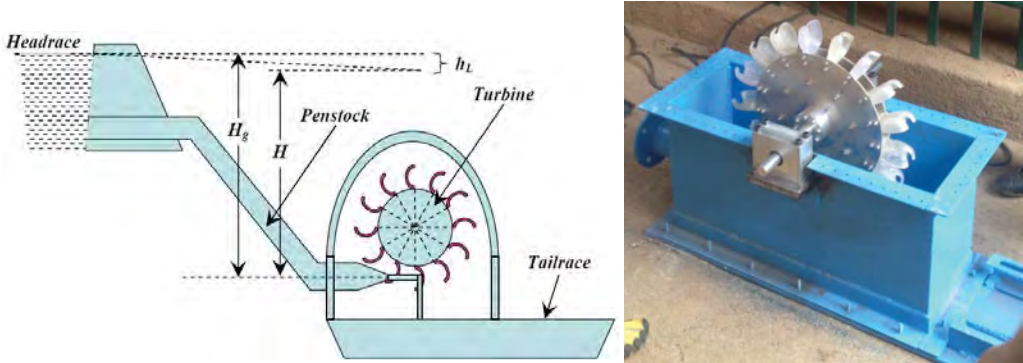


Figure 2.3.14: The general layout of a Pelton hydro turbine plant [19]

The flow rate of the water jet from the nozzle can be controlled with the use of a spear (evident in Figure 2.3.13). This spear helps to adjust the flow rate to balance the change caused by site conditions.

2.3.4 Methodology

This study, explored a simple design approach in SHP design and development processes, to facilitate rapid and increased uptake of SHP schemes in SSA. The design process was based on locally available material and manufacturing facilities. Calculus forms of equations were avoided and simple CAD drafting and simulation software was used.

2.3.4.1 Propeller turbine design for low head

Table 2.3.3: Nominal conditions for Kaplan/Propeller turbine design (refer to Figure 2.3.12) [22]

Step	Relevant Equations	Answer
Turbine capacity, P_{ii} .	$P_{ii} = \rho * g * Q * H_n$	6 kW
Specific speed, N_s	$N_s = \frac{N * \sqrt{Q}}{H_n^{0.75}}$	294
Velocity, u	$u = K_{ug} \sqrt{2gH_n}$	13.04 m/s
The angular velocity of the turbine runner, rad/s	$\omega = \frac{2\pi N}{60}$	157 rad/s
The blade tip radius, r_t	$r_t = \frac{K_{ug} \sqrt{2gH_n}}{\omega}$	0.083 m
The blade tip diameter, D_t	$D_t = 2r_t$	0.166 Mm 0056
The hub diameter, D_h	$\frac{D_h}{D_t} = 0.35$	0.058 m
Cross sectional area, A	$A = \frac{\pi}{4}(D_t^2 - D_h^2)$	0.019 m ²
Axial velocity [m/s]	$V_{axial} = \frac{4Q}{\pi(D_t^2 - D_h^2)}$	10.53 m/s
Flow coefficient, Φ :	$\Phi = \frac{Q}{ND_t^3}$	0.044
Power coefficient, Γ :	$\Gamma = \frac{P}{\rho N^3 D_t^5}$	1.4*10-8
Energy coefficient, Ψ :	$\Psi = \frac{gH}{N^2 D_t^2}$	4.7*10-4

Where A - area; Q - flow rate and; r_t - blade radius; r_h - hub radius; D_t - blade diameter and; D_h - hub diameter; K_{ug} , the tip-to-head velocity ratio (D_t/D_h); ρ - density of water (kg/m^3); g - acceleration due to gravity (9.81 m/s^2); H_n - net head (m) and; η_{tl} - total efficiency.

2.3.5 Design calculation and simulation of a Pelton bucket high head

2.3.5.1 Pelton design parameters

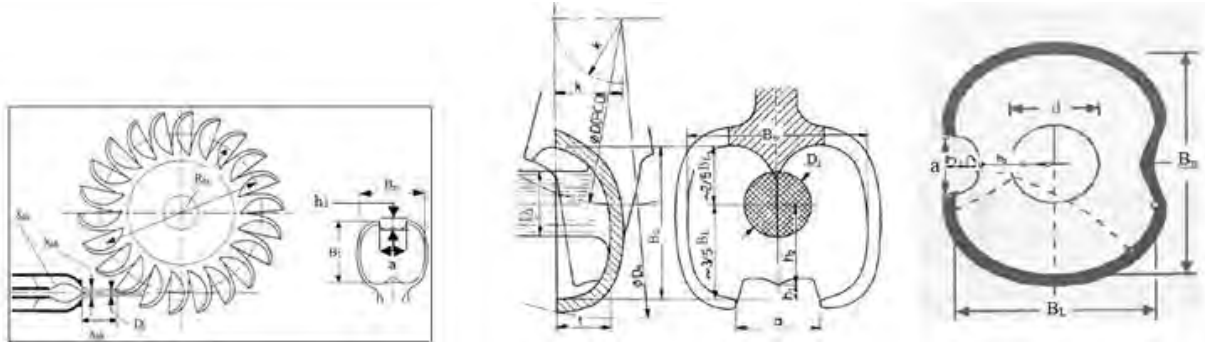


Figure 2.3.15: Runner and bucket parameters

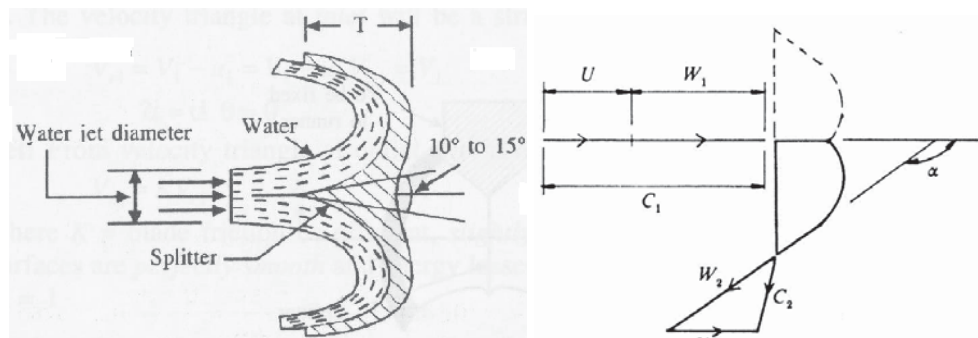


Figure 2.3.16: Turbine velocity diagrams

Table 2.3.4: Nominal conditions for Pelton turbine design (refer to Figures 2.3.15 and 2.3.16) [19, 21, 23, 24]

Given quantities: $Q = 0.015 \text{ m}^3/\text{s}$; $H_n = 60 \text{ m}$; $C_n = 0.98$; $\rho = 103 \text{ Kg/m}^3$; $x = 0.46$; $n_j = 1$; $L_{pt} = 100 \text{ m}$; $\psi = 0.98$ and; $\theta = 165^\circ$. The generator is rated at 120 watts, and the rotation (N) is 1500 rpm.

Parameters	Relevant Equations	Answer
The input power to the turbine, P_{ti}	$P_{ti} = \rho * g * C_n^2 * H_n * Q$	8.48 kW
Specific speed (N_s)	$N_s = \frac{N * \sqrt{P_{ti}}}{H_n^{\frac{5}{4}}}$	26.16
Jet velocity, V_j (m/s)	$V_j = C_n * \sqrt{2 * g * H_n}$	33.62 m/s
Jet/nozzle diameter, D_j	$D_j = \sqrt{\frac{4 * Q}{\pi * n_j * V_j}}$	0.024 m
Tangential velocity of the runner, V_{tr}	$V_{tr} = x * V_j$	15.47 m/s

Runner diameter D_r , (m)	$D_r = \frac{60 * V_{tr}}{\pi * N}$	0.20 m
Jet/nozzle cross sectional area, A_j	$A_j = \frac{\pi * D_j^2}{4}$	$4.5 * 10^{-4}$
Nozzle flow rate, Q_n (m^3/s)	$Q_n = V_j * A_j$	$0.015 m^3/s$
Distance between bucket and nozzle, x_{nb} (m)	$x_{nb} = 0.625 D_r$	0.125 m
Radius of bucket center of mass to runner center R_{br} (m)	$R_{br} = 0.47 D_r$	0.094 m
Bucket axial width, B_w (m)	$B_w = 3.4 D_j$	0.082 m
Bucket radial length, B_l (m)	$B_l = 3 D_j$	0.072 m
Bucket depth, B_d (m)	$B_d = 1.2 D_j$	0.029 m
Cavity Length, h_1 (m)	$h_1 = (0.35) D_j$	0.008 m
Length to Impact Point, h_2 (m)	$h_2 = (1.5) D_j$	0.036 m
Offset of Bucket, k (m)	$k = (0.17) D_j$	0.004 m
Cavity Width, a (m)	$a = (1.2) D_j$	0.029 m
Number of bucket n_a	$n_b = 15 + \frac{D_r}{2 D_j}$	19
Length of bucket moment arm, L_{ab} (m)	$L_{ab} = 0.195 D_r$	0.039 m
Volume of bucket, V_b (m^3)	$V_b = 0.0063 * D_r^3$	$5.04 * 10^{-5} m^3$
The output power to the turbine, P_{to} (kW)	$P_{to} = \rho * Q * V_{tr} \left[\frac{(V_j - V_{tr}) *}{(1 + \psi * \cos(\phi))} \right]$	8.20 kW
Turbine hydraulic efficiency, η_{th}	$\eta_{th} = \frac{P_{to}}{P_{ti}} * 100$	97 %
The torque produced by the turbine, T_t (N-m)	$T_t = \frac{P_{to}}{\omega} = Q * D_r * (V_j - V_{tr})$	0.054 N-m
The deflector required force, F_d :	$F_d = \rho * Q * V_j$	672.4 N
Force acting on the runner, F_A ;	$F_A = 2 * \rho * Q_n * (V_j - V_{tr})$	555.2 N


Where C_n – nozzle discharge coefficient (0.98); N – runner speed (rpm); x – ratio of V_{tr} to V_r ; Q - flow rate; g - acceleration due to gravity ($9.81 m/s^2$); H_n - net head (m); ρ - density of water (kg/m^3)

2.3.6 Material selection for Pelton bucket

Material selection is a very important part of design and manufacturing. One of the variables for design process iteration is material and it influences on the manufacturing process. In this study, the selection of material for the bucket was determined by availability, functional requirements, cost and manufacturing facilities available. Aluminium alloy (6061-T6) was

selected because aluminium is readily available in SSA and it can be easily worked. Table 2.3.5 shows the material's properties.


Table 2.3.5: Material (6061-T6 aluminium) properties

Model Reference	Volumetric Properties	
	Name: 6061-T6 aluminium alloy	Mass: 0.249492 kg
	Model type: Linear elastic isotropic	Volume: 9.24044e-005 m ³
	Yield strength: 2.75e+008 N/m ²	Density: 2700 kg/m ³
	Tensile strength: 3.1e+008 N/m ²	Weight: 2.44502 N
	Elastic modulus: 6.9e+010 N/m ²	Shear modulus: 2.6e+010 N/m ²
	Poisson's ratio: 0.33	Thermal expansion coefficient: 2.4e-005 /Kelvin

2.3.6.1 Evaluation of 6061-T6 Aluminium Alloy

The necessary design parameters in Table 2.3.4 were used in the simulation to validate the stress and fatigue of the part (bucket). The results of the simulation are shown in Tables 2.3.6 and 2.3.7 and Figures 2.3.12 and 2.3.13.

Table 2.3.6: Mesh information

	Mesh type	Solid Mesh	Total Nodes	14895
	Meshes Used:	Standard mesh	Total Elements	8568
	Total Nodes	14895	Maximum Aspect Ratio	19.602
	Total Elements	8568	% of elements with Aspect Ratio < 3	97.5
	Jacobian points	4 Points	% of elements with Aspect Ratio > 10	0.0817
	Element Size	4.52077 mm	% of distorted elements (Jacobian)	0
	Tolerance	0.226039 mm	Time to complete mesh(hh:mm:ss):	00:00:07
	Mesh Quality	High		

Static analysis (von Mises) shows that the highest stress (1.95904e+008 N/m²) as a result of the load is located at node 723 as indicated in Table 2.3.7 and Figure 2.3.12. This value is less than the material's yield stress of 2.75e+008 N/m² as presented in Table 2.3.5.

Table 2.3.7: Study results for stress, displacement and strain

Name	Type	Min	Max
Stress	VON: von Mises stress	1959.97 N/m ² Node: 812	1.95904e+008 N/m ² Node: 723

Displacement	URES: Resultant Displacement	0 mm Node: 177	0.209923 mm Node: 435
Strain	ESTRN: Equivalent Strain	5.56279e-008 Element: 3484	0.00172423 Element: 3816

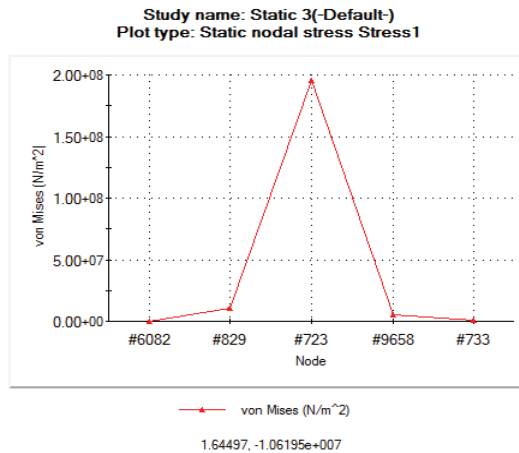
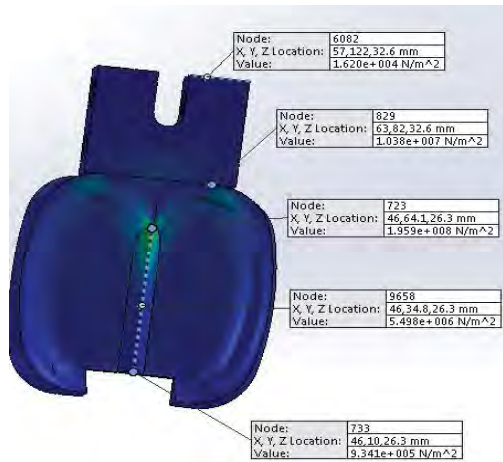
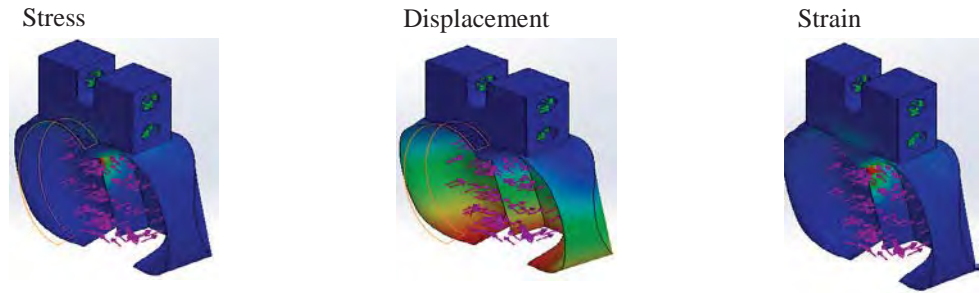


Figure 2.3.17: Nodal stress distribution

The fatigue distribution along the longitudinal section is shown in Figure 2.3.17. The highest fatigue value was recorded at nodal 723 as shown by Figure 2.3.18.

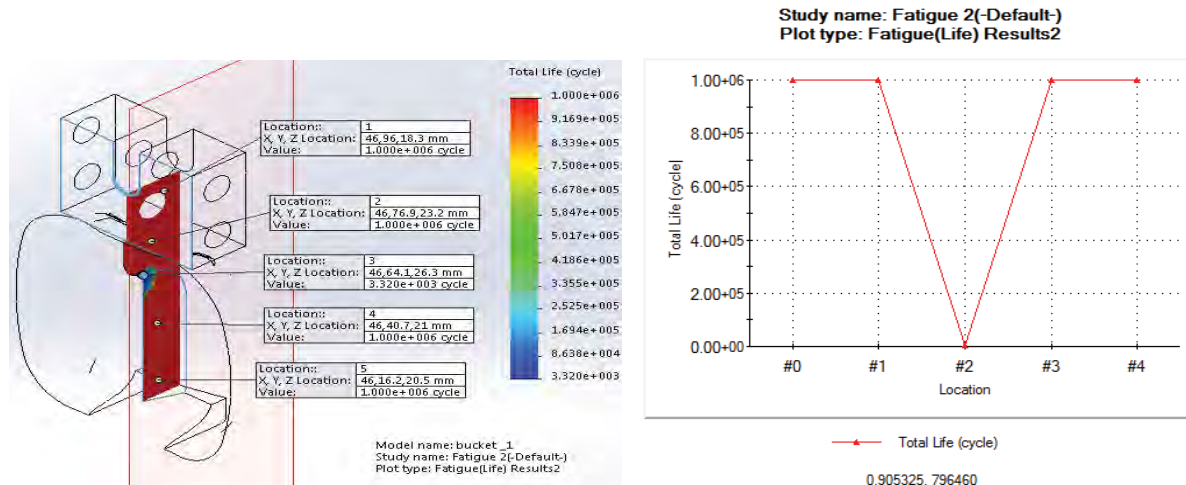


Figure 2.3.18: Nodal fatigue distribution

The minimum Factor of Safety (FOS) value is 1.404 and this value was recorded at nodal point 723 as show in Figure 2.3.19. However, the FOS is > 1. Using Solidworks software, the

FOS benchmark is 1.4. The value of FOS (1.404) recorded from the simulation validates the design.

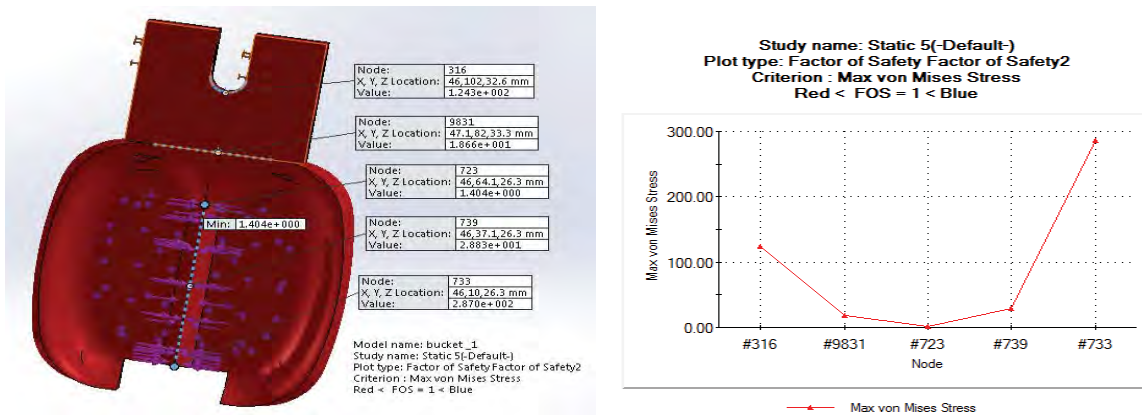


Figure 2.3.19: Factor of Safety distribution

2.3.7 Conclusion

The manufacturing infrastructure in SSA is inadequate to support energy sustainability. As a result, the region heavily depends on foreign technology and this leads to high cost of power projects. This has left the region's socio-economic situation in dire straights. In order to increase access to electricity in the region, it is therefore pertinent to building capacity in power technology. The design process should focus on local contents in terms material selection and manufacturing facility. This study recommends capacity building in SHP technology, establishment of joint regional energy research institutions, transformation of research findings into real products, and adoption of China's energy development approach of massive use of micro hydro turbines. The use of local materials should be encouraged as the performance of aluminium alloy (6061-T6) was shown by simulation results to be satisfactory.

Bibliography

- [1] A. Castellano, A. Kendall M. Mikomarov and T. Swemmer, "Brighter Africa: the growth potential of the sub-Saharan electricity sector," McKinsey & Company, New York, 2015.
- [2] International Renewable Energy Agency (IRENA). (2012, 19/03/2015). Prospects for the African Power Sector: scenarios and strategies for Africa project. Available: https://www.irena.org/DocumentDownloads/Publications/Prospects_for_the_African_PowerSector.pdf
- [3] International Renewable Energy Agency IEA, "A focus on energy prospects in Sub-Saharan Africa," *World Energy Outlook Special Report*, IEA, France, 2015.
- [4] W. S. Ebhota, A. C. Eloka-Eboka and F. I. Inambao, "Energy sustainability through domestication of energy technologies in Third World countries in Africa," *Proceedings of the Industrial and Commercial Use of Energy (ICUE), 2014 International Conference on "Energy efficiency in buildings"*. 2014, pp. 1-7.
- [5] K. Codi, Zambia electricity shortage highlights Africa's hydropower shortfalls, *Circle of Blue*, Jul 22, 2015. Available: <http://www.circleofblue.org/2015/world/zambia-electricity-shortage-highlights-africas-hydropower-shortfalls/2015>.
- [6] O. Mohammed, "Charted: how electricity problems are limiting growth in many African countries," *Quartz Africa*, June 08, 2015. Available: <http://qz.com/422357/charted-how-electricity-problems-are-limiting-growth-in-many-african-countries/>.
- [7] International Renewable Energy Agency (IEA), "CO₂ emissions from fuel combustion statistics highlights," IEA Statistics, 2014 Edition, , IEA, Paris, 2014.
- [8] Intergovernmental Panel on Climate Change (IPCC), "Revised 1996 IPCC Guidelines for National Greenhouse Gas Inventories " IPCC, Bracknell, UK, 2007.
- [9] M. Nachmany, S. Fankhauser, M. Townshend, T. Collins, T. Landesman, A. Matthews, et al., "The GLOBE climate legislation study: a review of climate change legislation in 66 countries," GLOBE International and the Grantham Research Institute, London School of Economics, London, 2014.

- [10] British Hydropower Association (BHA), "A guide to UK mini-hydro development," British Hydropower Association, Gussage St Michael, Wimborne, UK, 2012.
- [11] D. Basnyat, "Background material: fundamentals of small hydropower technologies," Renewable Energy and Energy Efficiency Partnership, Nairobi, Kenya, 2006.
- [12] D. J. Obadote, "Energy crisis in Nigeria: technical issues and solutions," presented at the Power Sector Prayer Conference, Nigeria, 2009.
- [13] P. Oliver, "Small hydropower: technology and current status. Renewable and sustainable," *Energy Reviews*, vol. 6, no. 6, pp. 537-556, 2002.
- [14] S. van der Wat, (2013, 2/11/2015). Hydro in Africa: navigating a continent of untapped potential. *HRW-Hydro Review Worldwide*. Available: <http://www.hydroworld.com/articles/print/volume-21/issue-6/articles/african-hydropower/hydro-in-africa-navigating-a-continent.html>.
- [15] M. Kimani, "Powering up Africa's economies: regional initiatives can help cover deficits," *Africa Renewal*, vol. 23, no. 3, p. 8, 2008.
- [16] B. A. Nasir, "Design of high efficiency Pelton turbine for micro hydropower plant," *International Journal of Electrical Engineering and Technology (IJEET)* vol. 4, no. 1, pp. 171-183, 2013.
- [17] L. Gudukeya and I. Madanhire, "Efficiency improvement of Pelton wheel and crossflow turbines in micro-hydropower plants: case study," *International Journal of Engineering and Computer Science* vol. 2, pp. 416-432, 2013.
- [18] L. Barelli, L. Liucci, A. Ottaviano and D. Valigi, "Mini-Hydro: a design approach in case of torrential rivers," *Energy*, vol. 58, pp. 695-706, 2013.
- [19] Energypedia, (2014, 02/06/2013). Hydropower Basics. Available: https://energypedia.info/wiki/Hydro_Power_Basics.
- [20] J. F. Claydon. (2015, 18/05/2015). *Turbines*. Available: <http://www.jfccivilengineer.com/turbines.htm>.
- [21] W. Stone, "Corazón del Bosque Hydroelectric Scheme: engineering design document," Appropriate Infrastructure Development Group (AIDG), Guatemala, May 2010.

- [22] T Flaspöhler, "Design of the runner of a Kaplan turbine for small hydroelectric power plants," Master's thesis, Mechanical Engineering, Tampere University of Applied Sciences, Tampere, Finland, 2007.
- [23] V. S. Obretenov, "Modernization of a Pelton water turbine," *Пробл. Машиностроения*, vol. 4, pp. 1-5, 2006.
- [24] A. Austegard and O. Schumacher. (n.d. 24/04/2015). Kaplan turbine from remote hydro light. Available: www.remotehydrolight.com

CHAPTER 3: DESIGN BASICS OF A SMALL HYDRO TURBINE PLANT FOR CAPACITY BUILDING IN SUB-SAHARAN AFRICA

W. S. Ebhota and F. L. Inambao, "Design basics of a small hydro turbine plant for capacity building in sub-Saharan Africa," *African Journal of Science, Technology, Innovation and Development*, vol. 8, no. 1, pp. 111-120, 2016. DOI: 10.1080/20421338.2015.1128039.



Design basics of a small hydro turbine plant for capacity building in sub-Saharan Africa

Williams S. Ebhota & Freddie Inambao

To cite this article: Williams S. Ebhota & Freddie Inambao (2016) Design basics of a small hydro turbine plant for capacity building in sub-Saharan Africa, African Journal of Science, Technology, Innovation and Development, 8:1, 111-120, DOI: [10.1080/20421338.2015.1128039](https://doi.org/10.1080/20421338.2015.1128039)

To link to this article: <http://dx.doi.org/10.1080/20421338.2015.1128039>



Published online: 29 Apr 2016.



Submit your article to this journal [↗](#)



Article views: 47



View related articles [↗](#)



View Crossmark data [↗](#)

Design basics of a small hydro turbine plant for capacity building in sub-Saharan Africa

Williams S. Ebhota* and Freddie Inambao

Department of Mechanical Engineering, University of KwaZulu-Natal, Durban, South Africa

**Corresponding author email: willymoon2001@yahoo.com*

This paper presents a simplified design considerations for a propeller hydro-turbine, including tabulated relevant mathematical expressions of operating parameters. In the design calculation, a 2.5 m head and 0.183 m³/s flow rate were used as river data for power of 2.61 kW. A four-blade propeller with an outer diameter of 0.226 m and a hub diameter of 0.079 m was considered suitable for the low head application. Dimensionless performance parameters for various power (2–10 kW) and flow rate (0.2–0.6 m³/s) were evaluated (using constant head and rotational speed), the results were tabulated and graphs plotted. The static axial force on the blade and hub analysis was carried out and results shown satisfactory performance of aluminum 6061-T6 alloy as the blade material. Popularisation of small hydro power (SHP) design and production technology in sub-Saharan Africa through domestic capacity building will accelerate local fabrication of SHP plants and components. The study recommends that the design process be based on available materials and manufacturing facilities. The provision of SHP for rural areas, industrial estates and standalone electrification will provoke commercial and industrial activities in sub-Saharan Africa. This will consequently raise the productivity and the standard of living of the people.

Keywords: energy, hub, hydroelectricity, hydrology, hydro-turbine, Pico, propeller, runner

JEL classification: P28, Q43, Q42, N57

Introduction

The third-world countries are faced with chronic electricity problems, which are barriers hindering economic growth, notwithstanding the availability of vast natural resources in these areas. The International Energy Agency (IEA) reported in 2014 that the population of sub-Saharan Africa without access to electricity is about 620 million people, equivalent to two-thirds of the population (IEA 2014). Design, manufacturing, and material development capacities for Pico hydro system applications are necessary in sub-Saharan Africa to increase access to energy for human survival and advancement (Ebhota, Eloka-Eboka, and Inambao 2014). On average, technologically advanced countries produce and consume more energy than developing and underdeveloped countries, while about 620 million people of sub-Saharan Africa have no access to electricity. It is imperative to provide adequate and affordable energy for citizens to improve livelihoods in sub-Saharan Africa and elsewhere (Cordeiro 2014, Etiosa et al. 2009). Social, economic and environmental aspects of the pico hydro turbine make it a viable alternative source of power. It also has the lowest generating and maintenance costs compared to other off-grid alternatives for remote areas. The environmental impact advantages of Pico hydro-turbine systems are the absence of the large civil works, massive ecosystem alterations and population displacement associated with large-scale hydro systems (Bryan 2011). They thus provide a better economic option for Africa.

Adequate access to power will provoke commercial and industrial activities in the developing countries of sub-Saharan Africa and consequently raise the productivity of the people and their standard of living. This can be achieved through popularisation of small hydro power (SHP) technology for the provision of power for rural areas, industrial estates and standalone electrification instead of relying on the national grid.

To boost power sustainability, the countries of sub-Saharan Africa should increase the continent's manufacturing profile. This is one way to fix the huge power problems in the continent. To do this there is a need to build SHP capacities for both human settlement and infrastructure that supports domestic manufacturing. The drive to increase the continent's local content in the manufacture of SHP equipment will ensure reduction in the cost of power projects from the present cost situation. Further, the ability to design and manufacture SHP equipment will address operation, maintenance and availability problems and jobs will be created.

Literature review

There are a lot of investigative studies of hydro turbine design, mainly centred on basic concepts, operating parameters and output efficiency (Zainuddin et al. 2009, Arriaga 2010, Weerapon and Sirivit 2009, Simpson and Williams 2006). Zainuddin et al. (2009) described the process of energy storage during domestic water distribution to houses by kinetic energy conversion of water flowing in the pipes into electricity. The energy can be used for regular domestic activities like cooking, and heating the water for bathing, and laundry. The study was conducted to design and produce a Pico-hydro generation system from water supplied to residential houses. In conclusion, head and flow rate were described as vital parameters in developing a Pico hydro system and wrong turbine selection and sizing as the main causes of failure (Zainuddin et al. 2009).

The concept of pumps as turbines was presented as a technically and economically viable additional alternative to Pico-hydro development in the Lao PDR was reported by Arriaga (2010). the report presents: feasibility study, design, and analysis of a 2 kW project in the Xiagnabouli province; estimation simulation of motor as generator to the needed

value excitation capacitance and induction loads impact in the system behaviour were regarded as positive approach; hastening to completion rather than focusing providing a sustainable electrical service for the village is an error and; enhancement of mechanical operational and electrical prediction model simulation.

A study was reported on feasibility analysis of a complementary power supply system to houses, offices, and industries using the combination of wind and pico-hydro turbines (Ehsan et al 2012). The hydro turbine was mounted along the path of inflow pipe to the storage tank and both turbines located on a high rise building roof. Pump installed at the ground floor fills tank with water at a very high velocity and this pushes the turbine to spin located along its flowing path. Turbine rotation is transferred via shaft to the generator that converts the kinetic energy to electrical energy that is stored by means of battery. Wind turbine installed also converts the kinetic energy in wind velocity into electrical energy and store in the same battery. The study pointed out that this system eliminates cost of fuel and generates clean power and eco-friendly environment as advantages.

Standard design procedure development for pico propeller turbines for local manufacture in developing countries was undertaken by Simpson and Williams (2006) in collaboration with Practical Action (ITDG). A demonstration 5 kW testing turbine was built on a site in Peru and the turbine design overall performance data were obtained with computational fluid dynamics (CFD). The preliminary CFD study results show a low efficiency rotor design and a mismatch between geometry flow and site conditions. A simplified manufacturing method was used to produce a new rotor with acceptable performance. Comparison of CFD simulations and field test results showed improvement of CFD modelling and measurement techniques used at the site.

Investigation of fluid flow pressure and velocity effects on blades for enhancement of hydro turbine efficiency were studied by Weerapon and Sirivit (2009). CFD simulation of pressure and velocity distributions on five blades of hydro bulb turbine rotating at 980 rpm with Fluent Software was performed. The large eddy simulation (LES) model of turbulence flow was used to check impacts of blade angles on a hydro turbine mounted on the Huai

Kum Dam drainage pipeline. The check was done under the realistic state of irregular and incompressible fluid flow. Simulation was performed at varying guide vane angles of 60°, 65° and 70° to establish the angle with maximum and minimum pressure on blades. Fixed simulation conditions were a 21 m head, a 25° blade twist angle and a 32° blade camber angle. The simulation results showed 213 kPa, 217 kPa and 207 kPa as maximum pressures at the leading pressure side for the angles 60°, 65° and 70° respectively, while -473 kPa, -465 kPa and -581 kPa as minimum pressures at the leading suction side for the angles 60°, 65° and 70° respectively. The study concluded that the guide vane angle affects pressure distribution and hydro turbine efficiency (Weerapon and Sirivit 2009).

Methodology

In the literature accessed, only a handful of studies have been done on alternative materials for hydro turbine blades, especially in the area that this study is focused on. This study explored a simple design approach in SHP design and development processes in order to facilitate rapid and larger involvement of local resources in SHP schemes. The design process was based on local available material and manufacturing facilities. Calculus forms of equations were avoided and simple CAD drafting and simulation softwares were used.

Hydro turbine design procedures

A simplified model of procedures can be categorised into twelve sequential steps as presented in Figure 1.

Hydrology: Flow duration curve

There are a lot of considerations to make in the design of a micro-turbine hydro-electrical plant. Fundamentally, the flow rate of the water source (river or stream), the speed, maximum head, turbine type and size must be considered. However, the maximum head and flow rate are the determining factors for the others. A hydrological study provides data for a flow duration curve (FDC), from which a mean flow rate is established that serves as the maximum flow rate of the river or stream. Estimation of a river's hydro potential is derived from its mean annual flow record (ESH Association 2010).

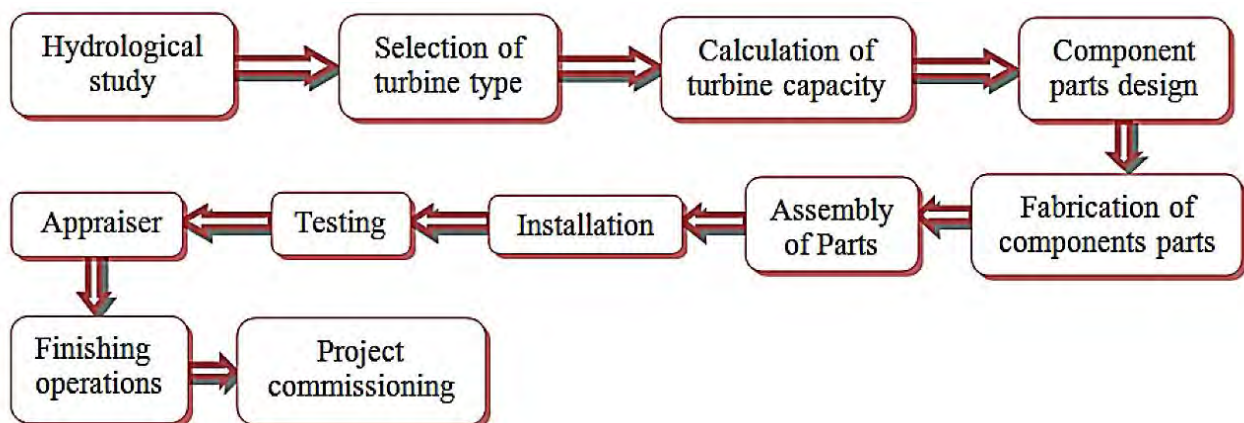


Figure 1: A production layout model of a pico hydro turbine system

Selection of turbine

The type of turbine to be used depends mostly on two factors derived from hydrological studies of the river or stream. They are the net head (H) and the flow rate (Q) of the river as represented in Figure 2. In general, there are turbines that are used for high pressure (50 m and above) and low head (below 10 m) domains for micro-hydro. For example, Pelton turbines are used for high heads while crossflow turbine and Kaplan turbine with fixed or movable are used for low heads. The Francis types of turbine are used for both high and low heads and have the largest range of usage in terms of head. It can be used for as low as 10 m heads for micro-hydro (ESH Association 2010).

Evaluation of characteristics of turbines and operational conditions

There are four most relevant parameters in turbine design and these are net head (H_n), flow rate (Q), rotational speed of the turbine (N) and the efficiency of the turbine (η). Two of these parameters (H_n and Q) are hydrological study data of the water source. Once the flow characteristics are known, the type of turbine, calculation of basic parts and the height or elevation above the tailrace water surface that the turbine will be installed to prevent cavitation can then be carried out.

In a pico hydropower plant (PHPP) system, the power generated depends on these variables:

- i. Flow rate (Q): This is the volume of water discharged per second. It is measured in m^3/s (SI unit)
- ii. Head (H): This is the vertical net distance between fore bay level and turbine level or tail water level and is measured in metres.
- iii. Rotational speed of the turbine (N) measured in revolutions per minute (rpm)
- iv. Efficiency (η): The pico hydropower plant (PHPP) has high efficiency, 60–80% (BHA 2006).

Power (P)

This is the energy generated at a given time and is measured in watts (W) is mathematically expressed as:

$$P = \eta \times \rho \times g \times Q \times H_n \tag{1}$$

where: η = efficiency (micro = 60–80%, small > 80%); ρ = density of water (1000 kg/m^3) and; g = acceleration due to gravity (9.81 m/s^2)

For $\eta = 70\%$ equation (1) becomes:

$$P = 6.87 \times Q \times H_n \text{ (kW)} \tag{2}$$

Specific speed

The four basic most significant parameters of hydro turbine operation as listed above are summed up in by a sole parameter. This parameter is often referred to as dimensionless parameter called specific speed (N_s) (Michele 2013, Gummer 2011, Cesar 1983):

$$N_s = \frac{N\sqrt{Q}}{H_n^{\frac{3}{4}}} \tag{3}$$

Although defined and called dimensionless by most authors, the value really depends on the parameters and units of

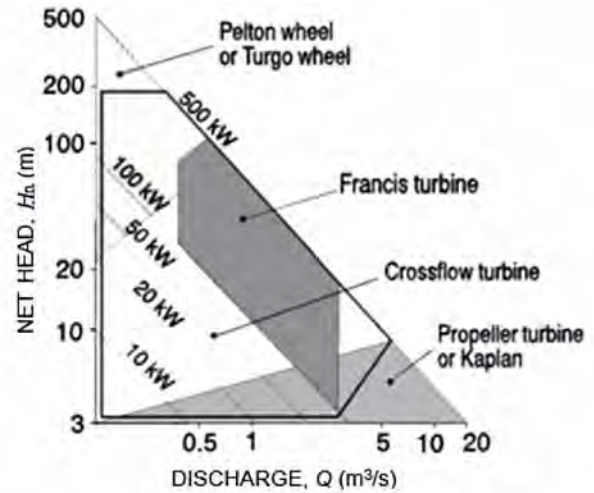


Figure 2: Flow rate and head for selection of small hydro turbines (Paish 2002).

measurement used. It is also being defined in terms of power and expressed as (Michele 2013, Cesar 1983):

$$N'_s = \frac{N\sqrt{P}}{H_n^{\frac{5}{4}}} \tag{4}$$

where N = turbine speed (rpm); H_n = net head (metres); Q = flow rate (m^3/s); and P = turbine power (kW). The expression with flow rate is preferred for the calculation of specific speed.

Turbines with identical geometric proportions have a specific speed (N_s), irrespective of their sizes (Celso 1998, Hofer and Gale 2011). The fundamental concept of N_s is to ascertain the optimal working conditions for a particular turbine design. Other useful dimensionless parameters that are often used to describe the flow rate, speed of rotation, turbine size and hydraulic head are (Michele 2013):

$$v = N \frac{D}{\sqrt{H}} \tag{5}$$

$$q = \frac{Q}{D^2\sqrt{H}} \tag{6}$$

The parameters are important to relate the performance of geometrically similar turbines, and are related to the specific speed:

$$v\sqrt{q} = N \frac{\sqrt{Q}}{H^{\frac{3}{4}}} = N_s \tag{7}$$

$$k = \omega \frac{\sqrt{Q}}{(gH)^{\frac{3}{4}}} \tag{8}$$

The specific speed is a criterion that determines the selection of turbine type and dimension. After determination of turbine speed (N), the gear box ratio and the generator type can be selected. Table 1 presents a summary of reference values of N_s for dissimilar hydraulic turbines.

Then the turbine speed in rpm can be determined as:

$$N = \frac{60\omega}{2\pi} \tag{9}$$

where ω = speed of the turbine in radians.

Recasting these expressions using units of radians:

$$\Omega_s = \frac{\omega\sqrt{Q}}{(gH)^{3/4}} \tag{10}$$

$$\Omega_{sp} = n \frac{\sqrt{(P_m/\rho)}}{(gH)^{5/4}} \tag{11}$$

where Ω_s = specific speed; Ω_{sp} = power specific speed and; ω = turbine speed with units radians/unit time.

The values of specific and power specific speeds are not dependent on turbine size but on turbine technology type as shown in Figure 3 (Bryan 2012).

Global hydraulic numbers and turbine parameters

The characteristics of the turbine and operational conditions are usually defined by three key dimensionless parameters; flow coefficient or discharge number (Φ), energy coefficient or head number (Ψ) and power coefficient (Γ) (Giosio 2015).

For a given head H_n , flow rate Q , specific energy E and angular velocity ω the following performance parameters can be defined Hofler and Gale 2011, Giosio 2015, Antonio et al. 2008:

Flow coefficient or discharge number, Φ :

$$\Phi = \frac{Q}{ND_t^3} \tag{12}$$

Energy coefficient or head number,

$$\Psi: \Psi = \frac{gH}{N^2D_t^2} = \frac{E}{N^2D_t^2} \tag{13}$$

Power coefficient, Γ :

$$\text{Specific diameter } \vartheta_e; \vartheta_e = \frac{\Psi_e^{0.25}}{\Phi_e^{0.5}} = \frac{\pi^{0.5}D_tE^{0.25}}{2^{0.75}Q^{0.5}} \tag{15}$$

$$\text{Torque number } \tau; \tau_e = \frac{2\Gamma}{\pi\rho\omega^2r_t^5} = \tau_e = \varphi_e\Psi_e\eta \tag{16}$$

$$\text{Efficiency } \eta; \eta = \frac{\tau_e}{\lambda_e} \tag{19}$$

$$\lambda_e = \varphi_e\Psi_e \tag{17}$$

$$\text{Velocity coefficient } v; v = \frac{\varphi_e^{0.5}}{\Psi_e^{0.75}} \tag{18}$$

where ρ = fluid density; r_t = radius of the blade tip; D_t = diameter of the blade tip and; T = blade torque.

Table 1: A summary of reference values of N_s for the types of hydraulic turbines (Michele 2013).

Type of turbine	N_s	Type of turbine	N_s
Pelton 1 jet	5–10	Francis (“medium”)	33–55
Pelton 2 jets	7–14	Francis (“fast”)	55–80
Pelton (>2 jets)	14–20	Francis (“ultrafast”)	80–120
Francis (“slow”)	15–33	Propeller, Kaplan	75–300

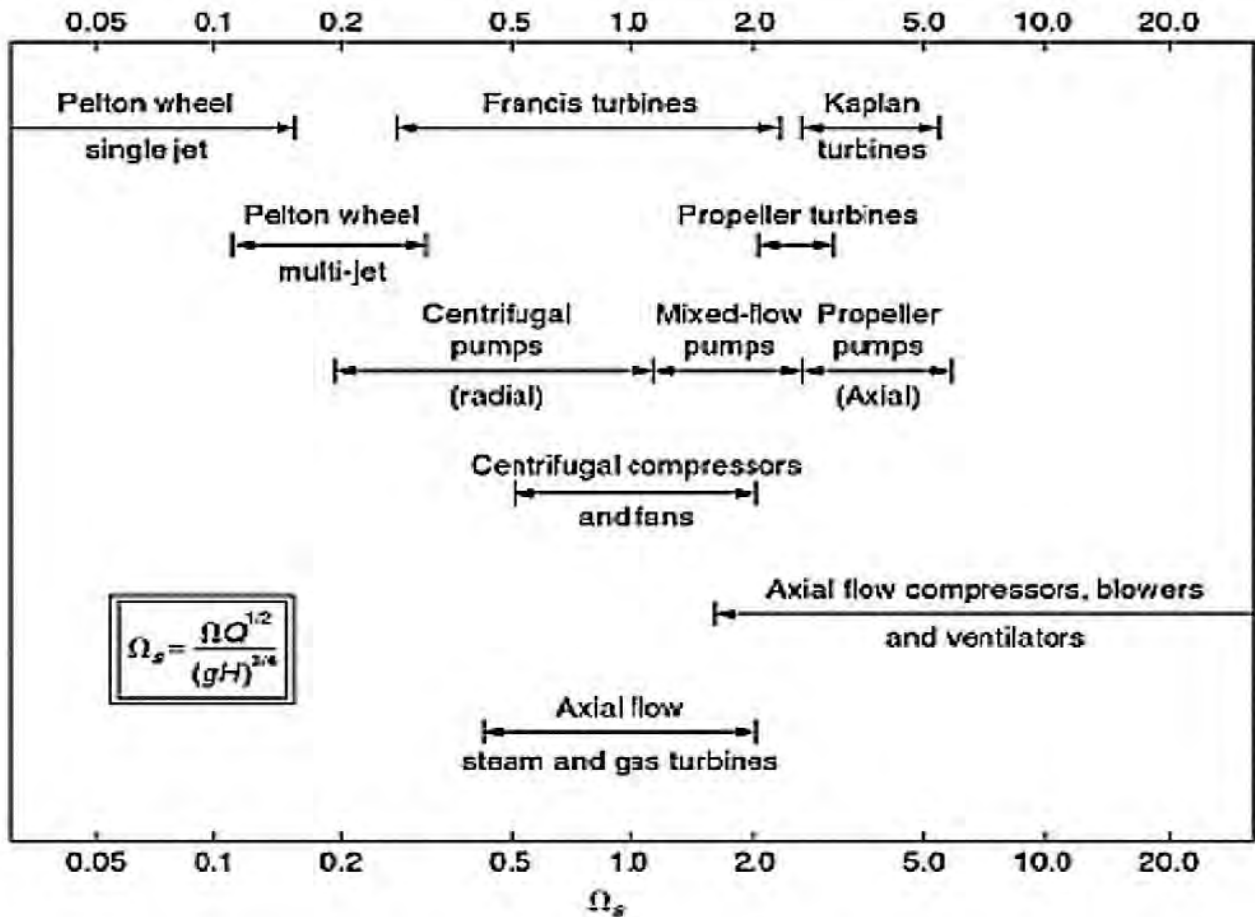


Figure 3: Specific speeds for different turbine technology (Dixon and Hall 2010)

The blade

The blade is the part that converts the water flow velocity into momentum that gives the torque that turns the generator. The blade is made up of the following features: blade angles, hub and tip diameter, curvature, twist and spacing.

The flow has both axial and tangential velocity components and angle of flow relative to the blade called blade angle (β) moving with tangential velocity ($r\omega$) defined by (Simon 1991):

$$\tan\beta = \frac{V_{axial}}{r\omega - V_{tan}} \tag{19}$$

$$V_{axial} = \frac{Q}{A} = \frac{4Q}{\pi(D_t^2 - D_h^2)} = \frac{Q}{\pi(r_t^2 - r_h^2)} \tag{20}$$

where A = area; Q = flow rate and; r_t = blade radius; r_h - hub radius; D_t = blade diameter; and D_h = hub diameter.

Equating power of turbine to change in momentum:

$$\eta\rho gHQ = \rho Q\Delta V_{tan} \tag{21}$$

assuming $V_{tan} = 0$ at the tail edge i.e. zero outlet swirl/tangential velocity, then, leading edge, $V_{tan} = \Delta V_{tan}$ then equation (8) becomes;

$$V_{tan} = \frac{\rho gH}{r\omega} \tag{22}$$

$$K_{ug} = \frac{r_t\omega}{\sqrt{2gH}} \tag{23}$$

$$\text{Round, } C_{round} \cdot C_{round} = \frac{D_t}{\sqrt{P}} \tag{24}$$

where r_t = radius of the blade tip and; D_t = diameter of the blade tip.

The force on the blade

The two velocity components on the turbine blade caused by the flow, tangential and axial velocities, produce corresponding force components on the blade, i.e. tangential and axial forces. The tangential force is responsible for the torque on the turbine shaft while the axial force makes the turbine shaft experience axial load (Simon 1991). The estimated axial load on the hub and the bodies is calculated using the expression of the total head pressure difference acting on the turbine:

$$F_{axial} = pA = \rho gH\pi\frac{D_t^2}{4} \tag{25}$$

assuming it acts over the entire hub and blade area.

There is always head lost and this affects effective head, usually less than the total head. This means that equation (27) was over-estimated. Therefore, the effective head will be taken as ηH . The effective axial force assumed to be acting across becomes:

$$F_{axial} = \eta\rho gH\pi\frac{D_t^2}{4} \tag{26}$$

Figure 1 is an adapted graph designed by Bohl (1991) centred on efficient Kaplan turbine can be used to determine hub-to-tip diameter ratio, K_{ug} , the tip-to-head velocity ratio (D_h/D_t) and the number of blades (Bohl 1991). The ratio of tip velocity and head velocity is an important parameter in sizing of a turbine. The ratio K_{ug} :

$$K_{ug} = \frac{r_t\omega}{\sqrt{2gH}} \tag{27}$$

where r_t = the blade tip radius; ω = the angular velocity of the turbine runner (rad/s) and; K_{ug} can be derived from the graph in Figure 4 based on the specific speed (Simpson and Williams 2011).

Figure 5 is an adapted graph designed by Bohl (1991) centred on efficient Kaplan turbine can be used to determine hub-to-tip diameter ratio, K_{ug} , the tip-to-head velocity ratio (D_h/D_t) and the number of blades (Bohl 1991).

where D_h – hub diameter; D_t – turbine blade tip diameter and; r_t – blade tip diameter

$$K_{ug} = \frac{r_t\omega}{\sqrt{2gH}} \tag{28}$$

$$\text{from equation (30): } r_t = \frac{K_{ug}\sqrt{2gH}}{\omega} \tag{29}$$

where ϕ_r = central angle shown in Figure 4(b).

Calculation: Pico Kaplan/propeller turbine

The four most significant parameters

Hydrological data

Head (H_n) = 2.5 m

Flow rate (Q) = 0.183 m³/s

Rotational speed (N) = 1000 rpm

Efficiency (η) = 60%

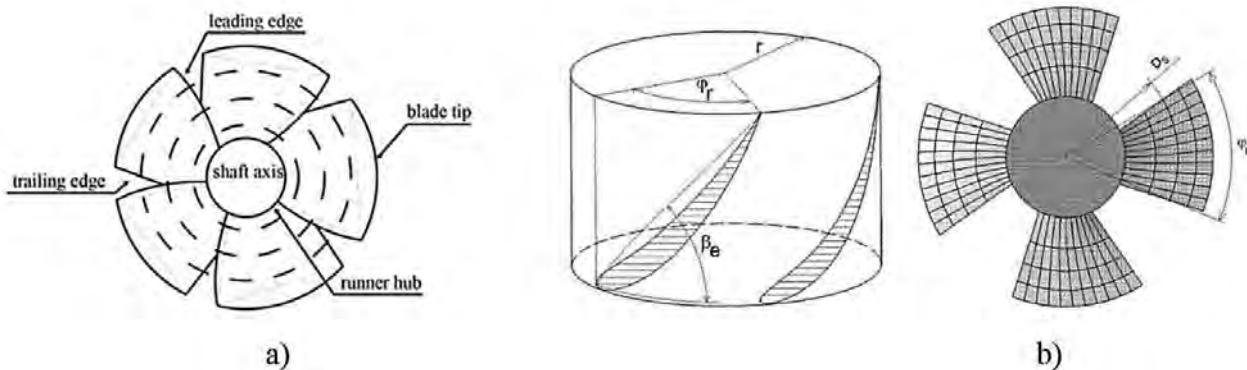


Figure 4: a) Configuration of the runner blade (Byeon and Kim 2013), b) View of the cylindrical blade sections

Downloaded by [UNIVERSITY OF KWAZULU-NATAL], [Williams Ebhota] at 02:08 01 June 2016

Turbine selection

Figures 2 and 5 were used in the selection of turbine type and number of turbines respectively. A propeller hydro turbine with four blades was considered suitable; the green lines in the Figure 5 refer. Table 2 shows the parameters required to define the nominal conditions of a hydro

turbine propeller. From Table 2, $N_s = 208$ and using this in Figure 5 (refer to the green lines):

Number of blade, $z = 4$; $\frac{D_h}{D_t} = 0.35$ and; $K_{ug} = 1.7$

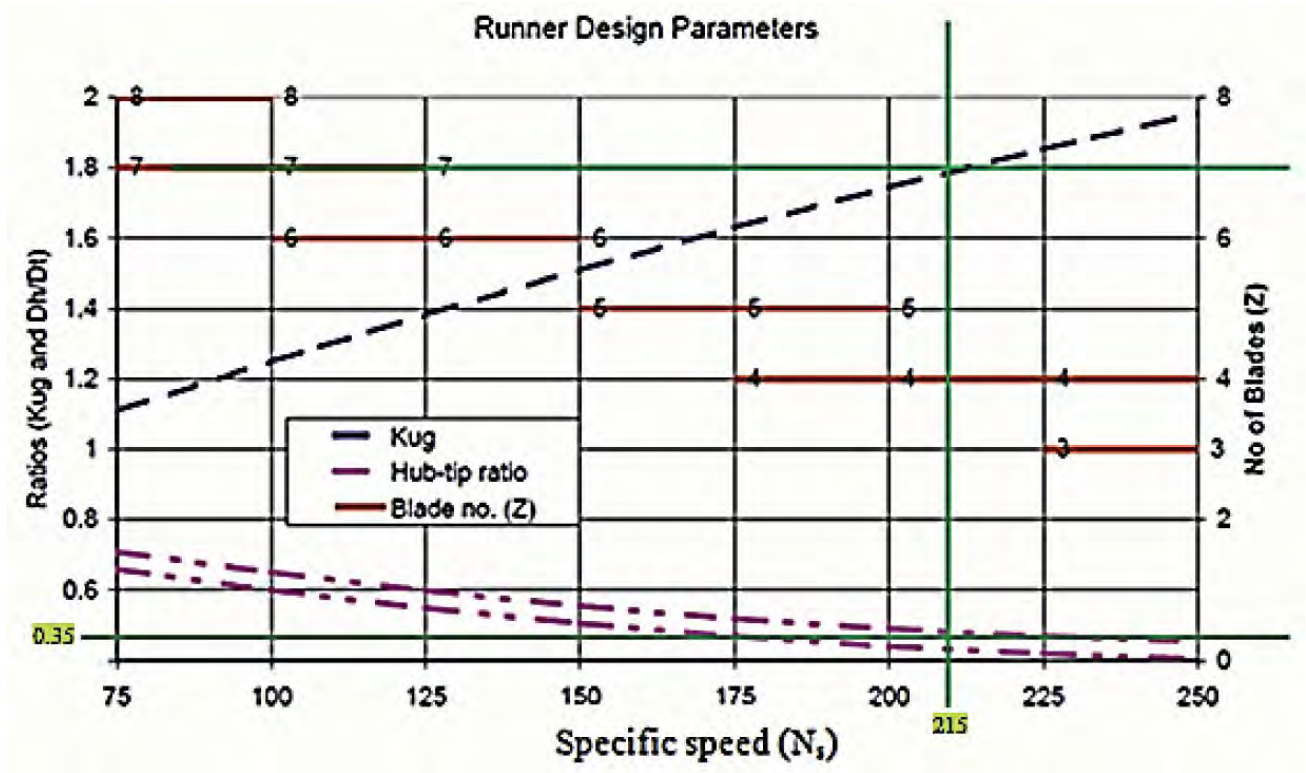


Figure 5: Number of blades functions chart (Michal 2013)

Table 2: Nominal conditions for the turbine design (Figure 5 refers)

S/N Step	Relevant equations	Input numerical value input	Answer
1 Turbine capacity, P	$P = 5.89 \times Q \times H$	$P = 5.89 \times 5.89 \times 2.5$	2.69 kW
2 Specific speed, N_s	$N_s = \frac{N \times \sqrt{Q}}{H^{0.75}}$	$N_s = \frac{1000 \times \sqrt{0.183}}{2.5^{0.75}}$	215
3 Velocity, u	$u = K_{ug} \sqrt{2gH}$	$u = 1.7 \times \sqrt{2 \times 9.81 \times 2.5}$	11.91 m/s
4 The angular velocity of the turbine runner, ω	$\omega = \frac{2\pi N}{60}$	$\omega = \frac{2 \times \pi \times 1000}{60}$	105 rad/s
5 The blade tip radius, r_t	$r_t = \frac{K_{ug} \sqrt{2gH}}{\omega}$	$r_t = \frac{1.7 \times \sqrt{2 \times 9.81 \times 2.5}}{105}$	0.113 m
6 The blade tip diameter, D_t	$D_t = 2r_t$	$D_t = 2 \times 0.113$	0.227 m
7 The hub diameter, D_h	$\frac{D_h}{D_t} = 0.35$	$D_h = 0.35 \times 0.226$	0.080 m
8 Cross sectional area, A	$A = \frac{\pi}{4}(D_t^2 - D_h^2)$	$A = \frac{\pi}{4} \times (0.226^2 - 0.079^2)$	0.035 m ²
9 Axial velocity, V_{axial}	$V_{axial} = \frac{4Q}{\pi(D_t^2 - D_h^2)}$	$V_{axial} = \frac{4 \times 0.183}{\pi \times (0.226^2 - 0.079^2)}$	5.20 m/s
10 Flow coefficient, Φ	$\Phi = \frac{Q}{ND_t^3}$	$\Phi = \frac{0.183}{1000 \times 0.226^3}$	0.0159
11 Power coefficient, Γ	$\Gamma = \frac{P}{\rho N^3 D_t^5}$	$\Gamma = \frac{2.69}{10^3 \times 1000^3 \times 0.226^5}$	4.6×10^{-9}
12 Energy coefficient, Ψ :	$\Psi = \frac{gH}{N^2 D_t^2}$	$\Psi = \frac{9.81 \times 2.5}{1000^2 \times 0.226^2}$	4.8×10^{-4}
13 Axial force on the blade, F_{axial}	$F_{axial} = \rho g H_n \pi \frac{D_t^2}{4}$	$F_{axial} = 1000 \times 9.81 \times 2.5 \times \pi \times \frac{0.227^2}{4}$	996 N

Dimensionless performance parameters

Three dimensionless performance parameters, flow coefficient (Φ), power coefficient (z) and energy coefficient (Ψ) were computed in Table 3 to establish their relation with operating parameters. The computation was done at constant head, H (3 m) and rotational speed, N (500 rpm).

Figures 6 and 7 represent dimensionless flow coefficient and power coefficient, both at constant rotational speed, respectively.

Blade model and simulation: Static analysis – Effects of axial force

The computer-aided design software, AutoCAD, was used for the drafting and dimensioning while Solidworks was used for the simulation to determine a suitable thickness. A 3 mm blade thickness gave satisfactory results and the propeller blade model is shown in Table 4 and Figure 8.

Material selection

As noted in the introduction, the level of manufacturing systems in sub-Saharan Africa is still too low to support the fabrication of some complex parts in terms of shape, composition, availability and the difficulty in working on certain materials. Presently, the best blade manufacturing process is fabrication or casting from stainless steel materials such as SS(16Cr5Ni), SS(13Cr4Ni) and SS(13Cr1Ni) (IEC 1991, Priyabrata et al. 2013). The foundries in the region cannot provide these materials adequately, or are unable to work on such materials and the costs are also an issue. The quest for alternative materials is vital to increase electricity access in the region. The blades need to be designed for strength, toughness, hardness and corrosion, cavitation-resistant and density. In this study, aluminum alloy, 6010-T6,

was considered, based on aluminum availability, cost and manufacturing facilities in sub-Saharan Africa. The properties of aluminum alloy, 6010-T6 are given in Table 4.

A summary of the simulation mesh results is contained in Table 5. The material selected for the blade is Aluminum 6010-T6 alloy and this choice was based on aluminum availability, cost and the level of manufacture infrastructure in the region.

Study results

The highest stress $5.037 \text{ e} + 005 \text{ N/m}^2$ was obtained at nodal point number 11063, as shown in Figure 9 and Table 6, which is a point in the fillet between the blade and hub. Aluminum 6010-T6 has a yield strength of $2.75 \text{ e} + 008 \text{ N/m}^2$, which exceeds the highest stress recorded. This validates the design as failure free.

The lowest factor of safety was noticed at nodal number 11603, as shown Figure 10, which is the point where the highest stress was measured.

Conclusion

The study presents the use of a SHP scheme as a viable method to increase access to electricity in sub-Saharan Africa and the sequential design steps of hydro turbine were discussed. Simplified mathematical expressions required for low head pico hydro turbine design were tabulated and used to calculate nominal operating parameters of a propeller turbine.

The study is of the view that:

- i. Small hydro power (SHP) technology should be popularised for rural areas, industrial estates and standalone electrification provision rather than the national grid.

Table 3: Dimensionless performance parameters

P (kW)	Q (m ³ /s)	N_s	K_{ug}	z	r_t (m)	D_t (m)	D_h (m)	Φ	Ψ	Γ
2	0.2	98	0.012	7	0.090	0.18	0.0630	0.0686	3.60×10^{-3}	0.0423
4	0.3	120	0.011	6	0.083	0.166	0.0581	0.1336	4.30×10^{-3}	0.1269
6	0.4	139	0.010	6	0.075	0.150	0.0525	0.237	5.20×10^{-3}	0.3160
8	0.5	156	0.009	5	0.068	0.136	0.0476	0.4064	6.40×10^{-3}	0.6878
10	0.6	170	0.008	4	0.060	0.120	0.0420	0.4877	8.20×10^{-3}	1.6075

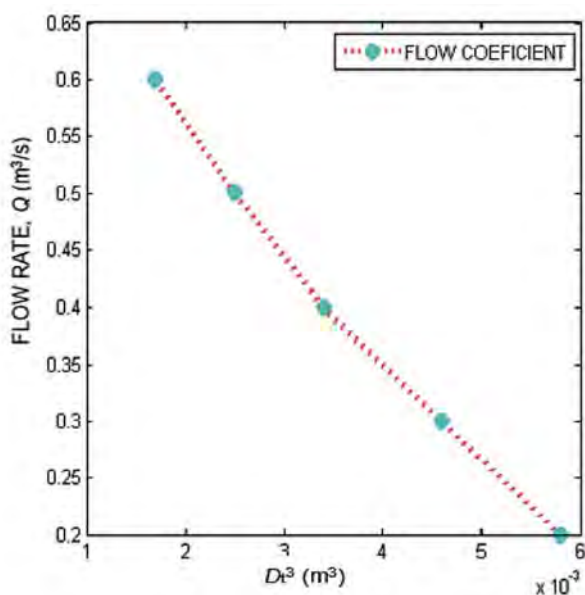


Figure 6: Plot of tip diameter against flow rate

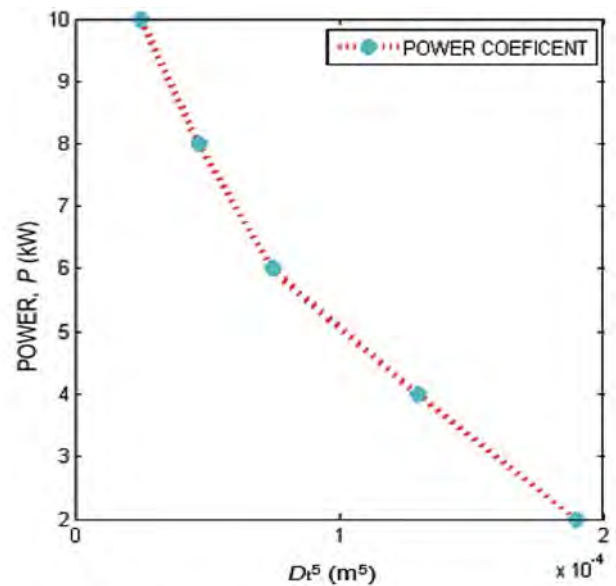


Figure 7: Plot of tip diameter against power


Downloaded by [UNIVERSITY OF KWAZULU-NATAL], [Williams Ebhota] at 02:08 01 June 2016

- ii. To boost power sustainability, countries of sub-Saharan Africa need to build human and infrastructure capacities that will support the local manufacturing of SHP plants and components in the region.
- iii. Increase in local contents in the manufacture of SHP equipment will reduce the cost of power projects as against the present cost situation.
- iv. The ability to design and manufacture will fix operation, maintenance and availability problems and jobs will be created.

The study found that a four-blade propeller with an outer diameter of 0.226 m and a hub diameter of 0.079 m was appropriate for a low head hydro turbine of 2.61 kW.

Simulation revealed that aluminum alloy 6010-6T shows good performance in terms of strength and density. However, the studied observed that hardness needs to be enhanced and suggests that reinforcement material should be introduced to the alloy matrix to form a composite.

Table 4: Material properties

Model reference	Properties	Volumetric properties
	Name: 6061-T6 (SS)	Mass: 1.12596 kg
	Model type: Linear elastic isotropic	Volume: 0.000417024 m ³
	Default failure criterion: Unknown	Density: 2700 kg/m ³
	Yield strength: 2.75 × 10 ⁸ N/m ²	Weight: 11.0345 N
	Tensile strength: 3.1 × 10 ⁸ N/m ²	
	Elastic modulus: 6.9 × 10 ¹⁰ N/m ²	
	Poisson's ratio: 0.33	
	Mass density: 2700 kg/m ³	
	Shear modulus: 2.6 × 10 ¹⁰ N/m ²	
	Thermal expansion coefficient: 2.4 × 10 ⁻⁵ /Kelvin	

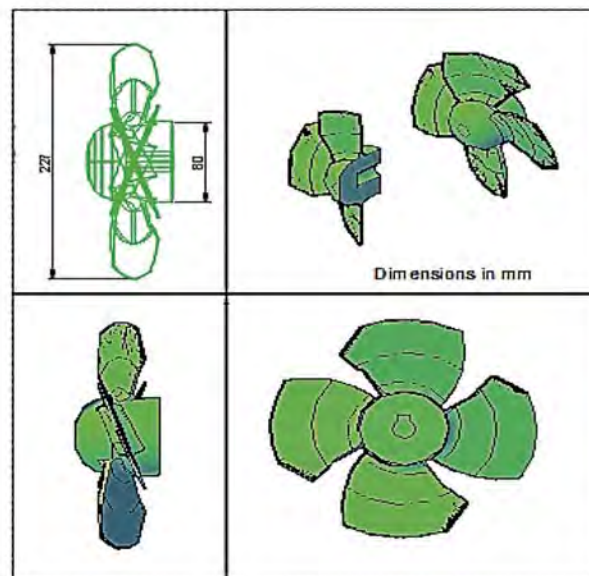


Figure 8: The blade model

Table 5: Mesh information


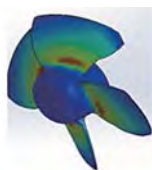
Mesh type	Solid mesh	Total nodes	17 339	
Mesher used	Standard mesh	Total elements	10 141	
Automatic transition	Off	Maximum aspect ratio	35.476	
Include mesh auto loops	Off	% of elements with aspect ratio < 3	78.5	
Jacobian points	4 Points	% of elements with aspect ratio > 10	2.04	
Element size	7.47305 mm	% of distorted elements (Jacobian)	0	
Tolerance	0.373652 mm	Time to complete mesh (hh:mm:ss)	00:00:03	
Mesh quality	High			

Table 6: Von Mises stress

Name	Type	Min	Max	
Stress	VON: von Mises stress	13 804.1 N/m ²	4.941 × 10 ⁷ N/m ²	
		Nodes: 12 293	Node: 1141	
Displacement	URES: Resultant displacement	0 mm	0.00763475 mm	
		Nodes: 107	Node: 687	
Strain	ESTRN: Equivalent strain	2.28658 × 10 ⁻⁹	3.37997 × 10 ⁻⁶	
		Elements: 4 201	Elements: 6 732	

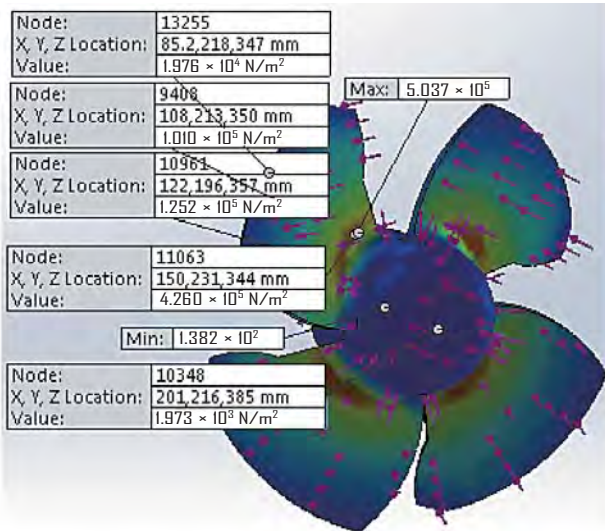


Figure 9: Von Mises nodal stress

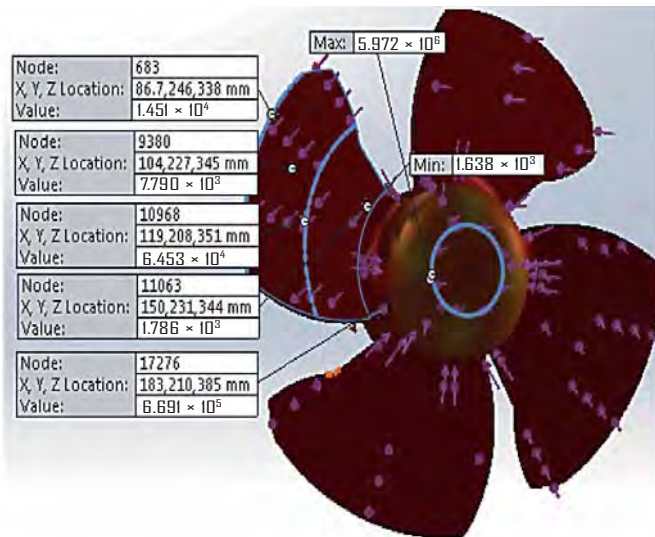
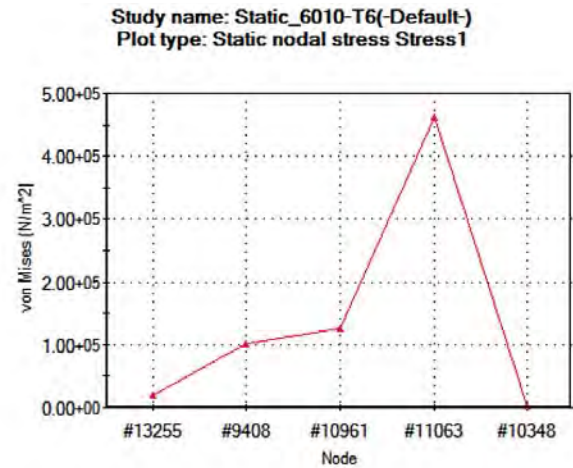
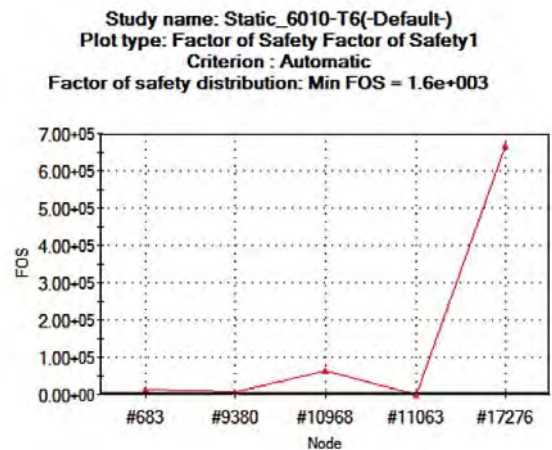


Figure 10: Depiction of factors of safety



Acknowledgement

The authors hereby acknowledge the Centre for Engineering Postgraduate Studies (CEPS)/HVDC/Smart grid Centre of the University of KwaZulu-Natal.

References

Arriaga, M. 2010. "Pump as turbine – A pico-hydro alternative in Lao People’s Democratic Republic." *Renewable Energy* 35 (5): 1109–1115. doi:10.1016/j.renene.2009.08.022.

BHA (British Hydropower Association) 2006. *A guide to UK mini hydro developments*. London: BHA.

Bohl, W. 1991. *Strömungsmaschinen 2: Berechnung und kalkulation*. Würzburg: Vogel Business Media.

Bryan, P. H.-Y. 2011. "Tesla turbine for pico hydro applications." *Guelph Engineering Journal* 4: 1–8.

Byeon, S.-S., and Y.-J. Kim. 2013. "Influence of blade number on the flow characteristics in the vertical axis propeller hydro turbine." *International Journal of Fluid Machinery and Systems* 6 (3): 144–51. doi:10.5293/IJFMS.2013.6.3.144.

Celso, P. 1998. *Layman’s guidebook on how to develop a small hydro site*, 2nd ed. Belgium: The European Small Hydropower Association (ESHA).

Cesar, F., A. Javier, C. Nicholas, and S. G. John. 1983. *Hydromechanics of variable speed turbines*. St. Anthony Falls Hydraulic Laboratory, University of Minnesota.

Cordeiro, J. L. 2014. *Energy 2020: A Vision of the Future*. Washington, DC: IEA and US Department of Energy.

Da Cruz, A. G. B., A. L. A. Mesquita, and C. J. C. Blanco. 2008. "Minimum pressure coefficient criterion applied in axial-flow hydraulic turbines." *Journal of the Brazilian Society of Mechanical Sciences and Engineering* 3. doi:10.1590/S1678-58782008000100005.

Dixon, S. L., and C. A. Hall. 2010. *Fluid mechanics and thermodynamics of turbomachinery*, 6th ed. Amsterdam: Butterworth-Heinemann.

Ebhota, W. S., A. C. Eloka-Eboka, and F. I. Inambao, "Energy sustainability through domestication of energy technologies in third world countries in Africa." Paper presented at the Industrial and Commercial Use of Energy (ICUE), 2014 International Conference on the Energy efficiency in buildings, Cape Town, 2014. 10.1109/ICUE.2014.6904197.

Ehsan, M. M., G. O. Enaiyat, F. S. Kazy, and S. M. Ferdous. 2012. "A novel approach of electrification of the high rise buildings at Dhaka City during load shedding hours." *International Journal of Renewable Energy Research* 2: 123–130.

ESH Association. 2010. "Energy recovery in existing infrastructures with small hydropower plants." Paper presented at the Sixth Framework Programme, Mhylab, Switzerland.

- Etiosa, U., A. Matthew, E. Agharese, O. G. Ogbemudia, P. U. Osaze, and G. O. Ose. 2009. *Energy Efficiency Survey in Nigeria – A Guide for Development Policy and Legislation*. <http://www.credcentre.org/Publications/EE%20Survey%20Nigeria.pdf>
- Giosio, D. R., A. D. Henderson, J. M. Walker, P. A. Brandner, J. E. Sargison, and P. Gautam. 2015. "Design and performance evaluation of a pump-as-turbine micro-hydro test facility with incorporated inlet flow control." *Renewable Energy* 78:1–6. doi:10.1016/j.renene.2014.12.027.
- Gummer, J. H. 2011. *Hydraulic turbines*. Thermopedia. doi:10.1615/AtoZ.h.hydraulic_turbines.
- Höfler, E., J. Gale, and A. Bergant. 2011. "Hydraulic design and analysis of the Saxo-type vertical axial turbine," *Transactions of the Canadian Society for Mechanical Engineering* 35 (1): 2011.
- IEA. 2014. *Factsheet: Energy in sub-Saharan Africa today*. International Energy Agency. Paris, France: World Energy Outlook.
- IEC (International Electrotechnical Commission). 1991. "Field acceptance tests to determine the hydraulic performance of hydraulic turbines, storage pumps and pump-turbines." Geneva: IEC.
- Michal, V., B. Tomas, and H. Peter. 2013. "Methodology of 3D hydraulic design of impeller of axial turbo machine." *Engineering Mechanics* 20 (2): 107–118.
- Michele, M. 2013. *Hydraulic turbines and hydroelectric power plants*. *Energy Systems course lecture notes*. Department of Industrial Engineering, University of Rome.
- Paish, O. 2002. "Small hydro power: Technology and current status. Renewable and sustainable." *Energy Reviews* 6:537–56.
- Priyabrata, A., K. R. Pankaj, and M. Asis. 2013. "Selection of hydro-turbine blade material: Application of fuzzy logic (MCDA)." *International Journal of Engineering Research and Applications* 3: 426–430.
- Simon, A. F. 1991. "A simplified low head propeller turbine for micro hydroelectric power." Master of Engineering thesis, University of Canterbury.
- Simpson, R., and A. Williams, 2006. "Application of computational fluid dynamics to the design of pico propeller turbines." In *Proceedings of the International Conference on Renewable Energy for Developing Countries*. Washington DC: University of the District of Columbia.
- Simpson, R., and A. Williams. 2011. *Design of propeller turbines for pico hydro*. Available: www.picohydro.org.uk
- Weerapon, N., and T. Sirivit. 2009. "Flow simulations on blades of hydro turbine." *International Journal of Renewable Energy Research* 4: 61–66.
- Zainuddin, H., M. S. Yahaya, J. M. Lazi, M. F. M. Basar, and Z. Ibrahim. 2009. "Design and development of pico-hydro generation system for energy storage using consuming water distributed to houses." *World Academy of Science, Engineering and Technology* 35: 154–159.

CHAPTER 4: PRINCIPLES AND BASELINE KNOWLEDGE OF FUNCTIONALLY GRADED ALUMINIUM MATRIX MATERIALS (FGAMMS): FABRICATION AND APPLICATIONS

W. S. Ebhota and F. L. Inambao, "Principles and baseline knowledge of functionally graded aluminium matrix materials (FGAMMs): fabrication techniques and applications," *International Journal of Engineering Research in Africa*, 2016, Vol. 26, pp 47-67. DOI:10.4028/www.scientific.net/JERA.26.47 (*Published*).

Principles and Baseline Knowledge of Functionally Graded Aluminium Matrix Materials (FGAMMs): Fabrication Techniques and Applications

Ebhota Williams S.^{1, a}, Akhil S. Karun^{2, b} and Inambao, Freddie L.^{3, c}

^{1,3}Discipline of Mechanical Engineering, Howard College, University of KwaZulu-Natal, Durban, South Africa.

²Materials Science and Technology Division, CSIR-National Institute for Interdisciplinary

^aEmail: willymoon2001@yahoo.com, ^bEmail: akhilskarun@gmail.com,

^cEmail: inambaof@ukzn.ac.za

Keywords: FGMs, fabrication techniques, aluminium matrix and ceramics reinforcements, squeeze casting, infiltration process, compocasting, centrifugal casting, stir casting, material prototyping

Abstract. This paper discusses the main Functionally Graded Materials (FGMs) and their bulk fabrication techniques, their development, principles and applications. The fabrication processes considered include powder metallurgy (PM), sintering, squeeze casting, infiltration process, compocasting, centrifugal casting, stir casting, material prototyping. The paper provides an overview of the FGM processing parameters including reinforcement particles size and volume %, temperature, pressure (for PM), and stirrer and mould rotational speeds (for stir and centrifugal casting processes respectively). The paper notes that the FGMs are widely used in the following sectors: automotive, medical, aerospace, aviation, nuclear energy, renewable energy, chemical, engineering, optics electronics etc.

Introduction

This paper focuses on the concept of bulk functionally graded materials (FGMs) production technologies of aluminium alloys and composites, their processing parameters and applications. This study reviews the past and present status of major bulk FGMs production techniques. The aim is to identify simple and cheap methods of production that can enhance the mechanical properties of aluminium alloys for hydro turbine blade production. Aluminium deposits are vast in sub-Saharan Africa and their alloys can be sourced locally. Hydropower technologies can help in tackling the perennial power problems in the region.

Functionally Graded Material (FGM) is a group of composite materials that have exceptional properties due to exploitation of the individual properties of the constituent materials. The materials are characterised by gradual transitions in material composition and microstructure in a specific direction [1, 2]. The possibility of manipulating the constituent materials of a FGM to meet functional requirements, makes this group of materials unique [3]. However, this class of advanced materials also occur in nature. Materials such as bone, teeth etc. are examples of FGMs that occur in nature [1]. Fig. 1 shows the path of modern materials, starting from base natural materials to FGM. The concept of FGM was modelled from nature in the quest to solving engineering problems [4].

Pure metals have little significance in engineering applications due to their deficiencies related to functional requirements. Quite often the requirements are conflicting and this occurrence makes most material in their natural form less valuable from an engineering point of view. For instance, a part may require hardness and ductility to function properly in a given working environment. It is more or less impossible to have such a material existing naturally. In this kind of situation, two different materials may be combined with each having one of the required properties. The combined materials could be metal and metal, metal and non-metal or non-metal and non-metal, and during merging they may be in the same state or not. The properties of the parent material are the summation of the properties of the different materials that are combined. Table 1 shows various forms of material combination that can be made, and their limitations [5].

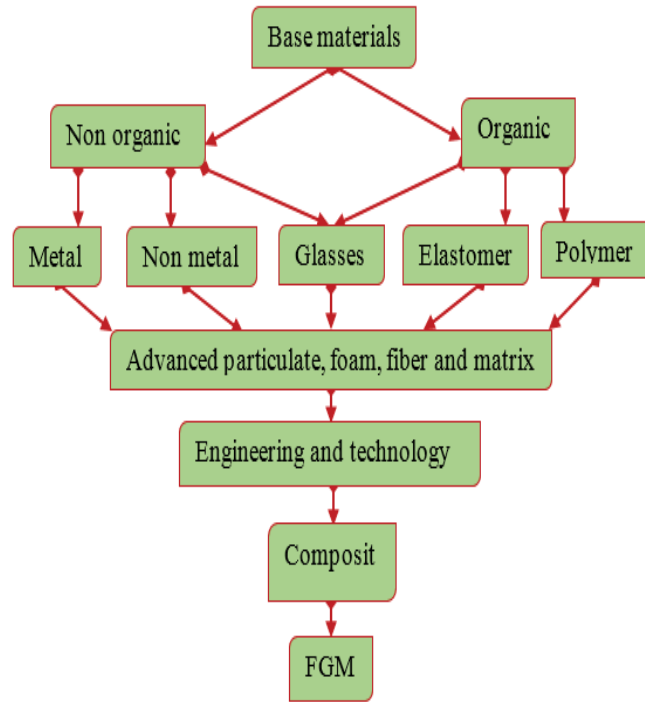


Figure 1: Order of modern material pattern as regards to FGM

Table 1: Production of engineering materials by materials combination [5].

Method	Combination of Materials	Limitation
Alloying	Molten state	Thermodynamic equilibrium limit (limit to which a material can dissolve in another material)
Powder metallurgy	Powder	Intricate shapes and features, porosity and strength,
Composite	Solid	Delamination (separation of fibres from the matrix at extreme working condition). This can happen for example, in high temperature application where two metals with different coefficient of expansion are used

FGMs have properties that are functions of location in the material as represented by Fig. 2. These properties include chemical composition, microstructure, and atomic arrangement.

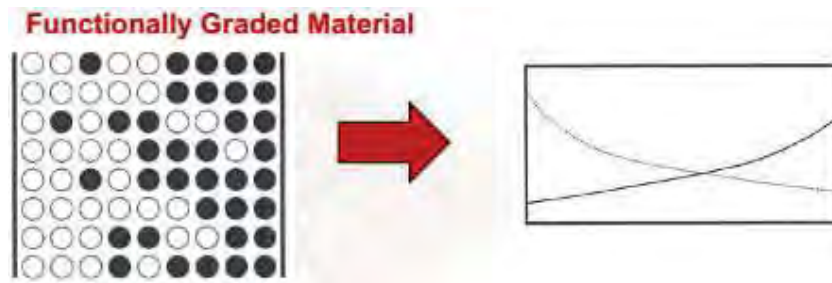


Figure 2: Functionally Graded Materials.

This group (FGM) of engineering materials evolved from composite materials. Composite materials belong to advanced engineering materials which are usually formed by two or more different materials in solid forms. These different materials that form composite material have individual chemical and physical properties. Composite materials offer better properties in combined form than the materials in their individual state. However, composite materials fail in certain harsh working conditions such as high temperature. These harsh conditions cause the fibres

to disintegrate from the matrix and this failure process is called delamination [4, 6]. Functionally graded materials can be divided into two broad groups namely [2, 5]:

- i. **Thin FGM** - Thin FGMs are relatively thin sections or thin surface coating, produced by physical or chemical vapour deposition (PVD/CVD), plasma spraying, self-propagating high temperature synthesis (SHS) etc.
- ii. **Bulk FGM** - Bulk FGMs are produced using powder metallurgy technique, centrifugal casting method, solid freeform technology etc.

Historical Background

Evolution of FGMs. The FGMs were initially introduced as a class of advanced composite materials with a single continuous or discontinuous inclination in terms of microstructure and composition as shown in Fig. 3 [7, 8]. The FGM chemical and physical properties change trend is 3-dimensional [9]. Although, several theoretical works were carried out and reported on FGMs in the 1970s, the influence of these studies was not great due to inadequate and suitable manufacturing techniques. The development of present day FGMs started in 1972 in relation to the study of composites and polymeric materials when Bever and Duwez investigated the properties of global material and re-examined the potential use of graded composites [10, 11].

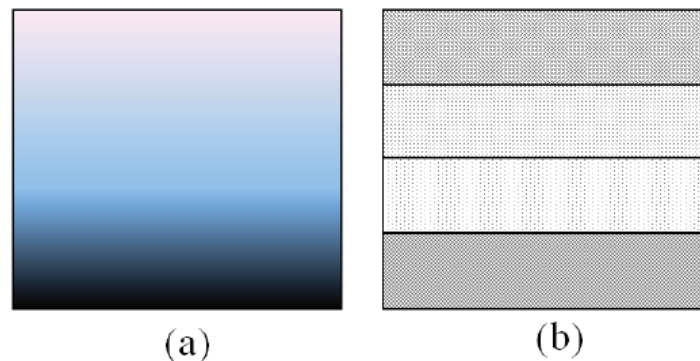


Figure 3: Type of FGM structure: (a) continuous and (b) discontinuous [12].

Shen and Bever submitted that variation of the chemical pattern of monomers, supramolecular structure or morphology and the molecular constitution of the polymers may influence the gradation of polymeric material. In this study, the material properties of chemical, mechanical, biomedical and transport and their applications were discussed. However, the study did not consider design, production and appraisal of the gradient of the structure [10]. The evolution of modern day FGMs started in the mid-1980s when Japanese engineers' encountered difficulty in finding a material for a particular barrier in a hypersonic space plane project. The thermal working condition requirements for the barrier were 1000 K inside temperature and 2000 K outside temperature with a thickness less than 10 mm. This material necessity pushed the engineers to come up with FGM [13]. The first national symposium on FGMs was held in Sendai, Japan in 1990 [14].

FGM technology was a popular programme from 1987 to 1991 in Japan and numerous production techniques were advanced for FGMs processing. These initial manufacturing processes include chemical vapour deposition, self-propagating high temperature synthesis (SHS) self-propagating, plasma spraying, powder metallurgy and self-propagating high temperature synthesis (SHS) and galvanofarming. From 1991 to the present many new techniques have been developed and used. FGMs fabrication methods have been categorised differently by authors. In 1999, Miyamoto et al. classified the manufacturing processes into four main categories; melt, layer, preform and bulk processes as shown in Fig. 4 [15]. The delamination problem that is associated with composite materials was eliminated in FGMs. The sharp interfaces that are mainly responsible for the failure in composites were substituted with gradient interfaces resulting in smooth transition between the materials in contact [4, 16]. In 1985, the application of continuous texture control was

introduced. This was to enhance binding strength and reduce the thermal stress present in ceramic coatings and joints being prepared for recycling in rocket engines [13].

The FGMs concept spread to Europe and it has become a popular manufacturing process in Germany. A transregional Collaborative Research Centre (SFB Transregio) was established in 2006, funded and mandated to exploit the potentials of thermomechanically coupled manufactured graded monomaterials such as aluminum, steel and polypropylene [17].

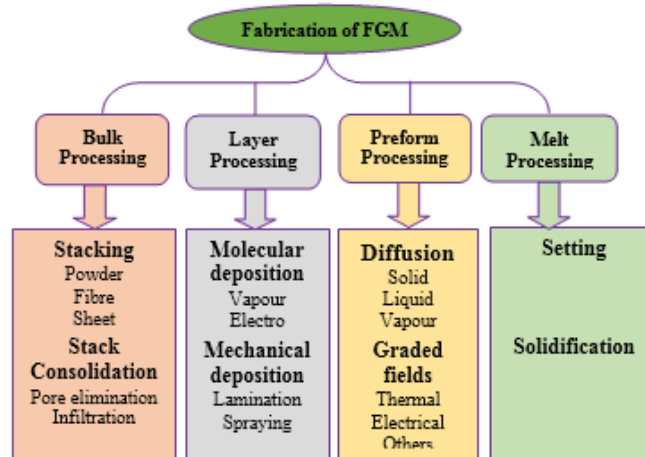


Figure 4: Classification of FGMs fabrication methods

Functional graded aluminium alloy matrix composites (FGAAMCs), Concepts and their Fabrication Techniques

The combination of aluminium alloy and ceramic material processed by certain techniques such as squeeze and centrifugal casting processes form functional graded aluminium alloy matrix composites (FGAAMCs). The industrial application of FGMs is increasing rapidly in automotive, aircraft and aerospace [18-20]. This interest is orchestrated by the possibility of determining the chemical and physical properties through manoeuvring of microstructure. It is possible in the FGM manufacturing process to have a material with high wear resistance at a high temperature. For example, this can be achieved by reinforcing the matrix with adequate distribution of ceramic material along the mass of the part with the required bulk toughness kept intact [21]. Many investigative works have been performed on FGMs using aluminium matrix alloys and ceramic as reinforced materials. Examples of metal matrix materials are aluminum, brass, bronze, titanium and magnesium. Regarding reinforcements, the most common used are nitrides (BN, ZrN, TiN), carbides (SiC, TiC, ZrC), borides (ZrB₂, TiB₂, SiB₂), oxides (Al₂O₃, MgO, TiO₂, ZrO₂), silicides (MoSi₂) and fine particles of various intermetallics (Fe₃Al, FeAl, NiAl, Ni₃Al, Ti₃Al, TiAl) [22]. FGMCs of Al/SiC_p have shown a lot of potential as engineering materials and have attracted material scientists and engineers. Since the Japanese engineers' breakthrough in the hypersonic space plane project in the 1980s till now, researchers have been investigating different aspects of FGMs, from characterisation of FGMs to their production techniques and applications.

There are various methods of manufacturing FGMs and an overview is presented in Table 2. These methods are physical and chemical in form. The method to be applied depends on the type of the materials, available manufacturing equipment for FGMs and potential application [23]. The methods of FGMs production have witnessed tremendous development in the past two decades. This dynamism has led to the emergence of several attractive engineering materials with striking properties that have been applied in different sectors such as automotive and aviation sectors. The production methods are broadly categorised into as follows [9]:

Constructive process – this process involves total automation of the management of the compositional gradient through piling of more than one set up material selectively until a stratum of layer formation is created. This method allows for a large layer.

Transport based process – This process is suitable for cases where movement of materials is based on natural occurrence to form microstructural and compositional gradients during manufacturing of FGMs. The dynamism in FGMs manufacturing technologies is rapid and the classification is presented in Table 2.

Table 2: FGM fabrication methods and their applications [24-27].

Method	Type	Group of FGM
Vapour deposition technique	Chemical vapour deposition (CVD) and physical vapour deposition (PVD)	Thin surface coating
Powder metallurgy (PM)	<i>Stepwise Compositional Control</i> : powder stacking, sheet lamination and wet powder spraying <i>Continuous Composition Control</i> : Centrifugal Powder forming (CPF), impeller dry blending, centrifugal sedimentation, electrophoretic deposition and pressure filtration / vacuum slip casting	Bulk
Melting processes	Centrifugal casting, sedimentation casting infiltration processing thermal spray processing	Bulk
Material prototyping/solid freeform (SFF) Fabrication	Laser based processes: laser cladding, melting, laser sintering, selective 3D-printing and selective laser	Bulk
Other methods	plasma spraying, electrodeposition, electrophoretic, ion beam assisted deposition (IBAD), self-propagating high-temperature synthesis (SHS)	Thin coating

Powder Metallurgy (PM). Powder metallurgy (PM) is a metal manufacturing process that makes semi-finished or finished components from mixed or alloyed powders. This process involves the following steps: production of powder metal, metalloids, metal alloys or compounds; blending and mixing of powders, compaction; sintering; and, in some cases, repeating the operation [9, 28, 29]. PM, therefore, is the production and exploitation of metal powders. Particles whose size is less than 100 nm (1 mm) are referred to as powder [30]. Metal powders' attributes depend on the following parameters: particle shape and size, particle size distribution, compressibility, apparent density, and flow rate. PM is known to be cost effective in the production of complex-shaped components as it minimises the application of secondary operations such as machining.

Notwithstanding the exceptional qualities of PM processes, porosity, production of parts with complex shape and features, and high strength are challenges [31]. There are pores in almost all of the PM parts and this has both advantages and disadvantages. One of the advantages is being able to produce self-lubricating bearings. The pores that are linked to the surface are impregnated with oil. However, the presence of voids in a part has serious effects on the thermal, mechanical, magnetic, physical, wear, and corrosion behaviour of that part [30]. The design engineer is always interested in material's elastic constants such as Young's modulus (E), shear modulus (G), and Poisson's ratio (ν). PM elastic constants are related by equation (1):

$$E = 2G(1 + \nu) \quad (1)$$

Beiss shows a relation between density (ρ) and Young's modulus (E) in equation (2):

$$E = E_o \left(\frac{\rho}{\rho_o} \right)^m \quad (2)$$

Where E_o is the pore-free material Young's modulus, and ρ_o is the pore-free material density and m is the exponent which is pore dependent, and ranges from 2.5 and 4.5.

Also, the PM materials mechanical properties are a function of the density [32, 33].

$$\frac{P}{P_o} = \left(\frac{\rho}{\rho_o} \right)^m \quad (3)$$

Where, P is the interest property, P_o is the pore-free material value, ρ is the material density, ρ_o is the pore-free material density, and m is an exponent the value of which depends on a given property.

PM is a technology that has a wide diversity in the manufacturing of automobile parts. In 2015 the Metal Powder Industries Federation (MPIF) PM received an award for excellence in design [34]. Some of the outstanding works listed in the award are: carrier and one-way rocker clutch assembly by GKN Sinter Metals; sector gear and fixed ring by Cloyes Gear & Products Inc.; variable valve timing (VVT) rotor adaptor assembly by GKN Sinter Metals; helical gear and spur pinion by Capstan Atlantic; powder metallurgy aluminum camshaft-bearing cap by Metal Powder Products Co., etc. Powder metallurgy is one of the key methods in the fabrication of functionally graded aluminium alloy and its composites, and several academic and industrial researches have been performed on this methodology.

Cylindrical specimens of iron powder-based graded products made from Distaloy SE powder having regions with varied carbon content, sintered by two methods, were investigated [35]. The sintering methods used are pressureless sintering and pressure-aided sintering, called Spark Plasma Sintering (SPS). Arising from this study, it was observed that:

- i. Sintering by means of the SPS technique produced slightly lower shrinkage compared to conventional sintering.
- ii. Microstructural studies of the manufactured products showed similar morphology of pores, with minor consequence of sintering techniques and parameters on pore size distribution.
- iii. The SPS sintered products showed an increased number of large pores, compared to the conventional method.
- iv. The SPS method cooling rate influenced the formation of numerous areas with bainitic structure causing an increase in outer layer hardness.

Investigative work was performed on the production of AlSi alloy with carbon nanotubes (CNTs) reinforcement for the purpose of obtaining FGM for engine piston ring applications.^[36] Wear and fatigue have been cited as the major cause of piston ring failure. FGMs fabricated by the PM process was seen as a solution to this problem, but existing manufacturing methods could only build cylinder specimens with limited gradients [37, 38] as cited by [36]. To address these limitations, new equipment was developed and then used to obtain an optimised AlSi-CNTs FGM for this purpose. This equipment permits the formation of varied continuous powder distribution along a given side of the sample. Various mechanical tests were carried out and discussed and including ultimate tensile and yield strengths, fatigue limit performance, tensile strain, and wear resistance tests. The results show that [36]: hot-pressing technique is good for the fabrication of AlSi-CNT FGM; the piston rings show varied gradient, about 2 wt.% of CNTs on the inner surface, 0 wt.% of CNTs in middle and 2 wt.% of CNTs on the outer surface of piston ring; AlSi-CNT FGMs provide better mechanical performance compared to AlSi unreinforced alloy; and, considering cost effectiveness, CNTs 2 wt.% gradient outer surfaces was considered best for piston ring material.

Sintering Process. Sintering is a PM consolidation process which is carried out alongside with the compaction process of FGM using hot pressing. Examples of sintering methods are spark plasma sintering (SPS), high frequency induction heating and electric furnace heating. The SPS sintering method was used in the production of HAP/Ti FGM and it was useful in stress relaxation of FGM [39]. Porosity is a measure of sintering effectiveness and sintering models have been created and analysed. Other factors that influence the behaviour of FGM fabricated by sintering methods are time, sintering atmosphere, temperature, and the isostatic condensation [40]. A study

on porosity using a sintered nickel/alumina (Ni/Al₂O₃) FGM revealed that porosity is directly related to the rate of shrinkage. Further, the study shows that a porosity reduction model is used to: check quality of particle-reinforced metal-ceramic FGM and predict changes in porosity reduction in particle dispersion development of FGMs [41, 42].

PM methods are continuously undergoing appraisal and modification for cost effectiveness, quality and suitability. According to Kieback et al. PM includes sedimentation, plasma spraying, electrophoretic deposition, slip casting, powder stacking, etc. as current FGMs manufacturing methods [37]. However, some of these methods produce sharp interfaces which lead to thermal expansion mismatch and residual thermal stresses. An example of such a PM method is sequential slip casting [43], but Po-Hua used sedimentation and vibration to scale up the production of aluminum and high-density polyethylene (Al-HDPE) FGMs to avoid thermal expansion mismatch and residual thermal stresses [44].

Squeeze Casting. Ghomashchi and Vikhrov in a review study categorised four basic steps in squeeze casting fabrication of FGMs: pouring of a calculated molten metal into the mould; closing the mould, pressure application; and, cast ejection [45]. However, there are other fundamental processes that are essential for quality squeeze casting. Other steps in the squeeze casting process of aluminium matrix FGM production include melting a specified metal, degassing, preheating of mould, pouring, and pressing. Regarding ceramic-metal functionally graded composite fabrication, further steps are particles preheating, addition of particles to the molten metal and stirring of the mixture.

The squeeze casting method produces finished or nearly finished castings with minor post production processes so as a result is considered to be a near net-shape manufacturing route. The pressure on the metal is released after solidification is completed. The applied pressure in squeeze casting enhances the bonding force between the matrix and the reinforcement, the wettability and solidification rate [46, 47]. Applying Clausius-Capeyron's expression in equation (4) to a metalostatic pressure as high as 200 MPa increases the melting point of the metal [48]. Epanchistov stated that the eutectic point in the A-Si structure changes to a higher silicon content.^[49]

$$\frac{\Delta T_f}{\Delta P} = T_f \frac{(V_l - V_s)}{\Delta H_f} \quad (4)$$

Where T_f = equilibrium freezing temperature; V_l and V_s = specific volumes of the liquid and solid, respectively; and ΔH_f = latent heat of fusion. A rough estimate of the effect of pressure can be determined by considering the liquid metal as an ideal gas and replacing the thermodynamic volume equation to have equation (5):

$$P = P_o \exp\left(\frac{-\Delta H_f}{RT_f}\right) \quad (5)$$

Where P_o , ΔH_f and R = constants.

Numerous research studies have been conducted in different parts of the world on aluminium and magnesium related metal matrix composites (MMCs) fabricated by the squeeze casting method. Over 700 journal articles published on MMCs research was reported in 2000 [45, 50]. The annual growth of the application of squeeze casting in aerospace, automotive, sport and leisure was put at 12 ± 15 % [51].

Infiltration Method. Infiltration is the process of metal matrix composites (MMCs) fabrication by means of ejecting a molten metal at a high pressure into a porous preform. Infiltration involves two stages: initiation of flow depicted by the dynamic wetting angle, and advancing the flow in the capillaries of the preform. The infiltration pressure threshold, P_0 , according to capillary law is [52]:

$$P_0 = 6\lambda\gamma_{lv} \cos\theta \left(\frac{V_p}{(1-V_p)D} \right) \quad (6)$$

Where θ is the contact angle; λ is the geometry depended factor; γ_{lv} is the tension of liquid-vapour surface; D is the mean diameter; and V_p is the volume fraction of the particulates.

The combination of squeeze casting and infiltration involves preform. The fabrication of a preform has these basic steps: liquid powder processing, pressing and shaping and sintering of the preform. The principle behind preform is the blending of a ceramic powder slurry with a sacrificial organic pore forming agent (PFA) that is pyrolysable. The mixture is then pressed and heat treated to pyrolyse the PFA to form preform pores. Preform processing parameters include a pore forming agent (PFA), green sintering temperature and green pressing pressure. Cellulose particles (PC) and carbon fibres (PF) are examples of PFAs. Table 3 shows some PFAs and their sintering temperature.

Table 3: Sintering temperatures for different preform formation [53, 54]

Ceramics	Pore forming additives	Sintering temperature (°C)
AO	PF	1500
AO	PC	1600
Al ₂ O ₃	Glassy frit binder (AG)	1000

The study of the behaviour of FGMs characterised by pure aluminium reinforced with Al₂O₃ (50 % volume) and B₄C particles with an average diameter of 30 µm was conducted. The composites were fabricated by pressure gas infiltration. The study observed that during monotonic loading, the composite materials measured 25 % elongation to failure; the ultimate tensile strengths recorded were 120 MPa and 200 MPa for Al-Al₂O₃ and Al-B₄C composites respectively; the tensile failure of Al-Al₂O₃ was due to particle fracture while matrix porosity was responsible for the failure in Al-B₄C. Degradation of Young modulus, and density decrease were used to measure the internal damage propagation. In another experiment, ceramic preforms with the same porosity level were produced by sintering of RA-207LS Al₂O₃ powder [55]. The preforms' porosity were based on polymer matrix cellular structure. Two types of pressure sources were used: pressure-vacuum infiltration (T = 720 °C, p = 15 MPa, t = 15 min), and gas-pressure infiltration (GPI) in an autoclave (T = 700 °C, p=4 MPa, t = 5 min). The study concluded that: ceramic-metal composites with interpenetrating of phases resulted from the two infiltration methods; GPI provided a higher degree of infiltration; and, better composites were obtained from preforms with the smallest pores. The flow of metal within the preforms depends on capillary size; the pressure variation along the capillary length; the metal liquid state preserving time within the capillary; and, the alloy viscosity dynamic. The study added that the composites produced by the GPI method are characterised by compressive strength, higher hardness, and an increase in Young's modulus. Fig. 5 shows the GPI set up.

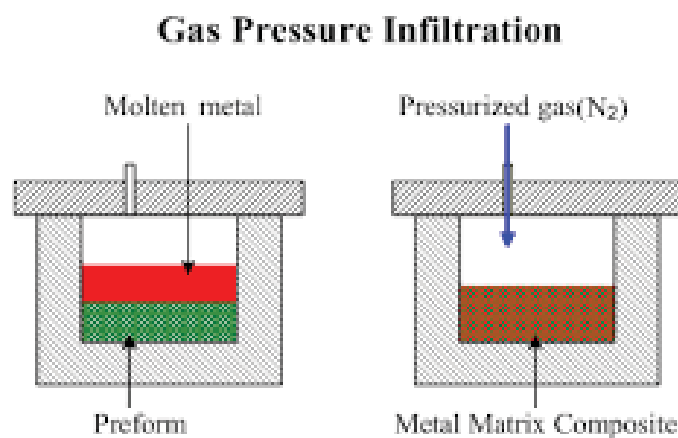


Figure 5: Schematic of GPI set up

Centrifugal casting. The fabrication of FGMs by the centrifugal casting technique involves the filling of a spinning mould and the cast is allow to solidify before rotation is stopped [20, 56]. The rotation creates centrifugal force that pushes the molten metal against the wall of the mould to produce the desired shape. This technique was first used by Dimitri Sensaud DeLavaud, a Brazilian

in 1918 [56]. The method is used in the casting of metal such as functionally graded materials (FGMs), alloy steels, corrosion- and heat-resistant steels, aluminum alloys, copper alloys, etc. It also used in the production of non-metal such as ceramics, plastics, glasses, and practically every material that can be melted into liquid or slurries. In centrifugal casting of hypereutectic alloys such as A390-5%Mg, the outer periphery will be a fibrous form of silicon. The large primary silicon and large α -aluminum dendrites will migrate to the inner region since they have almost the same density. In the case of particles and slurry, the particles will migrate to the outer region. For a slurry-slurry system, the heavier slurry with the higher density will move towards the mould wall. The magnitude of the segregation depends on the speed of rotation. The force generated equation and other common basic expression in centrifugal casting process is as follows:

The angular velocity, ω ;

$$\omega = \frac{v}{r} = \frac{2\pi N}{60} \quad (7)$$

Centrifugal force, F_c , acting on the particle of mass m at distance r ;

$$F_c = m\omega^2 r = m \frac{4\pi^2 N^2}{3600} \quad (8)$$

The ratio of centrifugal force to gravitational force, G , can be simplified as;

$$G = \frac{F_c}{F_g} = \frac{r\omega^2}{g} = \frac{r}{g} \left(\frac{2\pi N}{60} \right)^2 \quad (9)$$

Thornton recommends 50 G to 100 G range of speed for metal mould and 25 G to 50 G range of speed for sand cast mould. Speeds that are too high can cause hot tears to outside surfaces and excessive stresses [57]. The magnitude of centrifugal force possessed by particles in a molten metal depend on the density and size of the particles. The denser and larger particles migrate to the mould wall. The Stokes equation is used to explain this process for spherical shaped particles as in equation (10).

$$v = \frac{d^2 (\rho_p - \rho_l) g}{18\mu} \quad (10)$$

Where v is the particle velocity; d is the diameter of the particle; ρ_p is the particle density; ρ_l is the molten metal density; g is the gravitation force; and, μ is the viscosity of the molten metal.

The centrifugal method can be categorised in different ways: it can be based on mould arrangement and mould angle inclination to either vertical or horizontal planes [56]; and, it can be according to liquidus temperature of the matrix alloy. There are two types of centrifugal methods of fabrication by liquidus [58]. The ex situ or solid-particle centrifugal method involves temperature below the liquidus temperature of the matrix material and addition of pre-fabrication reinforcement to the liquid matrix metal by infiltration, vortex or casting method; and the centrifugal in situ method which involves temperature above liquidus temperature of the matrix and the reinforcement is precipitated in the matrix melt during cooling and solidification. The in situ method advantages compared to the ex situ technique, namely, good wettability, homogeneous distribution of reinforcement and reinforcement materials, and thermodynamic stability in the matrix alloy [59, 60].

Although many metal-ceramics FGMs have been developed by the centrifugal method, it is still in the development stage because of the inadequate knowledge of particle distribution and control [61]. The significant processing parameters for gradient microstructure control are: mould temperature; crucible temperature; pouring rate; thermal gradient through the mould; velocity of mould rotation; solidification rate etc. Temperature circulation is difficult to estimate during centrifugal casting due to the mould's fast rotation during pour and solidification. A schematic of a vertical centrifugal casting machine is shown in Fig. 6.

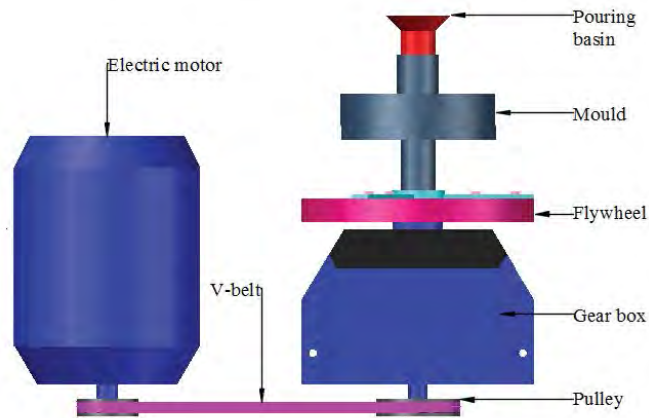


Figure 6: Schematic of a vertical centrifugal casting machine

Presently, the centrifugal casting method is one of the cheapest and simplest FGM fabrication methods. Gravity or centrifugal casting is the most economical to run [61]. The properties of a material depend greatly on its microstructure. Centrifugal process parameters are used to manipulate microstructure formation. Centrifugal technique processing parameters include pouring and mould temperatures, speed of mould rotation, and particle size. The application of this method is vital in the fabrication of disc, ring, and pipe components and as result it has attracted several academic and industrial research grants.

Gomes et al. carried out a comparative analysis between the wear behaviour of Al - SiC_p FGM and homogeneous Al - Si - Mg-20%SiC_p composite [62]. They were subjected to the slide the nodular cast iron (NCI) and the Pin-on disc tests without lubrication using 5N as normal load. The study revealed that Al - SiC_p FGM has lower wear coefficient than that of the homogeneous composite. This was attributed to the effects of SiC particles which serve as load-bearing elements. This shows that the presence of reinforcement particles in the matrix alloy enhances the wear resistance. However, it was demonstrated in other studies that the ratio of the matrix to reinforcement has a threshold that should not be exceeded. Exceeding the threshold can cause severe failure in the FGM matrix/reinforcement interface [63, 64].

Ramadan and Omer in their study produced functionally graded aluminum matrix composite (FGAMC) through the centrifugal casting method. In the FGAMC formation, Boron 1.2 % to 1.85 % by weight was dissolved in molten aluminum at 1400 °C through the addition of AlB₂ flake of 2.71 % to 4.20 % by weight. Centrifugal casting was carried out at 800 °C. It was reported in the results that two dissimilar regions were observed without smooth gradient as shown in Fig. 7, a zone (outer) with AlB₂ surplus and a zone (inner) with AlB₂ deficit. Further, the achievement of 64 % hardness and strength increase through the increase of reinforcement particles at the outer zone was reported [65].

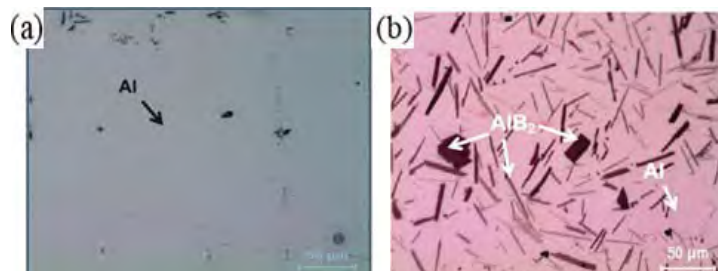


Figure 7: FGMMC Microstructure of AlB₂/Al (a) internal area and (b) external area [65]

Three samples of functionally graded rings were produced from aluminum A390 as a metal matrix alloy using centrifugal casting method by Rahvard et al. The three rings of A390 alloy had different amounts of Magnesium (Mg) of 0 %, 6 % and 12 % of weight Mg respectively. The effects of Mg volume variation on their mechanical and microstructural properties were investigated

in the samples of the metal matrix. This was used to know the particles distribution in the matrix alloy. Also examined was wear resistance by the three ring samples and a comparison analysis was made. It was observed in the work that [66]:

- i. The characteristics of A390 ring reinforced without Mg has the Si particles distributed in both inner and outer areas. This particle arrangement was attributed to the density of the primary Si being lower than that of the metal matrix alloy. This density difference will cause the particles to drift towards the inner region. However, the highest hardness was recorded in the outer region.
- ii. The second sample which is A390 alloy with 6%Mg displayed different particle distribution performance. The density of Mg_2Si is far lower than the aluminum alloy liquid density. The difference in densities causes the Mg_2Si particles to move to the inner region with a higher velocity. Subsequently, a distinctive alteration between the zones is obtained. It was reported that the inner region performed better in terms of hardness and wear resistance.
- iii. The third sample was 12%Mg ring with Mg_2Si as primary Mg_2Si reinforcement. The distribution was observed almost throughout the entire cross-section except for a narrow free reinforcement zone of 2mm thickness. The external layer was reported to possess the best performance for hardness and wear resistance.

The study of processing parameters like G number, caster and casting atmosphere influences on the cooling rate and microstructure formation were examined by Hisashi, Yoshimi and Yuko [67]. Samples of Al-Al₂Cu FGMs were produced through the centrifugal casting method at different casting conditions. The process parameters used were reinforcement volume fraction, pouring and mould temperatures, G number, mould diameter, degassing method, and cooling method. For experimental control and comparative analysis of the vacuum centrifugal casting, gravity casting was explored with the process parameters. Rod-shaped and pipe-shaped Al-Al₂Cu FGMs were produced by two kinds of vacuum centrifugal casters from Al-33mass%Cu eutectic alloy. Also, the distribution of lamellar spacing in the FGMs was evaluated. The study revealed that:

- i. The composition and microstructure in both rod-shaped and pipe-shaped FGMs samples were position dependent in the samples which are defined by production parameters such as cooling rate.
- ii. The samples of FGMs produced under vacuum show a comparatively abrupt profile of distribution of the Al₂Cu volume fraction compared to samples produced under atmospheric gas. This was attributed to cooling rate distribution.
- iii. There was a homogeneous distribution of cooling rate in smaller samples of FGMs compared to the larger samples. It was reported that G number and atmosphere influenced the cooling rate distribution and size of sample.
- iv. It was observed that lamellar spacing is a function of position.

Babu et al. developed analytical theory used for two-dimensional dynamics simulations to engineer metal-ceramic FGM for a preferred composition gradient employing the centrifugal casting technique.^[61] This work modelled the movement of ceramic particles in molten metal under centrifugal force and the combination of effects of solidification. The centrifugal method was used to produce FGM rings from the mixture of aluminum and silicon carbide (SiC) particles. Experimental results were to validate the simulation technique and then recommended for FGM composition gradient.

Material Prototyping or Solid Freeform (SFF) Fabrication Method. The dynamics of Material Prototyping or Solid Freeform (SFF) Fabrication Method method of material fabrication is very fast and has taken the centre stage of FGM production. Its benefits include production of complex shapes, fast production speed, material optimisation, not energy intensive, and fabrication of parts directly from CAD STL file. Five stages are involved in this method: CAD model data generation; CAD model data conversion to Standard Triangulation Language (STL) file; STL slicing into two dimensional cross section profiles; layer by layer deposition of component; and, removal and finishing operations [68, 69]. SFF technologies come in various types used in the fabrication of functionally graded materials. Prototyping technologies are still evolving with poor

surface finish and dimension accuracy challenges and current research efforts are being directed to these challenges.

Stir Casting. Stir casting simply means the blending of the melted matrix and particles before pouring the mixture into the mould as depicted by Fig. 8a. This is an aspect of the casting process that is vital for quality casting of FGAAMCs by melt casting. Stirring is employed to add and disperse the particles into the molten metal and to suspend the particles in the slurry. The introduction of particles into the matrix melt is an important step in FGMMCs fabrication and there are different methods to do this. These methods include: the insertion of particles restrained by inert gas carrier into the melt through injection gun; addition of the particles to the melt stream during pouring; use of a reciprocating piston to push particles into the molten metal; spray of particles along with atomised molten metal into a substrate; vortex method; distribution of particles in the molten metal by centrifugal process, etc. A complete set up of a stir casting facility is shown in Fig. 8b. The vortex method is known to be one of the best approaches to insert particles into the matrix melt, to distribute and suspend the particles in the slurry before it is cast. The stirring is introduced after the matrix has melted and the stirring is made vigorous in order to form a vortex at the surface of the matrix melt. The particles are then added to the matrix through the vortex and stirred for few minutes before the slurry mixture is cast. Stir casting is influenced by certain parameters such as pouring temperature, stirring time, stirrer blade angle, pouring rate, and gating systems [70, 71].

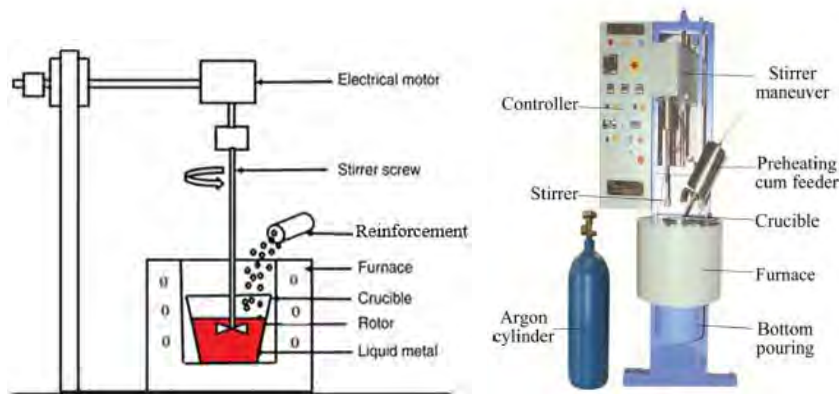


Figure 8: (a) A schematic stir casting set up; (b) a complete stir casting facility [71]

Compcasting. A lot of methods have been proposed and used to improve wettability and some of the methods are use of wettability fluxes and agents, preheating, ceramic coating, and oxidation [72, 73]. However, some of these methods are expensive and add to the production cost. The addition of reinforcement particles to a semi-solid matrix at lower casting temperature is termed slurry casting or compocasting. This modified stir casting method is regarded as an economical technique to enhance wettability [74].

There is always a quest to improve thermal, mechanical and chemical properties of materials to form new materials to meet the present material demands. As a result, many of the production technologies that have been or are in use are undergoing appraisal and new ideas are being added. Compcasting is one the casting technologies that is undergoing review and its investigation and application is expanding. Gladston et al. fabricated AA6061-RHA_p (rice husk ash particle) composite by compocasting technique. The study observed the formation of intergranular dispersion of particles and the improvement of macro hardness and ultimate tensile strength of RHA particles of FGMC [73]. The challenges of homogeneous distribution of SiC_p particles and the non-uniform dispersion of coarse Si fibres in Al-Si alloys cause poor mechanical properties. These setbacks were eliminated by the use of an accumulative roll bonding (ARB) process which operates on the principle of compocasting technique [75]. The ARB schematic is shown in Fig. 9. It was revealed that this process produced a composite with evenly distributed Si and SiC_p particles; finer and spheroidal Si particles; no Si and SiC particles free zone; minimised porosity; and, better matrix-particle bonding. The mechanical attributes of the composite were enhanced.

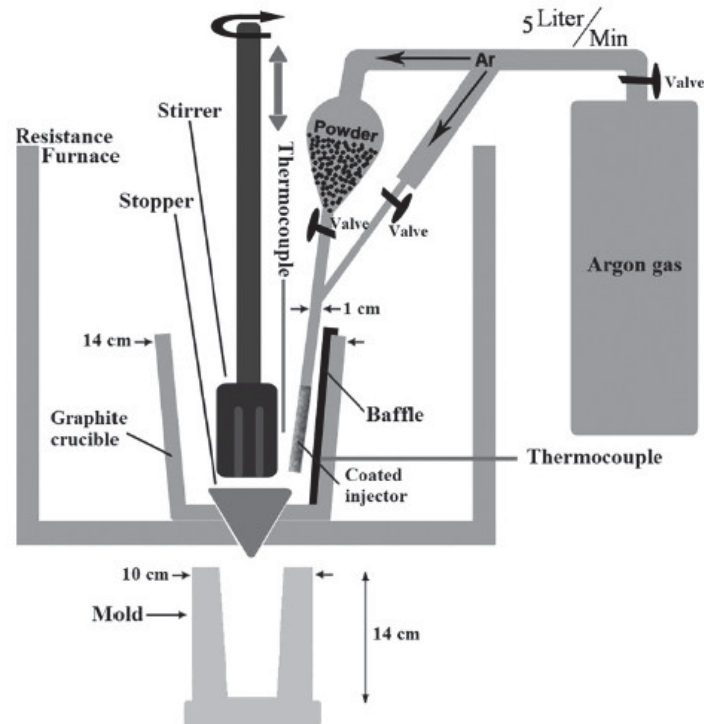


Figure 9: Schematic of ARB set-up [75]

Combination of Methods. Some of these methods are combined for effective production of FGAAMCs. Sintering is a major step in PM and in some cases it is combined with centrifugal the casting process. The stir casting process can also combine with other casting processes such as centrifugal casting, gravity casting and ultrasonic casting. Kunimine et al. combined sintering and centrifugal casting processes to fabricate copper/diamond FGMs for grinding wheels application [76]. The study investigated the influence of fabrication parameters such as casting and sintering temperatures, and the holding time on microstructure of a copper/diamond FGM. The novel FGM production stages are as shown in Fig. 10.

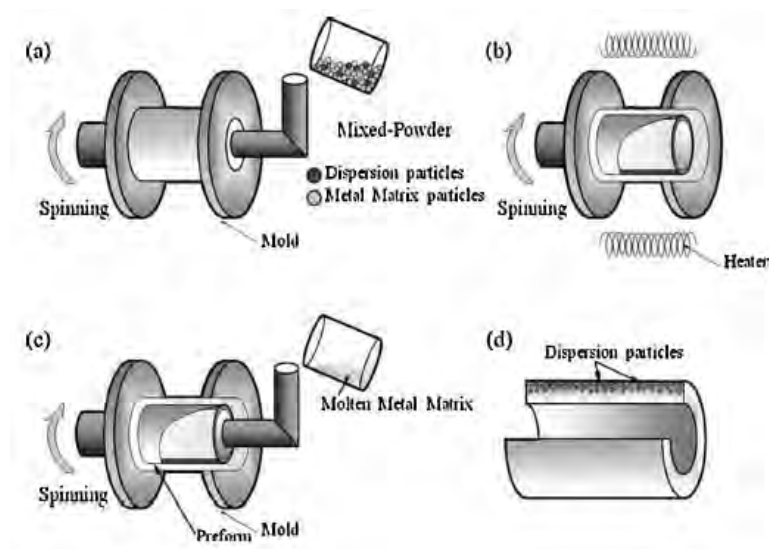


Figure 10: Schematic depiction of centrifugal sintered-casting method [76].

Kunimine et al. study revealed that: preform thickness can be controlled by choosing combinations of sintering holding time and temperature; copper/diamond FGMs were produced under casting temperatures of 1393 K and 1373 K by centrifugal sintered-casting technique and diamond abrasive grain fractions were controlled by processing parameters; the amount of pores in copper/diamond FGMs structure serve as chip spaces and were appropriate for grinding wheels for

machining carbon fibre-reinforced plastic (CFRP) application and gyro-driving grinding wheel systems provided with copper/diamond FGMs grinding wheel drilled on CFRP plate precisely without burring and delamination.

Erdemir et al. combined two techniques, hot press and consolidation method, to fabricate a number of layers of Al₂O₃/SiC FGMs. The study investigated the impact of SiC volume fraction on corrosion and wear resistance behaviour. The formation of FGMs of varied percentage of SiC (30 % to 60%) were used [77]. The study observed that: two layered FGMs with 50 wt.% SiC on outer layer composites showed excellent corrosion resistance in 3.5% NaCl solution; the macrohardness of Al₂O₃/SiC FGM with 40 wt.% SiC was 225 Hv while 30 wt.% SiC measured 170 Hv; increase in SiC content in Al₂O₃/SiC decreases wear rate while increase in the applied load increases wear loss. The study concludes that wear mechanism changes from adhesive wear to abrasive wear due to an increase in SiC particles content.

Effects of wettability and porosity in FGMs

Wettability. The spreading of a liquid around a solid surface is defined as wettability and it relates to the close contact between a solid and a liquid. The manner in which reinforcement particles are wet by melt is a measure of success of particle insertion into the casting in composite production. The addition of reactive elements, such as Zr, Ti, Mg, Ca, etc. to metal matrix stimulates wettability of matrix on particles. Young Dupre's equation describes the bonding force relationship between the matrix and the particles in terms of contact angle (θ) as shown is Fig. 11 as follows [78]: $\theta = 0^\circ$ (Perfect wettability); $\theta = 180^\circ$ (no wetting); $0 < \theta < 180^\circ$ (partial wetting).

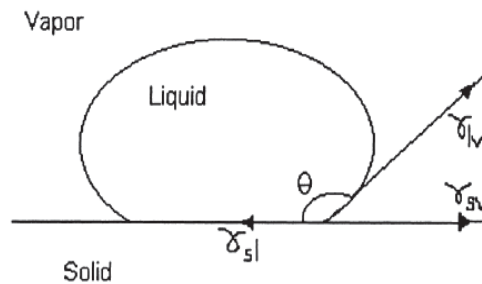


Figure 11: Schematic showing the contact angle between the solid phase and the liquid phase [70]

Where γ_{sv} is the solid–vapour; γ_{sl} is the solid–liquid interfacial energy; and γ_{lv} is the liquid–vapour interfacial energy.

A series of investigation on the influence of stirring casting on microstructure and wettability effects in FGAAMCs carried out by Hashim, Looney and Hashmi in which they carried out a series of wettability tests in aluminium FGAAMCs fabricated by stirring of semi-liquid slurry. A359 alloy, SiC_p and magnesium were used as matrix, reinforcement, and wetting agent respectively [70]. The study had stirring rotational speed, impeller size, holding temperature and stirrer location in the melt as the relevant fabrication processing parameters. A variety of mechanical properties can be achieved through this process by varying these processing parameters. This is because mechanical properties of the FGAAMCs largely depend on the reinforcement type, size, and its distribution pattern, the particles wet level by the matrix, and the quantity of porosity. The technique was described as cost effective, however, this greatly depends on how the production technical challenges are resolved.

The influence of processing parameters (temperature and holding time) on the dispersion of particles in a matrix and the subsequent mechanical behaviours was studied [79]. The matrix and reinforcement used were Al-11Si-Mg and SiC_p (40 μ m) respectively fabricated by stir casting at a constant rotation speed of 450 rpm. The formation of dendrites was conspicuously observed and the particles were evenly distributed in the specimens prepared at 700 °C, 750 °C, and 800 °C. Coupled with no significant pore formation, particle clustering was not seen in the SEM image. However,

significant pores and particles clustering were found in the specimens prepared at 850 °C and 900 °C. This condition was credited to the high viscosity which induces low shearing melt rate.

Abrasive wear property of Al6082-SiC-Gr hybrid composites produced by stir casting was examined and compared with Al6082 alloy and Al6082-SiC composites [80]. The study reported that: Al-SiC-Gr hybrid composites had a better wear resistance performance than Al6082 alloy and Al6082-SiC composites; 16.4 % and 27 % wear enhancement was observed of 200 mm grit size of Al-SiC-Gr composite, as-cast and T6 heat treated respectively when 15N load was applied; 100 mm grit size of Al-SiC-Gr composite, as-cast and T6 heat treated respectively, were found to be 19.6 % and 26.9 % wear resistance improved respectively.

Porosity. In most engineering materials, porosities are regarded as defects and as such material are made dense to minimise porosity and to enhance mechanical properties in FGAAMCs. Porosity formation is caused by air bubbles in a matrix melt, vapour from surfaces of reinforcing particles, gas entrapment and hydrogen evolution, and shrinkage during solidification [81]. Research works have shown that the porosity in a FGMMC is also a function of casting processing parameters. A decrease in the amount of porosity in FGMMC means an increase in the Poisson ratio, damping capacity, Young's modulus of elasticity and tensile and compressive strength. However, there are engineering and biomedical materials where porosity serves a useful purpose. Some of the engineering materials where porosity is useful are filters, catalyst supports and furnace lining bricks [82]. Applications of porous material includes solid oxide fuel cells porous electrodes, and isolating bacteria membranes used in bioreactors [83]. a series of production techniques have been invented and appraised to reduce porosity in cast FGMs and these include: vacuum casting, inert gas bubbling past the liquid metal, casting under pressure, compressing, rolling of material after casting to close the voids, and addition of hexachloroethane to melt.

Applications areas of FGMs

The FGM concept is described as a systematic process of bringing incompatible functions such as thermal, wear and corrosion resistance, toughness and machinability into a single part. This has expanded the application of FGMs in many sectors. Table 4 and Fig. 12 present FGMs application areas.

Table 4: FGMs application areas

Sectors	Applications
Engineering	Cutting tools, machine parts, engine components, etc.
Medical	Biomaterials: implants, artificial skin, drug delivery system
Energy	Thermionic and thermoelectric converters, fuel cells and solar batteries
Aerospace	Space plane nose, combustion chamber protective layer, body components etc.
Automotive	Crown of piston, cylinder liners, exhaust valves and valve seating
Nuclear	First wall of fusion reaction, fuel pellets
Optics	Optical fibre, lens
Chemical plants	Heat exchanger, heat pipe, slurry pump, reaction vessel
Electronics	Graded band semiconductor, substrate, sensor

Two FGMs in commercial status are high performer cutting tools, namely, tungsten carbide/cobalt and a razor blade of iron aluminum/stainless steel (FeAl/SS) FGM [15].

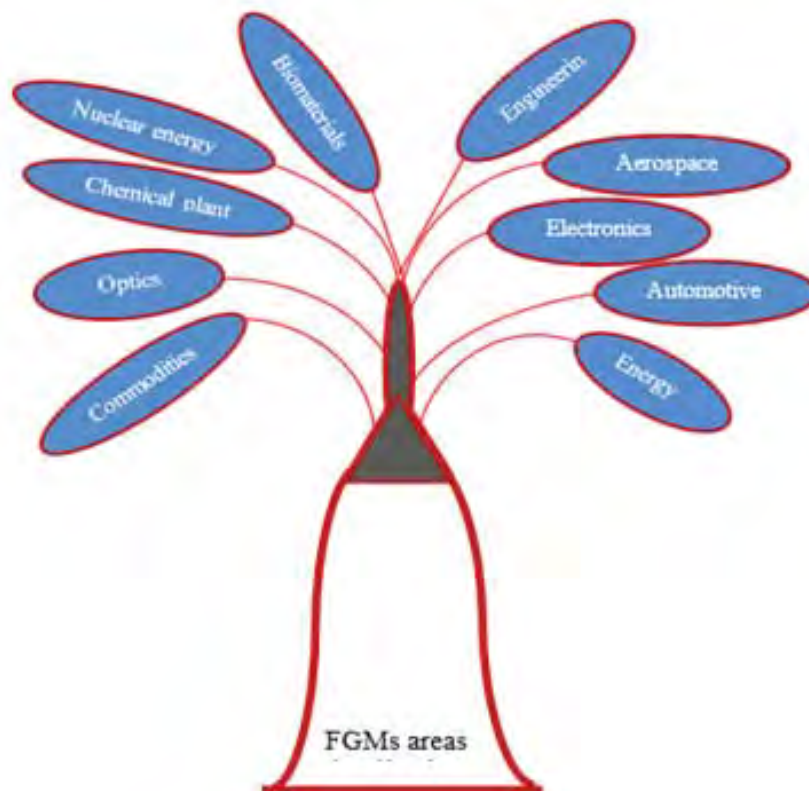


Figure 12: FGMs application areas

Conclusion

This paper presents an overview of the main FGMs bulk production techniques, their evolution, principles and applications. The fabrication processes include PM, sintering, squeeze casting, infiltration process, compocasting, centrifugal casting, stir casting, material prototyping. Despite the rapid development observed in all the techniques considered, challenges still abound in getting the desirable material without certain material attributes being a trade-off. The use of some of these techniques for mass production is challenging from cost of fabrication perspective. However, the combination of methods is seen as the most promising method of evolving new quality FGMs. Several FGAAMCs laboratory investigations have shown that the main processing parameters depends on the type of fabrication method used. However, reinforcement particle size, and casting temperature seem to be general while pressure, mould, and stirrer speed of rotational are for PM, centrifugal and stir castings respectively.

Acknowledgment

The authors hereby acknowledge the Centre for Engineering Postgraduate Studies (CEPS)/HVDC/Smart Grid Centre of the University of KwaZulu-Natal.

References

- [1] K. B. Shailendra, S. Ritesh, and R. M. Prabhat, "Functionally Graded Materials: A Critical Review," *International Journal of Research (IJR)* vol. 1, pp. 289-301, 2014.
- [2] G.E. Knoppers, J.W. Gunnink, J. Van Den Hout, and W. P. V. Vliet, "The Reality of Functionally Graded Material Products " presented at the International Solid Freeform Fabrication Symposium, University of Texas at Austin, Texas, 2004.
- [3] P. Shanmugavel, G. B. Bhaskar, M. Chandrasekaran, P. S. Mani, and S. P. Srinivasan, "An Overview of Fracture Analysis in Functionally Graded Materials," *European Journal of Scientific Research*, vol. 68, pp. 412-439, 2012.
- [4] S. S. Wang, "Fracture Mechanics for Delamination Problems in Composite Materials," *Journal of Composite Materials*, vol. 17, pp. 210-223, 1983.
- [5] M. M. Rasheedat, T. A. Esther, S. Mukul, and P. Sisa, "Functionally Graded Material: An Overview," in *Proceedings of the World Congress on Engineering, WCE*, London, U. K., 2012.
- [6] S. S. Wang and I. Choi, "The Interface Crack Between Dissimilar Anisotropic Composite Materials," *Journal of Applied Mechanics*, vol. 50, pp. 169-178, 1983.
- [7] J. J. Lannutti, "Functionally Graded Materials: Properties, Potential and Design Guidelines," *Compos. Eng. 4(1):81-94*, vol. 4, pp. 18-94, 1994.
- [8] A. Shukla, N. Jain, and R. Chona, "A Review Of Dynamic Fracture Studies In Functionally Graded Materials," *Strain* vol. 42, pp. 76-95, 2007.
- [9] N. S. J. Siti, M. Faizal, M. N. Dewan, and N. B. Shah, "A Review on the Fabrication Techniques of Functionally Graded Ceramic-Metallic Materials in Advanced Composites," *Scientific Research and Essays*, vol. 8, pp. 828-840, 2013.
- [10] M. Shen and M. B. Bever, "Gradient in Polymetric Materials," *Material Science and Engineering*, vol. 7, pp. 741-746, 1972.
- [11] M. B. Bever and P. F. Duwez, "Gradient in Composite Materials. ," *Materials Science and Engineering* vol. 10, pp. 1-8, 1972.
- [12] J. Saifulnizan, "Application of Functionally Graded Materials for Severe Plastic Deformation and Smart Materials: Experimental Study and Finite Element Analysis," PhD, Department of Engineering Physics, Electronics and Mechanics, Graduate School of Engineering, Nagoya Institute of Technology, 2012.
- [13] M. Niino, T. Hirai, and R. Watanabe, "The Functionally Gradient Materials," *J Jap Soc Compos Mat*, vol. 13, pp. 257-264, 1987.
- [14] B. M. Ankit and C. P. Khushbu, "A Review of Stress Analysis of Functionally Graded Material Plate with Cut-out," *International Journal of Engineering Research & Technology (IJERT)*, vol. 3 2014.
- [15] Y. Miyamoto, W. Kaysser, B. Rabin, A. Kawasaki, and R. Ford, *Functionally Graded Materials: Design, Processing and Applications.*: Kluwer Academic Publishers, 1999.
- [16] S. S. Wang, "Fracture Mechanics for Delamination Problems in Composite Materials," *Journal of Composite Materials*, vol. 17, pp. 210-223, 1983.
- [17] T. SFB. (2006, 22/7/2016). *Process-Integrated Manufacturing of Functionally Graded Structures on the Basis of Thermo-Mechanically Coupled Phenomena (Research for the Sustainable Products of Tomorrow ed.)*. Available: <http://web.archive.org/web/20150319184523/http://www.transregio-30.com/index.php?id=4&L=1>

- [18] A. C. Vieira, L. A. Rocha, and J. R. Gomes, "Influence of Sic Particles Incorporation on the Microstructure and Tribological Behaviour of Functional Graded Al/SiCp Composites," in *Proceedings of the IV Iberian Congress on Tribology*, Ibertrib, Bilbao, Spain, , 2007.
- [19] F. Erdemir, A. Canakci, and T. Varol, "Microstructural Characterization and Mechanical Properties of Functionally Graded Al₂O₃/SiC Composites Prepared by Powder Metallurgy Techniques," *Transaction Nonferrous Metallurgy Society China* vol. 25, p. 3569–3577, 2015.
- [20] A. C. Vieira, P. D. Sequeira, J. R. Gomes, and L. A. Rocha, "Dry Sliding Wear of Al Alloy/SiCp Functionally Graded Composites: Influence of Processing Conditions," *Wear* vol. 267 pp. 585–592., 2009.
- [21] Y. Watanabe, A. Kawamoto, and K. Matsuda, "Particle Size Distributions in Functionally Graded Materials Fabricated by Centrifugal Solid-Particle Method," *Composites Science and Technology* vol. 62, pp. 881–888, 2002.
- [22] A. Ibrahim, F. Mohamed, and E. Lavernia, " Particulate Reinforced Metal-Matrix Composites - A Review," *Journal of Materials Science* vol. 26, pp. 1137-1156, 1997.
- [23] M. Schwartz, "Encyclopedia of smart materials: Smart Materials," *Wiley-Interscience*, vol. 2, p. 1176, 2002.
- [24] R. Knoppers, J. W. Gunnink, d. H. J. Van, and V. W. Vliet, "The Rreality of Functionally Graded Material Products," TNO Science and Industry, Netherlands.
- [25] J. F. Groves and H. N. G. Wadley, "Functionally Graded Materials Synthesis via Low Vacuum Directed Vapor Deposition," in *Composites Part B: Engineering* vol. 28, ed, 1997.
- [26] D. W. Hutmacher, M. Sittinger, and M. V. Risbud, "Scaffoldbased Tissue Engineering: Rationale for Computer-Aided Design and Solid Freeform Fabrication Systems," *Trends Biotechnol*, vol. 22, pp. 354-62, 2004.
- [27] K. A. Mumtaz and N. Hopkinson, "Laser Melting Functionally Graded Composition of Waspaloy and Zirconia Powders," *Journal of Materials Science and Engineering*, vol. 42, pp. 7647-7656, 2007.
- [28] S. Kateřina, K. Miroslav, and S. Ivo, *Powder Metallurgy*. Ostrava: University Textbook, Technical University of Ostrava, 2014.
- [29] N. R. Ganesh. (n. d., 04/07/2016). *Powder Metallurgy: Basics and Applications*. Available: http://www.iitg.ernet.in/engfac/ganu/public_html/Powdermetallurgy.pdf
- [30] B. J. W., "Powder Metallurgy Methods and Applications," in *ASM Handbook, Powder Metallurgy*. vol. 7, P. Samal and J. Newkirk, Eds., ed: ASM International, 2015.
- [31] R. K. Rajput, *Manufacturing Technology: Manufacturing Processes*. New Delhi, DELHI, India: Laxmi Publications, 2008.
- [32] P. Beiss, "Principles of Metal Powder Compaction," presented at the European Powder Metallurgy Association Training Course,, Aachen, Germany, 2005.
- [33] P. Beiss, "Structural Mass Production Parts, Landolt-Bornstein: Numerical Data and Functional Relationships in Science and Technology," V. Group VIII Advanced Materials and Technologies, Materials, Sub-volume A, Powder Metallurgy Data, Ed., ed. Heidelberg, Germany: Springer.
- [34] MPIF. (2015, 04/07/2016). *Distinguished Service to Powder Metallurgy Award Recipients*. Available: <http://www.mpiif.org/AboutMPIF/PDFs/Distinguished-Service-Recipients.pdf>

- [35] Z. Krzysztof and P. Piotr, "Iron Powder-Based Graded Products Sintered by Conventional Method and by SPS," *Advanced Powder Technology* vol. 26, pp. 401-408, 2015.
- [36] O. Carvalho, M. Buciumeanu, S. Madeira, D. Soares, F. S. Silva, and M. G., "Optimization of AlSi-CNTs Functionally Graded Material Composites for Engine Piston Rings," *Materials and Design* vol. 80, pp. 163-173, 2015.
- [37] B. Kieback, A. Neubrand, and H. Riedel, "Processing Techniques for Functionally Graded Materials " *Materials Science and Engineering: A 362 (1-2)*, pp. 81-106, 2003.
- [38] J. Gandra, P. Vigarinho, D. Pereira, R. M. Miranda, A. Velhinho, and P. Vilaca, "Wear Characterization of Functionally Graded Al-SiC Composite Coatings Produced by Friction Surfacing," *Mater. Design*, vol. 52, pp. 373-383, 2013.
- [39] F. Watari, H. Kondo, S. Matsuo, R. Miyao, A. Yokoyama, M. Omori, *et al.*, "Development of Functionally Graded Implant and Dental Post for Bio-Medical Application," *Mater. Sci. Forum*, pp. 423-425:321-326, 2003.
- [40] L. A. Dobrzanski, B. Dolzanska, K. Golombek, and G. Matula, "Characteristics of Structure and Properties of a Sintered Graded Tool Materials with Cobalt Matrix," *Arch. Mater. Sci. Eng.* , vol. 47, pp. 69-76, 2011.
- [41] M. Pines and H. Bruck, "Pressure-Less Sintering of Particle-Reinforced Metal-Ceramic Composites for Functionally Graded Materials: Part II Sintering Model," *Acta Mater*, vol. 54, pp. 1467-1474, 2006.
- [42] N. B. Dhokey, V. A. Athavale, N. Narkhede, and M. Kamble, "Effect of Processing Conditions on Transient Liquid Phase Sintering of Premixed Aluminium Alloy Powders," *Adv. Mat. Lett.* , vol. 4, pp. 235-240, 2013.
- [43] J. S. Moya, A. J. Sanchezherencia, J. Requena, and R. Moreno, Sep. , "Functionally Gradient Ceramics by Sequential Slip Casting," *Materials Letters*, vol. 14, pp. 333-335, 1992.
- [44] L. Po-Hua, "Fabrication, Characterization and Modeling of Functionally Graded Materials," Doctor of Philosophy, Graduate School of Arts and Sciences, Columbia University, 2013.
- [45] M. R. Ghomashchi and A. Vikhrov, "Squeeze Casting: An Overview " *Journal of Materials Processing Technology*, vol. 101 pp. 1-9, 2000.
- [46] R. S. M. Seyed, "Processing of Squeeze Cast Al6061-30 vol% SiC Composites and their Characterisation," *Materials and Design*, vol. 27, pp. 216-222, 2006.
- [47] D. M. and K. V. S. Senthil, "Squeeze Casting of Aluminium Metal Matrix Composites- An Overview," presented at the 12th Global Congress on Manufacturing and Management, GCMM 2014, 2014.
- [48] S. Chatterjee and A. A. Daas, "Effects of Pressure on Solidification of some Commercial Aluminium-Base Casting Alloys," *The British Foundryman*, vol. 11, pp. 420-427, 1972.
- [49] O. G. Epanchistov, "Structure and Properties of Metals Solidified under High Pressure " 34-37, vol. 6, p. Russian Casting Production, 1972.
- [50] I. G. Crouch, "Aluminium Squeeze Casting Technology: European Researches Viewpoint " presented at the Australian Conference on Materials for Industrial Development, Christchurch, New Zealand, 1987
- [51] R. Di, E. and G. Piatti, "Metal matrix composites: state of the art,," *Alum. Mag.* , vol. 1, 1994.

- [52] J. Bear, *Dynamics of Fluids in Porous Media*. New York: American Elsevier Publishing Co, 1972.
- [53] D. Staudenecker, "Development of Porous Ceramic Preforms and Manufacture of Metal-Ceramic Composites," Diploma FH Aalen, FH Aalen Germany, 2001.
- [54] A. H. Bernd, "Pressure Infiltration Behaviour and Properties of Aluminium Alloy - Oxide Ceramic Preform Composites," Doctor of Philosophy, School of Metallurgy and Materials, The University of Birmingham, 2009.
- [55] A. Boczkowska, P. Chabera, A. J. Dolata, M. Dyzia, and A. Oziębło, "Porous Ceramic - Metal Composites Obtained by Infiltration Methods," *Metallurgija* vol. 52, pp. 345-348, 2013.
- [56] W. Sufei and L. Steve, "ASM Handbook: Centrifugal Casting," *ASM International*, vol. 15, pp. 667-673, 2008.
- [57] M. J. Amit. (n.d, 06/07/2016). *Aluminium Foundry Practice*. Available: <http://www.metalwebnews.com/howto/casting/casting.pdf>
- [58] Y. WATANABE, H. SATO, and Y. FUKUI, "Wear Properties of Intermetallic Compound Reinforced Functionally Graded Materials Fabricated by Centrifugal Solid-particle and In-Situ Methods," *Journal of Solid Mechanics and Materials Engineering*, vol. 2, pp. 842-853, 2008.
- [59] B. S. S. Daniel, V. S. R. Murthy, and G. S. Murty, "Metal-Ceramic Composites Via In-Situ Methods," *J Mater Process Technol*, vol. 68, pp. 132-155, 1997.
- [60] M. Hoseini and M. Meratian, "Tensile Properties of In-Situ Aluminium-Alumina Composites," *Mater Lett* vol. 59, pp. 3414-3418, 2005.
- [61] E. J. Babu, T. P. D. Rajan, S. Savithri, U. T. S. Pillai, and B. C. Pai, "Theoretical Analysis and Computer Simulation of the Particle Gradient Distribution in a Centrifugally Cast Functionally Graded Material," presented at the International Symposium of Research Students on Materials Science and Engineering, Chennai, India, 2004.
- [62] J. R. Gomes, L. A. Rocha, S. J. Crnkovic, R. F. Silva, and A. S. Miranda, "Friction and Wear Properties of Functionally Graded Aluminum Matrix Composites.," *Materials Science Forum* vol. 91, pp. 423-425, 2003.
- [63] J. R. Gomes, A. S. Miranda, L. A. Rocha, and R. F. Silva, "Effect of Functionally Graded Properties on the Tribological Behaviour of Aluminium Matrix Composites," *Key Engineering Materials* 2002.
- [64] R. Pippin and P. Weinert, "The Effective Threshold of Fatigue Crack Propagation in Aluminium Alloys: The influence of Particle Reinforcement," *Philosophical Magazine A*, vol. 77, pp. 875-886 1998.
- [65] K. Ramazan and S. Omer, "Fabrication and Properties of Functionally Graded Al/AlB₂ Composites," *Journal of Composite Materials*, vol. 0, pp. 1-9, 2014.
- [66] M. R. Masoud, T. Morteza, M. A. B. Seyed, and G. S. Sajad, "Characterization of the Graded Distribution of Primary Particles and Wear Behaviour in the A390 Alloy Ring with Various Mg Contents Fabricated by Centrifugal Casting," *Materials and Design* vol. 65, pp. 105-114, 2014.
- [67] Y. Watanabe, Y. Hattori, and H. Sato, "Distribution of Microstructure and Cooling Rate in Al-Al₂Cu Functionally Graded Materials Fabricated by a Centrifugal Method," *Journal of Materials Processing Technology*, vol. 221, pp. 197-204, 2015.
- [68] X. Lin and T. M. Yue, "Phase Formation and Microstructure Evolution in Laser Rapid Forming of Graded SS316L/Rene88DT Alloy," *Mater Sci Engng*, vol. A402, pp. 294-306, 2005.

- [69] M. A. Boboulos. (2015, 25/08/2015). *CAD-CAM & Rapid Prototyping Application Evaluation*. Available: www.bookBoom.com.
- [70] J. Hashim, L. Looney, and M. S. J. Hashmi, "Metal Matrix Composites: Production by the Stir Casting Method," *Journal of Materials Processing Technology*, vol. 92-93, pp. 1-7, 1999.
- [71] M. J. Jebeen, I. Dinaharan, and S. S. Joseph, "Prediction of Influence of Process Parameters on Tensile Strength of AA6061/TiC Aluminum Matrix Composites Produced using Stir Casting," *Transaction Nonferrous Metallurgy Society China*, vol. 26, p. 1498–1511, 2016.
- [72] K. B. Ashok and N. Murugan, "Metallurgical and Mechanical Characterization of Stir Cast AA6061-T6–AlNp Composite," *Materials and Design*, vol. 40, p. 52–58, 2012.
- [73] K. G. J. Allwyn, S. N. Mohamed, I. Dinaharan, and R. S. J. David, "Production and Characterization of Rich Husk Ash Particulate Reinforced AA6061 Aluminum Alloy Composites by Compocasting," *Transaction Nonferrous Metallurgy Society China*, vol. 25, p. 683–691, 2015.
- [74] L. Ceschini, G. Minak, and A. Morri, "Tensile and Fatigue Properties of the AA6061/20 vol.% Al₂O_{3p} and AA7005/10 vol.% Al₂O_{3p} Composites," *Composites Science and Technology*, vol. 66, p. 333–342, 2006.
- [75] S. Amirkhanlou, J. Roohollah, N. Behzad, and R. T. Mohammad, "Using ARB Process as a Solution for Dilemma of Si and SiC_p Distribution in Cast Al–Si/SiC_p Composites," *Materials Process Technology*, vol. 211, pp. 1159-1165, 2011.
- [76] K. Takahiro, S. Masafumi, S. Hisashi, and W. Yoshimi, "Fabrication of Copper/Diamond Functionally Graded Materials Forgrinding Wheels By Centrifugal Sintered-Casting," *Journal of Materials Processing Technology* vol. 217, pp. 294-301, 2015.
- [77] E. Fatih, C. Aykut, V. Temel, and O. Serdar, "Corrosion and Wear Behavior of Functionally Graded Al₂O₃/SiC Composites Produced by Hot Pressing and Consolidation," *Journal of Alloys and Compounds* vol. 644, pp. 589-596, 2015.
- [78] J. Narciso, A. Alonso, A. Pamies, C. Garcia-Cordovilla, and E. Louis, "Wettability of Binary and Ternary Alloys of the System Al-Si-Mg with SiC Particulates," *Scripta Metallurgy*, vol. 31, pp. 1495-1500, 1994.
- [79] G. G. Sozhamannan, P. S. Balasivanandha, and V. S. K. Venkatagalapathy, "Effect of Processing Paramters on Metal Matrix Composites: Stir Casting Process," *Journal of Surface Engineered Materials and Advanced Technology*, vol. 2, pp. 11-15, 2012.
- [80] N. C. Kaushik and R. N. Rao, "Effect of Grit Size on Two Body Abrasive Wear of Al6082 Hybrid Composites Produced by Stir Casting Method " *Tribology International* vol. 102, pp. 52-60, 2016.
- [81] S. N. Aqida, M. I. Ghazali, and J. Hashim, "Effects Of Porosity On Mechanical Properties Of Metal Matrix Composite: An Overview " *Jurnal Teknologi*, vol. 40, pp. 17-32, 2004.
- [82] M. Xigeng and S. Dan, "Graded/Gradient Porous Biomaterials," *Materials* vol. 3, pp. 26-47, 2010.
- [83] L. H. Larry, "Bioceramics," *Journal of the American Ceramic Society*, vol. 81, pp. 1705-1728, 1998.

**CHAPTER 5: CENTRIFUGAL CASTING TECHNIQUE BASELINE
KNOWLEDGE, APPLICATIONS, AND PROCESSING
PARAMETERS: OVERVIEW**

W. S. Ebhota and F. L. Inambao, "Centrifugal casting technique baseline knowledge, applications, and processing parameters: overview," *International Journal of Materials Research*, 2016. DOI: 10.3139/146.111423 (*Published*).

W. S. Ebhota et al.: Centrifugal casting technique baseline knowledge, applications, and processing parameters

Williams S. Ebhota^a, Akhil S. Karun^b, Freddie L. Inambao^c

^aDiscipline of Mechanical Engineering, Howard College, University of KwaZulu-Natal, Durban, South Africa

^bMaterials Science and Technology Division, CSIR-National Institute for Interdisciplinary Science and Technology, Thiruvananthapuram, India

^cDiscipline of Mechanical Engineering, Howard College, University of KwaZulu-Natal, Durban, South Africa

Centrifugal casting technique baseline knowledge, applications, and processing parameters: overview

The increasing need for materials with light weight, high resistance to corrosion and wear, toughness and strength, machinability, high thermal capacity etc. for various applications is unending. This demand has continued to stretch the exploitation and manipulation of various functionally graded materials (FGMs) and their production methods. This study explores one of the FGM production processes called the centrifugal casting technique (CCT). The centrifugal casting process has several potential advantages over traditional casting methods. This study provides information regarding the basic functionally graded production methods and their applications and also discusses categories of CCT, evolution and process parameters.

Keywords: Functionally graded materials; Centrifugal casting technique; Process parameters; Aluminium metal matrix; Reinforcement particles

1. Introduction

Functionally graded materials (FGMs) production methods are engineering materials and production processes which combine various functional attributes in one part. For instance, these attributes could be thermal, corrosion and

wear resistance, machinability and toughness. Several production techniques have been employed in the production of functionally graded aluminium matrix composites (FGAMCs) with exceptional properties and this has spurred their applications. Table 1 presents FGMs fabrication methods and their applications. Presently, FGAMCs are widely used in automotive, aerospace, sports, medicine, nuclear energy, renewable energy, chemical, optics, electronics, and general engineering industries [1–5]. The increase in the application of FGM aluminium composites is due to the following properties that they possess: high specific strength, low density, good wear and corrosion resistance, Young's modulus and high thermal capacity materials [6, 7]. Aluminium matrix composites have been reinforced with a variety of particles including: nitrides (BN, ZrN, TiN); carbides (SiC, TiC, ZrC); borides (ZrB₂, TiB₂, SiB₂); oxides (Al₂O₃, MgO, TiO₂, ZrO₂); silicides (MoSi₂); and fine particles of various intermetallics (Fe₃Al, FeAl, NiAl, Ni₃Al, Ti₃Al, TiAl) [8–11].

This study focuses on the centrifugal casting technique (CCT) which has several potential advantages over traditional casting methods. Empirically, alloy castability can be improved by mould rotation, as the magnitude of centrifugal force far exceeds that of gravity. This technique drives the molten metal into thin trailing edges and forces trapped air to escape [12–14]. However, low superheat is required as casting materials are sometimes very reactive,

coupled with high turbulent flow and gas trapping associated with high molten metal velocity [15–17].

1.1. Principle of CCT

The principle behind CCT is the use of forces generated from the centripetal acceleration of a rotating mould to distribute the metal matrix and particles into the mould. At the early stage of the history of this casting process, most moulds were cylindrical and mainly made from iron, graphite and steel. Sand or refractory lining materials were used to make cores. Objects with polynomial cross-sections, such as square and other shapes, can be produced by CCT, but such objects will have round inner surfaces. This technique was predominantly used for the manufacture of

tubes and pipes such as water supply lines, gas pipes, sewage pipes, rings, bushings, engine cylinder liners, pistons, streetlamp posts, brake drums etc.

Centrifugal forces play a significant role during the pouring and solidification phase in determining the properties of the cast. The force increases towards the outer region of the cast, away from the axis of rotation. This leads to a higher density at the outer surface than the nearest region to the axis, as represented in Fig. 1. The centrifugal force is a function of density and radius and is tangential to the circular path of rotation. This pushes the melt or particle to the periphery where it is retained by the wall of the mould. For a matrix and reinforcement particle, the component with higher density possesses greater centrifugal force and moves farther away from the centre of rotation.

Table 1. FGMs fabrication techniques and their applications.

Method	Type	Group of FGM
Vapour deposition techniques	Chemical vapour deposition (CVD) and physical vapour deposition (PVD)	Thin surface coating
Powder metallurgy (PM)	Stepwise Compositional Control: powder stacking, sheet lamination and wet powder spraying Continuous Composition Control: Centrifugal powder forming (CPF), impeller dry blending, centrifugal sedimentation, electrophoretic deposition and pressure filtration/vacuum slip casting	Bulk
Melting processes	Centrifugal casting, sedimentation casting infiltration processing thermal spray processing	Bulk
Material prototyping/solid freeform (SFF) fabrication	Laser-based processes: laser cladding, melting, laser sintering, selective D-printing and selective laser	Bulk
Compcasting	The liquid state process in which the addition of reinforcement to an agitated solidifying melt is carried out	Bulk
Other methods	plasma spraying, electrodeposition, electrophoretic, ion beam assisted deposition (IBAD), self-propagating high-temperature synthesis (SHS)	Thin coating

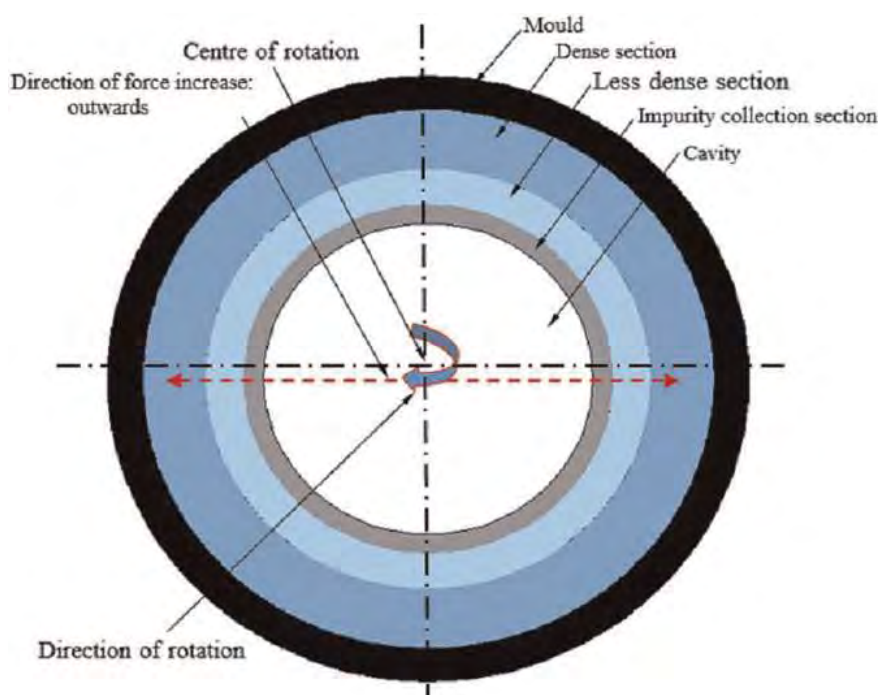


Fig. 1. A schematic of a true centrifugal casting system.

1.2. Advantages of CCT

1. Time-saving because it does not need gating system elements to direct the metal flow.
2. Quality castings in terms of accurate dimensions, good surface finish and porosity as gas porosity is limited in the region of the cast surface.
3. Solidification is faster with a high of quality metallurgical properties.
4. The force generated is about 150 times the force of gravity.
5. Simple and light machining operations are required.

1.3. FGMs by CCT

The CCT is a manufacturing process that involves pouring of molten metal into a rotating mould and the cast is allowed to solidify before rotation is stopped [18, 19]. Main components of a centrifugal cast machine are shown in Fig. 2. In the FGAMC context, CCT involves uniformly mixing particles with molten metal and pouring the mixture into a spinning mould forming a compositional gradient and it then being allowed to solidify [20]. CCT has been described as an exciting method due to the possibility of gradient control using process parameters. The rotation creates a centrifugal force that pushes the molten metal and the particles against the wall of the mould. This process ensures

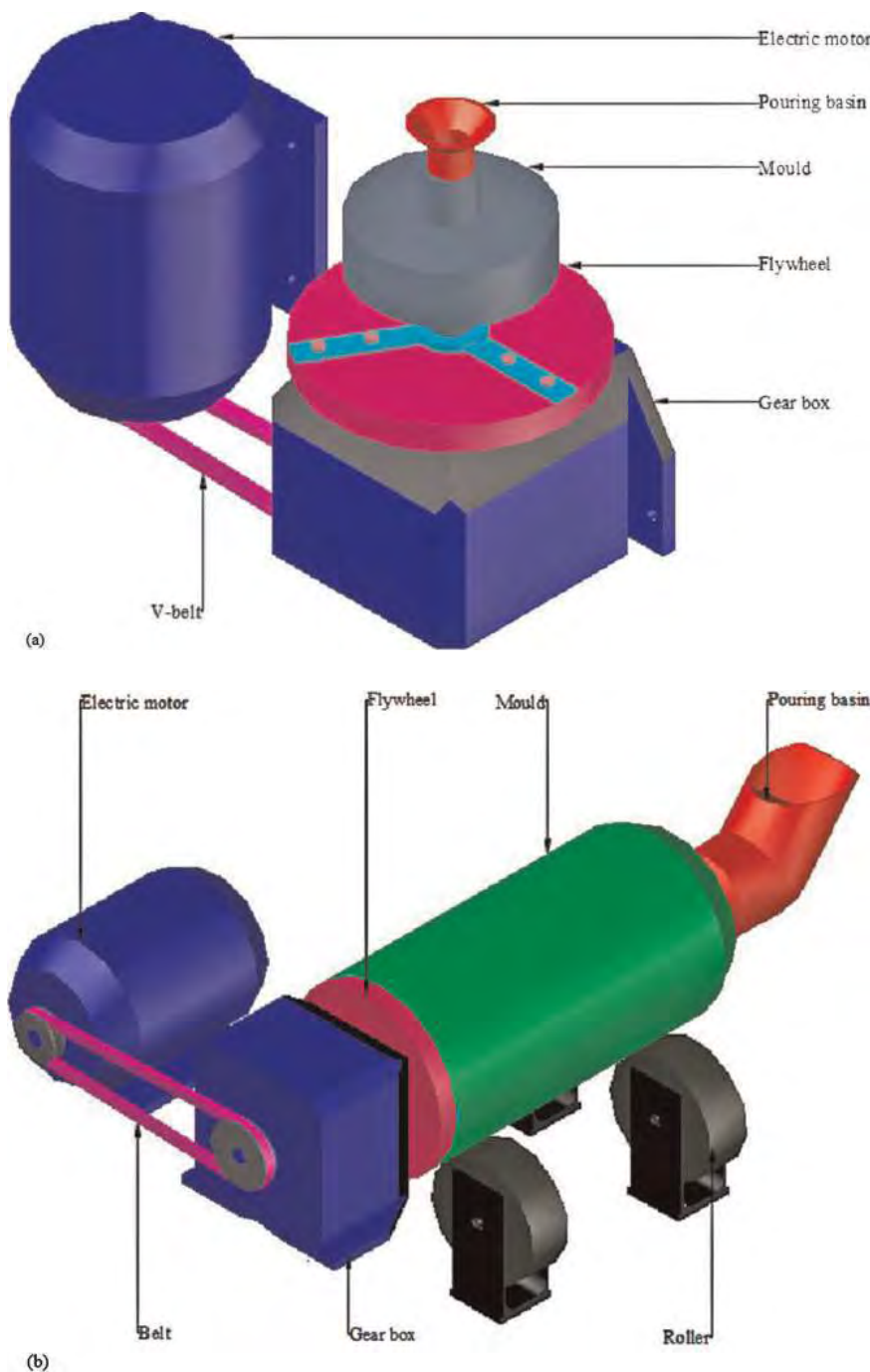


Fig. 2. Schematic of (a) vertical centrifugal casting machine, and (b) horizontal centrifugal casting machine.

the production of the desired shape, microstructural and compositional gradient. The method is used in the casting of metals such as steel alloys, magnesium alloys, aluminium alloys, copper alloys, etc.; non-metals such as ceramics, plastics, glass, and FGMs such as aluminium alloy ceramic composites, copper alloy–ceramic composites etc. Practically, the method can be used for every material that can be melted into liquid or slurries. Several functionally attractive metal–ceramic based FGMs have been developed through this technique for a range of engineering applications such as an automobile, aircraft and aerospace, general engineering industries, etc.

The current methods of bulk and mass production of FGMs in large quantities or for large parts are not yet reliable and are expensive. Amongst the known fabrication techniques, CCT is the most attractive and economical to execute [21–23]. Several FGMs of pure metal–ceramics, metal alloy–ceramics and metal–intermetallic compounds have been developed by CCT and experimental and numerical studies performed.

1.4. Classification of CCT

Centrifugal casting methods are classified into two groups. The first group is based on centrifugal machine arrangement and the second group is based on temperature. The first group includes two main types, namely, horizontal centrifugal casting and vertical centrifugal casting, as shown in Fig. 2. However, this group can be further categorised into horizontal true centrifugal casting process, inclined true centrifugal casting process, vertical true centrifugal casting process, and semi-vertical centrifugal casting process. Schematic diagrams in Fig. 3 show a wider centrifugal casting machine classification [19]. The second group is based on the temperature of the matrix alloy and includes the ex-situ

solid-particle centrifugal method and the in-situ centrifugal method [24–26]. The ex-situ solid-particle centrifugal method involves a temperature below the liquidus temperature of the matrix material and addition of prefabricated reinforcement to the metal matrix by infiltration, vortex or casting methods. The in-situ centrifugal method involves a temperature exceeding matrix liquidus temperature and reinforcement precipitation in the matrix melt during cooling and solidification. This method is advantageous compared to the ex-situ technique in terms of good wettability, uniform distribution of reinforcement and reinforcement material thermodynamic stability in the matrix alloy [27, 28].

2. Evolution

The use of CCT is as old as the 16th century involving Benvenuto Cellini and others who founded the art. Eckhardt obtained the first recorded patent on CCT in 1809 in England while in the USA Baltimore made the first industrial application of the process in 1848 [29]. A Brazilian, Dimitri Sensaud DeLavaud, invented a new CCT machine in 1918 which was characterised by the absence of cores [19]. Non-professional craftsmen got access to centrifugal casting methods after its adoption in 1940 for jewellery manufacturing. Experimentation regarding the combination of centrifugal and vacuum castings was conducted in 1935, and patents were issued in 1940–42. The first successful vacuum centrifugal casting was achieved by A.L. Englehardt in 1948. The technique was initially (before the mid-1980s) used solely for the fabrication of symmetrical components such as shafts, bushings, cylinders, pipes, rolls for steel mills and other shapes. The method has evolved tremendously through research and development and has been described by several authors as the simplest and cheapest technique in FGM fabrication [30].

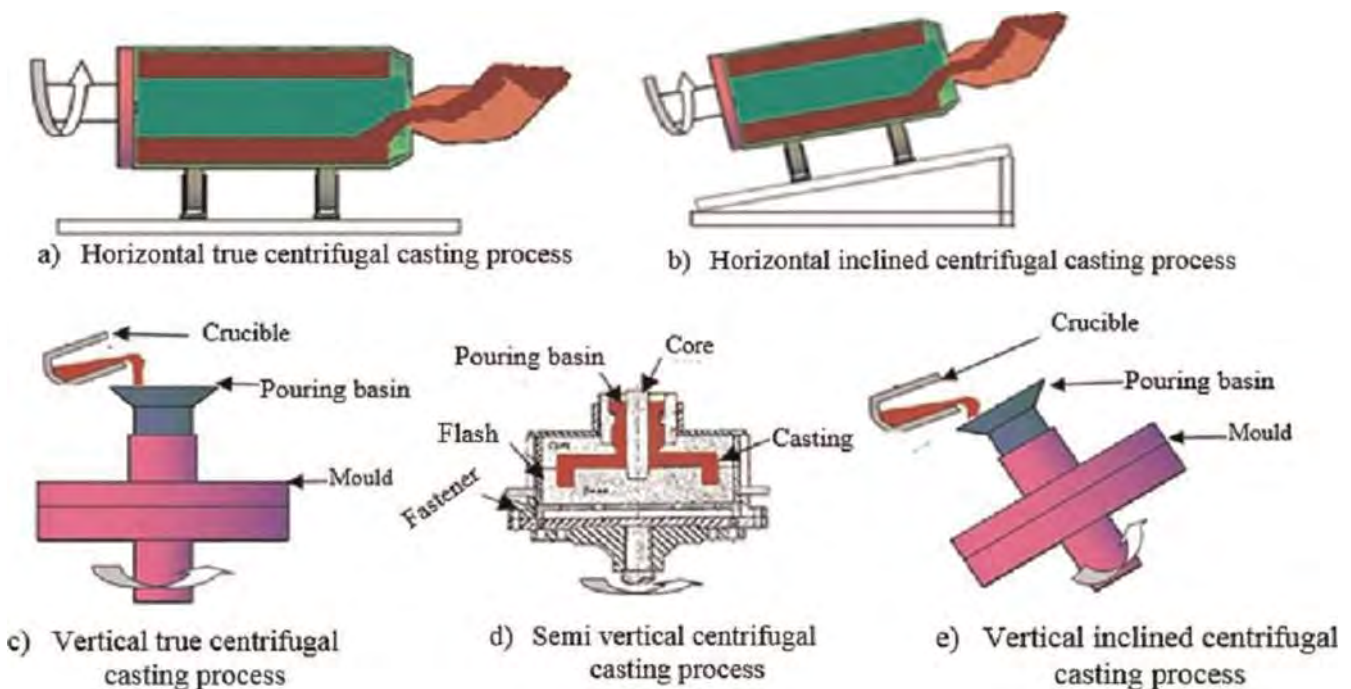


Fig. 3. Classification of centrifugal casting methods based on mould rotation [19].

Presently, all the known FGM manufacturing techniques are expensive to execute for mass production of large parts and some are complex to perform. These methods include powder metallurgy, chemical vapour deposition, solidification processing, spray atomisation and co-deposition and centrifugal. The centrifugal casting process is regarded as an economical casting technique [22] and has these advantages: fast solidification with quality metallurgical properties; limited gas porosity in the cast inner surface; force generated is about 150 times the force of gravity; risers and core are not needed; and simple and light machining operation is required.

2.1. FGMs manufacturing by means of CCT

The CCT in FGM manufacturing involves the uniform mixing of particles with molten metal and pouring the resultant mixture into a spinning mould forming a compositional gradient and allowing it to solidify. The centrifugal casting method is exciting due to the possibility of gradient control using process parameters. The centrifugal casting process is developing rapidly and has the potential to dominate the field of FGM production. However, it is still in the development stage due to inadequate knowledge of particle distribution and control [22].

The manufacture of FGMs by centrifugation is characterised by the discontinuous distribution of reinforcing particles in a radially graded pattern. The metal matrix and reinforcing particle density difference causes segregation in which the higher density particles migrate to the outer periphery and lower density particles migrate to the inner surface. The grading determines the functionality and can be regulated and enhanced by certain processing parameters such as particle size and volume, centrifugal rotation speed, mould temperature, molten metal alloying temperature, and cast geometry [31]. The size and concentration of the ceramic particle in a matrix has a correlation with hardness and wear.

Experimental works have proved that centrifugal casting can separate phases of dissimilar densities. Many functionally graded aluminium composites (FGACs) have been fabricated successfully through one or other of the types of centrifugal casting techniques. Investigations have revealed that Al/SiC, Al/Shirasu and Al/Al₃Ti can be manufactured via centrifugal solid-particle methods while Al/Al₃Ni and Al/Al₂Cu can be fabricated using the in-situ method [25]. The fabrication of Al/(Al₃Ti+Al₃Ni) hybrid FGMs needs the combination of solid-particle and in-situ production methods.

Ferreira et al. [32] have used the centrifugal method to manufacture Al/Al₃Ti and Al/Al₃Zr FGMs from the following compositions: Al-5 mass% Ti and Al-5 mass% Zr, respectively. The magnitudes of centrifugal force used are 30 G, 60 G and 120 G where G is the ratio of the centrifugal force to gravity force. The results of the characterisation show that an increase in the volume of particles and centrifugal force will affect both gradient and particle concentration at the outer surface, and that better tribocorrosion performance was found in the sample with the highest volume of particles.

Vieira et al. [18] have studied the factors in CCT that affect the wear of FGM (Al alloy/SiC_p). The matrix material was aluminium alloy with chemical composition of Al-10Si-4.5Cu-2Mg and the reinforcement particles of SiC_p

with particle average size of 37.8 μm. The speeds of 1 500 rpm and 2 000 rpm were used as rotational speeds for two different moulds, to produce cast rings. The authors observed that the centrifugal casting process:

1. Aided microstructure gradient and hardness in the centrifuged alloy without reinforcement and the material was characterised by serious wear of adhesive wear type.
2. The gradient of FGM at 2 000 rpm was sharper than the one cast with 1 500 rpm.
3. An increase in the volume of the SiC particles to 5 % in the mixture reduces the rate of FGM wear, but severe wear was reported in the volume of SiC particles below 2 %.
4. The mechanisms of wear found in the FGMAC considered are two-body abrasion wear, delamination, adhesion and oxidative wear.

The gradient of FGMs fabricated by the centrifugal technique is a function of the following: speed of rotation, process duration, and dispersive fluid and particle contents. The centrifugal casting of Fe-TiC FGM requires a self-generating high-temperature production reaction as an additional step. It was observed in the Fe-TiC FGM specimen that the hardness increased inwardly and the inner part performed better than the outer surface in wear tests [33].

Watanabe et al. [34] have produced an Al-Al₂Cu FGM ring from Al-3 %Cu using the centrifugal in-situ method. In this study, it was reported that: the α-Al particles drifted towards the outer surface after the centrifugal process as the density of α-Al crystal is higher than the molten aluminium alloy, the concentration of Cu in the ring was massive towards the inner part, the hardness of the Al-Al₂Cu FGM ring fabricated increases down the inner region, and the hardness of the specimen appreciated tremendously due to heat treatment.

A review of wear properties of two types of aluminium matrix FGMs, Al-Al₃Ti FGM and Al-Al₃Ni FGM, was conducted by Watanabe et al. [24]. Two fabrication methods were used to produce FGM rings: the centrifugal solid particle method and the centrifugal in-situ method. The authors reported that size, shape, volume fraction, and orientation of the reinforcements are parameters defining properties of the FGMs. In summary, the findings were [24]:

1. The wear property was found to be anisotropic and depended on the direction of the wear test relative to the Al₃Ti particle alignment. Figure 4 depicts the alignments of the Al₃Ti.
2. Larger alignment parameters resulted in greater anisotropic wear resistance.
3. A wear resistance gradient of Al-Al₃Ni FGMs was noticed along the thickness of the ring proportional to the volume fraction and particle size reduction.
4. Mechanical properties of the FGM fabricated by the centrifugal in-situ technique depend on the particle size gradient.
5. FGMs wear resistance can be enhanced by particle size, volume fraction and the alignment dispersal of the reinforcements in the FGMs.

FGMs fabricated by centrifugation of different reinforcement particles of B₄C, SiC, SiC primary silicon, graphite hybrid, Mg₂Si and Al₃Ni on aluminium matrix were investigated by Rajan and Pai [35]. The study reported that rein-

forcement sizes and densities are relevant factors that affect the gradient formation of the microstructure. High-density SiC and Al₃Ni particles were found near the outer surface while low-density particles of graphite, primary silicon and Mg₂Si were arranged near the inner surface. B₄C particles with the closest density to aluminium spread more than others.

2.2. Centrifugal mixed-powder method (CMPM)

To fix the centrifugal limitation, the centrifugal mixed powder method (CMPM) was introduced in the production of FGMs with nano size reinforcement. A CMPM schematic is shown in Fig. 5 [36]. CMPM has advanced to the reactive centrifugal mixed powder method (RCMPM) which ex-

hibits better surface properties of FGMs manufactured by this method [37].

Radhika and Raghu [38] investigated the production of Al–Al₃Ti/Ti₃Al FGM by means of the RCMPM. They reported that the particles move more slowly in distribution at a greater temperature and the FGMs produced with RCMPM change significantly in both intermetallic and morphology with processing temperature. The Ti₃Al intermetallic compound, fine granular Al₃Ti particles, and unreacted Ti phase were found at relatively low temperatures (1150°C to 1250°C). At 1350°C casting temperature, granular Al₃Ti particles were not observed but coarse Al₃Ti platelet particles were found. Further increase in the casting temperature (145 K) resulted in obtaining more coarse Al₃Ti platelet particles. It was observed in the fabricated FGMs that hardness is a function of particle type and size, and their processing temperature.

The centrifugal mixed powder method has been described as a novel method for the fabrication of a nano-particle distributed FGM and the steps are depicted in Fig. 5. Stages of CMPM are as follows [36]:

1. Mixing of powder functional nanoparticles and metal matrix particles in a spinning mould (see Fig. 5a).
2. Melting of metal matrix ingot and pouring the molten metal into the rotating mould that contains the powder mixture (see Fig. 5b).
3. The molten metal matrix is forced into the spaces between the particles of the powder mixture by centrifugal force (see Fig. 5c). The heat in the molten metal matrix melts the matrix powder and forms a composite with the nano-particles (see Fig. 5d). The functional nanoparticles migrate to the outer region of the fabricated FGM ring (see Fig. 5e).

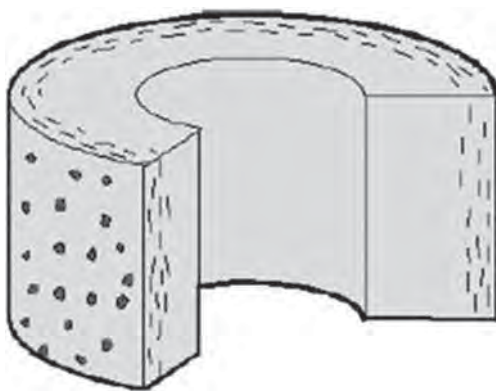


Fig. 4. Schematic alignments of the Al₃Ti particles in an Al–Al₃Ti FGM ring.

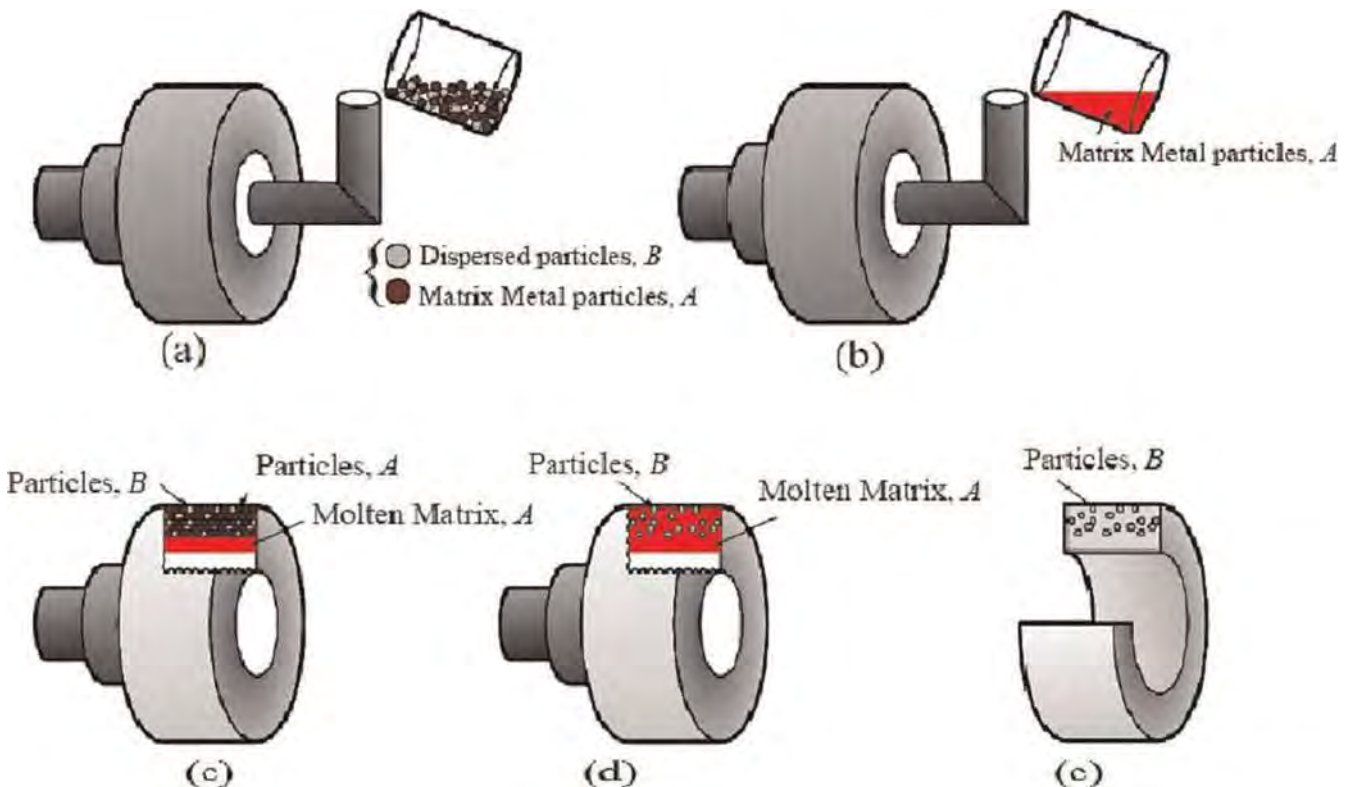


Fig. 5. The schematic description of a CMPM process [36].

Cu–SiC and Al–TiO₂ FGMs were produced with CMPM and characterised [39]. Results showed that:

1. Nanoparticles were dispersed only on the surface of the fabricated FGMs ring.
2. Nano-particle dispersion in the FGM is not density difference dependent between the matrix and the particle.
3. Fabricated FGM surface hardness was enhanced by CMPM.
4. CMPM is effective for fabrication of FGMs which have nano-particles.

3. CCT significant process parameters

While many metal–ceramic FGMs have been developed by means of the centrifugal casting method, this method is still in development because of inadequate knowledge of particle distribution and control [22]. The significant processing parameters for gradient microstructure control are mould temperature, pouring temperature, pouring rate, thermal gradient through the mould, velocity of mould rotation, solidification rate, etc. Temperature circulation is difficult to estimate during centrifugal casting due to the high speed of mould rotation during pour and solidification. The investigation of centrifugal casting process parameters shows that [40–43]:

1. If $\Delta\rho = \rho_p - \rho_m$ is positive, the concentration of ceramic particles will be higher at the outer region, where ρ_p and ρ_m are particle and metal matrix densities.
2. Increasing the particle volume fraction increases the packed and gradient regions, but decreases the particle-free zone, as shown in Fig. 6a.
3. Higher rotational speed migrates more particles to the outer region, causing a thicker zone without ceramic particles called the free region. Rotation of 1500 rpm results in three distinct regions as shown in Fig. 6b: packed region, gradient region, and particle-free zone.
4. Larger particles possess bigger centrifugal acceleration and form a packed bed more easily, as shown in Fig. 6c.

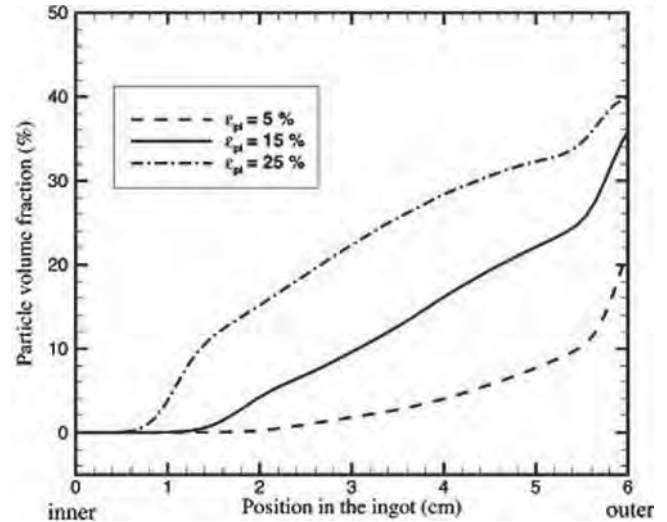
The microstructure, particle distribution and hardness of FGMs cylindrical parts fabricated by horizontal centrifugal casting at 1100 rpm were studied by Rajan et al. [44]. Two metal matrix composites (MMCs) were formed from aluminium alloys and SiC reinforcement particles of size 23 μm , namely, A356 (Al-7.5Si-0.35Mg); A2124 (Al-4.5Cu-1.6Mg-0.25Zn-0.2Si). Both formations had 15% of reinforcement particle concentration. A356 alloy was subjected to solution heat treatment at 535 °C for 10 h with warm quenching and artificial ageing at 165 °C for 8 h. A2124 alloy was subjected to solution heat treatment at 495 °C for 4 h with warm quenching and artificial ageing at 190 °C for 5 h. Microstructures of SiC particle distribution in A356–SiC are shown in Fig. 9.

The study reported that:

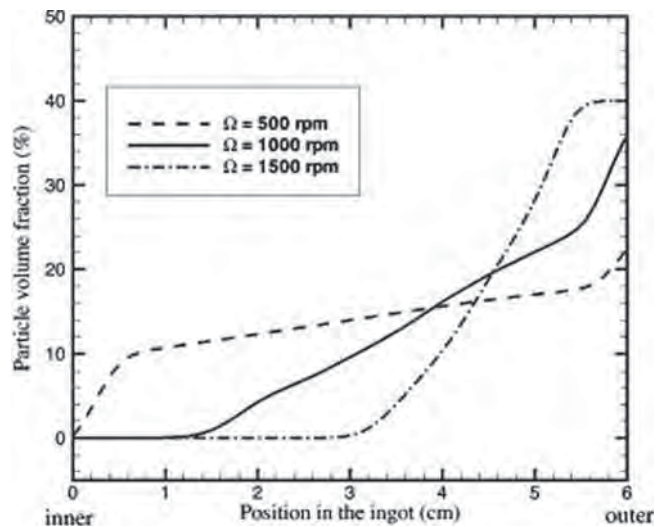
1. The hardness of the non-heated FGMC ring sample was highest at the edge, 98 BHN and lowest in the inner region, 58–60 BHN. A hardness of 155 BHN and 145 BHN were observed at the outer periphery of Al356–SiC and Al212–SiC composites respectively after heat treatment. Figures 7 and 8 show the trends of SiC particle distribution and hardness in the FGM cast ring starting from the outer edge.

2. FGM ring sample SiC particle concentration was higher at the outer periphery (about 45% of the volume of SiC) than the inner region, as shown in Fig. 9.

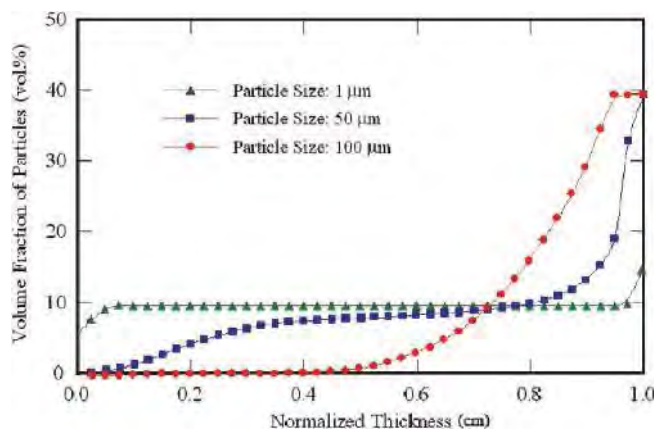
Micrographs of the microstructure of Al356–SiC composite are presented in Fig. 9 and show the particle distribution



(a)



(b)



(c)

Fig. 6. (a) particle volume fraction, (b) rotational speed effects on particles distribution, and (c) effects on particle sizes [36, 42].

and composite gradient. The gradient of the FGM in Fig. 9 has three distinct regions due to the centrifuge: outer region (Fig. 9a and b), mid region (Fig. 9d and e) and inner region (Fig. 9f). The SiC particles have higher density than the matrix and as a result the SiC particles migrate to the outer region. The mid region is predominantly the matrix with large α -Al dendrites, iron intermetallic and eutectic silicon while the inner region has a lot of large voids. It was reported that the A2124-SiC composite has the same pattern of the microstructure. The trend of the mechanical properties reflected this gradient and increase down the outer periphery as indicated by the direction of the arrow. The hardness increases towards the edge for both non-heat treated and heat treated. Maximum hardness of 155 BHN and 145 BHN were recorded at the outer periphery of Al356-SiC and A2124-SiC FGMs respectively.

An investigative study on the influence of vertical CCT on mechanical and metallurgical behaviour of a hypereu-

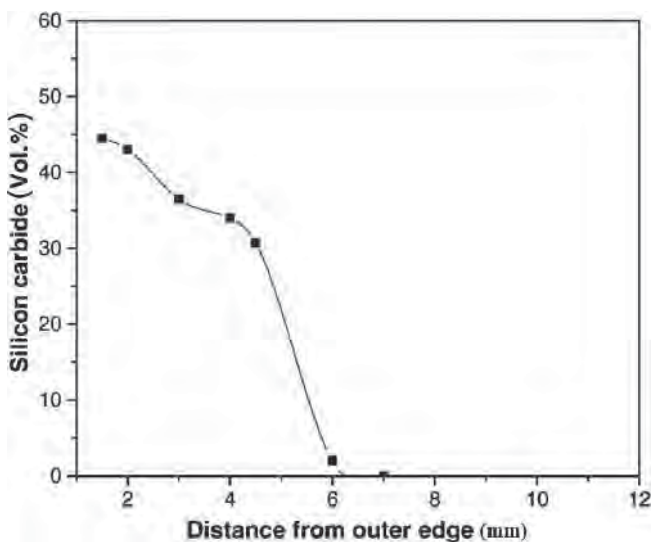


Fig. 7. Graph of SiC particle distribution in the functionally graded Al(356)-SiC cast ring starting from the outer edge [44].

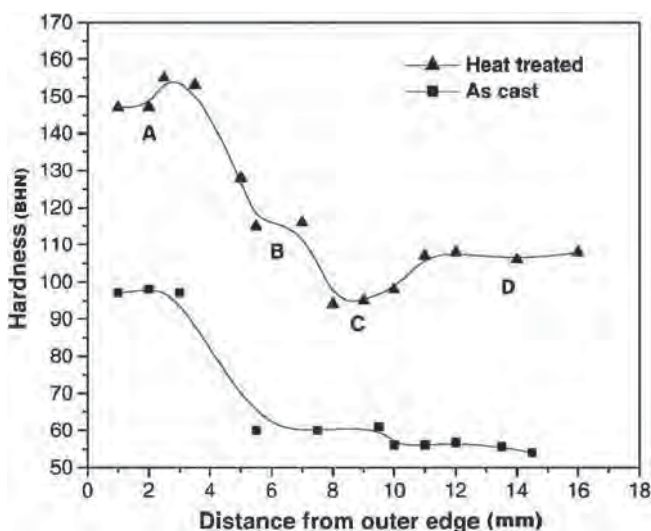


Fig. 8. The graph of hardness trend in non-heat treated and heat treated Al(356)-SiC functionally graded composites starting from the outer edge [44].

tectic Al-18Si alloy was carried out by Chirita et al. [45]. Three different casting techniques, namely, gravity, gravity with vibration and centrifugal casting were used to produce the specimens. All the castings were made from commercially available Al-18Si alloy and a vacuum induction furnace was used for the melting and pouring. The melt was automatically poured into the mould. A frequency of 8 Hz and an amplitude of 0.5 mm in one direction were recorded in the centrifugal casting equipment. Tests to ascertain the effects of their individual production process on the properties of the specimens were carried out. This study concluded that:

1. The mechanical properties of the castings were enhanced tremendously by CCT.
2. No significant influence was observed on casting properties with centrifugal pressure.
3. The innate vibration and faster cooling rate of the vertical CCT are the main factors responsible for the substantial effect on casting mechanical attributes.

In a study, the effect of the vertical CCT and gravity casting technique on the different Al-Si alloys (hypoeutectic, eutectic and hypereutectic alloy) on the mechanical properties of the specimens was compared [46]. Three casting specimens, A (7% Si), B (12% Si), and C (18% Si), were made from commercially available Al-Si alloys. A vacuum induction furnace was used for the melting at 100°C above their liquidus temperature and pouring into a permanent mould preheated at 130°C and rotating at 450 rpm. The melt was automatically poured into the mould. The same melting conditions for the CCT were used for gravity casting but manually poured into the mould. The study reported that:

1. The centrifuge influence was observed to be most sensitive in specimen C (18% Si).
2. The force generated during centrifugation refines the morphology of the alloy.
3. Better mechanical properties are obtainable in the outer surface of the casting.

4. Conclusion

The centrifugal casting process has evolved for several years and much investigative work has been carried out on various aspects including processing facility and parameters. However, from the works considered, the processing parameters are similar. In conclusion, this overview showed that:

1. The possibility of systematic incorporation of incompatible functions such as thermal capacity, toughness, machinability, wear and corrosion resistance into a single part can be achieved by application of CCT.
2. Main processing parameters are size of reinforcement particles, pre-heating and pouring temperatures, and rotational speed.
3. The centrifugal casting method is simple and cost effective to execute.
4. The literature generally sees CCT as a casting process that has several advantages over the traditional gravity casting method.
5. There are challenges in its application in relation to certain shapes (only effective for cylindrical parts) and mass production.

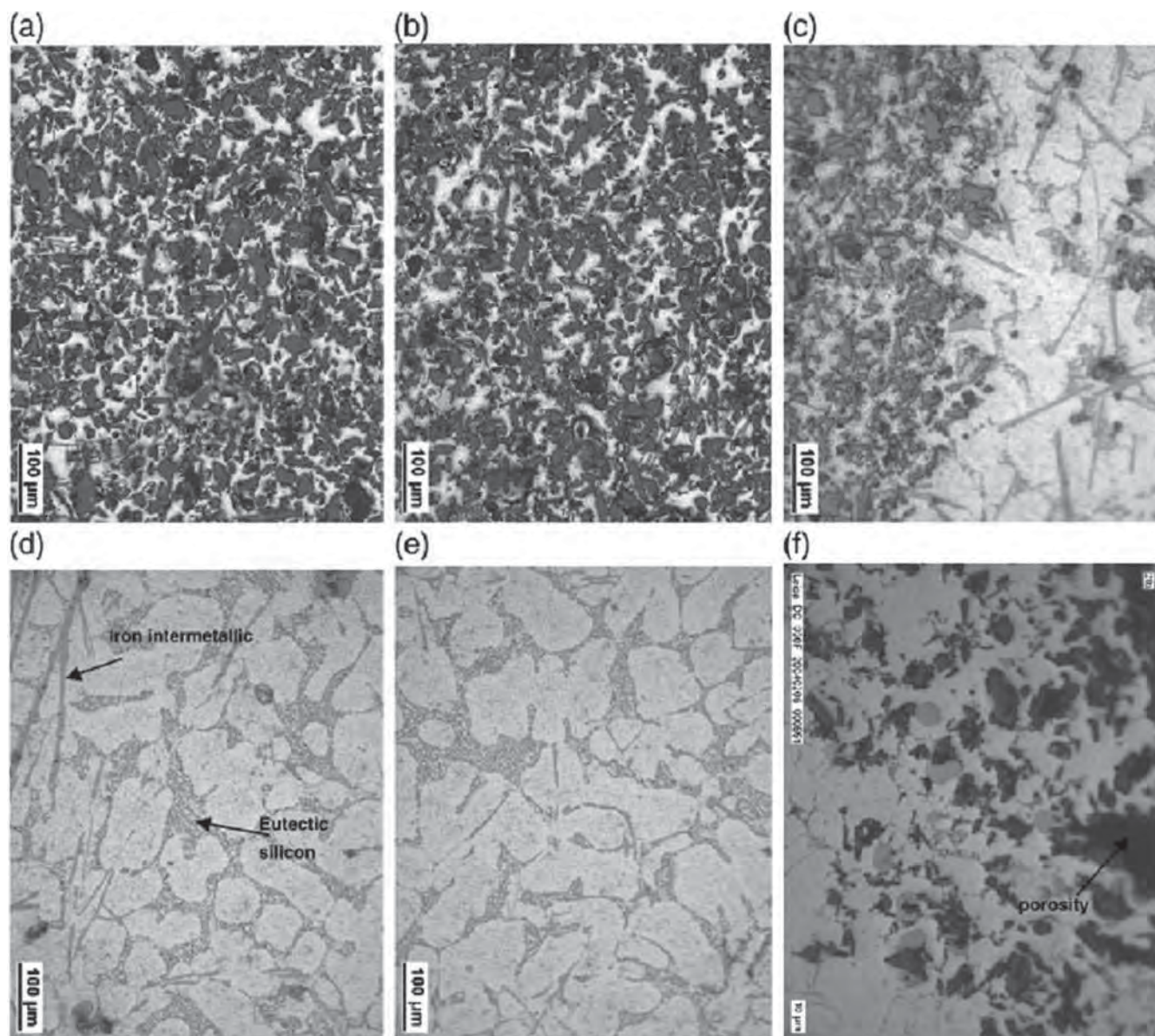


Fig. 9. Microstructures showing SiC particle distribution in Al(356)–SiC FGMs cast ring. Sequence starting from the outer to inner periphery in mm: (a) 1.5 mm; (b) 3.5 mm; (c) 5.5 mm; (d) 6.5 mm; (e) 12 mm; (f) 15 mm [44].

The authors acknowledge the Centre for Engineering Postgraduate Studies (CEPS)/HVDC/Smart grid Centre of the University of KwaZulu-Natal.

References

- [1] A. Ayyar, K.K. Chawla: *Compos. Sci. Technol.* 66 (2006) 1980. DOI:10.1016/j.compscitech.2006.01.007
- [2] A. Kelly: *Mater. Sci.* 41 (2006) 905. DOI:10.1007/s10853-013-7719-5
- [3] P.M. Ashraf, S.M.A. Shibli: *J. Alloys Compd.* 484 (2009) 47. DOI:10.1016/j.jallcom.2009.04.134
- [4] I. Bharti, N. Gupta, K.M. Gupta: *Int. J. Mater. Mech. Manuf.* 1 (2013) 221. DOI:10.7763/IJMMM.2013.V1.47
- [5] S.S. Wang: *J. Compos. Mater.* 17 (1983) 210–223. DOI:10.1177/002199838301700302
- [6] X. Lin, C. Liu, H. Xiao: *Composites Part B* 45 (2012) 8. DOI:10.1016/j.compositesb.2012.09.001
- [7] Y. Miyamoto, W. Kaysser, B. Rabin, A. Kawasaki, R. Ford (Eds.): *Functionally Graded Materials: Design, Processing and Applications*. Kluwer Academic Publishers, Dordrecht, The Netherlands (1999). DOI:10.1007/978-1-4615-5301-4
- [8] S. Naher, D. Brabazon, L. Looney: *J. Mater. Process. Technol.* 143–144 (2003) 567. DOI:10.1016/S0924-0136(03)00368-6
- [9] A. Onat, H. Akbulut, F. Yilmaz: *J. Alloys Compd.* 436 (2007) 375. DOI:10.1016/j.jallcom.2006.07.057
- [10] A. Ibrahim, F. Mohamed, E. Lavernia: *J. Mater. Sci.* 26 (1997) 1137. DOI:10.1007/BF00544448
- [11] G. Mohsen, N. Behzad, P. Masoud: *Met Mater. Int.* 18 (2012) 149. DOI:10.1007/s12540-012-0018-x
- [12] R.A. Harding, M. Wickins, Y.G. Li, in: *Progress Towards the Production of High Quality γ -TiAl Castings, Structural Intermetallics*, 3rd Int. Symp. Structural Intermetallics, Jackson Hole, WY, USA (2001) 181–189.
- [13] G. Chirita, D. Soares, F.S. Silva: *Mater. Des.* 29 (2008) 20. DOI:10.1016/j.matdes.2006.12.011
- [14] N.J. Humphreys, D. McBride, D.M. Shevchenko, T.N. Croft, P. Withey, N.R. Green, M. Cross: *Appl. Math. Modell.* 37 (2013) 7633. DOI:10.1016/j.apm.2013.03.030
- [15] Z.J. Zhang, J.X. Zhou, M.Y. Zhang, S.Y. Pang, D.M. Liao, Y.J. Yin, X. Shen: *Adv. Mater. Res.* 314–316 (2011) 364. DOI:10.4028/www.scientific.net/AMR.314-316.364
- [16] X. Wu: *Intermetallics* 14 (2006) 1114. DOI:10.1016/j.intermet.2005.10.019
- [17] J. Campbell: *Castings*, Butterworth-Heinemann, Oxford, UK (2003).

- [18] A.C. Vieira, P.D. Sequeira, J.R. Gomes, L.A. Rocha: *Wear* 267 (2009) 585. DOI:10.1016/j.wear.2009.01.041
- [19] S. Wei, S. Lampman: *ASM Handbook*, Vol. 15, Casting (2008) 667. DOI:10.1361/asmhba0005257
- [20] T.P.D. Rajan, B.C. Pai: *Acta Metall. Sin. (Engl. Lett.)* 27 (2014) 825. DOI:10.1007/s40195-014-0142-3
- [21] J.W. Gao, C.Y. Wang: *J. Heat Transfer* 123 (2000) 368. DOI:10.1115/1.1339976
- [22] E.J. Babu, T.P.D. Rajan, S. Savithri, U.T.S. Pillai, B.C. Pai: *Int. Symp. of Research Students on Mater. Sci. Eng.*, Chennai, India (2004). DOI:10.1557/PROC-845-AA9.10
- [23] A. Saiyathibrahim, N.S.S. Mohamed, P. Dhanapal in: *Int. Conf. on Systems, Science, Control, Communication, Engineering and Technology*, Karpagam Institutions, Coimbatore, India (2015).
- [24] Y. Watanabe, H. Sato, Y. Fukui: *J. Solid Mech. Mater. Eng.* 2 (2008) 842. DOI:10.1299/jmmp.2.842
- [25] Y. Watanabe, I.S. Kim, Y. Fukui: *Met. Mater. Int.* 11 (2005) 391. DOI:10.1007/BF03027510
- [26] Y. Watanabe, S. Oike: *Acta Mater.* 53 (2005) 1631. DOI:10.1016/j.actamat.2004.12.013
- [27] B.S.S. Daniel, V.S.R. Murthy, G.S. Murty: *J. Mater. Process. Technol.* 68 (1997) 132. DOI:10.1016/S0924-0136(96)00020-9
- [28] S. Jayalakshmi, M. Gupta: *Springer Briefs in Materials* (2015) 7–58. DOI:10.1007/978-3-319-15016-1_2
- [29] A. Royer, S. Vasseur: *ASM Handbook*, Vol. 15, Castings, ASM International, Ohio, UAS (1988).
- [30] A. Royer, S. Vasseur: *ASM Hand book – Castings*, ASM International, Ohio, 15 (1988) 296.
- [31] E. Panda, S.P. Mehrotra, D. Mazumdar: *Metall. Mater. Trans. A* 37 (2006) 1675–1687. DOI:10.1007/s11661-006-0109-8
- [32] S.C. Ferreira, P.D. Sequeira, W. Yoshimi, E. Arizaa, L.A. Rocha: *Wear* 270 (2011) 806. DOI:10.1016/j.wear.2011.02.007
- [33] L. Jaworska, M. Rozmus, B. Króllicka, A. Twardowska: *J. Archive. Mater. Manuf. Eng.* 17 (2006) 73.
- [34] Y. Watanabe, H. Sato, T. Ogawa, I.S. Kim: *Mater. Trans., JIM* 48 (2007) 2945. DOI:10.2320/matertrans.MB200710
- [35] T.P.D. Rajan, B.C. Pai: *Trans. Indian Inst. Met.* 62 (2009) 383. DOI:10.1007/s12666-009-0067-0
- [36] Y. Watanabe, Y. Inaguma, H. Sato, E. Miura-Fujiwara: *Materials* 2 (2009) 2510. DOI:10.3390/ma2042510
- [37] S. El-Hadad, H. Sato, E. Miura-Fujiwara, Y. Watanabe: *Materials* 3 (2010) 4639. DOI:10.3390/ma3094639
- [38] N. Radhika, R. Raghu: *Trans. Nonferrous Met. Soc. China* 26 (2016) 905–916. DOI:10.1016/S1003-6326(16)64185-7
- [39] H. Sato, Y. Inaguma, Y. Watanabe: *Mater. Sci. Forum* 638–642 (2010) 2160. DOI:10.4028/www.scientific.net/MSF.638-642.2160
- [40] C.G. Kang, P.K. Rohatgi: *Met. Mater. Trans. B* 27 (1996) 277. DOI:10.1007/BF02915054
- [41] Q. Liu, Y. Jiao, Z. Hu: *Met. Mater. Trans. B* 27 (1996) 1025. DOI:10.1007/s11663-996-0017-8
- [42] J.W. Gao, C.Y. Wang: *Mater. Sci. Eng.* 292 (2000) 207. DOI:10.1016/S0921-5093(00)01014-5
- [43] F. Bonollo, A. Moret, S. Gallo, C. Mus, in: *6th Int. Seminar on Experimental Techniques and Design in Composite Materials*, Vicenza, Italy (2003).
- [44] T.P.D. Rajan, R.M. Pillai, B.C. Pai: *Mater. Charact.* 61 (2010) 923. DOI:10.1016/j.matchar.2010.06.002
- [45] G. Chirita, I. Stefanescu, J. Barbosa, H. Puga, D. Soares, F.S. Silva: *Int. J. Cast Met. Res.* 22 (2009) 382. DOI:10.1179/174313309X380422
- [46] G. Chirita, I. Stefanescu, D. Cruz, D. Soares, F.S. Silva: *Mater. Des.* 31 (2010) 2867. DOI:10.1016/j.matdes.2009.12.045

(Received February 9, 2016; accepted July 1, 2016; colour online only; online since August 4, 2016)

Correspondence address

Mr. Williams S. Ebhota, M.Eng.
Discipline of Mechanical Engineering
University of KwaZulu-Natal
9 Mountain Rise Road
Glenmore, Durban 4001
South Africa
Tel.: +27 633840252
E-mail: willymoon2001@yahoo.com

Bibliography

DOI 10.3139/146.111423
Int. J. Mater. Res. (formerly Z. Metallkd.)
107 (2016) 10; page 960–969
© Carl Hanser Verlag GmbH & Co. KG
ISSN 1862-5282

**CHAPTER 6: FUNCTIONALLY GRADED METAL MATRIX
COMPOSITE BY CENTRIFUGAL CASTING TECHNIQUE
MATHEMATICAL CORRELATION**

W. S. Ebhota and F. L. Inambao, "Functionally graded metal matrix composite by centrifugal casting technique mathematical correlation," *African Journal of Science, Technology, Innovation and Development*, 2016. (*Submitted*)

Functionally Graded Metal Matrix Composite by Centrifugal Casting Technique

Mathematical Correlation

Williams S. Ebhota^a and Freddie L. Inambao^b

^{a, b}Discipline of Mechanical Engineering, Howard College, University of KwaZulu-Natal,
Durban, South Africa.

***Correspondence email: wilymoon2001@yahoo.com**

Abstract–The functionally graded materials (FGMs) solidification process has complicated movement phenomena of fluid, solute and heat. These phenomena control the segregation of particles in a molten matrix, interactions of particles with a solidification front and the integration of particles in the solidifying matrix. The desired particle distribution in a solidified component can be achieved by manipulating the time of solidification and this makes the study of particle motion during solidification important. This study involves the analysis of particle/matrix configuration, solid/liquid interface shape within the vicinity of the particle, thermal conductivity and the pushing/engulfment transition. An overview of the mathematical models of centrifugal casting of FGMs is presented and these include forces acting on the particle; melt particle and solid/liquid interface forces; composite thermal conductivity; heat-transfer coefficient composites; volume fraction resolution; and, particle matrix field temperature configuration.

Keywords: Functionally graded materials; Centrifugal casting process; Composite solidification and segregation; Molten matrix and reinforcement particles; Modelling of centrifugal casting.

6.1 Introduction

Mathematical models of centrifugal casting of functionally graded materials (FGMs) that describe the relationship between metal matrix and reinforcement particles, have been provided by several authors [1, 2]. The solidification process of FGMs has complex transport phenomena of fluid, heat and solute. This process governs the segregation of particles in a molten matrix, interactions of particles with the solidification front and the integration of particles in the solidifying matrix. Solidification time manipulation helps in achieving the desired particle distribution in a solidified component. Thus, the study of particle motion in solidification process is pertinent.

The growing solidification of melts containing reinforcement particles rejects the suspended particles at the solid/liquid interface which is known as the pushing phenomenon [3]. On a microscopic scale the non-uniform distribution of particles in a fully solidified part is caused by the pushing phenomenon. The distribution of particles in the solidified material is improved by growing solid/liquid interfaces resulting from particle entrapping by the solidification front. Segregation in the interdendritic zones is avoided by entrapping particles uniting with the matrix to form a composite resulting in improved properties of the composite. Study of the interaction between solid/liquid interfaces and particles is important to the particle distribution in the matrix which defines composite properties.

In the 1980's and 1990's several theoretical, experimental and review studies were carried out on solid/liquid interfaces and particle relationships using different systems [4, 5]. The studies described particle pushing based on:

- i. Thermodynamic variations in total energy when a particle is entrapped by a progressing solidification front. Thermodynamic free energy change is affected by the properties of the solid/particle interface during entrapping of the particle by the solidification front involving small velocities.
- ii. Plane thermal conductivity and thermal diffusivity ratio between the particle and the liquid [6].
- iii. Kinetic importance and critical interface velocities above which the particles are entrapped irrespective of the thermodynamic criterion. Several models linked the particle pushing phenomenon to the threshold velocity of the interface above which particle entrapment occurs.

Thermal parameter differences of solid, liquid, and particle influence the planar interface, which changes shape as it approaches the particle. The heat of the fusion of melt, temperature gradient, undercooling, comparative heat capacities of solid, liquid and particle affect the shape of interface following the particle. The study of interface shape and curvature facilitates the understanding of the interaction between the particle and the interface [3].

Shangguan, Ahuja and Stefanescu stated that melt thermal conductivity is less than particle thermal conductivity and that the shape following the particle is concave [7]. Pang, Stefanescu and Dhindaw study have a contrary view of the succinonitrile-polystyrene particle system in relation to Shangguan, Ahuja and Stefanescu's prediction on melt thermal conductivity [8]. Their view is that the interaction area between particle and interface affects

the forces acting on the particle and this depends on interface shape and curvature behind the particle.

Various studies have revealed that temperature gradient variation affects the critical velocity of the interface (V_c) proportionally [9, 10]. Cissé and Bolling showed that in an ice-water system with copper particles, as melt temperature gradient decreases, V_c increases [11]. The authors further stated that the indistinctiveness of critical interface velocity on the temperature gradient function may signal the presence of the following: the specific temperature inclination that the temperature gradient relies on for critical interface velocity tends to reverse; and, the function of melt and particle relative thermal properties depend on the thermal gradient effect [11].

A study by Kim and Rohatgi expressed solid/liquid interface shape and curvature in terms of the ratio between particle thermal conductivity and melt thermal conductivity; melt viscosity; solid/liquid interface surface tension; melt heat of fusion; and, imposed solid/liquid interface temperature gradient. The study calculated the critical interface velocity exploiting attractive and repulsive forces acting force balance [3].

Hanumanth and Irons investigated both numerical and experimental solidification of FGMs, aluminium alloy-SiC composites and developed a one-dimensional enthalpy model [12]. This study used the Richardson-Zaki hindered settling correlation to estimate particle velocity. This can cause significant phase velocity overestimation of particles by a factor of $1/1-\epsilon_p$ because the methodology means liquid counter-current displacement flow resulting from particle sedimentation which is unaccounted for, where ϵ_p is the particle phase velocity. The study includes the investigation of thermal conductivity effects and the cooling rate of SiC particles. The Scheil equation was used to explain mushy zone evolution. For an accurate depiction of cooling rates and particle settling, SiC particle thermal conductivity on the order of a single crystal was planned. However, the recommended cooling condition resulted in very little settling.

A multiphase model for alloy solidification of metal matrix particle composites with convection was developed by Feller and Beckermann [13]. The Happel hindered settling function model was applied to several one- and two-dimensional Al-7wt%Si/SiC systems applications. Simulation and experimental sedimentation results of A356 systems with clustering and non-clustering SiC particles showed good conformity [14]. Initial studies had

negligible information on time evolution of the coupled solidification and sedimentation activities and their main focus was on final particle distribution.

This study resulted in undefinable solidifying matrix particle segregation mechanisms, which are required for FGM design. In the past, detailed data on the time evolution of particle concentration distribution of solidifying matrix was insufficient due to limited experimental work. Experimental data availability is necessary to accurately authenticate complex FGM solidification models (Gao and Wang 2001). To bridge this gap, Gao and Wang studied the solidification relationship between particle transport and freezing front dynamics [15]. In their study, the gravity casting solidification process of FGMs was numerically and experimentally investigated. A fixed-grid, the finite-volume method, was used to solve numerically one-dimensional multiphase solidification model equations developed by the study. Experimental results were used to validate the model which was applied in Al-SiC FGM efficient computational prototyping. The experimental setup is shown in Figure 6.1.

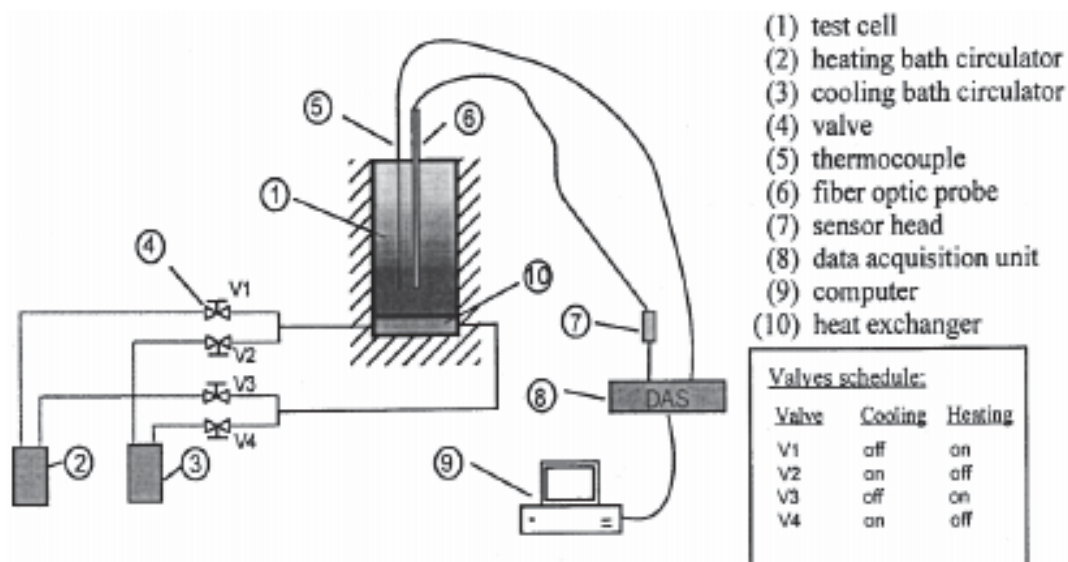


Figure 6.1: Schematic of Gao and Wang experimental setup [15]

Distilled water and succinonitrile (SCN) were used as matrix liquids and glass beads as particles in a rectangular ingot transparent model experiment. Important processing parameters effects were studied and the solidified ingot showed a graded particle distribution zone towards the bottom and a particle free zone in the top portion. The study observed that:

- i. Higher superheat causes slower solidification which results in a thicker particle-free zone and higher particle concentration towards the bottom.
- ii. A thinner particle-free region resulting from higher initial particle volume fraction.
- iii. Particle settling was suppressed by lower cooling temperatures.

- iv. The desired gradient attribute of the solidified component can be manipulated with optimisation of processing parameters such as particle size, particle volume fraction, cooling rate and superheat. This was obtained from simulations results of Al/SiC FGMs.

Investigation of suspended ceramic particles in aluminium melts was performed during the fabrication of FGM (Al-SiC) by means of the vertical centrifugal casting method [16]. Forces acting on the particle, force balance and motion of the particle in the melt during vertical centrifugal casting were modelled mathematically and simulated using Matlab. Process parameters such as solidification rate, mould rotational speed, mould temperature, particle size and particle fraction of segregation were examined. The results show that with the particle at an initial position of 0.005, the process at 800 rpm gave the particle a radial distance of 21 mm while 400 rpm reduces the penetration by 62 %. 1200 rpm increased the penetration by 57 %.

Balout and Litwin conducted experiments on aluminium alloy A356 reinforced by 10 % volume of 12 μm SiC fabricated with CCT for particle distribution modelling [17]. The study revealed that particle distribution in the outer surface varies according to viscosity. Different pouring temperatures (650 °C, 680 °C, and 700 °C) and mould temperatures (30 °C, 100 °C, 350 °C, and 400 °C) were used. The study defined and modelled the following parameters: particle velocity; deceleration; displacement; and, segregation during the cooling process. The study concluded that:

- i. Behaviour of particles varies with time, position and viscosity.
- ii. Melt viscosity and centrifugal radius variations during centrifugation change on particle segregation process.
- iii. Particle segregation is heightened by increasing mould and pouring temperatures and this favours higher particle volume fractions in the periphery of the casting.

A study by Emila, Dipak, and Mehrotra developed a prediction model for centrifugally cast FGM particle segregation patterns and one-dimensional transient heat-transfer coupled with casting and mould temperatures distribution and solidification time [18]. The force balance equation containing centrifugal, drag and repulsive (force possessed by a particle in the solid/liquid interface neighbourhood) forces was discussed. The pure implicit finite volume method was applied to find model equation solutions using time-step technique transformed variables. The study noted that the particle-rich region thickness in FGM decreases with increase in rotational speed; particle size; initial pouring and mould temperatures; and,

particles and molten matrix density difference. Other observations made by the study are: heat transfer coefficient reduction at the casting/mould interface increases solidification time and solid-particles segregation formation; solidification time and particle-rich region thickness increases with reinforcing particles volume fraction increase; initial volume fraction of particles in the outer layers of Al-Al₂O₃ and Al-SiC FGMs remains the same or less using finer particles, lower rotational speeds, and an enhanced heat transfer coefficient at the casting/mould interface; heat-transfer coefficients reduction and increase in rotational speed and particles size results in intense segregation at the outer region of FGMs, although intense segregation at the innermost layers was predicted for the Al-Gr system.

6.2 Mathematical expressions

In this section of the study, analysis of the particle/matrix configuration, solid/liquid interface shape within the vicinity of the particle, thermal conductivity and pushing/engulfment transition critical condition will be carried out.

Several authors based their model formation on the following assumptions [17-21]:

- i. One-dimensional heat flow perpendicular to the mould wall.
- ii. Homogeneously distributed solid particles and metal matrix instantaneously fill the mould.
- iii. Solid particles and metal matrix thermal properties at invariant temperature.
- iv. Solidification is accelerated by casting/graphite mould interface caused by casting contraction.
- v. Buoyancy causes natural convection and movement of particles is neglected.
- vi. Solid and liquid regions interface considered planar.
- vii. Thermal resistance between particles and molten metal is zero.
- viii. Shape of reinforcement particles is considered as spherical.
- ix. Liquidus front stops particle motion.
- x. The volume fraction of large solid particles in the molten metal retards particle movement. The apparent viscosity, v_c : $v_c = v \left[1 + 2.5v_f(t) + 10.05v_f^2(t) \right]$.
- xi. Maximum volume fraction for segregation of particles occurrence is 52 %.

6.2.1 Particle and solid/liquid interface

The analysis of particle and solid/liquid interface encompasses a discussion on Stokes' flotation velocity, $V_f =$ particle matrix field temperature configuration; evaluation of

solid/liquid interface shape on the vicinity of the particle; evaluation of forces on the particle; and, defining a critical condition for pushing/engulfment transition.

6.2.1.1 The discussion on Stokes' flotation velocity

For acceleration = 0, the spherical particle velocity according to Stoke's law is:

$$V_f = \frac{4R^2 \Delta\rho \omega^2 r}{18\mu} \quad \text{_____} \quad (6.1)$$

Where R = radius of the particle; ω = angular velocity; r = particle position, μ = melt viscosity; $\Delta\rho = \rho_P - \rho_m$ = density difference; and, ρ_P and ρ_m particle and molten metal densities respectively.

The solid/liquid front moves against gravity in a solid/liquid system with a steady state velocity, V. As a result, it experiences force of gravity and Stokes' flotation velocity, V_f :

The following conditions may occur in a system:

$V_f > V$ (particle float away); $V > V_f < 0$ (particle approach interface; sedimentation); $V > V_f$ only when particle approaches and interaction is occurring. V_f is therefore referred to as the threshold velocity.

6.2.1.2 Evaluation of solid/liquid interface shape in particle vicinity

Figure 6.2 describes the relationship between the spherical particle and the solid/liquid interface as the particle approaches the interface. The particle presence affects the velocity of the interface and this velocity is categorised in two ways: not affected by the particle, V_1 ; and, affected by the particle, V_2 .

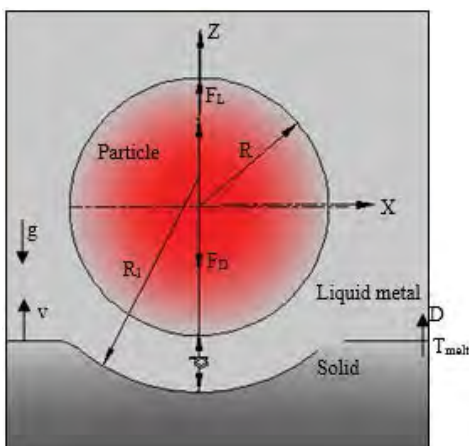


Figure 6.2: Representation of a particle near solid/liquid interface and the forces acting on the particle [7]

Considering Figure 6.2, the distance between the particle and interface at $Z = 0$ is d . This means:

$$T_m [X = 0, Z = -(R + d)] = T_{melt} \quad \text{_____ (6.2)}$$

For isothermal,

$$\frac{R + d \left(1 + \frac{a}{b}\right)}{r \left[1 + a \left(\frac{R}{r}\right)^3\right]} = \cos \theta \quad \text{_____ (6.3)}$$

$$\text{Where } a = \frac{1 - \alpha}{2 + \alpha} \quad \text{_____ (6.4)}$$

$$b = 1 + \frac{d}{R} \quad \text{_____ (6.5)}$$

Figures 6.3 and 6.4 depict solid/liquid interface shapes at a constant d and varied thermal conductivity ratio, α , derived from equation (3).

At $\alpha < 1$, the bump is created (pushing is made easier); at $\alpha = 1$, the planar surface is formed; at $\alpha > 1$, the trough is created (conductive for engulfment).

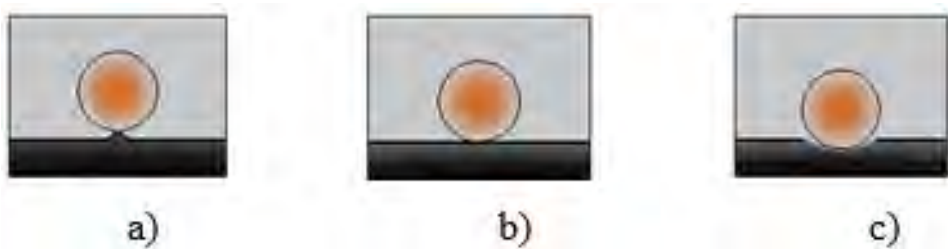


Figure 6.3: Depiction of solid/liquid interface shapes evolution, a) $\alpha < 0.1$; b) $\alpha = 1$; and c) $\alpha > 1$

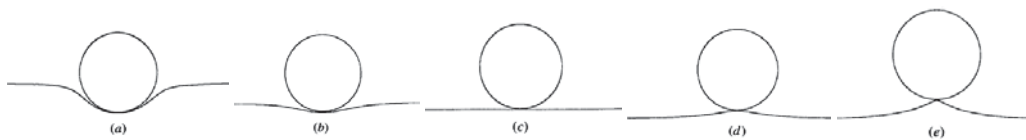


Figure 6.4: Depiction of solid/liquid interface shapes for various conditions

Conditions: At constant d and varied thermal conductivity ratio a) $\alpha = 11.1$; b) $\alpha = 2.0$; c) $\alpha = 1.0$; and d) $\alpha = 0.06$

Interface radius of curvature at $X = 0$, is given by:

$$R_l = \frac{2a - b}{3a} (R + d) \quad \text{_____ (6.6)}$$

When $d < R$,

$$R_l = \left(\frac{2a - b}{3a}\right) R = \left(\frac{\alpha}{\alpha - 1}\right) R \quad \text{_____ (6.7)}$$

$$f = \frac{R_l}{R_l - R} = \alpha \quad \text{_____ (6.8)}$$

6.2.2 Forces acting on particle in a melt

A particle suspended in molten metal during vertical centrifugal casting is subjected to four different forces as represented in Figure 6.5: gravitational force, F_G ; centrifugal force caused by mould rotation, F_C ; drag force due to viscosity effect, F_D ; and, repulsive force or van der Waal forces caused by solid-liquid interface movement, F_L . Force of gravity is often neglected because it is very small compared to centrifugal force [17, 18, 22, 23].

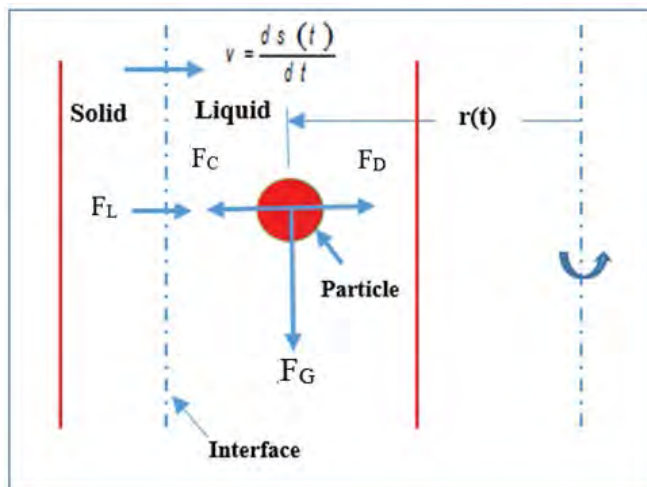


Figure 6.5: Representation of forces acting on a particle moving in molten metal

The three forces are defined as follows:

6.2.2.1 Gravitational force

Gravitational force, F_G and its direction are functions of the density difference between the particle and the melt. F_G is mathematically expressed as:

$$F_G = \frac{4}{3} \pi R^3 \Delta \rho g \quad \text{_____ (6.9)}$$

Where R = particle radius; g = gravitational acceleration; μ = melt viscosity; $\Delta \rho = \rho_p - \rho_m$ = density difference; and, ρ_p and ρ_m particle and molten metal densities respectively.

6.2.2.2 Drag force

Drag force, F_D , is given by Stokes' law:

$$F_D = 6\pi\eta VR \quad \text{_____ (6.10)}$$

When $d < R$ for planar surface:

$$F_D = 6\pi\eta V \frac{R^2}{d} \quad \text{_____ (6.11)}$$

When $d < R$ for non-planer surface

$$F_D = 6\pi\eta V \frac{R^2}{d} \left(\frac{R_l}{R_l - R} \right) \quad \text{_____ (6.12)}$$

$$= 6\pi\eta V \frac{R^2}{d} \alpha^2 \quad \text{_____ (6.13)}$$

If $R_l > 0$ as for $\alpha > 1$, concave interface will be formed with greater F_D while lesser F_D and convex are formed by $R_l < 0$ and $\alpha < 1$.

6.2.2.3 Repulsive/Van der Waals force

This force is due to the interface energy between the liquid and solid phases, σ_{sl} ; between liquid phase and particle, σ_{lp} ; and between solid phase and particle, σ_{sp} ;

This energy is defined as

$$F_l = 2\pi R \Delta\sigma \quad \text{_____ (6.14)}$$

$$\Delta\sigma = \Delta\sigma_0 \left(\frac{a_0}{a_0 + d} \right) \quad \text{_____ (6.15)}$$

When $a_0 = r_p + r =$ sum of radii of atoms at the surface layer of the particle and the solid, n is 2 to 7

$$\Delta\sigma_0 = \sigma_{sp} - \sigma_{lp} - \sigma_{sl} \quad \text{_____ (6.16)}$$

So that,

$$F_l = 2\pi R \Delta\sigma_0 \left(\frac{a_0}{a_0 + d} \right)^n \quad \text{_____ (6.17)}$$

Potschke and Rogge assumed van der Waals force for two particles with radii $R + R_l$:

$$F_l = 2\pi R \Delta\sigma_0 \left(\frac{a_0}{a_0 + d} \right)^2 \frac{R_l}{R_l - R} \quad \text{_____ (6.18)}$$

exerted on a fish as it approaches the water tank wall. Several factors define fish behaviour in a water tank and these include swimming ability; velocity relative to the ambient water; interaction among the individuals; swimming speed uniformity; the direction of movements within the school; and, repulsion and attraction near the wall. The psychological phenomenon of a fish as a living entity comes into play by averting the possibility of it striking the wall as it gets close. Dispersed particles in solidifying liquid do not possess such psychological phenomena so cannot avert the possibility of striking the wall and are not rejected by the solidification front. Their velocities reduce at the influence zone and are finally trapped and absorbed by the solidification zone. The investigation was based on *repulsive force not independent of the tank shape and size in parameters estimation* according to Sannomiya and Matuda [7].

6.2.2.4 Force balance equation, F_{net}

The force balance equation, F_{net} is taken as:

$$F_{net} = F_C - F_D - F_L \quad (6.20)$$

The repulsive force is associated particles within a solid wall or solid-liquid interface. The dynamic force balance that is not induced by solid wall/interface is:

$$F_{net} = F_C - F_G \quad (6.21)$$

The force balance equation with the assumption that the fluid flow is laminar ($Re \leq 1$) is:

$$4/3 * \pi * R^3 * \rho_p (d^2 r/dt) = 4/3 * \pi * R^2 (\rho_p - \rho_m) \omega^2 * r - 6 * \pi * R * \mu (dr/dt) \quad (6.22)$$

The solution of net force without repulsive force of a particle at a given position moving at constant velocity at any given time, t , is:

$$r(t) = r_0 \exp \left[\frac{4\omega^2 (\rho_p - \rho_m) R^2 t}{18\mu} \right] \quad (6.23)$$

Where r_0 = position of the particle at time $t = 0$.

6.2.3 Significant conditions for pushing/engulfment transition

The three forces (F_G , F_D and F_L) acting on the particle play separate roles in pushing/engulfment transition. Upward growth condition:

F_G = conducive to pushing when $\Delta\rho > 0$

F_L = conducive to pushing when $\sigma_0 > 0$

F_D = conducive to engulfment when

For F_G and F_L the condition is vice versa while F_D is always engulfment.

F_D is a function of V and d while F_L is a function of d . At equilibrium velocity, V_e :

$$F_G + F_L - F_D \text{ ————— (6.24)}$$

That is:

$$\frac{4}{3} \pi R^3 \Delta \rho g + 2 \pi R \Delta \sigma_0 \left(\frac{a_0}{a_0 + d} \right)^n \alpha - 6 \pi \eta V_e \frac{R^2}{d} \alpha^2 = 0 \text{ ————— (6.25)}$$

So that,

$$V_e = \frac{d}{3 \eta \alpha} \left[\frac{\Delta \sigma_0}{R} \left(\frac{a_0}{a_0 + d} \right)^n + \frac{2 R \Delta \rho g}{3 \alpha} \right] \text{ ————— (6.26)}$$

If $R \gg R^* = \sqrt{\left[\frac{3 \Delta \sigma_0 \alpha}{8 / (\Delta \rho / g)} \right]}$, F_G is neglected because is very small compared to F_D and

F_L , equation (30) becomes:

$$V_e = \frac{\Delta \sigma_0}{3 \eta \alpha} \frac{d}{R} \left[\left(\frac{a_0}{a_0 + d} \right)^n \right] \text{ ————— (6.27)}$$

From equation (27), critical distance can be expressed, d_c :

$$d_c = \frac{a_0}{n-1} \text{ ————— (6.28)}$$

Critical velocity then becomes, V_c :

$$V_c = \frac{a_0}{3 \eta \alpha (n-1)} * \frac{\Delta \sigma_0}{R} \left(\frac{n-1}{n} \right)^n \text{ ————— (6.29)}$$

When $n = 2$ and $d_c = a_0$;

$$V_c = \frac{a_0 \Delta \sigma_0}{12 \eta \alpha R} \text{ ————— (6.30)}$$

6.2.4 Volume fraction resolution

Discretisation of cast thickness into n numbers of equal sizes is used in determining liquid metal matrix fraction variation and segment nodal points are considered at the extreme positions. The segment volume fraction of particles is defined as:

$$V_{fs} = \frac{V_s}{V_s + V_l} = \frac{1}{1 + \frac{\rho_s m_l}{\rho_l m_s}} \quad (6.31)$$

Where V_{fs} = volume fraction of the particle; V_s = volume of reinforced particles and; V_l = volume of the metal matrix in each segment.

Solid particles and matrix melt volumes and masses are defined from the correlations:

$$V_s = V_{fs} V \quad V_l = V - V_s \quad (6.32)$$

$$m_s = V_s \rho_s \quad m_l = V_l \rho_l \quad (6.33)$$

Where V = total volume of each segment; m_s = mass of solid in each segment, and m_l = total mass of liquid in each segment.

Initial time $t = 0$ particle positions are considered at the nodal points for easiness. New positions $t + \Delta t$ are defined by equation (23) or (25). Particle velocities at different nodal points vary due to particle motion dependence on location in the liquid melt. The particle's new position could be in the node or segment and both the number of particles in a segment and volume can be calculated. Segment volume is constant at all times while the new volume fraction of particles at $t = 1$ per unit length can be estimated. Calculated new positions become initial locations for particles in the next time.

6.2.5 Particle matrix field temperature configuration 153

In the temperature configuration analysis, the following assumptions were made [7]: conduction heat transfer was considered while convection and viscous heat dissipation were neglected; solid/liquid interface latent heat release was ignored; solid and liquid phases have the same thermal conductivity; material parameters are not depending on temperature matrix which is considered as an isotropic medium; and Azimuthal symmetry, the heat conduction equation in spherical coordinates.

Considering Figure 1, the heat by Fourier's law is defined as:

$$\frac{1}{r^2} * \frac{\partial}{\partial r} \left(\frac{r^2 \partial T}{\partial r} \right) + \frac{1}{r^2 \sin \theta} * \frac{\partial}{\partial \theta} \left(\sin \theta \frac{\partial T}{\partial \theta} \right) = 0 \quad (6.34)$$

6.2.6 Boundary conditions

In Z-direction far away from the particle at constant temperature gradient:

$$\left(\frac{\partial T}{\partial r} \right)_{r \rightarrow \infty} = G \quad (6.35)$$

Particle/matrix temperature continuity across the interface:

$$(T_m)_{r=R} = (T_p)_{r=R} \quad (6.36)$$

Reference temperature T_0 :

$$(T_m)_{z \rightarrow \infty} = T_0 \quad (6.37)$$

Applying the boundary conditions to equation (12) defines temperature distribution in the matrix, T_m as well as in the particle, T_p :

$$T_p = T_0 - \left(\frac{3}{\alpha + 2} \right) Gr \cos \theta \quad (16) \quad T_m = T_0 - \left[1 + \left(\frac{1 - \alpha}{2 + \alpha} \right) \left(\frac{R}{r} \right)^3 \right] Gr \cos \theta \quad (6.38)$$

Where T_0 = reference temperature; G = imposed thermal gradient on solid/liquid interface away from the particle; R = particle radius; $r = R + d$; d = distance between particle surface and solid/liquid interface; and $\alpha = \frac{K_p}{K_m}$, ratio of particle thermal conductivity (K_p) to melt thermal conductivity (K_m). The ratio $\alpha = 1$ if conductivities are equal.

The value of α affects the heat flow flux as follows (see Figure 6.6) (Shangguan, Ahuja, and Stefanescu 1992):

- i. When $\alpha = 1$, global heat flows in Z-direction and isothermals are parallel and at a 90° angle to the heat flux line.
- ii. When $\alpha \neq 1$, isothermal is deflected, (Figure 6.2a).
- iii. When $\alpha < 1$, heat flux diverges from the particle (Figure 6.2b).
- iv. When $\alpha > 1$, heat flux converges toward the particle (Figure 6.2c).

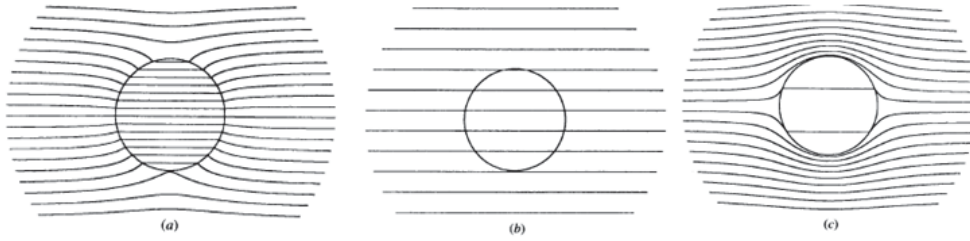


Figure 6.6: Effects of thermal conductivity ratio, α , on heat flux: a) $\alpha < 1$; b) $\alpha = 1$; c) $\alpha > 1$

6.2.7 Heat conduction expression

The schematic in Figure 6.7, represents the centrifugal casting system of MMCs which have been used by several authors in mathematical model formulation [4, 18]. During casting, solidification starts by heat conduction from the molten region to the surrounding area through the solidified composite region, graphite mould and steel mould respectively. Further, some of the heat is radiated from the cast inner surface. The direction of heat flow in a centrifugal casting process is shown in Figure 6.7.

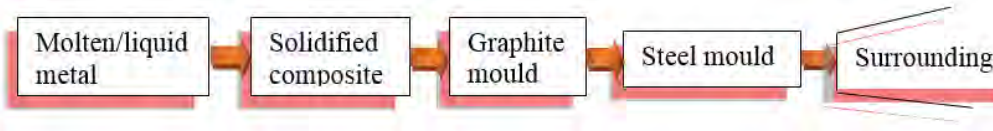


Figure 6.7: Direction of heat flows in a centrifugal casting system

6.2.8 Governing expression

The heat transfer of casting and the mould is controlled by the unsteady-state heat one-dimensional conduction equation in cylindrical coordinate forms:

$$\rho_i c_i \left(\frac{\partial T_i}{\partial t} \right) = \frac{1}{r} \frac{\partial}{\partial r} \left(r k_i \frac{\partial T_i}{\partial r} \right) \quad (6.39)$$

Where $i = l_c, s_c$, and g depict regions; molten composite, solid composite graphite, and steel mould respectively.

6.2.9 Composites thermophysical properties

Rule of mixtures defines densities, thermal conductivities, and specific heats of composites in solid or liquid regions as a function of the volume fraction of particles, $V_f(t)$ at any time t :

$$P_c = (1 - v_f(t)) P_m + v_f(t) P_p \quad (6.40)$$

Where P_c = property of the composite being considered; P_m and P_p = properties of matrix and particles, respectively.

6.2.10 Centrifugal casting system initial conditions

Considering a centrifugal casting system as depicted in Figure 6.8, the mould is preheated to a temperature (T_M) which is a step to avoid thermal shock. Temperature distribution before pouring at $t = 0$ is given as:

$$T_{lc} = T_p$$

$$T_g = T_m = T_M$$

Where T_p = molten metal before pouring

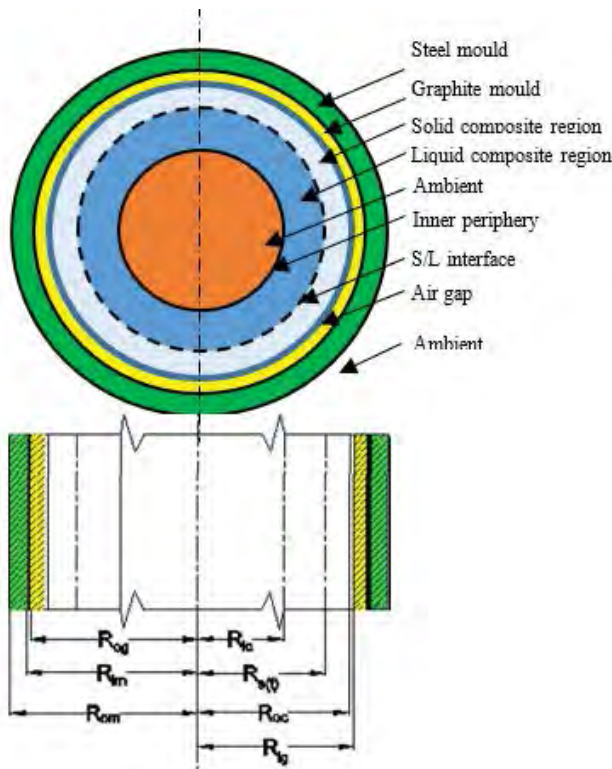


Figure 6.8: Schematic depiction of centrifugal cast system of metal matrix composites

6.2.11 Boundary conditions

The regions' boundary conditions in casting and mould are as follows.

- i. Casting inner surface, at $r = R_{ic}$

$$-k_k \frac{\partial T_{lc}}{\partial r} = h_2 (T_{ci} - T_\beta) \quad \text{_____} \quad (6.41)$$

- ii. Graphite mould outer surface, at $r = R_{og}$

$$-k_{sc} \frac{\partial T_{sc}}{\partial r} = h_1 (T_{co} - T_{gi}) \quad \text{_____} \quad (6.42)$$

iii. Casting outer surface, at $r = R_{oc}$

$$-k_g \frac{\partial T_g}{\partial r} = h_1 (T_{co} - T_{gi}) \quad (6.43)$$

iv. Graphite mould inner surface, at $r = R_{ig}$

$$-k_g \frac{\partial T_g}{\partial r} = h_4 (T_{go} - T_{mi}) \quad (6.44)$$

v. Steel mould inner surface of the, at $r = R_{im}$

$$-k_m \frac{\partial T_m}{\partial r} = h_4 (T_{go} - T_{mi}) \quad (6.45)$$

vi. Steel mould outer surface of the, at $r = R_{om}$

$$-k_m \frac{\partial T_m}{\partial r} = h_3 (T_{mo} - T_\alpha) \quad (6.46)$$

vii. Solid-liquid interface, at $r = R_s(t)$

$$T_{sc} = T_{lc} = T_f$$

viii. The sum of the rate of heat provided to liquid-phase and heat released during solidification at the interface is equal to the rate of solid phase heat removal. This defines the energy balance at the interface at $r = R_s(t)$

$$-k_{sc} \frac{\partial T_{sc}}{\partial r} = -k_{lc} \frac{\partial T_{lc}}{\partial r} + \rho_{sc} H \frac{\partial s(t)}{\partial t} \quad (6.47)$$

6.2.12 Formulation of heat-transfer coefficient

The rate of liquid composite solidification is affected substantially by the casting-graphite mould interface created by contraction of the casting; thermal expansion of the mould during solidification; and, the graphite-steel air gap formed by imperfect contact. The casting and graphite mould heat transfer coefficient varies due to air gap and is assumed as [28]:

$$h_1 = h_i \left(\frac{h_f}{h_i} \right)^{\frac{s(t)}{r_i}} \quad (6.48)$$

Where h_i = initial heat-transfer coefficient; h_f = final heat-transfer coefficient; $s(t)$ = solidified thickness, and; r_i = total casting thickness.

6.2.13 Composite thermal conductivity, K

Calculation of thermal conductivity, K , of the composite according to the effective middle theory (EMT) [29]:

$$K = K_m \frac{(1 - V_p)}{(1 + 0.5V_p)} \quad (6.49)$$

Where K_m = matrix thermal conductivity (W/m K); and V_p = particle volume fraction.

Calculation of particle concentration:

$$C_p^{Ai} \Big|_{i=0}^A = \frac{m_p^{Ai}}{m_T^{Ai}} \times 100\% \quad (6.50)$$

Where $C_p^{Ai} \Big|_{i=0}^A$ = concentration of the particles in an area A_i ; m_p^{Ai} = mass of the particles in an area A_i ; and m_T^{Ai} = total mass of the whole microstructure in an area A_i .

6.3 Conclusion

A FGM component is useful in a place where the part is needed to function in an environment under various working conditions. For instance, a piston receives both high pressure and high temperature on its top surface. It is, therefore, desirable to have particular particles at the surface for better wear and thermal resistance. On the other hand, uniform particle distribution may be required for part functionality. There are factors in macro and micro forms that control the pattern of particle distribution in metal matrix composites (MMCs). For macro forms, uniform distribution of particles is achieved by application of mechanical or magnetic stirring. Uniform particle distribution is achieved microscopically by rapid cooling to accelerate particle engulfment. Wettability between the particle and melt is another factor that determines particle distribution pattern. Particle distribution prediction modelling helps in designing MMCs as desired by functionality need.

Bibliography

- [1] S. V. Gawali and V. B. Tungikar. "Improvement in tribological properties by improving geometry of reinforcement particles." *International Journal of Engineering Science and Technology (IJEST)*, vol. 3, pp. 8289-8297, 2011.
- [2] R. Zagórski and J. Sleziona, "Pouring mould during centrifugal casting process," *Archives of Materials Science and Engineering*, vol. 28, pp. 441-444, 2007.
- [3] J. K. Kim and P. K. Rohatgi, "An analytical solution of the critical interface velocity for the capturing of insoluble particles by a moving solid/liquid interface," *Metallurgical and Materials Transactions A*, vol. 29A, pp. 351-358, 1998.
- [4] P. K. Rohatgi, R. Asthana and F. Yarandi, "Formation of solidification microstructures in cast metal matrix particle composites." In: *Solidification of Metal Matrix Composites, Proceedings of the Conference*, Indianapolis, Indiana, USA, Oct. 1-5, 1989 (A91-54879 23-24). Minerals, Metals, and Materials Society, Warrendale, Pennsylvania, pp. 51-57, 1990.
- [5] D. M. Stefanescu and B. K. Dhindaw, *Metals Handbook*, vol. 15. Metals Park, OH: ASM International, 1988.
- [6] B. V. Derjaguin, *Theory of Stability of Colloids and Thin Films*. New York, NY: Consultants Bureau, 1989.
- [7] D. Shangguan, S. Ahuja and D. M. Stefanescu, "An analytical model for the interaction between an insoluble particle and an advancing solid/liquid interface," *Metallurgical Transactions A*, vol. 23A, pp. 669-680, 1992.
- [8] H. Pang, D. M. Stefanescu and B. K. Dhindaw, "Influence of interface morphology on the pushing/engulfment transition of polystyrene particles in succinonitrile + water matrices," In *Proceedings of the 2nd International Conference on Cast Metal Matrix Composites*, Tuscaloosa, Alabama, pp 57-69, October, 1993.
- [9] A. A. Chernov, D. E. Temkin and A. M. Melnikova, "Theory of the capture of solid inclusions during the growth of crystals from the melt." *Soviet Physics Crystallography*, vol. 21, pp. 369-374, 1976.
- [10] R. P. Smith, D. Li, D. W. Francis, J. Chappuis and A. W. Newmann, "Experimental study of the relationship between the free energy of adhesion and the repulsive force

- between a particle and a solidification front." *Journal of Colloid and Interface Science*, vol. 157, pp. 478-484, 1993.
- [11] J. Cissé and G. F. Bolling, "The steady-state rejection of insoluble particles by salol grown from the melt," *Journal of Crystal Growth*, vol. 11, pp. 25-28, 1971.
- [12] G. S. Hanumanth and G. A. Irons, "Solidification of particle-reinforced metal-matrix composites," *Metallurgical and Materials Transactions B*, vol. 27B, pp. 663-671, 1996.
- [13] R. J. Feller and C. Beckermann, "Modeling of solidification of metal-matrix particulate composites with convection," *Metallurgical and Materials Transactions B*, vol. 28B, pp. 1165-1183, 1996.
- [14] J. Happel, "Viscous flow in multiparticle systems: slow motion of fluids relative to beds of spherical particles," *AIChE Journal*, vol. 4, pp. 197-201, 1958.
- [15] J. W. Gao and C. Y. Wang, "Transport phenomena during solidification processing of functionally graded composites by sedimentation." *Journal of Heat Transfer*, vol. 123, pp. 1-8, 2001.
- [16] S. P. A. Abdul, K. Sandeep and P. R. Shalij, "Mathematical modeling and computer simulation of particle gradient distribution in a vertical centrifugally cast functionally gradient composite," *International Journal of Innovative Research in Science, Engineering and Technology*, vol. 3 pp. 14441-14447, 2014.
- [17] B. Balout and J. Litwin, "Mathematical modeling of particle segregation during centrifugal casting of metal matrix composites," *Journal of Materials Engineering and Performance*, vol. 21, pp. 450-462, 2012.
- [18] P. Emila, M. Dipak, and S. P. Mehrotra, "Mathematical modeling of particle segregation during centrifugal casting of metal matrix composites," *Metallurgical and Materials Transactions* vol. 37A, pp. 1675-1687, 2006.
- [19] J. Szekely, *Fluid Flow Phenomena in Metal Processing*. New York, NY: Academic Press, 1979.
- [20] E. J. Babu, T. P. D. Rajan, S. Savithri, U. T. S. Pillai and B. C. Pai, "Theoretical analysis and computer simulation of the particle gradient distribution in a centrifugally cast functionally gradient material," presented at the International Symposium of

- Research Students on Materials Science and Engineering, Chennai, India, 20-22 December, 2004.
- [21] F. Bonollo, A. Moret, S. Gallo and C. Mus, "Cylinder liners in aluminium matrix composite by centrifugal casting," presented at the 6th International Seminar on Experimental Techniques and Design in Composite Materials, Vicenza, Italy, 18-20 June, 2003.
- [22] J. S. Jerzy and D. Ludmil, "Metallic functionally graded materials: a specific class of advanced composites," *Journal of Material Science Technology*, vol. 29, pp. 297-316, 2013.
- [23] A. W. Rempel and M. G. Worster, "Particle trapping at an advancing solidification front with interfacial-curvature effects," *Journal of Crystal Growth*, vol. 223, pp. 420-432, 2001.
- [24] R. J. Dashwood, Y. M. Youssef and P. D. Lee, "Effect of clustering on particle pushing and solidification behaviour in Tib reinforced aluminium Pmmcs." *Composites A*, vol. 36, pp. 747-763, 2005.
- [25] A. W. Rempel and M. G. Worster, "The interaction between a particle and an advancing solidification front," *Journal of Crystal Growth*, vol. 205, pp. 427-440, 1999.
- [26] R. Sasikumar and T. R. Ramamohan, "Distortion of the temperature and solute concentration fields due to the presence of particles at the solidification front—effects on particle pushing," *Acta Metallurgica et Materialia*, vol. 39 pp. 517-522, 1991.
- [27] G. F. Bolling and J. Cissé, "A theory for the interaction of particles with a solidifying front," *Journal of Crystal Growth*, vol. 10, pp. 56-66, 1971.
- [28] L. Lajoie and M. Suery, "Modelling of particle segregation during centrifugal casting of Al-Matrix composites," In *Cast Reinforced Metal Composites. Proceedings of the World Materials Congress, 24-28 September Chicago*, S. G. Fishman and A. K. Dhingra, Eds, Materials Park, OH: ASM International, 1988.
- [29] A. Grabowski, M. Nowak and J. Sleziona, "Optical and conductive properties of AlSi-Alloy/SiC composites: application in modelling CO₂ laser processing of composites," *Optical Lasers Engineering*, vol. 43, pp. 233-246, 2005.

**CHAPTER 7: SMART DESIGN AND DEVELOPMENT OF A SMALL
HYDROPOWER SYSTEM AND EXPLOITATION OF LOCALLY
SOURCED MATERIAL FOR PELTON TURBINE BUCKET
PRODUCTION**

W. S. Ebhota and F. L. Inambao, "Smart design and development of small hydropower system and exploiting of locally sourced material for Pelton turbine bucket production," *Iranian Journal of Science and Technology, Transactions of Mechanical Engineering*, 2016. *(Under review.)*

Smart Design and Development of a Small Hydropower System and Exploitation of Locally Sourced Material for Pelton Turbine Bucket Production

Williams S. Ebhota^a and Freddie L. Inambao^b

^{a, b}Discipline of Mechanical Engineering, Howard College, University of KwaZulu-Natal, Durban, South Africa.

Correspondence email: willymoon2001@yahoo.com

Abstract–Small hydropower (SHP) systems are known to be an environmentally friendly, cost effective and simple form of renewable energy production, appropriate for rural electrification in sub-Saharan Africa (SSA). Greater access to power in SSA can be facilitated through domestic design and development of SHP components and systems. Domestic participation in the design, manufacturing of SHP components and application of SHP systems can be promoted through SHP capacity building and use of locally sourced materials. This study, therefore, involves the design of both civil and mechanical aspects of SHP, and the use of locally sourced materials and manufacturing processes, in the design and production of Pelton turbine buckets. The study succeeded in the coding of a SHP system design and development of design charts using Matlab. A390 and A390-5Mg cast aluminium alloys were selected and investigated as Pelton bucket materials using Solidworks modelling and simulation software. The materials performances measured by von Mises, displacement and strain results were outstanding.

7.1 Introduction

Energy is an indispensable component of human survival, national economic growth, and promotion of health, manufacturing, security, research and development and transportation systems. Adequate access to reliable, quality and affordable energy is a prerequisite and critical to national security, employment, and an acceptable standard of living. Small hydropower (SHP) has been identified as a non-polluting, cost effective and environmentally benign renewable energy source suitable for rural electrification [1-3]. To boost energy accessibility and sustainability sufficiently in sub-Saharan Africa (SSA) requires the region's active participation in the manufacture of SHP equipment, as this will ensure a reduction in the cost of power projects execution compared to the present cost situation. Further, the ability to design and manufacture will solve operational, maintenance and parts availability problems and jobs will be created. Adequate access to power in the region will stimulate commercial and industrial activities and, consequently, raise the productivity and standard of

living of the people [4, 5]. This can be achieved through the popularisation of SHP off grid technology for rural areas, industrial estates and standalone electrification independent of national grids [6].

Literature shows that a lot of theoretical design, research and practical works have been carried out in SHP system development. Some are tied to existing projects but are not necessarily designed for capacity building [7, 8]. Very little is seen in terms of blade materials research and development of locally sourced materials. The discussion on how to domesticate SHP technologies in SSA, a region that has abundant untapped SHP potentials yet is bedevilled with frequent blackouts, is virtually non-existent. This study is, therefore, designed to bridge these limitations and further simplify SHP design for greater participation, especially for SSA. This study is divided into the following components: theoretical framework and design considerations (civil work and design of a Pelton turbine bucket); selection of Pelton bucket materials and possible manufacturing processes; and results of execution of the SHP design parameters chart developed with Matlab.

7.2 Review

In a study, micro Pelton turbine operating and other necessary parameters were calculated based on a maximum efficiency of 97 % [9]. These parameters include turbine power, runner diameter, turbine torque, bucket dimensions, number of buckets, runner length, runner speed, specific speed and nozzle dimension. The paper obtained values of head and flow rate at an efficiency of 97 %. Alnakhilani et al. studied the highest obtainable efficiency at Energy Conversion Laboratory of Sebelas Maret University. In the study, different Pelton turbines were modified using key parameters such as bucket volume nozzle needle seat ring, bucket angle attack, and nozzle needle tip [1]. A theoretical and experimental study was carried out on Pelton wheel bucket design and analysis using the standard thumb rules and bucket modelling using CATIA V5 software [8]. Gudukeya and Madanhire investigated the effects of material, surface texture and fabrication methods on the efficiency of a hydropower plant project within an acceptable cost range. The study concluded that manufacturing of more efficient financially viable Pelton turbines for micro hydropower system (MHS) are possible. In their project, more electricity was produced at a reduced cost per unit kW improving its viability [10]. A theoretical micro-hydroelectric plant design for off-grid applications was carried out to produce green power for remote farms or cottages. A prototype of the system was built to test the design [11].

A study on the modelling and validation of results empirically, using locally available materials in Kenya, was carried out [12]. In the study, stress reduction of 14.2 % was achieved by modifying the profile of the Pelton bucket. Recycled A356 aluminium alloy was found to withstand the stress of 150 Mpa, produced by the generated 5 kW power [12]. A pico Pelton turbine was designed and manufactured using chopped glass fibres reinforced epoxy matrix composite as the bucket material [13]. A 50,000 litres capacity storage tank in a 10 storied tower was used as a water source to operate the turbine. In the study, 1.5 kW was generated out the 2.793 kW that it was theoretically designed for. In the design study of Nava and Siva, CATIA V5 design and modelling software was used to design and optimise a Pelton turbine considering three materials in the analysis [14]. Efficiency and stress in relation to the number of buckets were studied in the work. In the three bucket materials selected (steel, cast iron and fibreglass reinforced plastic matrix), the study concluded that fibreglass reinforced plastic matrix shows exceptional performance compared to cast iron.

7.3 Theoretical framework and design considerations

7.3.1 SHP system and principle of operation

Small- or micro-hydropower systems are required to convert the hydraulic energy of flowing water into mechanical or electrical power depending on the energy needed. In a typical SHP system arrangement, water is diverted from the source by a weir via the intake into an open channel called the headrace. The water then flows past a settling basin for silt and other particles removal and into a storage tank called the forebay. The water then passes through the penstock to the turbine in the powerhouse. The water via the guide vane or nozzle hits the turbine blade that is fixed to a shaft. This mechanism converts the hydraulic energy of the moving water into a rotational motion (mechanical energy). The shaft is linked to a mechanical machine that needs a rotary motion to operate an alternator to generate electricity. Figure 7.1 shows a schematic of a hydropower system and the direction of water flow.

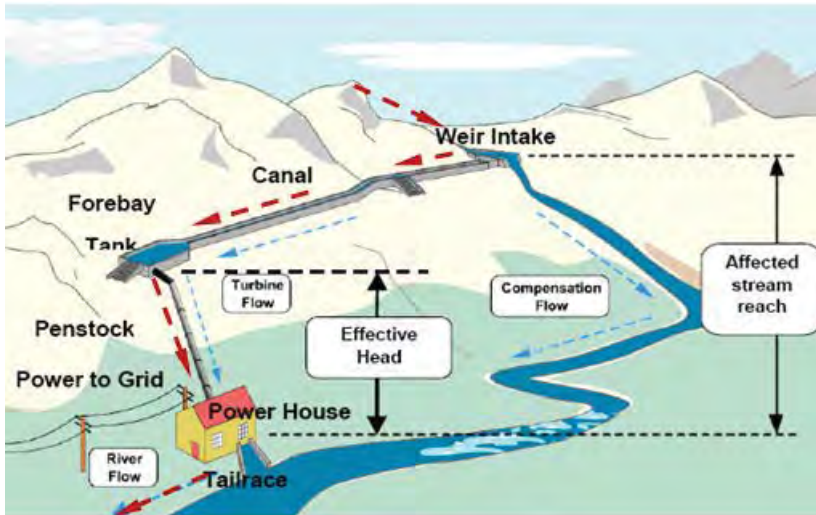


Figure 7.1: Schematic of a hydropower system and the direction of flow

7.3.2 Designing and development of key components of a SHP system

The design and development of a SHP system involves many considerations which can be divided into three stages, as illustrated in Figure 7.2. The stages are hydrological study/survey, design system and manufacturing process. The entire process starts with the evaluation of hydro potentials of a water source such as stream, river, etc. [15]. The design starting parameters are derived from the Flow Duration Curve (FDC) which is prepared from the mean annual flow record of the hydro potentials such as a river or stream. The fundamental hydro potentials needed to kick start the SHP design process are flow rate, velocity, and gross head [16]. The design system can be grouped into civil work design, mechanical design and electrical design.



Figure 7.2: SHP development stages

The design and development processes can further be broken down into components, as shown in the schematic in Figure 7.3 [5].

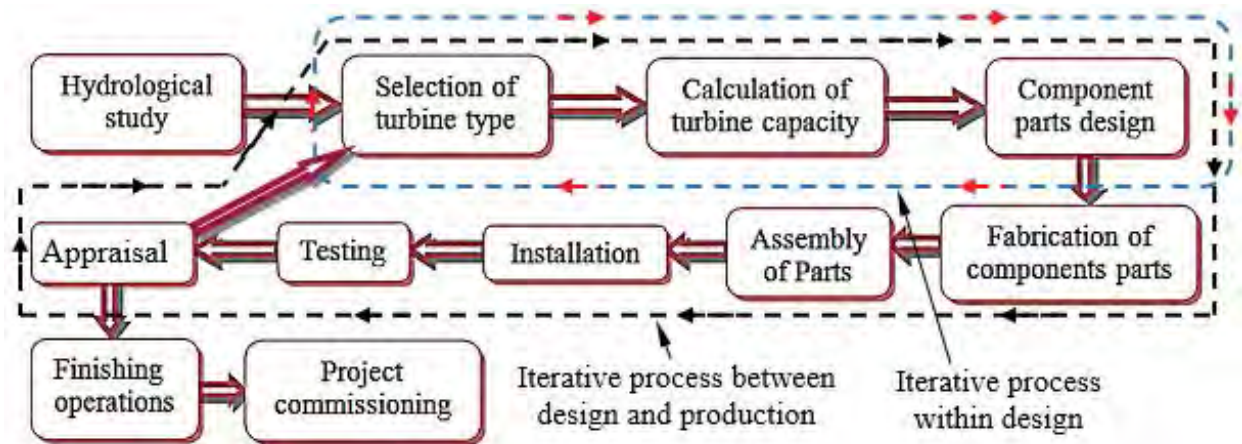


Figure 7.3: SHP design and development layout

7.3.3 Civil design

The SHP system can be divided into subsystems as follows: water source; water diversion and storage system (weir, silt settling basin, forebay or tank and spillway); water conduction system (headrace canal, tunnel or Penstock, and tailrace); powerhouse; generation; and, control system.

7.3.3.1 Weir and intake

The river flow benchmark for micro turbine application is about $4 \text{ m}^3/\text{s}$. In the case of a flow less than this benchmark, it may be possible to build a weir i.e. a low wall or dam across it to be gauged with a notch through which all the water may be channelled, as shown in Figure 7.4. There are different types of notch that could be used and commonest ones are rectangular, Vee and trapezoidal [17, 18], as presented in Table 7.1. In designing a weir, the width, b , is chosen and the depth, h , is taken as $2b$. The notch material may be metal plate or hardwood with sharp edges.

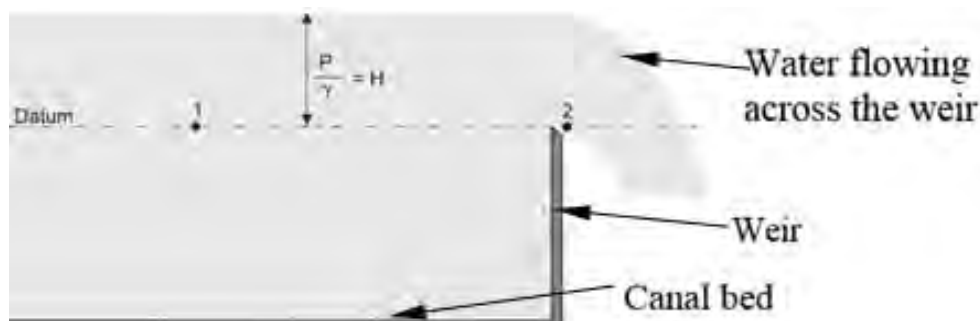
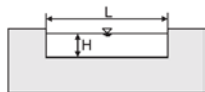
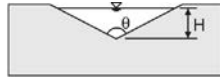
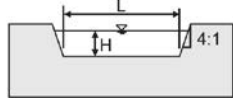
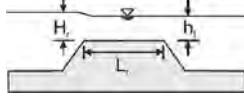


Figure 7.4: Schematic of a weir

Table 7.1: Common types of weir and intake flow rate [18, 19]

Weir	Schematic	Mathematical expression	Value of C
Rectangular notch		$Q = C(b - 0.2h)h^{1.5}$	1.84
V-notch		$Q = C\left(\frac{8}{15}\right)\sqrt{2g} \tan \theta \left(\frac{h}{2}\right)^{1.5}$	0.570 & 1.0611 C(H,Q)
Cipolletti notch		$Q = Cbh^{1.5}$	1.86
Broad notch		$Q_d = Cbh_1^{1.5}$	1.25-3.1
Intake			
Intake orifice flow, Q (m ³ /s)		$Q = CA_{or}\sqrt{2g(h_r - h_f)}$	

Where A_{or} = area of the orifice; C = discharge coefficient (0.6 and 0.8 for a sharp and smooth edges respectively); g = gravity acceleration; h_r = upstream orifice water level; and h_h = downstream orifice water level.

The intake design discharge $Q_{din} = 1.15Q_d$ where Q_d is the set design discharge and 1.15 accounts for the seepage losses between the intake and the forebay. A velocity value between 1.0 m/s to 1.5 m/s and more than 3.0 m/s should be set for stone masonry and concrete intakes respectively [20, 21]. The mathematical equation for intake orifice is in Table 7.1. Figure 7.5 is a submerged intake schematic.

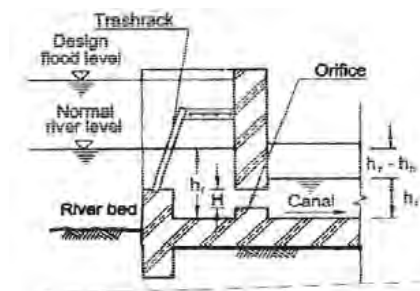


Figure 7.5: Schematic of a submerged intake

7.3.3.2 Headrace canal/open channel

The common types of headrace canal cross sections are shown in Figure 7.6.

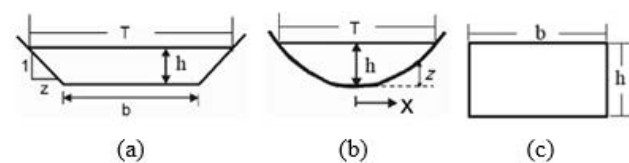


Figure 7.6: Common channel cross sections a) trapezoidal channel b) parabolic c) rectangular

It is recommended that the headrace should be slightly elevated to avoid erosion of the channel surface caused by the flowing water. Headrace design expressions are presented in Table 7.2. In an open channel foundation two requirements must be satisfied [22]:

- i. The channel must be a rigid structure and not permit deformations to guarantee stability.
- ii. The channel should allow uniform flow and this is achieved when:
 - a. The water depth, area and velocity in every cross-section of the channel are constant.
 - b. The energy gradient line, surface line and bottom channel line are parallel to each other.

Table 7.2: Headrace canal/channel design equations

Parameter	Equation	Parameter	Equation
From the continuity equation, discharge, Q (m ³ /s)	$Q = A_{ch} V_{ch}$	Critical velocity, for effective water flow, $V_c < 0.8V_c$	$V_c = \left(\sqrt{\frac{A_{ch} g}{T}} \right)$
Manning the mathematical expression, Q (m ³ /s)	$Q = s_f \left(\frac{1}{n_{ch}} \right) s_{ch}^{\frac{1}{2}}$	channel bottom line slope (hydraulic gradient), S_{ch}	$S_{ch} = \left(\frac{Q \times n_{ch}^{\frac{2}{3}}}{A_{ch} \times R_{ch}^{\frac{2}{3}}} \right)^2$
Wetted perimeter, P_w	$P_w = b_{ch} + 2h_{ch}$	Chezy's C , C_c	$C_c = \frac{1}{n_p} R_{ch}^{0.1667}$
Hydraulic radius of the section area, R_{ch}	$R_{ch} = \frac{A_{ch}}{P_w}$	Shape optimisation coefficient, x	$x = 2\sqrt{(1+N^2)} - 2N$
Normal open channel velocity, V_{ch} (m/s)	$V_{ch} = \frac{Q}{A_{ch}}$	Depth of the water in the canal, h_{ch} (m)	$h_{ch} = \frac{\sqrt{A_{ch}}}{x+N}$
From Chezy equation, the open channel velocity, V_{chc} (m/s)	$V_{chc} = C\sqrt{R_{ch}S_{ch}}$	Canal bed width, b_{ch} (m/s)	$b_{ch} = h_{ch} + x$
Hazen-Williams velocity equation, V_{chw} (m/s)	$V_{chw} = kCR_{ch}^{0.64}S_{ch}^{0.54}$	Canal top width, T (m/s)	$T = h_{ch} + (2h_{ch}N)$
Darcy-Weisbach velocity equation, V_{chd} (m/s)	$V_{chd} = \sqrt{\frac{8g}{f} R_{ch}S_{ch}}$	Head Loss, H_{loss}	$H_{loss} = L_{ch}S_{ch}$
From Manning's equation, V_{chm}	$V_{ch} = \frac{R_{ch}^{\frac{2}{3}}S_{ch}^{\frac{1}{2}}}{n_{ch}}$	Largest particle that can move through the canal, d_{ch}	$d_{ch} = 11R_{ch}S_{ch}$

Where n_{ch} = roughness coefficient ($n_{ch} = 0.012$ – 0.014 for concrete channels); S_{ch} = % slope of sides; C_c = Chezy's C ; A_{ch} = open channel cross-sectional area (it could be rectangular, trapezoid or circular); f = Darcy-Weisbach friction factor; and $k = 0.85$ for SI units or 1.32 for U.S. units.

The Chézy equation is frequently used in sanitary sewer channel design and analysis. The Hazen-Williams equation is commonly used in the design and analysis of pressure pipe systems. The Darcy-Weisbach equation which is a theoretically based is usually used in the analysis of pressure pipe systems.

The recommended headrace canal/channel velocity (V_{ch}) is between 1 m/s to 1.5 m/s, as shown Table 7.3.

Table 7.3: Recommended headrace canal/channel velocity (V_{ch}) and roughness coefficient (C)

Material	Slope (h/v)	Recommended canal velocity (V_{ch})	
		> 0.3 m depth	> 1 m depth
Stone masonry with mud mortar	0.5–1.0	1	1
Stone masonry with cement	0–1.5	1.5	1.5
Roughness coefficient, (C)			
Masonry canals	Brickwork		0.015
	masonry with cement mortar		0.017
	Coarse rubble masonry		0.02

7.3.3.3 Spillway and settling basin

Figure 7.7 shows a schematic of the cross section and longitudinal section of a spillway.

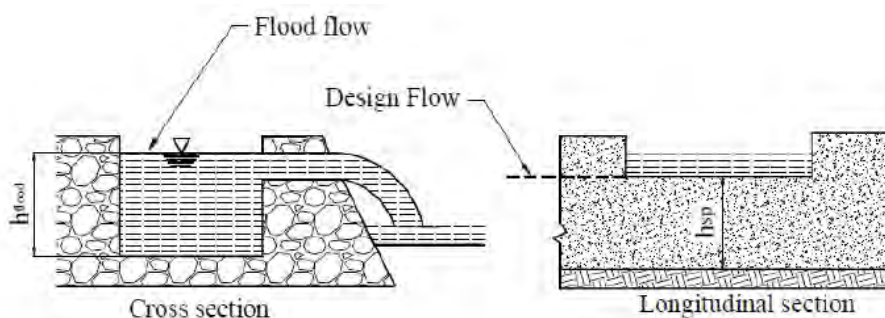


Figure 7.7: Normal spillway in a SHP system

The minimum size of particle to be considered to settle in the basin is 0.2 mm. The width of the basin which is about 2–5 times the width of the approach canal is fixed and followed by setting of the safety factor (1–2) which takes care of the turbulence in the flow. Figure 7.8 shows the different views (side and top views) of a settling basin. The mathematical relations for designing a settling basin are presented in Table 7.4.

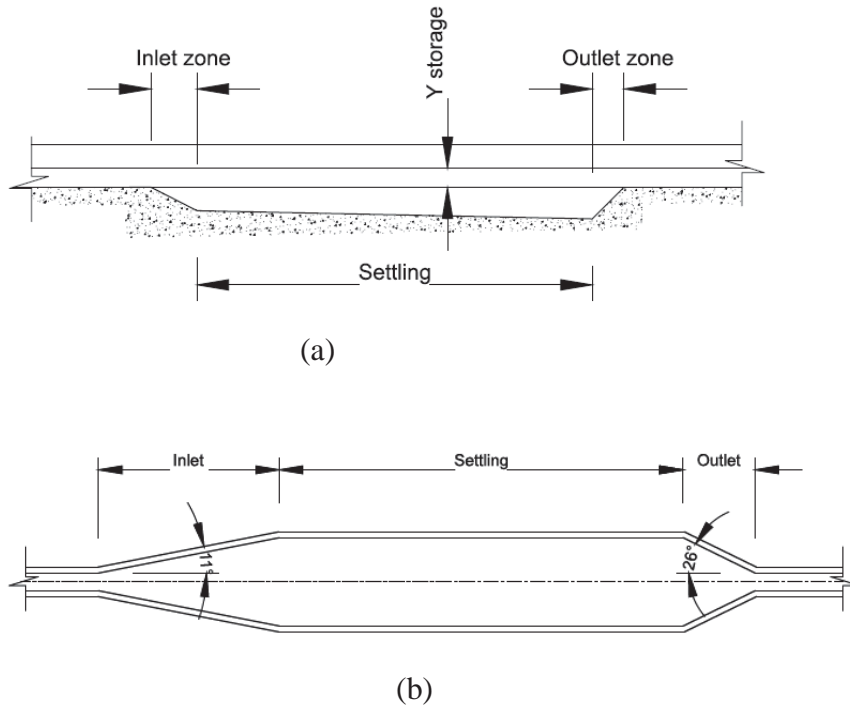


Figure 7.8: (a) Side view and (b) Top view of a settling basin

Table 7.4: Calculation for design of a settling basin

Parameter	Equation	Parameter	Equation
The length of the spillway, L_{sp} (m)	$L_{sp} = \frac{(Q_{fld} - Q_{ch})}{C_w (h_{overtop})^{1.5}}$ $h_{overtop} = h_{fld} - h_{sp}$	Silt load S_{load} (kg),	$S_{load} = Q_{ch} T_{silt} C$
		Volume of the silt in basin, V_{silt}	$V_{silt} = \frac{S_{load}}{\rho_{silt} P_{factor}}$
The length of the settling basin (L_{set})	$L_{set} = \frac{2Q_{ch}}{WV_{vert}}$	The average settling basin depth (D_{col})	$D_{col} = \frac{V_{silt}}{L_{set} W}$

Where Q_{fld} = flood flow through the intake (m^3/s); Q_{ch} = designed flow rate in the channel (headrace canal) (m^3/s); C_w = spillway profile coefficient ($C_w = 0.6$ for sharp edge profile) and h_{fld} = flood level height in the canal (m); h_{sp} = of the spillway crest height from canal bed (m); W = suitable basin width (m); (V_{vert} = fall velocity (velocity fall of 0.03 m/s is used for settling particles of 0.3 mm diameter); T_{silt} = silt emptying frequency in seconds (12 hours or 43,200 seconds is used in SHP project); C_{silt} = silt concentration of incoming flow (kg/m^3), and the value can be $0.5 kg/m^3$, ρ_{silt} = density of silt ($2.600 kg/m^3$ is commonly used); P_{factor} = sediments submerged in water packing factor (50 % is normally used).

7.3.3.4 Trash rack design

Horizontal slanting bars inclined at about 60° to 80° at certain spacing are placed at the entrance of flow to prevent the trash getting in. These bars are called trash rack bars and the number depends on the turbine type and manufacturer. However, conventional values are 20 mm to 30 mm for Pelton turbines, 40 mm to 50 mm for Francis turbines and 80 mm to 100 mm for Kaplan turbines [22, 23]. Also at the entrance is a grill or screen that prevents the

debris from entering. The passage of the water through the rack leads to loss of head. The trash rack has a coefficient (K_{tr}) that depends on the shape of the bar and ranges from 0.8–2.4.

7.3.3.5 Forebay and penstock design

Choose the width, b_f , and set the length equal to 2 to 2.5 times the b_f . The clearance of the penstock from the forebay bed commonly ranges from 0.30 m to 0.50 m. In the forebay design, an equivalent of 15 seconds volume buffer is supplied as an auxiliary for the turbine to be able to cope with flow variations during standard operating conditions. The design of the forebay and the settling basin are similar but the forebay is connected to the penstock. Figure 7.9 shows the normal forebay features in a SHP system. The calculation of the submergence head should be done with care to avoid being undersized as this could lead to flow variation in the penstock as well as an explosion in the penstock pipe.

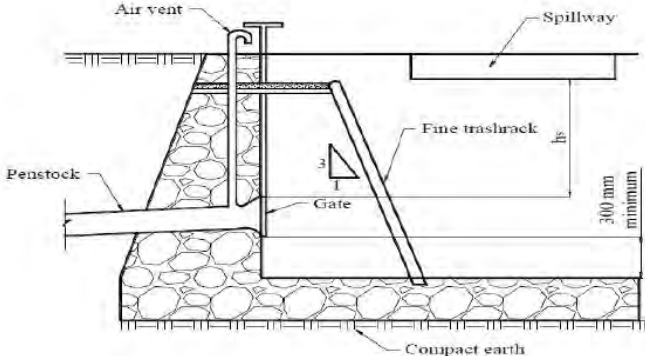


Figure 7.9: Schematic showing normal forebay in SHP system

The pipes that connect the forebay to the turbine are called penstocks. The connection could be surface or underground depending on the topography of the ground, the material the penstock is made of, the ambient temperature and other environmental requirements as the case may be [22]. In real fluid flows, friction head losses exist and these losses are classified into major losses (energy loss per length of pipe) and minor losses (bends, fittings, valves, etc.). The losses are due to the friction imposed by the pipe walls and fittings on the flowing fluid. For optimisation, the velocity of flow in the penstock should be considered, as represented in Table 7.5.

Table 7.5: Penstock flow velocity

Head (m)	Low Head $H_g < 50$	Medium Head $50 \leq H_g \leq 250$	High Head $H_g > 250$
Velocity (m/s)	2–3	3–4	4–5

The penstock diameter has an effect on head loss: a smaller diameter gives greater continuous head loss. However, the head loss should be within 5 % to 10 % of the gross head. Mild steel of ultimate tensile strength of $3.5 \text{ N/m}^2 \times 108 \text{ N/m}^2$ is commonly considered for penstock material. The penstock thickness should be large enough to withstand both the static and dynamic hydraulic pressure of the water and the safety factor, SF, should not be less than 3.5. Corrosion allowance of 1 mm is set for the penstock [21]. Figure 7.10 shows the penstock assembly in a SHP system.

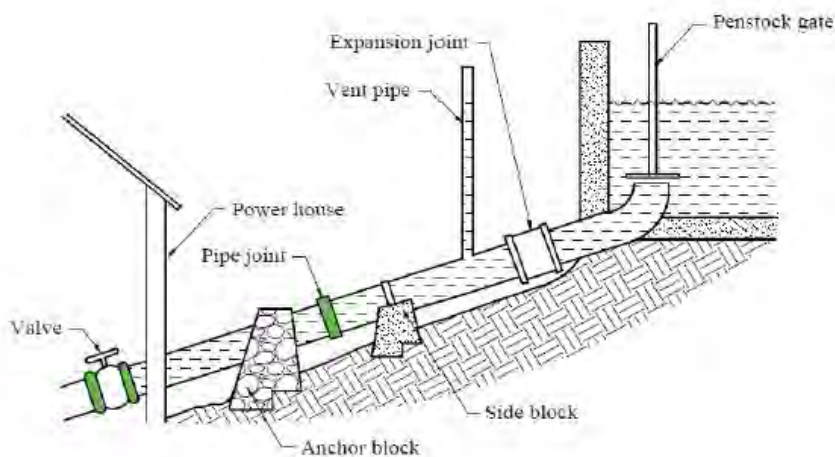


Figure 7.10: Components of the penstock assembly [24]

Sizing of the penstock is mainly controlled by the estimated flow rate, length of pipe and gross head as shown in the following expression below. The wall thickness of the penstock depends on the materials of pipe, its strength (tensile), pipe diameter and the operating pressure. The pipe should be rigid enough to be handled without danger of deformation in the field. The penstock is provided with air vents to conduct out the air resulting from rapid closure of the valve, thereby preventing the air going into the penstock. Table 7.6 presents mathematical expressions for forebay penstock design. To accurately calculate the head loss in the penstock, the following parameters are set:

- Penstock material roughness factor, k (for steel $k = 1.5 \times 10^{-4} \text{ m}$).
- Trash rack bars thickness t_b , typically at 1 cm to 2 cm, but this largely depends on the selected turbine – 2 cm or 3 cm can be considered for preliminary design. The smaller the space between the bars, the more the turbine is protected, but this causes head loss due to clogging therefore requires regular cleaning.
- The trash rack angle, α , is set at 72° to the horizontal plane and this is equivalent to a slope of 1:3 ($H:V$).
- Cross-sectional area factor, β , is set according to the bar shape.

- The entrance factor, k_e ; due to the shape of the transition between the forebay and the penstock. 0.05 can be considered for k_e for this kind of transition.
- Bend factor, ζ , according to the angle of bend, θ , and this is obtained from a reference table.

Table 7.6: Expressions for forebay and penstock design

Parameter	Mathematical relation	Parameter	Mathematical relation
Submergence head, H_s	$H_s = 1.5V_p^2 / 2g$	Head lost for n penstocks, h_{ln} (m)	$h_{ln} = h_l \sqrt{n}$
Internal penstock diameter, D_p (m)	$D_p = 2.69 \left(n_p^2 \times Q_p^2 \times \frac{L_p}{H_g} \right)^{0.1875}$	Penstock wall thickness t_p , (m)	$t_p = \frac{pD}{2\sigma}$
Minimum wall thickness, t_p (m)	$t_p = \frac{D_p + 508}{400} + 1.2$	Penstock wall thickness t_p + allowance, t_{pt} (m)	$t_{pt} = \frac{pD_p}{2\sigma} + t_{extr}$
The total head net, H_n , (m)	$H_n = H_g - \Delta h_l$	n Penstock arrangement wall thickness t_{pn} , (m)	$t_{pn} = \frac{t_p}{\sqrt{n}}$
Single penstock installation head loss due to friction, h_l (m)	$h_l = \frac{2fL_p}{2g\pi} \left(\frac{Q_p^2}{D_p^5} \right)$	The diameter of n penstock, D_{pn} , (m)	$D_{pn} = \frac{D_p}{\sqrt[5]{n^2}}$
	$a_1 = \frac{2fL_p}{2g\pi} = 0.26fL_p$	n penstocks flow velocity, V_{pn} , (m ³ /s)	$V_{pn} = \frac{V_p}{\sqrt[5]{n}}$
	$h_l = 0.26fL_p \left(\frac{Q_p^2}{D_p^5} \right)$	Air vent diameter, d_{vent} (m)	$d_{vent} = Q_p^{0.5} \left[\left(\frac{F}{E} \right) \left(\frac{D_p}{t_{ef} f} \right)^3 \right]$
Minor head loss	$h_{lmin} = \frac{V_p^2}{2g} (K_{ent} + K_{ben} + K_{cont} + K_{val})$		

Where V_p = penstock velocity; Q_p = water flow rate (m³/s); L_p = penstock length in (m) and; H_g = gross head in (m) (surge tank is needed if $H_g/L_p > 5$); D_p = penstock diameter in (mm) and; t_p = minimum penstock thickness in (mm); Δh_l = total loss and it should not be more than 5–10 % of H_g and the value can be checked by penstock diameter variations; p = internal pressure (kg/m²); E = Young's modulus for the penstock (N/m²); t_{ef} = effective penstock wall thickness at upper end (mm); F = safety factor (for buried penstock pipe F is 5 and for exposed pipe F is 10); σ = Tensile stress; and f = dimensionless friction factor for pipe material which can be obtained from Moody Chart ($f = 0.0014$); n_p = Manning's coefficient (see Table 9.7 for Manning's coefficient); p = the desired pressure ($1.5 H_g$); t_{extr} = extra thickness for corrosion (1-3 mm) [25]; K_{ent} = Loss of head through entrance; K_{ben} = Loss of head through bend; K_{con} = Loss of head through contraction; K_{val} = Loss of head through valves.

Table 7.7: Manning's roughness coefficients, n_p , for common channel materials [26]

Surface Material	Mild steel pipe	Concrete (Cement) - finished	Concrete - wooden forms	Concrete - centrifugally spun	Copper	PVC
n_p	0.008–0.012	0.012	0.015	0.013	0.011	0.009–0.011

Empirical calculation of the internal diameter (D_p) of a penstock

There are various relations that have been proposed by researchers for calculating the internal diameter of a penstock as shown in Table 7.8. These relations, which are based on either flow rate (Q), capacity (P_t), or gross head (H_g) – or their combination – are products of empirical and field statistical data analysis [27]. Figure 11 shows the penstock and powerhouse arrangement and the relation between gross head and loss head.

Table 7.8: Relations to calculate the internal diameter (D_p) of a penstock

Relation	Proposed by	$D_p = F(Q, P_t, H_g)$	Limitation
$D_p = 0.72Q^{0.5}$	Warnick et al. [28]	$D_p = F(Q)$	Optimum D_p for SHP
$D_p = 0.176 \left(\frac{P_t}{H_g} \right) 0.466$	Bier [27]	$D_p = F(P_t, H_g)$	Optimum D_p for large hydroelectric
$D_p = \frac{0.71P_t^{0.43}}{H_g^{0.65}}$	Sarkaria [29]	$D_p = F(P_t, H_g)$	Optimum D_p for large hydroelectric
$D_p = \frac{0.72P_t^{0.43}}{H_g^{0.63}}$	Warnick et al. [28]	$D_p = F(P_t, H_g)$	Optimum D_p for large hydroelectric
$D_p = \frac{0.52P_t^{0.43}}{H_g^{0.6}}$	Moffat et al.	$D_p = F(P_t, H_g)$	Optimum D_p for large hydroelectric
$D_p = \frac{1.517Q^{0.5}}{H_g^{0.25}}$	USBR [30]	$D_p = F(Q, H_g)$	$Q > 0.56$ m ³ /s
$D_p = \frac{1.127Q^{0.45}}{H_g^{0.12}}$	Fahlbusch [31]	$D_p = F(Q, H_g)$	$Q > 0.56$ m ³ /s
$D_p = 0.05 \left(\frac{SMheQ^3 P_{wf}}{WCH_r} \right)$	ASCE [32]	$D_p = F(Q, P_t, H_g)$	$Q > 0.56$ m ³ /s
$D_p = \sqrt[3]{0.05Q^3}$	Ludin–Bundschu [33]	$D_p = F(Q, H_g)$	$H_g < 100$ m
$D_p = \sqrt[3]{\frac{5.2Q^3}{H_g}}$	Ludin–Bundschu	$D_p = F(Q, H_g)$	$H_g > 100$ m

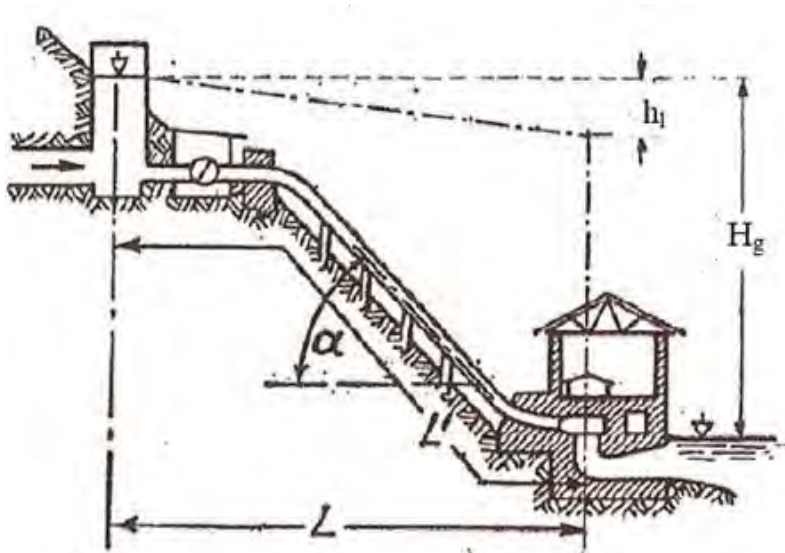


Figure 7.11: Penstock and powerhouse arrangement

7.3.4 Hydro Pelton turbine mechanical design

A Pelton turbine system is made of a weir, forebay, headrace, penstock, nozzle, runner and generator. The runner is a subassembly of the system that consists of several buckets fixed around the circumference of a circular disc, bearing, seal and a shaft. The shaft connects the wheel either vertically or horizontally to the alternator or generator. This idealised Pelton turbine system is schematised in Figure 7.12. The water pressure is converted into kinetic energy (KE) by the nozzle before it strikes the bucket. The jet, with KE, is impinged on the splitter of the bucket through a nozzle at a right angle. The KE of the streaming jet is totally converted by the bucket into mechanical energy in the generator, which subsequently converts the mechanical energy into electrical energy [10, 11, 34]. The splitter prevents a central area of the bucket from acting as a dead spot and this makes it more efficient in deflecting the water jet away [35]. Details of the design are presented in Table 7.3.

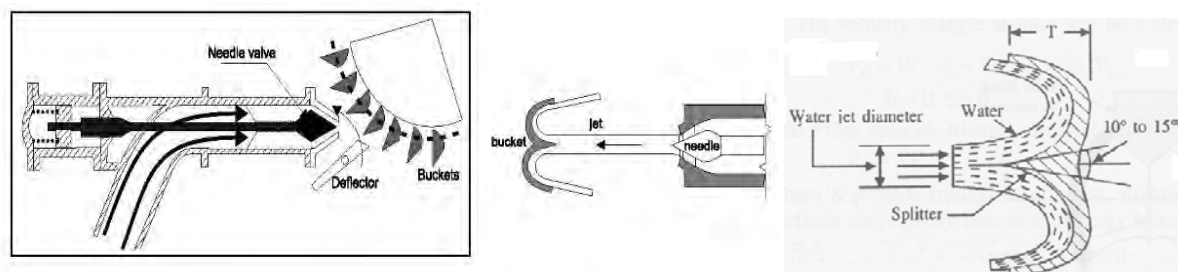


Figure 7.12: Streaming jet impinges on splitter of a bucket

7.3.4.1 Main categories of turbine and their applications

The schematic diagram in Figure 7.13 shows the different types of the turbine while Table 7.9 presents their applications.

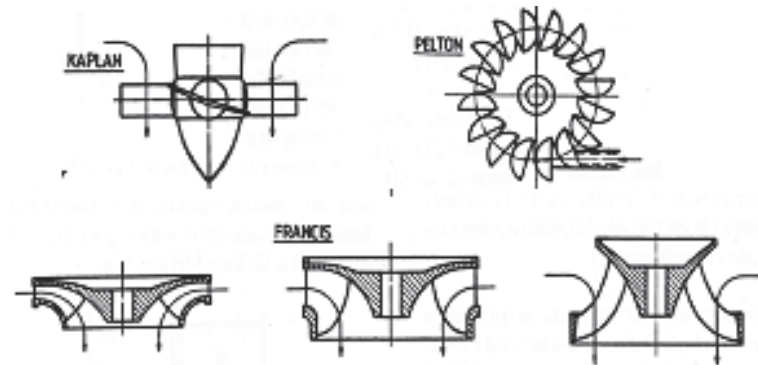


Figure 7.13: The different types of turbine

Table 7.9: Types of hydro turbine and their applications [36].

Turbine	Head Classification		
	High (> 50 m)	Medium (10 m to 50 m)	Low (< 10 m)
Impulse	Pelton, Turgo, Multi-jet Pelton	Crossflow, Pelton, Turgo, Multi-jet Pelton	Crossflow
Reaction		Francis (spiral case)	Francis (open-flume), Propeller, Kaplan, Darius

Turbine design governing equations were developed from Euler general turbine equations, using the Pelton wheel velocities triangle schematic diagram in Figure 7.14 [37].

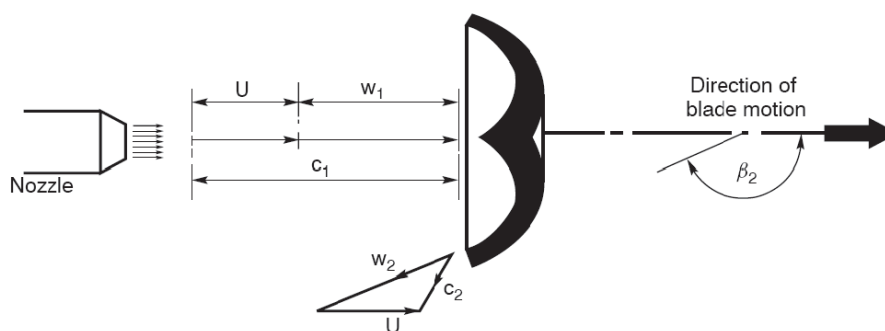


Figure 7.14: The Pelton wheel velocities triangle, showing the relative and absolute velocities of the flow

7.3.4.2 Euler equation

$$\Delta W = U_1 C_{w1} - U_2 C_{w2} \quad (7.1)$$

But for Pelton, C_{w2} is always negative, so that equation 4 becomes:

$$\Delta W = U_1 C_{w1} + U_2 C_{w2} \text{-----} (7.2)$$

Where ΔW = work done; U_1 = bucket speed; U_2 = bucket speed vector; C_{w1} = input velocity of the whirl; and, C_{w2} = exit velocity of the whirl.

7.3.4.3 For Pelton turbine

$$U_1 = U_2 = U = V_{tr} \text{-----} (7.3) \quad C_1 = C_{w1} = V_j = U + w_1 \text{-----} (7.4)$$

$$C_{w2} = U + w_2 \cos \beta_2 \text{-----} (7.5) \text{ Where } \beta < 0$$

Using equations (2–5) in equation (1), it becomes:

$$\Delta W = U [U + w_1 - (U + w_2 \cos \beta_2)] = U (w_1 + w_2 \cos \beta_2) \text{-----} (7.6)$$

Where C_1 = jet velocity; U_1 = bucket speed; w_1 = relative velocity at the inlet; w_2 = relative velocity at the exit; β_2 = angle inclined to the horizontal plane by the jet; C_2 = the absolute velocity at the exit and; U_2 = speed vector at the exit.

For 100 % hydraulic efficiency, β_2 will be 180° . But in practice, the jet is deflected by buckets through an angle, β_2 , of about 160° to 165° in the same plane of the jet. The Pelton wheel casing is a non-hydraulic function part but serves as a guide for protecting water splashing and for runner accidents [38].

Considering impact of loss due to friction, the loss factor, k is incorporated, see Figure 7.15:

$$k = \frac{w_2}{w_1} \text{-----} (7.7)$$

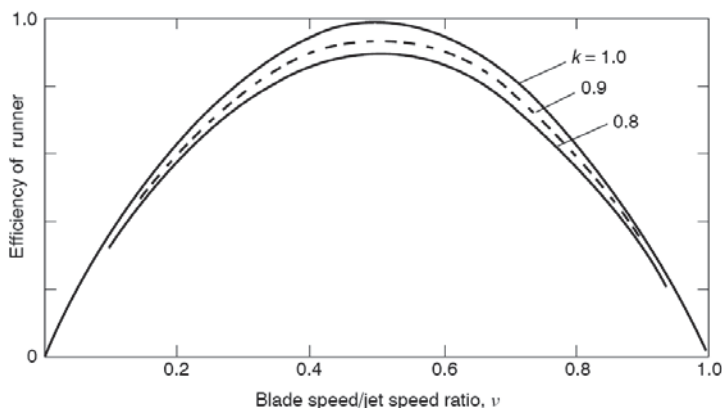


Figure 7.15: Theoretical variation of runner efficiency for a Pelton wheel with blade speed to jet speed ratio for several values of friction factor k

From equation (7):

$$w_2 = kw_1$$

Where $k < 1$, so that (6) becomes:

$$\Delta W = U w_1 (1 - k \cos \beta_2) = U (C_1 - U) (1 - k \cos \beta_2) \quad (7.8)$$

$$\eta_t = \frac{2\Delta W}{C_1^2} = 2 \frac{U}{C_1} \left[1 - \frac{U}{C_1} \right] (1 - k \cos \beta_2) \quad (7.9)$$

7.3.4.4 The real Pelton runner

There are always losses in the Pelton runner, therefore, $\eta_t < 1$ [37]. The schematic of the runner is shown in Figures 7.16 and 7.17. The design calculation details of a turbine id presented in Table 7.10:

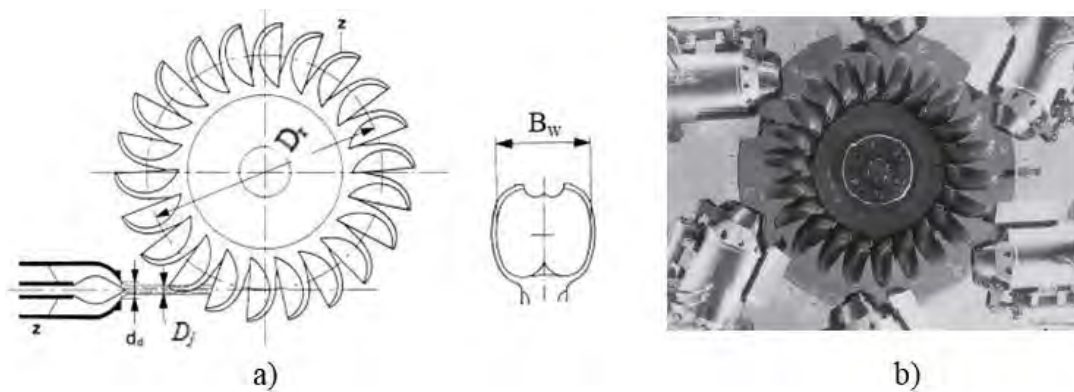


Figure 7.16: The arrangement of a runner a) the bucket and nozzle relation; b) 6-Nozzle Pelton runner [39]

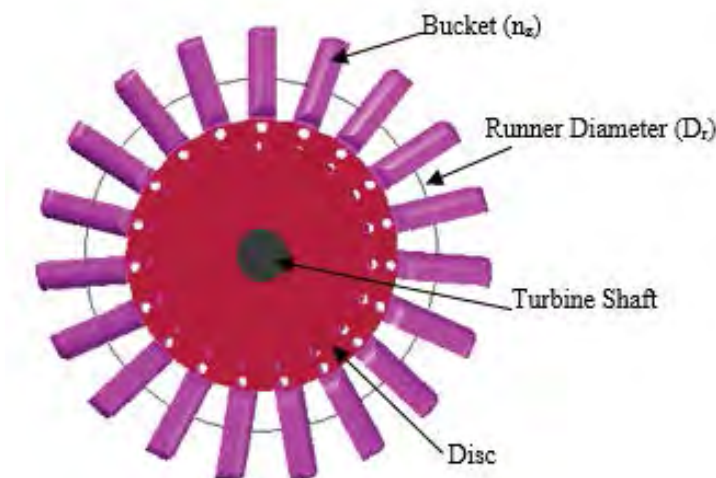


Figure 7.17: Assembly of buckets on a runner

Table 7.10: The calculation details of a turbine design [11, 40-42]

Parameters	Relevant Equations	Parameters	Relevant Equations
The input power to the turbine, P_{ii} (kW)	$P_{ii} = \frac{\rho * g * \eta_t * H_n * Q}{1000}$	Bucket depth, B_d (m)	$B_d = 1.2D_j$
Specific speed (N_s)	$N_s = \frac{N * \sqrt{P_{ii}}}{H_n^{\frac{5}{4}}}$	Cavity Length, h_1 (m)	$h_1 = (0.35)D_j$
Jet velocity, V_j (m/s)	$V_j = C_n * \sqrt{2 * g * H_n}$	Length to Impact Point, h_2 (m)	$h_2 = (1.5)D_j$
Jet/nozzle diameter, D_j	$D_j = \sqrt{\frac{4 * Q}{\pi * n_z * V_j}}$	Offset of Bucket, k (m)	$k = (0.17)D_j$
Tangential velocity of the runner, V_{tr}	$V_{tr} = x * V_j$	Cavity Width, a (m)	$a = (1.2)D_j$
Runner diameter, D_r , (m)	$D_r = \frac{60 * V_{tr}}{\pi * N}$	Number of buckets n_z	$n_z = 15 + \frac{D_r}{2D_j}$
nozzle cross-sectional area, A_j	$A_j = \frac{\pi * D_j^2}{4}$	Length of bucket moment arm, L_{ab} (m)	$L_{ab} = 0.195D_r$
Nozzle flow rate, Q_n (m ³ /s)	$Q_n = V_j * A_j$	Absolute reaction forces acting on the Pelton runner	$F = 2\rho Q(V_j - V_{tr})$
Distance between bucket and nozzle, x_{nb} (m)	$x_{nb} = 0.625D_r$	The torque on the runner is T_r :	$T_r = \frac{D_r}{2} F = \rho Q D_r (V_j -$
Radius of bucket centre of mass to runner centre, R_{br} (m)	$R_{br} = 0.47D_r$	Turbine shaft diameter D_{shaft} (mm)	$D_{shaft} = 105 \left(\frac{P_t}{N} \right)^{0.35}$
Bucket axial width, B_w (m)	$B_w = 3.2D_j$	Number poles of the generator, Z_p	$N = \frac{3000}{Z_p}$
Bucket radial length, B_l (m)	$B_l = 3D_j$		

Where η_t = efficiency of the wheel; N = generator rotation (*rpm*); x = ratio of V_{tr} to V_j (at maximum η_t , $x = 0.5$); Q = flow rate (m³/s); g = acceleration due to gravity (9.81m/s²); H_n = net head (m); ρ = density of water (kg/m³) and; n_z = no of nozzle; V_j = absolute velocity of water jet (ms⁻¹); C_n = nozzle coefficient ($C_n = 0.96...0.98$); g = gravitational constant, 9.81 (ms⁻²) and, H_n = net head (m); k_u = Coefficient after Impact ($k_u = 0.45$ to 0.49) assume worst case 0.45 ; n_z = number of nozzles ($n_z \geq 17$); Q = flow rate (m³/s);

Rules of thumb: $B_w = 3.1D_j$ for 1 nozzle; $B_w = 3.2D_j$ for 2 nozzles; $B_w = 3.3D_j$ for 4-5 nozzles and $B_w > 3.3D_j$ for

6 nozzles. The general relation between B_w and D_j : $3.1 > \frac{B_w}{D_j} \geq 3.4$

There are always losses in Pelton runner, therefore, $\eta_t < 1$.

7.3.4.5 Turbine shaft diameter

Shaft diameter is an important part of a hydro turbine in determining the preliminary runner geometry. Enough space should be provided in accordance with the design in a runner for a structurally safe shaft.

7.4 Pelton turbine bucket production

7.4.1 Selection of material

The environment in which the runner of a turbine works is aggressive and hostile. The bucket is prone to corrosion and erosion wear caused by impinging free jets that may contain sand and chemically aggressive elements. Fabrication, assembly and installation of buckets are also associated with challenges, especially in an environment with poor manufacturing infrastructure, as is the case in SSA presently. Buckets are sometimes used in seawater which is the most corroding natural medium containing corrosive halide reagents such as NaCl and MgCl₂. The compositional content of seawater depends on geographical location and varies over a wide range, however, the salt content of the world's oceans is approximately constant, about 3.1 % [5, 6]. To satisfy both rigidity and environment requirements, stainless steels have been the common materials for buckets [43-45], coated with epoxy or polyurethane based resins materials. However, considering present functionally graded aluminium alloys and composites, this group of materials seems feasible for the production of Pelton turbine buckets.

Corrosion and erosion wear are problems shortening the life span of a bucket, and therefore are major factors to be considered and tackled during design and manufacture processes. According to this study, there are basically two methods to ameliorate the challenges posed to the life span of the bucket and other turbine parts: enhancing desilting in the basin to prevent sand and other particles from getting to the bucket; and, improving the wear and corrosion resistance of the selected material used in the manufacturing process.

7.4.2 Manufacturing of a Pelton turbine bucket

The production processes of steel materials are complex, very expensive and require huge energy for casting and welding. The dwindling power and manufacturing sectors in SSA cannot adequately support the production of Pelton buckets. Despite these limitations, a lot can still be achieved in the production of hydro turbine components with a design process that takes into consideration materials and manufacturing inadequacies. Quite often, projects fail

or take longer time than necessary when the design process fails to sufficiently capture the relation that exists between material and manufacturing process. For manufacturing purposes, the choice of material is governed not only by operational requirements but also by cost, availability, and the manufacturing methods available [5].

If the desirable is not available, the available becomes desirable. The use of locally sourced materials can be enhanced through manufacturing and heat treatment processes as an alternative to stainless steel, and this should be promoted. This study, therefore, exploits locally sourced aluminium alloy and composites whose mechanical properties can be improved by functionally graded manufacturing method (FGM) techniques for Pelton bucket production. Aluminium based materials are locally sourced in SSA and possess good aerodynamics and natural corrosion resistance attributes and can be enhanced by manufacturing and heat treatment processes. The FGM method of centrifugal casting combined with heat treatment have been chosen for the production of a Pelton bucket due to the simplicity and cost-effectiveness of the processes involved [46]. The manufacturing process of a Pelton turbine bucket has two steps: production of a permanent mould; and, centrifugal casting process. The concept is to produce a bucket that has hardness and strength properties in gradient form, such that the inner surface denoted by (a), as shown in Figure 7.18, is the hardest and toughest zone.

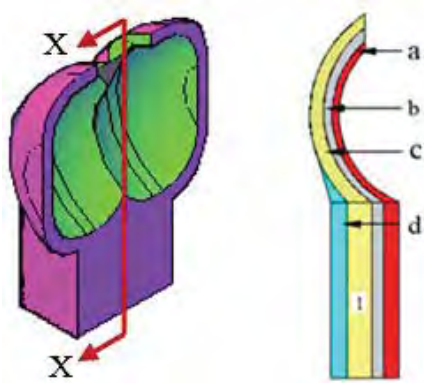


Figure 7.18: An offset of section X-X of a Pelton bucket

7.5 SHP system design results

The design of the SHP system was executed by Matlab software for civil and mechanical sections and the bucket was simulated with Solidworks. The entire process started with the hydrological data in Table 7.10. The civil components considered include the intake, weir, open channel (canal), settling basin, forebay, and penstock. In the mechanical design, the

main operating parameters of a Pelton hydro turbine were considered and design charts developed. The Matlab codes are presented in appendixes 3 and 4

7.5.1 Civil works design charts for SHP

Figure 7.19 shows the relation between intake sectional area and intake discharge when $h_r - h_h = 0.3$ m; where h_r = normal river water level (m) and h_h = headrace level (m). Figure 7.20 depicts the correlation that exists between headrace canal sectional area and discharge at canal velocity of 1.4 m/s and width of 0.3 m.

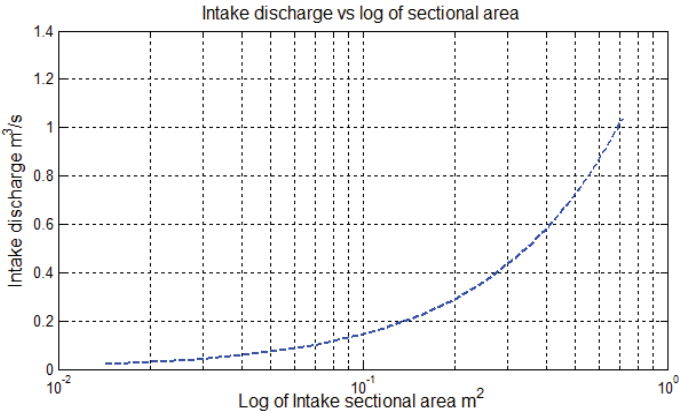


Figure 7.19: Intake discharge vs sectional area

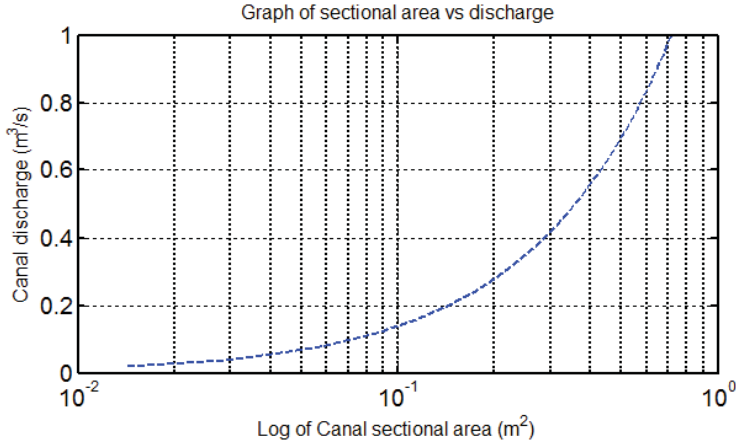


Figure 7.20: Canal discharge vs sectional area

Figure 7.21 shows the link between headrace canal sectional area and depth for rectangular and radius for the circular canal. Notch discharge against weir depth at a width of 0.3 m for both Vee notch and the rectangular notch is shown in Figure 7.22.

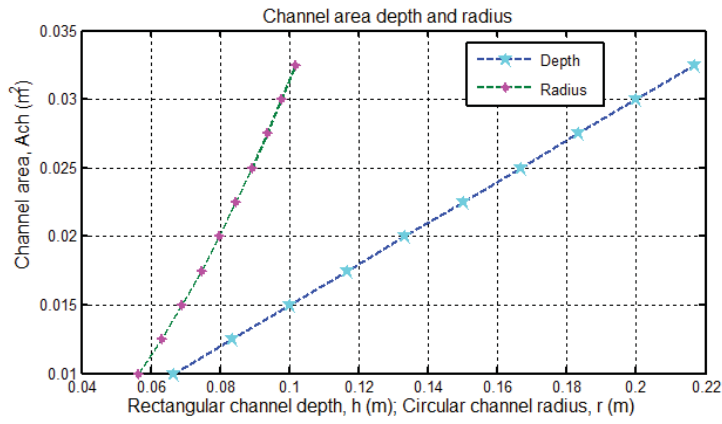


Figure 7.21: Canal area vs depth and radius

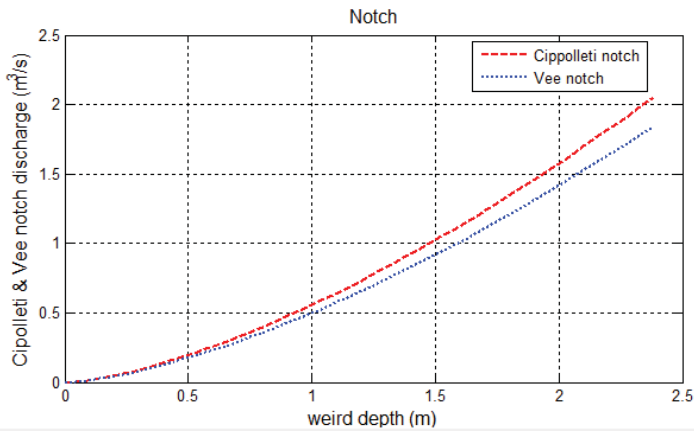


Figure 7.22: Notch discharge vs weir depth

Variations of the headrace canal sectional area and perimeter wet at the width of 0.3 m and velocity of 1.4 m/s is shown in Figure 7.23. Figure 7.24 shows the relationship between length and volume of settling basin silt emptying frequency of 43,200 seconds.

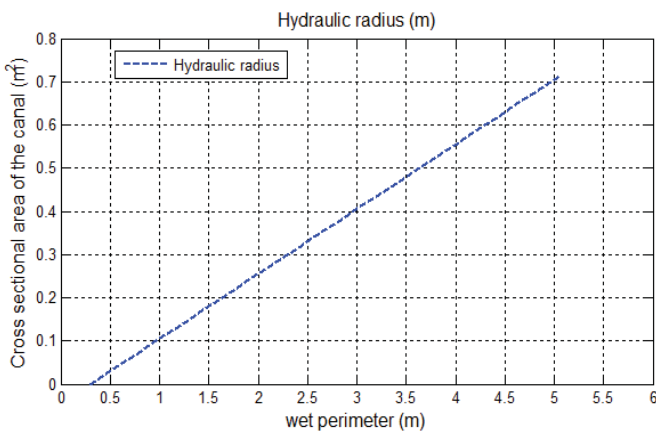


Figure 7.23: Canal sectional area vs perimeter wet

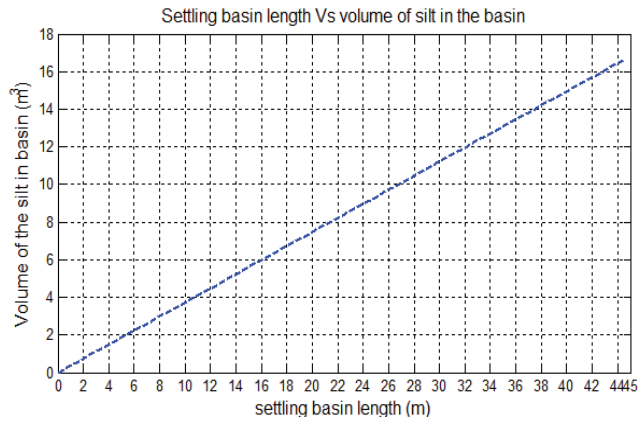


Figure 7.24: Length vs volume of settling basin

Figures 7.25 and 7.26 show variations of penstock flow rate against internal diameter and penstock thickness using theoretical and empirical relations according to Warnick et al. [28] and United States Department of the Interior, Bureau of Reclamation [30].

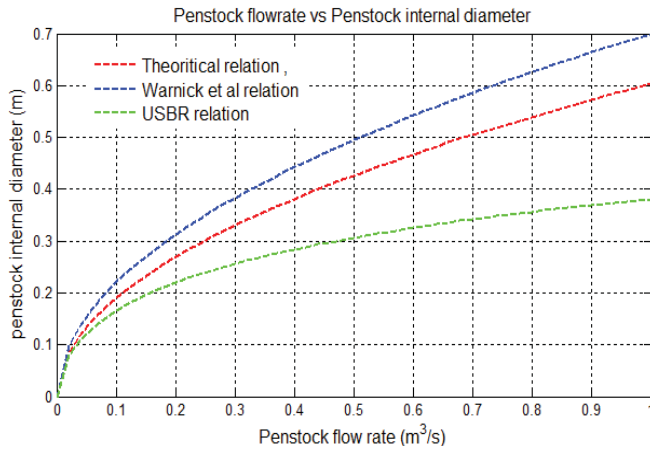


Figure 7.25: Discharge vs penstock internal diameter

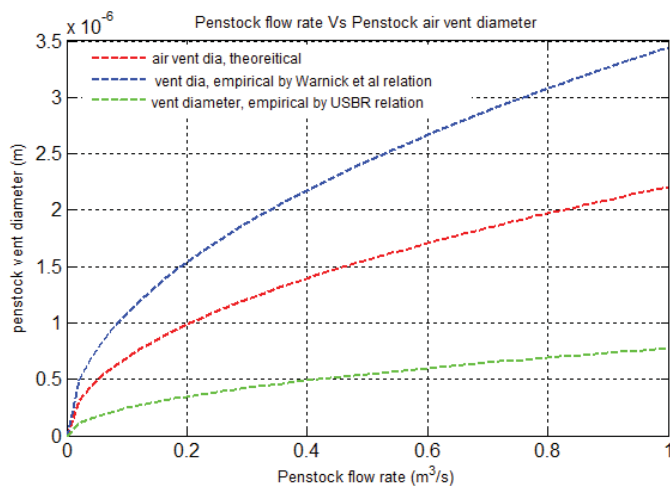


Figure 7.26: Discharge vs Penstock vent diameter

7.5.2 Pelton turbine bucket design charts

Figure 7.27 shows the relation between flow rate and turbine power when turbine efficiency is 83 %. Figure 7.28 shows the variations of flow rate against water jet diameter for two nozzles.

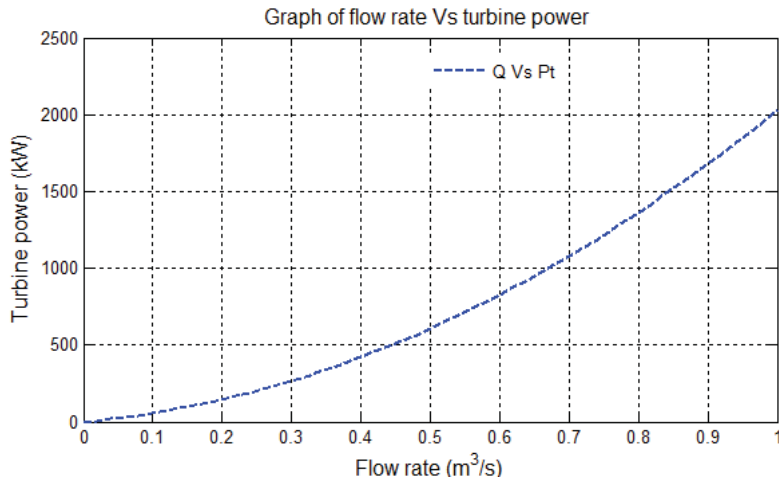


Figure 7.27: Discharge vs power of turbine

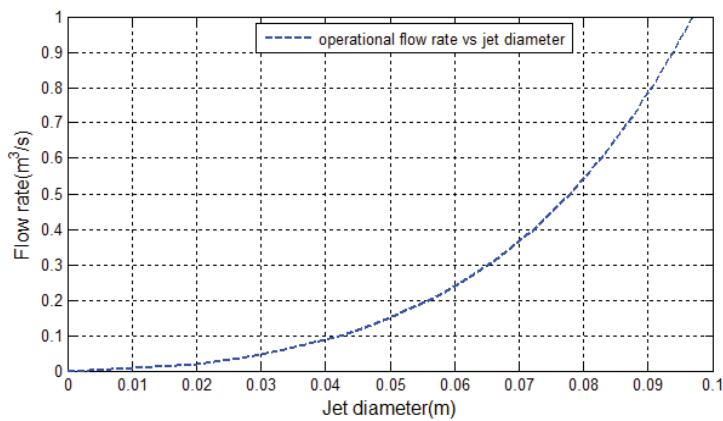


Figure 7.28: Discharge vs Jet diameter

The variations of runner tangential velocity against runner diameter at different speeds of rotation are shown in Figure 7.29, while the relation between bucket features and jet diameter is presented in Figure 7.30.

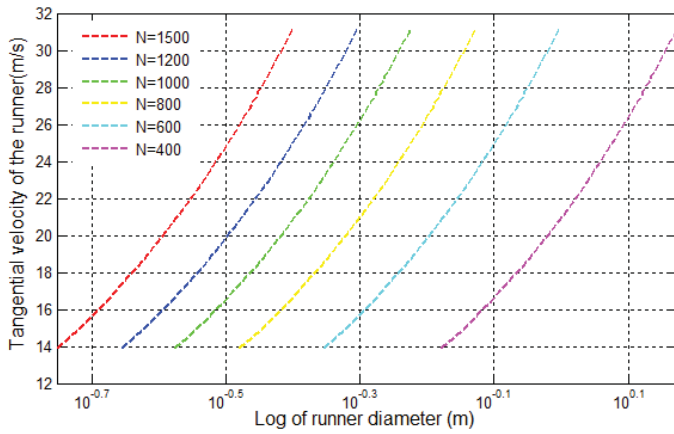


Figure 7.29: Velocity vs runner diameter of a turbine

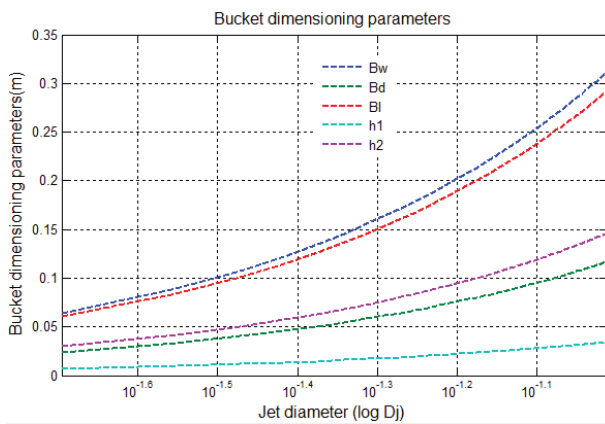


Figure 7.30: Bucket design parameters

Figure 7.31 shows the correlation between the operational flow rate and specific speed at varying rotational speed. The efficiency against turbine power at varying net heads is shown in Figure 7.32.

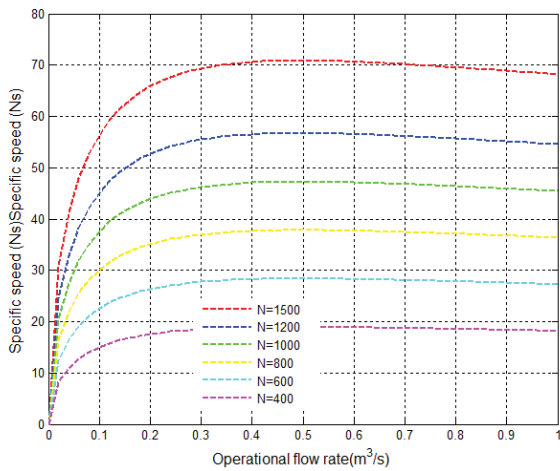


Figure 7.31: Rotational speed vs specific speed

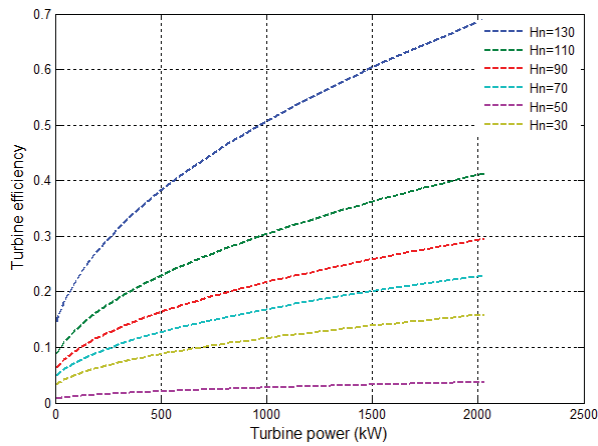


Figure 7.32: Turbine power vs turbine efficiency

The relationship between the runner torque and reaction force shows proportionality; the resulting curve is shown in Figure 7.33. The graph of turbine shaft against turbine power at different rotation speeds is shown in Figure 34.

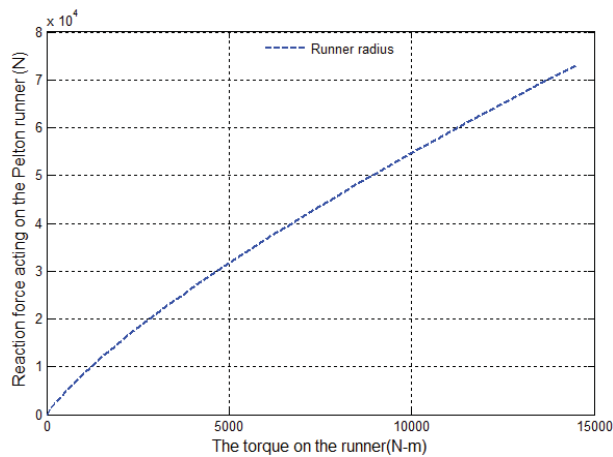


Figure 7.33: Graph of torque against reaction force

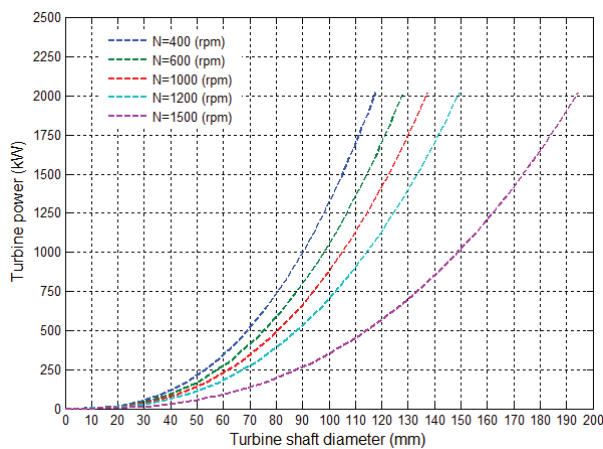


Figure 7.34: Graph of turbine shaft against power

7.6 Prototype design parameters

A prototype bucket was designed and Table 7.11 contains the results of the design calculation.

Table 7.11: Main turbine design parameters and constants

<i>Given quantities:</i> $Q = 0.033 \text{ m}^3/\text{s}$; $H_n = 60 \text{ m}$; $g = 9.81 \text{ m/s}^2$; $C_n = 0.97$; $k_u = 0.46$; $\rho = 10^3 \text{ Kg/m}^3$; $x = 0.46$; $n_z = 2$; $N = 1500 \text{ rpm}$; and $\eta_t = 95\%$			
Parameters	Calculated Value	Parameters	Calculated Value
The input power to the turbine, P_{ii} (kW)	18.45 kW	Bucket radial length, B_1 (m)	0.75 m
Specific speed (N_s)	8.98	Bucket depth, B_d (m)	0.03 m
Jet velocity, V_j (m/s)	33.28 m/s	Cavity Length, h_1 (m)	0.009 m
Jet/nozzle diameter, D_j	0.025 m	Length to Impact Point, h_2 (m)	0.038 m
Tangential velocity of the runner, V_{tr}	15.31 m/s	Offset of Bucket, k (m)	0.004 m
Runner diameter D_r , (m)	0.19 m	Cavity Width, a (m)	0.03 m
nozzle cross-sectional area, A_j	0.0005 m	Number of buckets n_z	19
Nozzle flow rate, Q_n (m^3/s)	0.017 m^3/s	Length of bucket moment arm, L_{ab} (m)	0.049 m
Distance between bucket and nozzle, x_{nb} (m)	0.119 m	Absolute reaction force acting on the Pelton runner, F (N)	1,186 N
Radius of bucket centre of mass to runner centre R_{br} (m)	0.089 m	The torque on the runner is T_i :	112.67 N/m
Bucket axial width, B_w (m)	0.08 m		

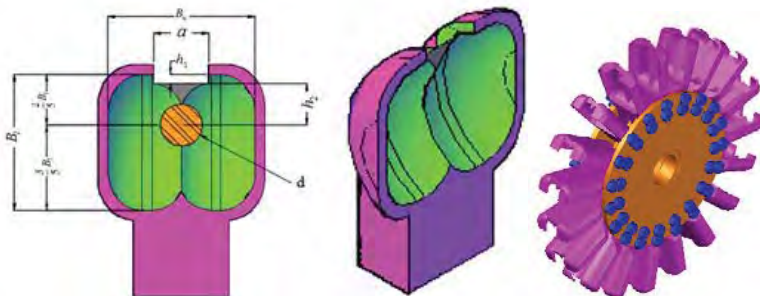


Figure 7.35: The designed bucket prototype

7.7 Pelton bucket simulation results

The Pelton designed as shown in Figure 7.35 was simulated with Solidworks software and the simulation results were reported. Table 7.12 contains information regarding the name and mechanical properties of the bucket material.

Table 7.12: Mechanical properties of the bucket material

Name:	356.0-T6 (Permanent Mould cast)	Elastic modulus:	7.24e+010 N/m ²
Model type:	Linear Elastic Isotropic	Poisson's ratio:	0.33
Yield strength:	1.52e + 008 N/m ²	Mass density:	2680 kg/m ³

Tensile strength:	2.28e + 008 N/m ²	Shear modulus:	2.72e + 010 N/m ²
Compressive strength:	1.85e + 008 N/m ²	Thermal expansion coefficient:	2.1e-005 / Kelvin

Table 7.13 presents information about the simulation study properties.

Table 7.13: Study properties

Study name	Static stress
Analysis type	Static
Mesh type	Solid Mesh
Type of load applied	Normal force
Load value	1186 N

Figure 7.36(a-e) shows the simulation processes: (a) the computer aided drafting (CAD) of the bucket; (b) the areas of force application and the fixtures; (c) the mesh pattern; (d) the von Mises representation of static stress; and, (e) the von Mises static stress results in colour bar. Table 7.14 and Figure 7.36e present the maximum stress of $6.723 \times 10^7 \text{ N/m}^2$, recorded in the upper part of the splitter, denoted as S in Figure 7.36d. This value is less than the yield strength ($1.52 \times 10^8 \text{ N/m}^2$) of the bucket material (A356-T6). This means that the design is safe.

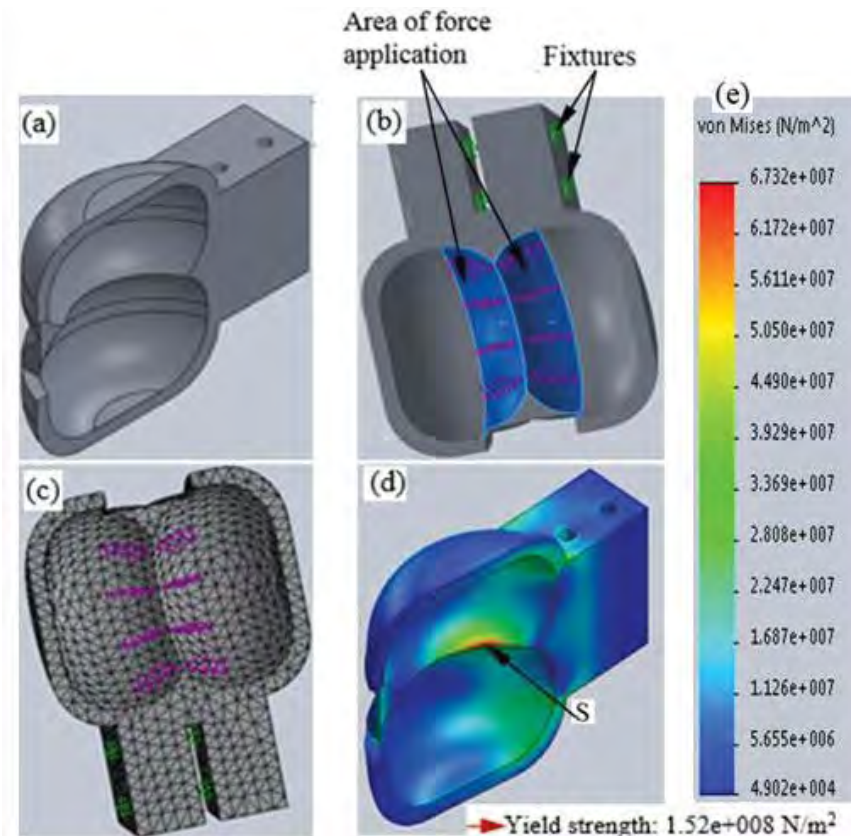


Figure 7.36: Diagrammatic representation of simulation process and von Mises result

Table 7.14 presents the von Mises stress, displacement, and strain performance of the prototype Pelton bucket.

Table 7.14: von Mises stress, displacement, and strain results

Name	Type	Min	Max
Stress	VON: von Mises Stress	49016.3 N/m ² Node: 10307	6.73216e+007 N/m ² Node: 7460
Displacement	URES: Resultant Displacement	0 mm Node: 370	0.172845 mm Node: 1289
Strain	ESTRN: Equivalent Strain	4.82532e-007 Element: 2977	0.000622133 Element: 8721

7.8 Conclusion

Adequate access to reliable, quality and affordable power is a necessity to enhance the standard of living in SSA. Inadequate power supply has hindered economic development in the region, especially in the rural areas, for decades, yet the huge SHP potentials available in the region are untapped. Small hydropower systems have been identified as environmentally friendly, cost effective and simple renewable energy schemes suitable for rural electrification in the region. There is a need to popularise SHP schemes for rural areas, industrial estates and standalone electrification rather than for national grids in SSA. Domestic design and development of SHP components and systems will facilitate greater access to power in the region. Small hydropower capacity building and use of locally sourced materials will promote domestic participation in the design, manufacturing of SHP components and application of SHP systems. This study, therefore, developed SHP system design codes and charts using Matlab and a simplified SHP design process and considered materials and manufacturing techniques available locally. A390 and A390-5Mg cast aluminium alloys were investigated for a Pelton bucket using Solidworks simulation software. The materials performances measured by von Mises, displacement and strain results were outstanding.

Bibliography

- [1] M. M. Alnakhilani, Mukhtar Mukhtar, D. A. Himawanto, A. Alkurtehi and D. Danardono, "Effect of the bucket and nozzle dimension on the performance of a pelton water turbine," *Modern Applied Science*, vol. 9, pp. 25-33, 2015.
- [2] M. Mohibullah, A. M. Radzi and M. I. A. Hakim, "Basic design aspects of micro-hydro-power plant and its potential development in Malaysia," presented at the National Power and Energy Conference (PECon), Pan Pacific Glenmarie Kuala Lumpur, Malaysia, 2004.
- [3] B. A. Nasir, "Design of micro-hydro-electric power station," *International Journal of Engineering and Advanced Technology (IJEAT)*, vol. 2, pp. 39-47, 2013.
- [4] W. S. Ebhota and F. L. Inambao, "electricity insufficiency in Africa: a product of inadequate manufacturing capacity," *African Journal of Science, Technology, Innovation and Development*, vol. 8, pp. 197-204, 2016.
- [5] W. S. Ebhota and F. L. Inambao, "Design basics of a small hydro turbine plant for capacity building in sub-Saharan Africa" *African Journal of Science, Technology, Innovation and Development*, vol. 8, pp. 111-120, 2016.
- [6] O. Paish, "Small Hydropower: technology and current status. renewable and sustainable," *Energy Reviews*, vol. 6 pp. 537-556, 2002.
- [7] UNIDO Projects for the Promotion of Small Hydropower for Productive Use (11/10/2016). Independent Thematic Review. Available: https://www.unido.org/fileadmin/user_media/About_UNIDO/Evaluation/Project_reports/e-book_small-hydro.PDF.
- [8] S. Sebin, A. A. Tom, J. G. Nikhil and C. A. Ashwin, "Design and modelling of a pelton wheel bucket: theoretical validation and software comparison," *International Journal of Engineering Research & Technology (IJERT)*, vol. 3, 2014.
- [9] B. A. Nasir, "Design of high-efficiency pelton turbine for micro-hydropower plant," *International Journal of Electrical Engineering and Technology (IJEET)*, vol. 4, no. 1, pp. 171-183, 2013.
- [10] L. Gudukeya and I. Madanhire, "Efficiency improvement of pelton wheel and crossflow turbines in micro-hydropower plants: case study," *International Journal of Engineering and Computer Science*, vol. 2, pp. 416-432, 2013.
- [11] W. Bolon, V. Sharma and M. Singh, "Green mechatronics project: pelton wheel driven micro-hydro plant," Mechanical Engineering University of Ottawa, 2010.

- [12] R. N. Mbiu, S. M. Maranga and H. Ndiritu, "Performance of aluminium A356 alloy based buckets towards bending forces on Pelton turbines," in *Proceedings of the Sustainable Research and Innovation (SRI) Conference*, Nairobi, Kenya, 2015, pp. 134-138.
- [13] A. K. M. K. Islam, S. Bhuyan and F. A. Chowdhury, "Advanced composite Pelton wheel design and study its performance for pico/micro hydropower plant application," *International Journal of Engineering and Innovative Technology (IJEIT)*, vol. 2, no. 11, pp. 126-132, 2013.
- [14] N. N. I. Reddy and T. S. Prasad, "Design and static analysis of Pelton turbine bucket" *International Journal of Science Technology and Management*, vol. 4, pp. 19-25, 2015.
- [15] W. S. Ebhota and F. L. Inambao, "Design basics of a small hydro turbine plant for capacity building in sub-Saharan Africa," *African Journal of Science, Technology, Innovation and Development*, vol. 8, pp. 111-120, 2016.
- [16] European Small Hydropower Association (ESHA), "Energy recovery in existing infrastructures with small hydropower plants," presented at the Sixth Framework Programme, Mhylab, Switzerland, 2010.
- [17] V. T. Chow, *Open-Channel Hydraulics*. Michigan: McGraw-Hill, 1959.
- [18] M. E. S. Haestad and E. M. Michael, *Computer Applications in Hydraulic Engineering: Basic Hydraulic Principles*. Waterbury, CT: Haestad Methods, Inc., 2002.
- [19] British Hydropower Association (BHA), "A guide to UK mini-hydro development," Wimborne, United Kingdom: British Hydropower Association 2012.
- [20] A. Kunwor, "Technical specifications of micro hydropower system design and its implementation: feasibility analysis and design of Lamaya Khola micro hydropower plant," Bachelor's Degree Thesis, Industrial Management, Arcada Polytechnic, Nepal, 2012.
- [21] Pakistan Poverty Alleviation Fund (PPAF), *Renewable Energy Guidelines: Micro/Mini Hydropower Design Aspects* vol. 11. Islamabad: Pakistan Poverty Alleviation Fund, 2013.
- [22] C. Penche, *Layman's Guidebook on How to Develop a Small Hydro Site*, Second edition ed. Belgium: The European Small Hydropower Association (ESHA), 1998.
- [23] B. A. Nasir, "Design consideration of micro hydro-electric power plant," *Energy Procedia*, vol. 50, pp. 19–29, 2014.

- [24] Y. Amarjeet and P. G. Shriram, "Prospect of micro hydropower in hilly area," *International Journal of Scientific Research and Development*, vol. 2, pp. 2321-0613, 2014.
- [25] Indonesian Renewable Energy Commission (IREC). (2015, 10/08/2016). Penstock thickness calculation (case study). Available: <http://indmicrohydro.blogspot.co.za/search/label/Penstocks>.
- [26] The Engineering ToolBox. (2016, 19/07/2016). Manning's roughness coefficients for common materials. Available: www.engineeringtoolbox.com/mannings-roughness-d_799.html.
- [27] M. K. Singhal and A. Kumar, "Optimum design of penstock for hydro projects," *International Journal of Energy and Power Engineering*, vol. 4, pp. 216-226, 2015.
- [28] C. C. Warnick, H. A. Mayo, J. L. Carson and L. H. Sheldon, *Hydropower Engineering*. Englewood Cliffs, NJ: Prentice-Hall Inc., 1984.
- [29] G. S. Sarkaria, "Economic penstock diameter: a 20-year review," *Water Power and Dam Construction November*, vol. 31, pp. 70-72, 1979.
- [30] United States Department of the Interior, Bureau of Reclamation, "Welded steel penstocks," Engineering Monograph No. 3, Washington, 1986.
- [31] F. Fablbusch, "Determining diameters for power tunnels and pressure shafts" *Water Power and Dam Construction*, February, 1987.
- [32] American Society of Civil Engineers (ASCE), *Steel Penstocks Manuals and Reports on Engineering Practice No. 79*. New York: American Society of Civil Engineers, 1993.
- [33] A. Bulu. (no date, 30/07/2016). Hydroelectric power plants. Available: web.itu.edu.tr/~bulu/hydroelectric.../lecture_notes_12.pdf.
- [34] O. Zia, O. A. Ghani, S. T. Wasif and Z. Hamid, "Design, fabrication and installation of a micro-hydropower plant," Mechanical Engineering, GIK Institute of Engineering Sciences & Technology, 2010.
- [35] American Society of Mechanical Engineers (ASME) Hydropower Technical Committee, *The Guide to Hydropower Mechanical Design*. New York, NY: American Society of Mechanical Engineers, 1996.
- [36] J. F. Claydon. (2015, 18/05/2015). Turbines. Available: <http://www.jfccivilengineer.com/turbines.htm>.
- [37] S. L. Dixon and C. A. Hall, *Fluid Mechanics and Thermodynamics of Turbomachinery-Chapter 9 – Hydraulic Turbines*, 7th ed. Oxford: Elsevier Inc, 2014.

- [38] E. Logan and R. Roy, *Handbook of Turbomachinery*, New York, NY: Marcel Dekker Inc, 2003
- [39] P. Henry, *Turbomachines Hydrauliques*, 1st ed. Ecublens, Switzerland,: PPUR, 1992.
- [40] H. Brekke, *Pumper & Turbiner*. Trondheim: Vannkraftlaboratoriet NTNU, 2003.
- [41] M. F. White, *Fluid Mechanics*. New York, NY: McGraw Hill 2008.
- [42] G. Okhay, "Utilisation of CFD tools in the design process of a Francis turbine," Master thesis, Middle East Technical University, Ankara, Turkey, 2010.
- [43] International Energy Agency (IEC), "Field acceptance tests to determine the hydraulic performance of hydraulic turbines, storage pumps and pump-turbines," IEC International standard 60041, 3rd ed, 1991.
- [44] North American Electric Reliability Corporation (NERC), "Appendix F, performance indexes and equations," Atlanta, GA: North American Electric Reliability Corporation, 2011.
- [45] P. Adhikary, P. K Roy and A, Mazumdar, "Selection of hydro-turbine blade material: application of fuzzy logic (MCDA)," *International Journal of Engineering Research and Applications*, vol. 3, pp. 426-430, 2013.
- [46] W. S. Ebhota, A. S. Karun and F. L. Inambao, "Centrifugal casting technique baseline knowledge, applications, and processing parameters: overview," *International Journal of Materials Research*, 04 August, 2016.

CHAPTER 8: INVESTIGATION OF FUNCTIONALLY GRADED ALUMINIUM A356 ALLOY AND A356-10%SiC_p COMPOSITE FOR HYDRO TURBINE BUCKET APPLICATION

W. S. Ebhota and F. L. Inambao, "Investigation of Functionally Graded Aluminium A356 Alloy and A356-10%SiC_p Composite for Hydro Turbine Bucket Application," *International Journal of Engineering Research in Africa*, 2016, Vol. 26, pp 30-46. DOI:10.4028/www.scientific.net/JERA.26.30 (*Published*).

Investigation of Functionally Graded Aluminium A356 Alloy and A356-10%SiC_p Composite for Hydro Turbine Bucket Application

Ebhota Williams S.^{1, a}, Akhil S. Karun^{2, b} and Inambao, Freddie L.^{3, c}

^{1, 3}Discipline of Mechanical Engineering, Howard College, University of KwaZulu-Natal, Durban, South Africa.

²Materials Science and Technology Division, CSIR-National Institute for Interdisciplinary

^aEmail: willymoon2001@yahoo.com, ^bEmail: akhilskarun@gmail.com,

^cEmail: inambaof@ukzn.ac.za

Keywords: Functionally graded materials; centrifugal casting; A356 alloy; A356-10%SiC_p composite; Pelton bucket; turbine blade

Abstract. The study investigates the application of centrifugal casting process in the production of a complex shape component, Pelton turbine bucket. The bucket materials examined were functionally graded aluminium A356 alloy and A356-10%SiC_p composite. A permanent mould for the casting of the bucket was designed with a Solidworks software and fabricated by the combination of CNC machining and welding. Oil hardening non-shrinking die steel (OHNS) was chosen for the mould material. The OHNS was heat treated and a hardness of 432 BHN was obtained. The mould was put into use, the buckets of A356 Alloy and A356-10%SiC_p composite were cast, cut and machined into specimens. Some of the specimens were given T6 heat treatment and the specimens were prepared according to the designed investigations. The micrographs of A356-10%SiC_p composite shows more concentration of SiC_p particles at the inner periphery of the bucket. The maximum hardness of As-Cast A356 and A356-10%SiC_p composite were 60 BRN and 95BRN respectively, recorded at the inner periphery of the bucket. And these values appreciated to 98BRN and 122BRN for A356 alloy and A356-10%SiC_p composite respectively after heat treatment. The prediction curves of the ultimate tensile stress and yield tensile stress show the same trend as the hardness curves.

Introduction

The study focuses on the wear and strength properties enhancement of A356 aluminium alloy and A356-10%SiC_p composite, exploring manufacturing process (casting) and heat treatment process for Pelton bucket production. The use of locally sourced materials for SHP hydro turbine components and their manufacturing technologies, is very crucial to energy provision and sustainability in sub-Saharan Africa (SSA). Domestication of SHP technology, is the key to the perennial rural electrification problems in the region. To effectively tackle the perennial power in Sub Sahara Africa (SSA), the electricity generation and distribution technologies should be domesticated in the region. This will ensure that challenges as regards to high cost of power project, duration of project execution, installation, operation, maintenance and repair and downtime will be tackled and sustained. Several authors and energy research organisations see small and micro power system of renewable energy are the best option for rural and off grid areas in SSA [1, 2]. It therefore, imperative for countries of SSA to develop small and micro renewable energy system for her economic gains.

Technical capacities building for hydro turbine components and system; design, material selection and manufacturing should be promoted through regional joint effort, academic research, exchange programme with the developed countries, etc. [3]. The capacity building, should be such that will increase local participation in SHP technology domestication in the region. SSA with a lot of untapped SHP potentials as presented in Table 1, needs to explore merits of SHP for greater access to power [4].

Table 1: SHP potential in SSA [4]

Regions in SSA	Available SHP potential (MW)	Installed capacity (MW)	Installed capacity (%)
Eastern Africa	6,262	209	3.3
Middle Africa	328	76	23.1
South Africa	384.5	43	11.2
West Africa	742.5	82	11.1

Review

Loice and Ignatio investigated the effects of material, surface texture and fabrication methods on efficiency of hydro power plant within an acceptable cost range. The study concluded that manufacturing of more efficient financially viable Pelton turbines for SHP is possible. In their project, more electricity was generated at a reduced cost per unit kW [5]. A theoretical micro-hydroelectric plant design for off grid applications was carried out to produce a green power for remote farms or cottage. A prototype of the system was built to test the design [6].

A study on the modelling and validation of results empirically, using locally available materials was carried out in Kenyan [7]. In the study, 14.2 % stress reduction was achieved by modifying the profile of the Pelton bucket. A recycled A356 aluminium alloy, was found to withstand stress of 150Mpa, produced by the generated 5 kW power [7]. A Pelton turbine was designed and manufactured for Pico Pelton turbine, using chopped glass fibres reinforced epoxy matrix composite as the bucket material [8]. A 50,000 litres capacity storage tank in a 10 storey tower was used as a water source to operate the turbine. In the study, 1.5 kW was generated out the 2.793 kW that was theoretically designed for. In the design study of Nava and Siva, CATIA V5 design and modelling software was used to designed and optimised Pelton turbine considering three materials in the analysis [9]. Efficient and stress in relation with the number of buckets were studied in the work. In the three bucket materials selected (steel, cast iron and fibre glass reinforced plastic matrix), the study concluded that fibre glass reinforced plastic matrix shows exceptional performance compared to cast iron. However, there are striking limitation in that are associated with the use fibre reinforced composite. It requires depth expertise, most of the material constituents are imported, and forms solid waste it is damage as most cases recycling and decomposition are not possible. A lot of theoretical design work of hydro turbine have been studied. However, only few is known of the use of aluminium alloys and their composites for the fabrication of Pelton turbine bucket. Present applications of aluminium alloys and their composites, hypothetically suggest that aluminium alloys and composites are promising materials for Pelton turbine bucket and turbine blade fabrication.

Application of A356 alloy and A356-SiCp composite suitability for Pelton turbine bucket

Previous studies of hydro turbine plants, revealed that silt erosion affects the underwater components greatly which include turbine blade [10-12]. In some cases, water is stored in a reservoir or in a settling basin to be used when the need arises. Over a period of time, sediments that includes silts and hard abrasive sand settle at the bottom of the reservoir or basin. This problem must be taken care of by sediment settling systems in power plants. However, a lot of unsettled sediment still pass through the turbine every year and the turbine runner is therefore, exposed to severe erosion wear. This sediments are often prevented from go through the turbine by incorporating sediment settling systems in the power plant. However, there are still possibilities of unsettled sediment passing through the turbine and this occurrence causes serious erosion to the nozzle system and the turbine runner. The parts that are vulnerable to silt erosion are bucket/blade, faceplates and seal rings. Studies have shown that, silt erosion menace is more severe during the raining season [12, 13].

The effects of erosion on turbine depends on certain water and turbine material factors. The factors include water flow velocity and discharge, water salt concentration, silt quantity and size, and wear and corrosion resistance, hardness and strength of the turbine material. To effectively guide against turbine failure and to enhance its life span, the design consideration of these features is vital. However, wear and corrosion resistance enhancement of the turbine blade can be achieved through manufacturing method. This attribute improvement helps the blade to withstand the effect of the water salt concentration, and the moving unsettled silt and hard abrasive sand.

Metal Reaction in Environment

Presently, hydro turbine blades are made from metals and they show three types of behaviour when immersed in the environment: Immune behaviour, active behaviour and passive behaviour as shown in Fig 1 [14]. The noble metals like gold, silver and platinum show immune behaviour as they do not react with the environment and therefore, no corrosion. A metal is said to have an active behaviour when it corrodes in a solution and forms soluble, non-protective corrosion product. This active behaviour is associated with higher weight loss of the metal and example is mild steel immersion in NaCl solution (seawater). In the third behaviour, the metal corrodes in a solution, but forms an insoluble protective film that makes it to have a passive state. Passive films are different from paints for coating as some people hold. Sodium, potassium, and magnesium are active in almost all aqueous media. Titanium and tantalum are passive nearly in all aqueous environments. Aluminium and zinc are passive in some media, but are very active metals and show active character in many environments.

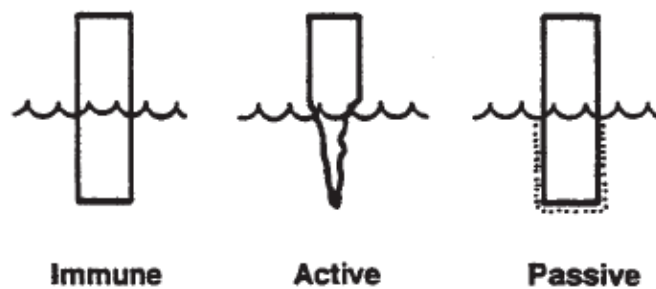


Fig 1: Three metal characters in an environment [14]

Seawater is the most corrodent natural medium where metals are commonly used and its composition has corrosive reagents, halides (NaCl and MgCl_2). The compositional content of seawater depends on geographical location and varies over a wide range, however, the salt content of World Ocean is approximately constant, about 3.1% [15, 16]. The world seas salt compositions are shown in table 2.

Table 2: Contents of salt in world Oceans and river water [16]

Oceans	salt content, %
Atlantic Ocean	3.5–3.8
Pacific Ocean	3.4–3.7
Mediterranean Sea	3.7–3.9
Red Sea	4.1
Sea of Azov	0.9–1.2
Baltic Sea	0.2–0.45
White Sea	1.9–3.3
Caspian Sea	1.0–1.5
Black Sea	1.7–1.85
Rivers	0.01–0.05

Aluminum alloys susceptibility to corrosion are reasonably differ, as a result, aluminum alloys can be categorised into two groups, according to their seawater corrosion resistance:

- i. High corrosion resistance alloys but vulnerable to pitting corrosion
- ii. Alloys vulnerable to intergranular corrosion (IGC) exfoliation corrosion (EC) and corrosion cracking (CC) the structural corrosion types.

Empirically, conducting laboratory corrosion test with traditional seawater is not always accurate due to the effects of other impurities apart from chlorides in seawater. Table 3 presents other impurities in seawater. The impurities affect structural corrosion types (EC, IGC and CC) susceptibility of metal.

Table 3: The standard seawater composition [17-19]

Salts	g/l water	%
NaCl	27.2	77.8
MgCl ₂	3.8	10.9
MgSO ₄	1.7	4.7
CaSO ₄	1.2	3.6
K ₂ SO ₄	0.9	2.5
CaCO ₃	0.1	0.3
MgBr ₂	0.1	0.2
Totally	35	100

The Al-Si cast alloys and their composites, are known for superior properties like corrosion and wear resistance, high strength, low thermal coefficient, excellent castability, etc. This has make them relevant materials for number of applications in airspace and other engineering industries. Various methods are used to develop and improve the properties of Al-Si cast alloys and composites. These properties are depended on microstructure of the matrix, and the size, shape, type and volume of reinforcement in the matrix. Wear resistance and other mechanical properties are function of the hardness of the second phase particles in the matrix [20, 21].

Functionally graded manufacturing technique: Centrifugal casting technique

Centrifugal casting technique was chosen due to its mechanical and microstructural enhancing advantages. The process aids microstructure gradient and improve hardness of alloys even without reinforcement and therefore, gives the material a better wear and corrosion resistance [22]. The mechanical properties of aluminium–silicon alloys are often improved by casting technology [23]. Quite often, hypoeutectic and near eutectic Al-Si alloys are applied when corrosion resistance and good castability are needed and with little quantity of Mg and Cu for heat treatment enhancement. It has been revealed that centrifugal can increase: rupture strain by 160% and rupture strength by 35%; young modulus by 18% and; fatigue life by 1.5% [24].

Methodology of the Study

The study is divided into two parts: manufacturing of Pelton turbine bucket by centrifugal casting technique and; characterisation of Pelton turbine bucket materials.

Manufacturing of Pelton turbine bucket

The fabrication of Pelton turbine bucket has two stages: Production of permanent mould and; centrifugal casting of the Pelton bucket. The 3D model of the bucket is shown in Fig 2. In this study, the bucket was designed for a capacity of 18.45kW turbine power.

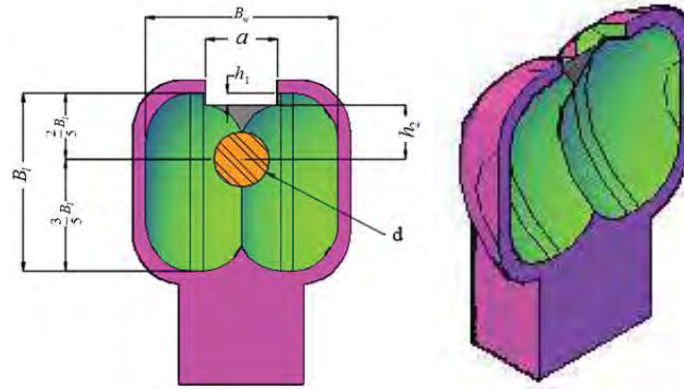
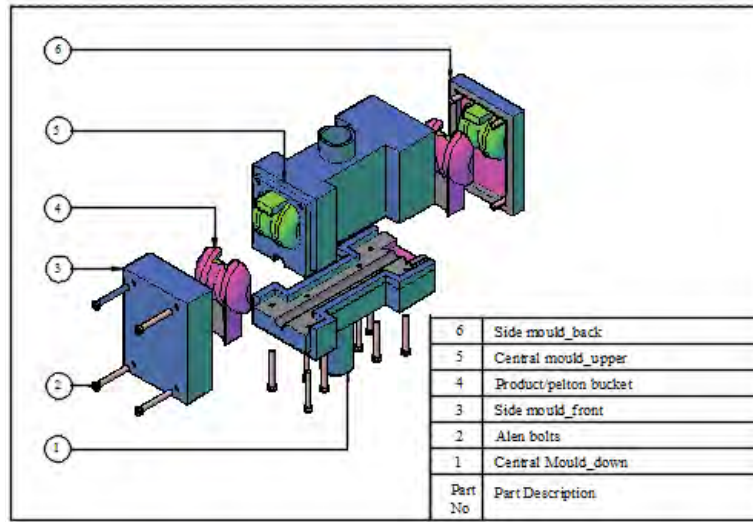
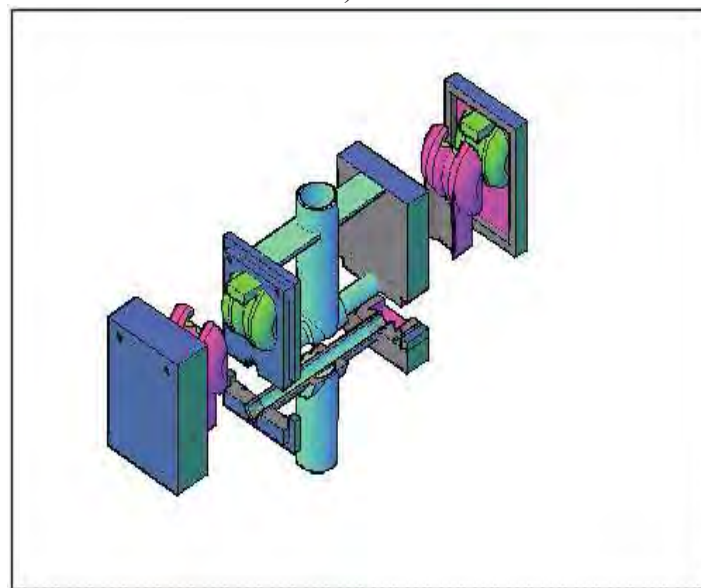


Fig 6: The diagram shows the design parameters of a bucket

Production of Mould. The mould was designed with Solidworks software where the IGES files of the mould components were generated. Computer numerical control (CNC) machining centre was used to machine the components of the permanent mould. The computer aided design (CAD) drawing of the mould as designed and as produced are shown in Fig 3(a) and (b) respectively.



a)



b)

Fig 3: a) Exploded diagram of the Pelton bucket mould as designed; b) Exploded diagram of the Pelton bucket mould as fabricated

Mould Material. Oil Hardening Non Shrinking Die Steel (OHNS) was used as the mould material and the components were heat treated before they were put to use. The chemical composition is shown in Table 4. OHNS steel is a reliable material for gauging, blanking and cutting tools as well as for hardness and elevated temperature performance [25]. The hardening temperature used was 800 °C and had a hardness of about 432 of Brinell 3000Kgf standard. The fabricated Pelton bucket mould components are shown in Fig 4

Table 4: Chemical composition of the OHNS material used for the Pelton bucket mould.

Element	C	Mn	Cr	W	V
%	0.95	1.1	0.6	0.6	0.2

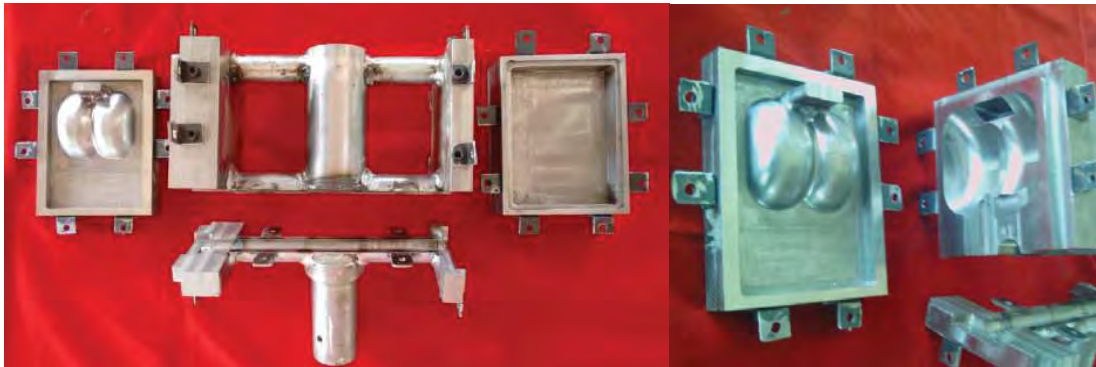


Fig 4: The fabricated Pelton bucket mould components

Centrifugal Casting of Pelton Bucket. The functionally graded materials (FGMs), A356 alloy and A356-10%SiC_p are under investigation. The chemical composition of A356 used is shown in Table 5.

Table 5: A356 alloy chemical composition

Elements	Cu	Mg	Mn	Si	Fe	Ti	Zn	Al
%	0.25	0.30	0.35	7.5	0.35	0.05	0.10	91.10

Casting of A356 Alloy. Clay graphite crucible was used to process the alloy. Hexachloroethane was applied at 720 °C for degassing of the molten metal to prevent hydrogen entrapment. The molten metal was superheated to 750 °C, above its Liquidus temperature. The liquid metal was then poured into a spinning Pelton bucket mould (centrifugal casting) and a stationary rectangular mould (gravity casting). The moulds were preheated to 300 °C and the Pelton bucket mould was rotated at 1500 RPM during pouring and solidification. The rotation was stopped 5 minutes after pouring.

Casting of A356-10%SiC_p Composite. The same melting conditions for A356 alloy as stated above, were followed for the casting of A356-10%SiC_p composite. The 25 µm SiC particle was preheated to 600 °C before inserting it into the A356 molten and the mixture was stirred with electric motor driven impeller at a speed of 300 RPM. The particle feed rate to the molten metal is about 1gm/s and the mixture was stirred 15 minutes more after the particle addition.

In the mould configuration, it is designed to produce castings in one operation. The arrangement is such that the faces are in the same direction as depicted in Fig 5.

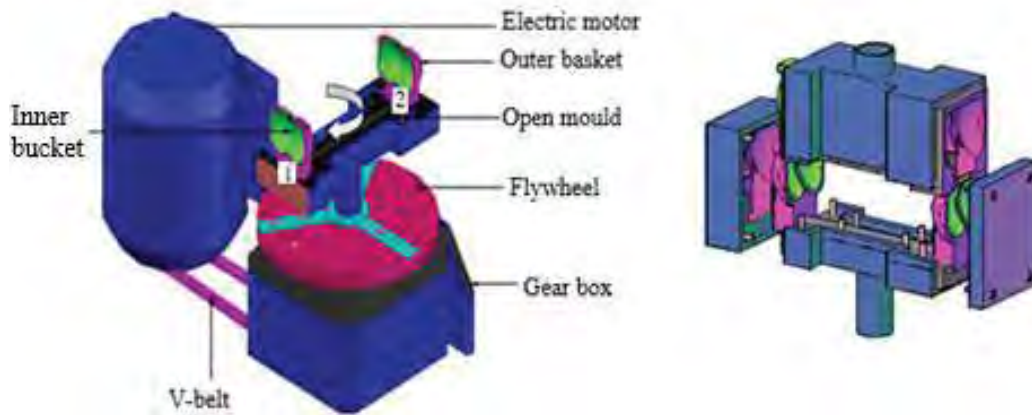


Fig 5: Centrifugal casting machine with an opened mould in which the buckets are facing the same direction

Preparation of test specimen

Microstructure Examination. The cast bucket of both materials under investigation were sliced at the middle (plan X-X, see Fig 6a) into two parts and both halves were prepared for microstructural examination and hardness test. The samples for the microstructural view were polished using the following grades of grit emery papers of 80, 100, 320, 400, 600 and 1000 consecutively. The emery paper polishing was followed by cloth polishing with 6 μm , 3 μm and 1 μm SiC_p particle pastes. The prepared samples for microstructural examination are shown in Fig 6. The polished sample was subjected to Leica optical microscopy for transverse viewing as shown by the arrow in Fig 6d and capturing.

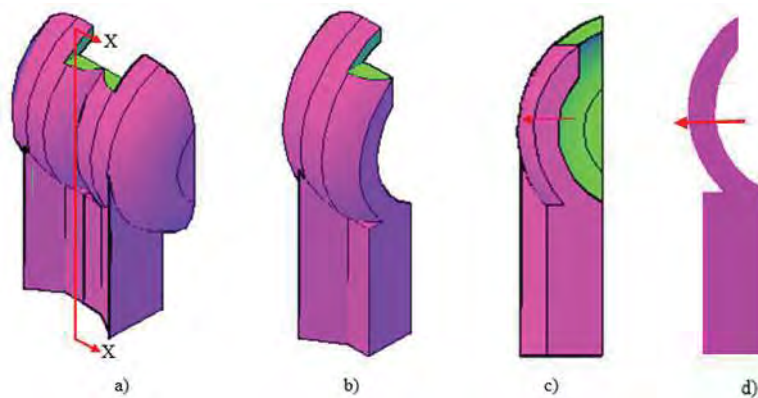


Fig 6: Method of preparing the samples for microstructural examination and hardness test

Hardness Test. The second half of the sample was prepared for Brinell hardness test and was only subjected to polishing using grades of grit emery papers of 80, 100, 320, 400, 600 and 1000 respectively. The specimens for hardness test are shown in Fig 7. The polished sample was subjected to 62.5Kgf load of Tinius Olsen hardness test machine transversely as shown by the dots in Fig 7b.

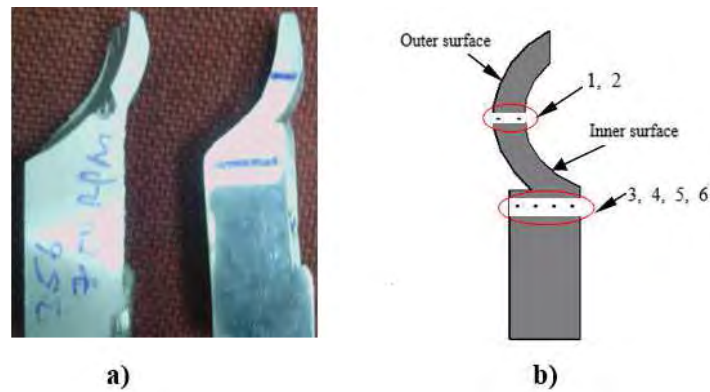


Fig 7: a) Specimens for microstructural examination and for hardness test; b) offset of the face of the specimen

Heat Treatment. The solution heat treatment (T6), is the most widely used for the improvement of the combination of strength and ductility. A356 alloy test sample was treated according to T6 heat treatment standard for A356 alloy for hardness, strength and ductility enhancement. The specimen was heated to 540 °C and held for 4 hours and quenching in a water of 65 °C temperature according to earlier studies [26, 27]. Artificial aging was carried out at 165 °C for 6 hours and the process profile is shown in Fig 8. A356-10%SiC_p composite specimen was heated to 520 °C, held for 8 hours and quenching in a water of 80 °C temperature. The artificial aging was done at 160 °C and held for 20 hours [28]. The heat treatment process for A356-10%SiC_p is represented in Fig 9. Quenching was done in accordance with the B-917 ASTM standard, with the cooling from 400 °C to 260 °C and the quenching delay time was less than 10 seconds. These precaution measures were necessary to prevent the formation of premature precipitate.

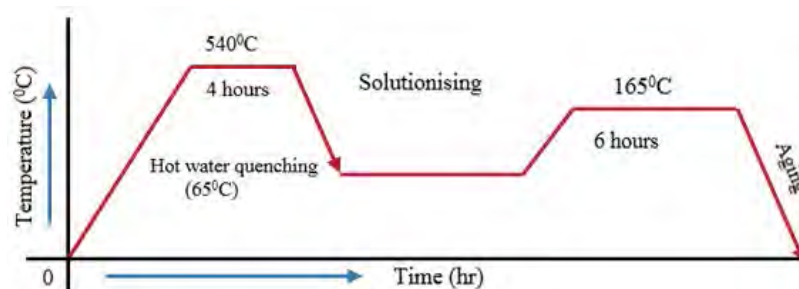


Fig 8: Schematic of T6 Heat Treatment of A356 Alloy profile

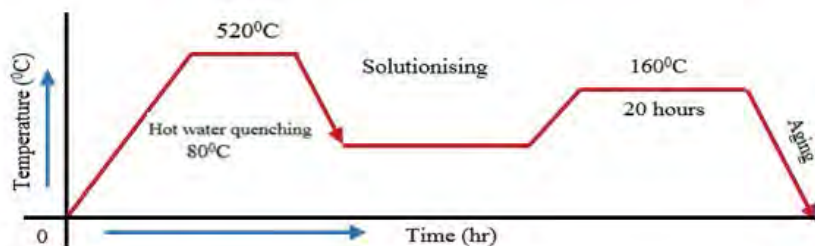


Fig 9: Schematic of T6 Heat Treatment of A356-10%SiC composite profile

Results and Discussion

Casting of Pelton bucket by centrifugal process

The first few castings shown the same defect as the one shown in Fig 10a. The defect was caused by the centrifugal force effect on the cast bucket. This was a major challenge in this study. Several attempts were made by changing the process variables before a good cast was made. In centrifugal casting, there is the tendency of the surface of the cast, towards the centre of rotation, to form a parabola of revolution as depicted in the schematic in Fig 10b.

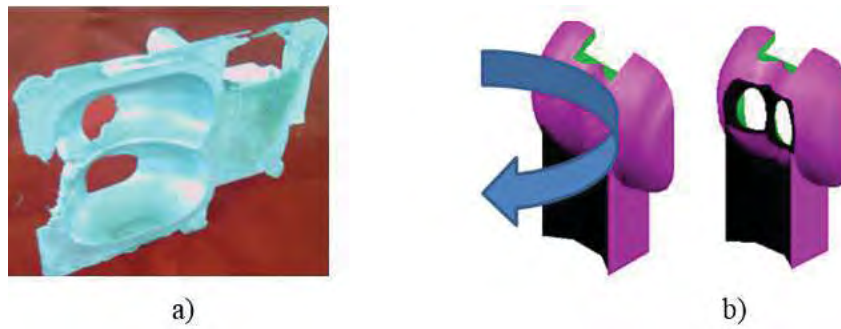


Fig 10: a) a defected cast caused by centrifuge; b) schematic of the effect of centrifuge cast

The curve formed is a function of these parameters: the rotational speed; the cast geometry and; pouring and mould temperatures. In this work, the defect was corrected significantly by geometry and Fig 11 shows the defect free Pelton bucket cast.



Fig 11: The defect free Pelton bucket cast

Microstructural examination

The micrograph of buckets 1 and 2 is shown in Fig 12. It was observed that the two buckets have the same gradient trend. However, the trend in 2 was in opposite direction of 1. For the purpose of the operational performance of the bucket, especially for wear resistance, bucket 1 arrangement in Fig 5 is preferred. Figs 12 and 13 show the pattern of microstructure gradient of the alloy and composite respectively used in bucket 1.

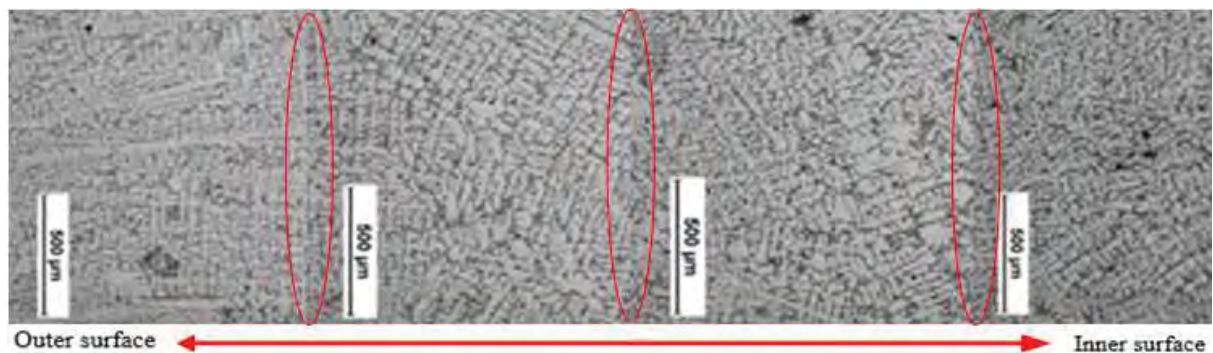


Fig 12: The micrgraph the gradient of cast bucket 1 of A356 alloy.

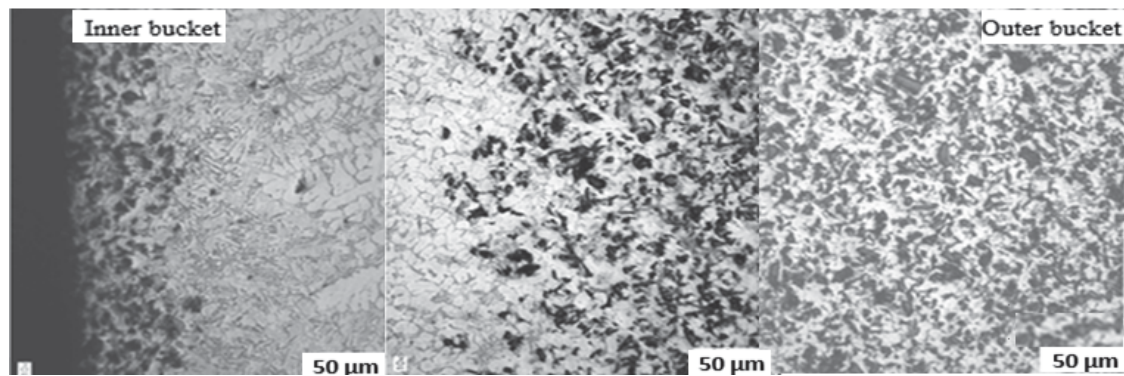


Fig 13: The micrograph the gradient of cast bucket 1 of A356-10%SiC_p composite

Effect of T6 heat treatment and centrifugal casting technique on hardness

A356 alloy, which has Al-7.5%Si-0.3Mg is widely used in engineering industries like automotive, aerospace and military applications for high strength parts. It offers good combination of mechanical properties such as castability, strength, corrosion resistance and pressure tightness in both the permanent mould and sand cast condition. Despite these attributes, in most cases, A356 alloy is not used as-cast, as the presence of eutectic silicon causes it to perform below optimal value. Generally, mechanical properties of aluminium alloys and composites are reduced by coarse grain, cavities and needle shape eutectic silicon. Modification and refinement improve the mechanical properties of alloy such as tensile strength, impact strength, wear resistance and hardness significantly [29, 30]. Rapid solidification, vibration, heat treatment and chemical treatment are the basic methods of manipulating the morphology of an alloy for properties enhancement. In chemical treatment, small amount of sodium is added to the melt and this changes the eutectic silicon phase morphology from coarse acicular to fine fibrous. The process results in enhancement of mechanical property. [31-33].

Centrifugal Casting. The large dendritic cells, large flakes of silicon and large inter-dendrite arm spacing of α -aluminum dendrites that are produced by low solidification rate. These morphological features need to be refined and modified for the alloy to possess better mechanical properties. High solidification rate gives small dendritic cells, small inter-dendrite arm spacing and small flakes of silicon and morphologically changed from acicular to fibrous [34]. Centrifugal casting influences the rate of solidification and consequently enhances the quality of casting.

The rate at which centrifuge affects the microstructure of an alloy is speed of rotation depended. Studies have shown that the optimum centrifugal is between 1200-1500 RPM [34, 35]. At the speed of 1500 RPM, the microstructure of the bucket experiences the following: transformation of large primary silicon into needle shaped eutectic silicon in the inner; long needle-shaped eutectic silicon are converted into fine primary silicon at the outer and; there is the formation of fine grain. The transformations and the high rate of solidification, enhanced the hardness value of both A356 alloy and A356-10%SiC_p composite. This transformation is evidently pronounced in Fig 14: Long needle-shaped eutectic silicon are seen broken into fine primary silicon at the outer of the bucket; while at the inner, large primary silicon are being converted into needle-shaped eutectic silicon. The maximum hardness of 60 BRN was recorded at 5 mm from the surface of the inner part of the bucket and 55 BRN was recorded at the outer region as show in Fig 16.

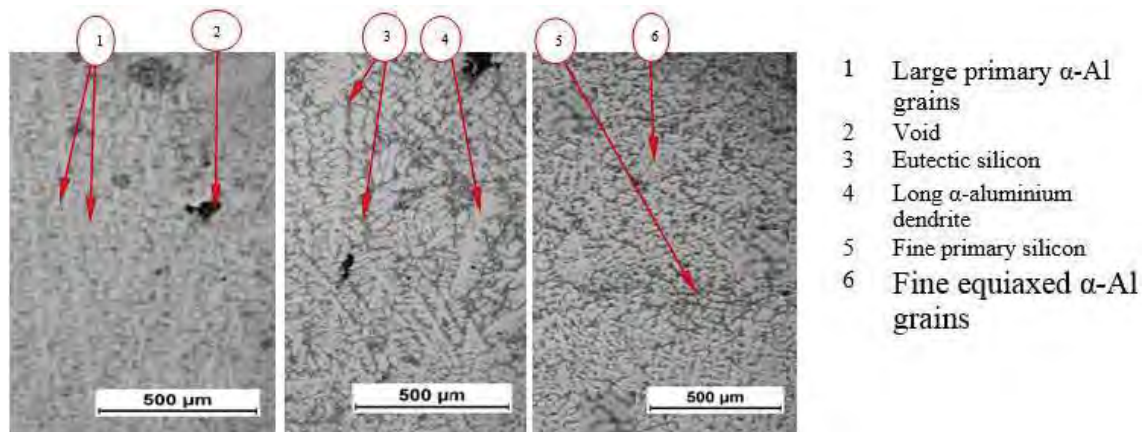


Fig 14: The features of the micrograph of the bucket made from A356 alloy by centrifugal cast

Heat Treatment. The heat treatment of A356 can be classified into three, based on soaking temperatures: Soaking at high temperature of 560°C [26, 27]; soaking temperature slightly below the eutectic temperature, 540°C [36-38] and; soaking temperature at 500°C . Quite often, hypoeutectic and near eutectic Al-Si alloys are applied when corrosion resistance and good castability are needed and with little quantity of Mg and Cu for heat treatment enhancement. In certain heat treatment conditions, as in the case T6 treatment of A356, precipitation of Mg_2Si and that of silicon occur [31]. The micrograph of the microstructure examination of T6 treated A356 is shown in Fig 15.

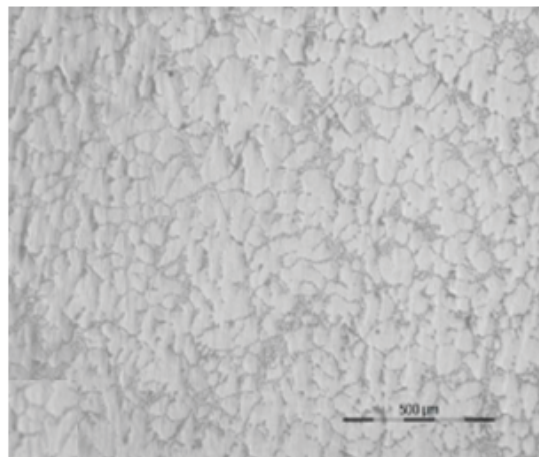


Fig 15: Optical micrograph of alloy A356 after solution treatment at 540°C for 4 hours

The hardness of both alloy and composite samples increased appreciably after the heat treatment. Maximum hardness (98 BRN and 122 BRN for alloy and composite respectively) were recorded at about 5 mm from the inner face in both samples. Lower hardness values were recorded, at 3 mm from the inner surface in all the samples. This is due to the rapid solidification at the inner periphery caused by fast cooling facilitated by the mould rotation.

The increase the hardness observed is due to supersaturated solid solution production that occurred during the soaking of A356 alloy at 540°C for 4 hours. This process causes the dissolution of hardening elements (Mg_2Si) in the matrix into globular primary $\alpha\text{-Al}$, spheroidisation of eutectic silicon and casting homogenisation [10, 11, 39]. Fig 16 shows hardness trends in the samples.

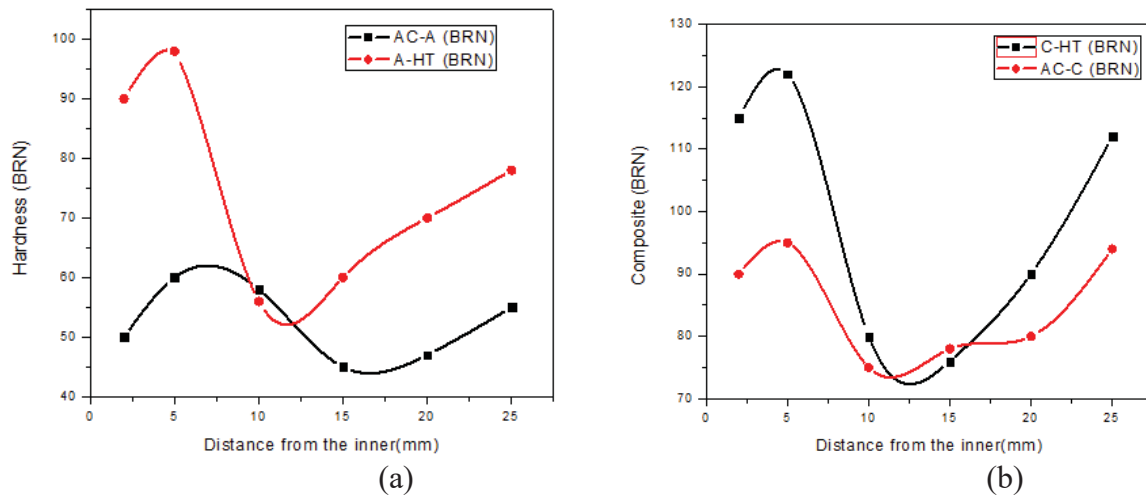


Fig 16: Brinell micro-hardness plot for a) A356 alloy as-cast and heat treated and; b) A356-10%SiC_p as cast and heat treated.

Where AC = as-cast A356 alloy; A- HT = A356 alloy heat treated; AC-C = As-cast A356-10%SiC composite; C-HT = A356-10%SiC composite heat treated

The dissolution of Mg₂Si, Spheroidisation and homogenisation of eutectic silicon in A356, happen within 5 minutes of soaking at 540^oC. The diagram of the Pseudo-binary of Al-Mg₂Si phase is shown in Fig 17

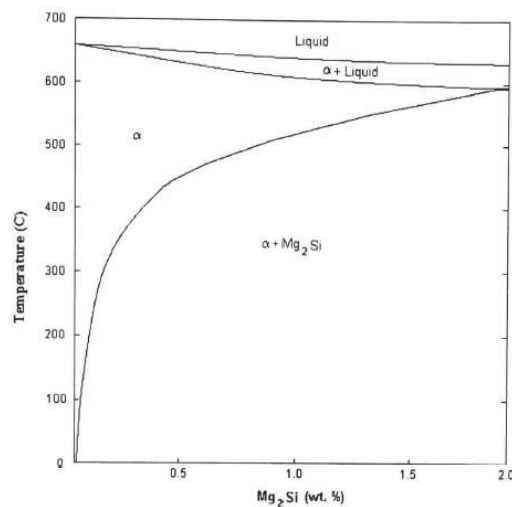


Fig 17: Pseudo-binary of Al-Mg₂Si phase diagram

Yield strength (YS) and Ultimate tensile strength (UTS) predictions

The strength of A356-T6 and A356-SiC-T6 can be predicted using this relation in equation (1) [11]:

$$YS = 3.03 \times VHN \times (0.055)^n \quad (1)$$

Where YS - yield strength, VHN – Vickers hardness number and; n - strain hardening exponent (0.091). The YS and UTS prediction curves for the samples are shown in Figs 18, 19 and 20.

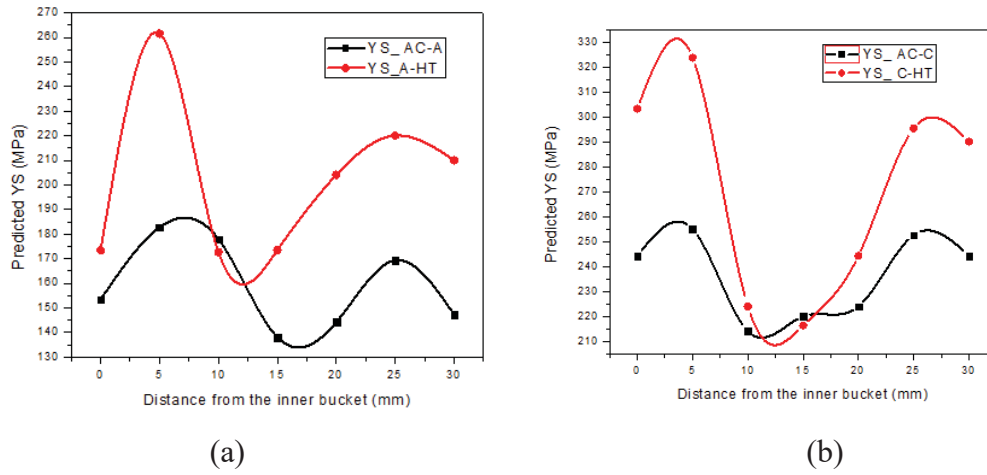


Fig 18: Yield strength prediction of a) A356 as cast (YS_AC-A) and heat treated (YS_AC-HT) and b) A356-SiCp as cast (YS_A-C) and heat treated (YS_C-HT)

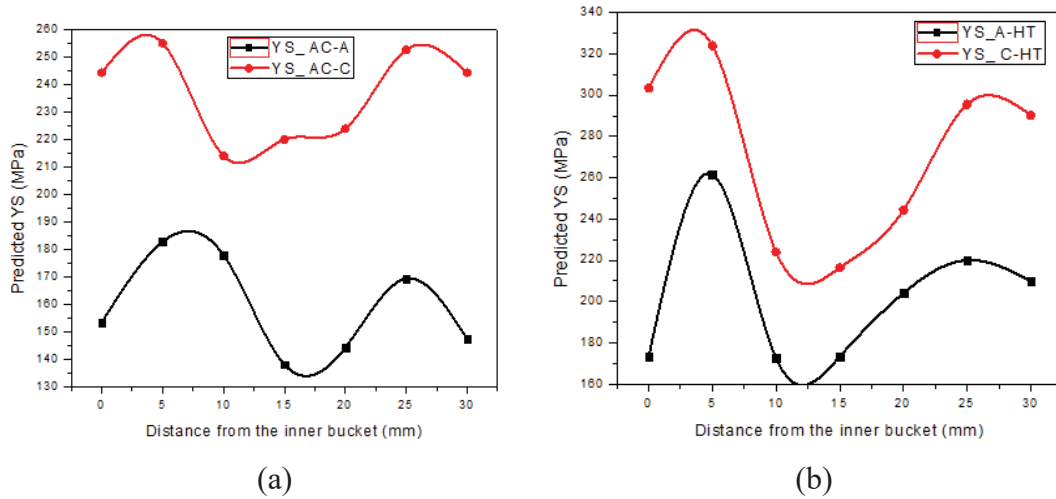


Fig 19: Yield strength prediction of a) A356 as cast (YS_AC-A) and A356-SiCp as cast (YS_A-C) and b) A356 heat treated (YS_A-HT) and A356-SiCp heat treated (YS_C-HT)

Again, YS-UTS ratio, can be predicted in terms of n, using the expressions (2) and (3):

$$YS_{0.2\%}/UTS = \frac{[(0.002)^n (exp n)]}{(n)^n} \tag{2}$$

$$UTS = \frac{YS_{0.2\%} n^n}{[(0.002)^n (exp n)]} \tag{3}$$

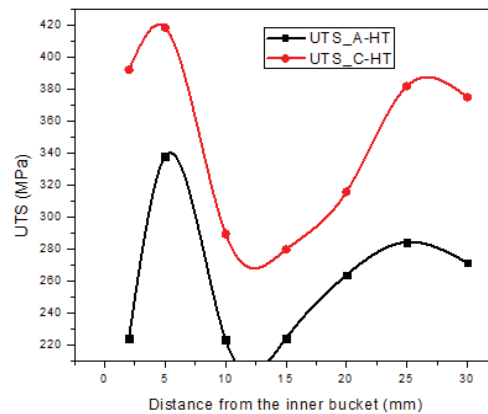


Fig 20: UTS prediction of heat treated a) A356 (UTS_A-HT) and A356-SiC_p (UTS_C-HT)

From Figs 18-20, it was observed that, the YS and UTS, appreciated greatly across the surface for both A356 alloy and A356-SiC_p composite after heat treatment.

Protective Coating of Pelton Bucket

Despite the wear and corrosion resistance of A356 alloy and A356-SiC_p composite, they are still very much susceptible to seawater corrosion and silt erosion over time. For better operation performance and longer life span, coating the inner surface of the bucket with tougher and hardened material is recommendable. Coating Pelton bucket with ceramic is will be effective due to the provision of the following protective service to the surface of the bucket: Wear and corrosion protection; impingement protection, silt erosion protection and surface hardness improvement. This study recommends ceramic coating of Al₂O₃ implanted Fe micrograins, and microarc oxidation (MAO) or plasma electrolytic oxidation (PEO).

Conclusion

Domestication of SHP technologies was noted as a significant way of reliably tackling rural electrification problems in SSA and the use of FGMs production technique was considered vital. In engineering sectors, such as aerospace, automotive and energy, FGMs play a vital role in ensuring that the desired attributes of components as regards their functionality are achieved. The needed operational properties of parts have pushed the material engineers and scientists to develop different FGMs production methods. This study, therefore, exploits the FGMs production method to enhance locally sourced aluminium alloy for Pelton hydro turbine bucket production. However, the cost of production, complexity of technique, and mass production of parts are some of the major barriers to the application of these fabrication techniques. This notwithstanding, centrifugal casting technique was identified as a simple and cost-effective process that enhances the mechanical properties of aluminium alloys and composites. This study then concludes that:

- i. To genuinely turn around the perennial power issues in SSA, power should be generated from the abundant small hydro potentials with the application of indigenous technology and made from locally sourced materials.
- ii. Use of centrifugal casting method and heat treatment improved the mechanical properties of A356 alloy and A356-SiC_p composite, making them more suitable for Pelton bucket production.
- iii. Heat treated A356 alloy and A356-SiC_p composite, will be suitable for turbine materials for water storage turbine system. This is due to minimal % of silt in the stored water and the enhanced corrosion and wear resistance property of the materials.
- iv. To further improve the life span of bucket, hard surface coating should be applied

Acknowledgement

The authors hereby acknowledge the Centre for Engineering Postgraduate Studies (CEPS)/HVDC/Smart grid Centre of the University of KwaZulu-Natal.

References

- [1] BETP. (2012, 14/02/ 2016). *Hydraulic Turbines*. Available: <http://www.betp.net/2012/01/pelton-wheelturbine/>
- [2] P. H.-Y. Bryan, "Design of a Low Head Pico Hydro Turbine for Rural Electrification in Cameroon," *Engineering and International Development*, The University of Guelph, Guelph, Ontario, Canada, 2012.
- [3] W. S. Ebhota, A. C. Eloka-Eboka, and F. L. Inambao, "Energy sustainability through domestication of energy technologies in third world countries in Africa," in *Industrial and Commercial Use of Energy (ICUE), 2014 International Conference on the "Energy efficiency in buildings"*. 2014, pp. 1-7.
- [4] H. Liu, D. Masera, and L. Esser, "World Hydropower Development Report 2013.," *United Nation Industrial Development Organisation (UNIDO) and Intertional Centre on Small Hydropower (ICSHP)*, 2013.
- [5] G. Loice and M. Ignatio, "Efficiency Improvement of Pelton Wheel and Crossflow Turbines in Micro-Hydro Power Plants: Case Study," *International Journal of Engineering and Computer Science* vol. 2, pp. 416-432, 2013.
- [6] B. William, S. Vasu, and S. Manjot, "Green Mechatronics Project: Pelton Wheel Driven Micro-Hydro Plant," *Mechanical Engineering University of Ottawa*, 2010.
- [7] R. N. Mbiu¹, S. M. Maranga, and H. Ndiritu, "Performance of Aluminium A356 Alloy Based Buckets Towards Bending Forces on Pelton Turbines," in *Sustainable Research and Innovation (SRI) Conference*, Nairobi, Kenya, 2015, pp. 134-138.
- [8] I. A. K. M. Khabirul, B. Sahnewaz, and A. C. Farooque, "Advanced Composite Pelton Wheel Design and Study its Performance for Pico/Micro Hydro Power Plant Application," *International Journal of Engineering and Innovative Technology (IJEIT)*, vol. 2, pp. 126-132, 2013.
- [9] N. I. R. Nava and T. S. Prasad, "Design and Static Analysis of Pelton Turbine Bucket " *International Journal of Science Technology and Management*, vol. 4, pp. 19-25, 2015.
- [10] D. V. Khera and R. S. Chadhawork, "Silt Erosion. Trouble for Turbines," *International Water Power and Dam Construction* vol. 53, pp. 22-3, 2001.
- [11] M. K. Padhy and R. P. Saini, "Effect of Size and Concentration of Silt Particles on Erosion of Pelton Turbine Buckets," *Energy* vol. 34, pp. 1477-1483, 2009.
- [12] A. Negi, R. S. Virendra, and S. S. Samant, "Effect of Cr₂O₃ and TiN Coatings on 13Cr-4Ni Turbine Blade Material by HVOF Process: A Review," *International Journal of Water & Hydro Constructions – IJWHC* vol. 1 2014.
- [13] T. R. Bajracharya, B. Acharya, J. C. B., R. P. Saini, and O. G. Dahlhaug, "Sand Erosion of Pelton Turbine Nozzles and Buckets: A Case Study of Chilime Hydropower Plant," *Wear* vol. 264, pp. 177-184, 2008.
- [14] ASM, *Corrosion: Understanding the Basics*. ASM International, Materials Park, Ohio American Technical Publishers Ltd, 2000.

- [15] G. V. Akimov, *Theory and Methods of Studying Metal Corrosion*. Moscow AN SSSR, 1945.
- [16] V. S. Sinyavskii and V. D. Kalinin, "Marine Corrosion and Protection of Aluminum Alloys According to their Composition and Structure," *Protection of Metals*, vol. 41, pp. 317-328, 2005.
- [17] V. S. Sinyavskii, V. D. Val'kov, and V. D. Kalinin, *Corrosion and Protection of Aluminum Alloys* Moscow: Metallurgiya, 1986.
- [18] M. korroziya, *Handbook on Marine Corrosion* Shumakher, M.M. ed. Moscow: Metallurgiya, 1983.
- [19] H. P. Godard, "The Corrosion of Light Metals: Aluminum," *John Wiley, Inc*, vol. Y-L-S, p. 218, 1967.
- [20] H. Torabian, J. P. Pathak, and S. N. Tiwari, "Wear Characteristics of Al-Si Alloys," *Wear*, vol. 172, pp. 49-58, 1994.
- [21] P. K. Rohatgi and B. C. Pai, "Effect of Microstructure and Mechanical Properties on the Seizure Resistance of Cast Aluminium Alloys.," *Wear*, vol. 28, pp. 353-367, 1974.
- [22] A. C. Vieira, P. D. Sequeira, J. R. Gomes, and L. A. Rocha, "Dry Sliding Wear of Al Alloy/SiCp Functionally Graded Composites: Influence of Processing Conditions," *Wear* vol. 267 pp. 585-592., 2009.
- [23] *Casting Metal handbook*, 9th ed. vol. 15: ASM International, 1997.
- [24] G. Chirita, I. Stefanescu, D. Cruz, D. Soares, and F. S. Silva, "Sensitivity of Different Al-Si Alloys to Centrifugal Casting Effect," *Materials and Design* vol. 31 pp. 2867-2877, 2010.
- [25] SAAJ. (2014, 23/03/2016). *Die Steel Grade OHNS*. Available: http://saajsteel.com/?page_id=1055
- [26] D. L. Zhang, L. Zheng, and D. H. StJohn, "Effect of Solution Treatment Temperature on Tensile Properties of Al-7Si-0.3 (wt-%) Alloy," *Materials Science and Technology*, vol. 14, pp. 619-625, 1998.
- [27] S. Shivkumar, S. Ricci, B. Steenhoff, and D. Apelian, "An Experimental Study to Optimize the Heat Treatment of A356 alloy " *American Foundry Society Transaction*, vol. 97, pp. 791-810., 1989.
- [28] M. Drouzy, S. Jacob, and M. Richard, "Interpretation of Tensile Results by Means of Quality Index and Probable Yield Strength," *AFS International Cast Metals Research Journal*, vol. 5, pp. 43-50, 1980.
- [29] K. G. Basavakumar, P. G. Mukunda, and M. Chakraborty, "Impact Toughness in Al -12Si and Al-12Si-3Cu Cast Alloys- Part - I: Effect of Process Variables And Microstructure," *International Journal of Impact Engineering*, vol. 25, pp. 199-205, 2008.
- [30] T. M. Chandrashekharaiah and S. A. Kori, "Effect of Grain Refinement and Modification on the Dry Sliding Wear Behaviour of Eutectic Al-Si Alloys," *Tribology International*, vol. 42, pp. 59-65, 2009.
- [31] F. H. P. Juan, "Heat Treatment and Precipitation in A356 Aluminum Alloy," Doctor of Philosophy, Mining, Metals and Materials Engineering, McGill University, Montreal, Canada, 2003.
- [32] L. Heusler and W. Schneider, "Recent Investigations of Influence of P on Na and Sr Modification of Al-Si Alloys " *American Foundry Society Transaction*, vol. 97, pp. 915-921, 1997.

- [33] B. C. a. J. E. Gruzleski:, "Mechanical Properties of A356.0 Alloys Modified with Pure Strontium " *American Foundry Society Transaction*, pp. 453-464, 1982.
- [34] B. P. Vikramkumar, "Investigations on the Properties of Al-Si Alloy Synthesized By Centrifugal Casting Process," *Metallurgical Engineering*, Ganpat Uniiversity, Kherva, India, 2014.
- [35] A. S. Rao, S. T. Mahantesh, and S. R. Shrikantha, "Understanding Melt Flow Behavior for Al-Si Alloys Processed Through Vertical Centrifugal Casting," *Materials and Manufacturing Processes*, vol. 30, pp. 1305-1311, 2015.
- [36] M. Ishak, A. Amir, and A. Hadi, "Effect of Solution Treatment Temperature on Microstructure and Mechanical Properties of A356 Alloy," presented at the International Conference on Mechanical Engineering Research (ICMER2013), Bukit Gambang Resort City, Kuantan, Pahang, Malaysia, 2013.
- [37] B. A. Dewhirst, "Optimization of the Heat Treatment of Semi Solid Processed A356 Aluminum Alloy," *Masters Worcester Polytechnic Institute*,, 2005.
- [38] M. Rosso and G. M. Actis, "Optimization of Heat Treatment Cycles for Automotive Parts Produced By Rheocasting Process.," *Solid State Phenom.* , vol. 116-117, pp. 505-8, 2006.
- [39] W. S. Miller, L. Zhuang, J. Bottema, A. J. Wittebrood, P. De Smet, A. Haszler, *et al.*, "Recent Development in Aluminium Alloys for the Automotive Industry," *Material Science Engineering A*, vol. 280, pp. 37-49, 2000.

**CHAPTER 9: ENHANCING THE WEAR AND CORROSION
RESISTANCE OF A PELTON TURBINE BUCKET SURFACE BY
CENTRIFUGAL CASTING TECHNIQUE AND HEAT TREATMENT**

W. S. Ebhota and F. L. Inambao, "Enhancing the wear and corrosion resistance of a Pelton turbine bucket surface by centrifugal casting technique and heat treatment," *Australian Journal of Mechanical Engineering*, 2016. (*Under review.*)

Enhancing the Wear and Corrosion Resistance of a Pelton Turbine Bucket Surface by Centrifugal Casting Technique and Heat Treatment

Williams S. Ebhota^a and Freddie L. Inambao^b

^{a, b}Discipline of Mechanical Engineering, Howard College, University of KwaZulu-Natal, Durban, South Africa.

Correspondence email: wilymoon2001@yahoo.com

Abstract–This study examines the possibility of fabricating a complex, non-cylindrical shaped Pelton turbine bucket by centrifugal casting technique. The functionally graded aluminium A356 alloy and A356-10%SiCp composite produced were characterised for hydro turbine bucket application. Oil Hardening Non-Shrinking Die Steel (OHNS) steel was selected for the permanent mould material, machined with CNC and heat treated to a hardness of 432 BHN. Aluminium alloys A390 and A390-5%Mg were considered as the Pelton materials, cast and characterised. Gravity casting of A390 and A390-5%Mg were done for comparison purposes. For detailed investigation, a cylindrical shape cast of A390-5%Mg was fabricated. The effects of the casting method and heat treatment on the mechanical properties and corrosion resistance of A390 and A390-5%Mg alloys were investigated. A hardness of 150 BHN (maximum) was recorded near the inner surface of the bucket and 157 BHN (maximum) was recorded in the inner periphery of the cylindrical cast. From the corrosion test, it was observed that A360-5%Mg by gravity casting shows higher corrosion resistance than the base alloy A390, and the specimen from the inner zone of the circular cast shows a higher corrosion resistance than the specimen from the outer periphery.

Keywords: A360-5%Mg alloy; Centrifugal casting technique; Electrochemical corrosion test; T6-heat treatment; Pelton turbine bucket.

9.1 Introduction

Functionally Graded Materials (FGMs) are a class of composite materials that have unique properties as a consequence of the gradual transition of the constituent materials. This group of knowledge-based materials occurs in nature such as bone and teeth [1, 2]. The concept of FGM was modelled from nature in the quest of solving engineering problems [3]. Most metals in their pure nature have little significance in engineering application as their properties sometimes conflict with what is required of them. For instance, a part may require hardness and ductility for proper functioning in a given working environment. Naturally, such material is hard to find. This kind of scenario has driven scientists and the engineers to

develop various material fabrication processes. These processes are used to combine different elements or compounds in order to explore the comparative advantages of the individual elements or compounds.

In the case of aluminium and its alloys, microstructures are modified chemically or mechanically. The properties of a material are defined by its microstructure characteristics. In chemical modification, certain elements or chemicals are added to the matrix depending on the attribute required from the material. The grain size distribution, primary silicon (Si) and morphology of the microstructure are mainly responsible for the properties of hypereutectic Al-Si-Mg alloys. However, the mechanical properties are affected by the presence of coarse massive irregular or star shaped primary Si which are usually associated with typical casting methods.

The centrifugal casting process generates radial forces that segregate composite materials including the matrix into zones with the denser components farthest away from the axis of rotation. In addition to the centrifugal effect, the rotation of the mould after pouring facilitates rapid cooling and solidification. In the centrifugal casting of ceramic particle reinforced aluminium matrix, two distinct regions are created: a particle-enriched zone and a particle-depleted zone. However, the meeting point of this segregation is in a gradual transition, not sharp. In the case of SiC in an aluminium matrix, experiments have shown that SiC will segregate to the outer periphery of the cast [4, 5]. The particle-enriched zone thickness is reduced by the increase in rotation speed and pouring temperature.

In a study, the hypereutectic aluminium alloy was physically modified with intensive melt shearing while solidifying and the effect on the microstructure was examined [6]. The results revealed that the shearing greatly refined the primary silicon with heat treatment playing a significant role. 660 °C was recorded as the optimum temperature for Al-20wt%Si alloy Si particles refinement. A centrifugal in-situ process was used to fabricate an Al-Al₂Cu FGM ring from Al-3%Cu in a study which reported the following findings: the α -Al particles drifted to the outer periphery of the ring; the presence of Cu in the ring was massive in the inner part; the hardness of the Al₂Cu FGM ring increased towards the inner region; and the specimen hardness increased tremendously after heat treatment [7]. This occurrence suggests that the α -Al particle is denser than Cu.

An investigative work was conducted on the different aluminium matrices reinforcing particles of B₄C, SiC, graphite hybrid, primary silicon, Al₃Ni and Mg₂Si produced by a

centrifugation process. The study observed that reinforcement density and size are the parameters that affect the microstructure gradient. Denser SiC and Al₃Ni particles were observed close to the outer surface while less dense particles of graphite, primary silicon and Mg₂Si were found close to the inner surface. B₄C particles were more frequently distributed around the matrix than others because it has the closest density to the aluminium matrix. Mechanical stir and electromagnetic stir casting techniques were used to fabricate A356-SiC metal matrix composites with varying weight proportions of SiC particles. The study investigated macrostructure, microstructure and mechanical properties of the castings and observed that the trend of mechanical properties improvement corresponds to the trend in the increase of reinforcement particles in all cases, and a lesser number of the void was produced by electromagnetic stir casting than stir casting. K. Patel, H. Patel and F. Patel examined the effect of the rotation speed of a horizontal centrifugal casting process on the tribological and hardness properties of a hyper-eutectic (Al-17Si) alloy [8]. According to the study, hardness and wear rate followed the same trend – their values increased toward the outer periphery; the primary silicon was refined by the increase in the spinning speed from coarse shape to fine shape; and 700 RPM was considered to be the optimal mould rotation speed at which the wear rate at the outer periphery was minimised.

9.1.1 Pelton turbine material and fabrication

The turbine bucket is basically designed for aerodynamics, strength, wear and corrosion resistance, and cavitation attributes. In a Pelton turbine, nozzle and bucket are severely affected by silt erosion and high velocity jet water. Stainless steels SS(16Cr-5Ni), SS(13Cr-4Ni), SS(13Cr-Ni) etc. are the commonest materials used for hydro turbines and water pumps because of their mechanical performance attributes [9]. However, these materials are expensive, complex to formulate, require huge energy to cast, are not erosive wear resistant, and are comparatively difficult to machine and weld. The manufacturing infrastructure in most countries in sub-Saharan Africa is inadequate to sufficiently support stainless steel production and working with stainless steel. This has made the production of hydro turbines blades out of reach in the region despite the need to generate more electricity. Aluminium based materials have reasonable corrosion wear resistance naturally that could be improved through various production and modification processes.

This study aimed to cast an irregularly shaped component, a Pelton turbine bucket, by vertical centrifugal casting technique with A390 and A390-5%Mg as bucket materials. Previous

studies consulted regarding the centrifugal casting process have considered perfect cylindrical bodies in their investigations. This study hypothetically identifies the successful designing and fabrication of a permanent mould as the most important outcome in this research work.

9.2 Experimental method

9.2.1 Fabrication of a permanent mould for a Pelton turbine bucket

The fabrication of a Pelton turbine bucket was divided into two stages: production of a permanent mould and centrifugal casting of the Pelton bucket. The CAD model of the bucket is shown in Figure 9.1 and was designed for a capacity of 18.45 kW turbine power.

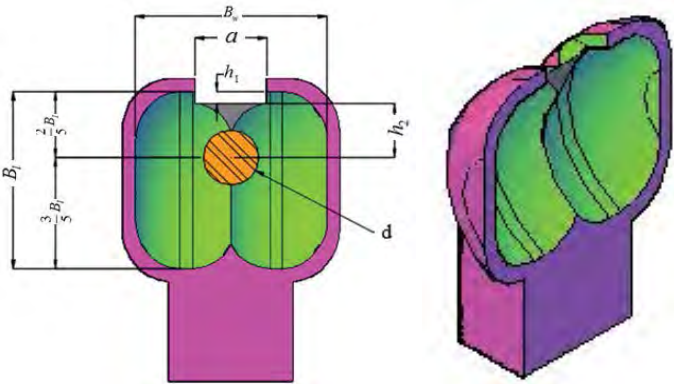
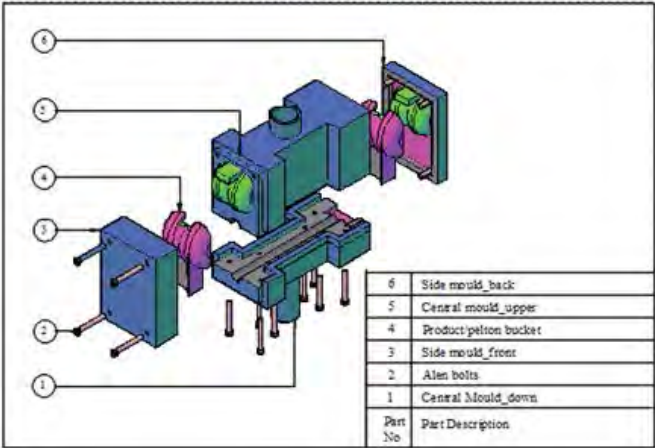


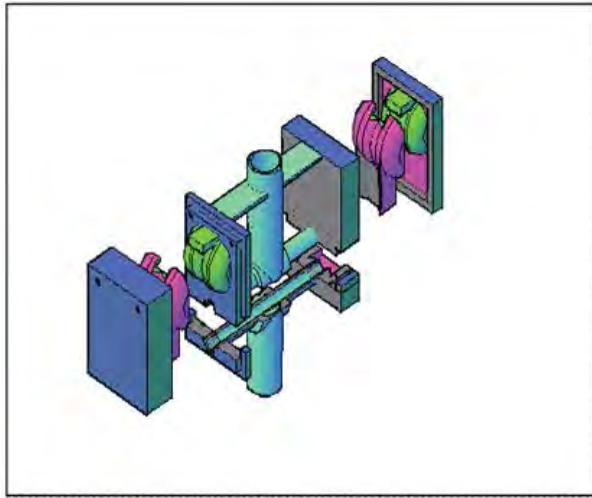
Figure 9.1: The design parameters of a bucket

9.2.2 Production of the mould

Solidworks software was used for the mould design and generation of IGES files of the mould components for CNC machining application. The mould parts were machined according to the specifications stated in the IGES files. Figures 9.2(a) and 9.2(b) show the exploded assembly of the mould as designed and as fabricated respectively.



a)



b)

Figure 9.2: a) Exploded view of Pelton bucket mould assembly as designed; b) Exploded view of Pelton bucket mould assembly as fabricated

9.2.3 Mould material

Oil Hardening Non-Shrinking Die Steel (OHNS) was selected as the material for the mould production. The OHNS chemical composition is shown in Table 9.1. OHNS steel is a reliable material for gauging, blanking and cutting tools as well as for hardness and elevated temperature performance [10]. The CNC machined components of the mould were heat treated as follows: 800 °C was used as hardening temperature and 432 BHN was recorded after the heat treatment. A photograph of the manufactured components for the Pelton bucket mould is shown Figure 9.3.

Table 9.1: OHNS material chemical composition

Element	C	Mn	Cr	W	V
%	0.95	1.1	0.6	0.6	0.2

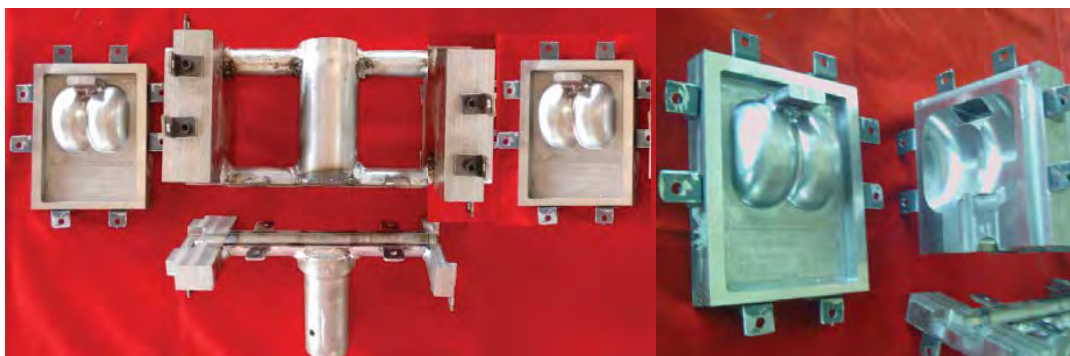


Figure 9.3: The manufactured mould components for Pelton bucket

9.2.4 A390-aluminium alloy formation

The chemical composition of A390 aluminium alloy is contained in Table 9.2. A calculated kilogramme of the commercial A390 was charged into the induction furnace. The alloy was processed in clay graphite crucibles. Degassing of the molten metal to prevent hydrogen entrapment was done at 720 °C by rotary impeller degassing (RID) machine, shown in Figure 9.4. The RID set parameters were: rotor speed - 500 rpm, gas (Nitrogen) flow rate - 0.4 m³/h and refining time - 15 min, in accordance with previous studies [11]. The rotary shaft was placed about 50 mm from the centreline in order to avoid vortex formation. The molten metal was poured into a circular mould rotating at a constant speed of 1200 rpm and held at this speed for 5 minutes before it was stopped.

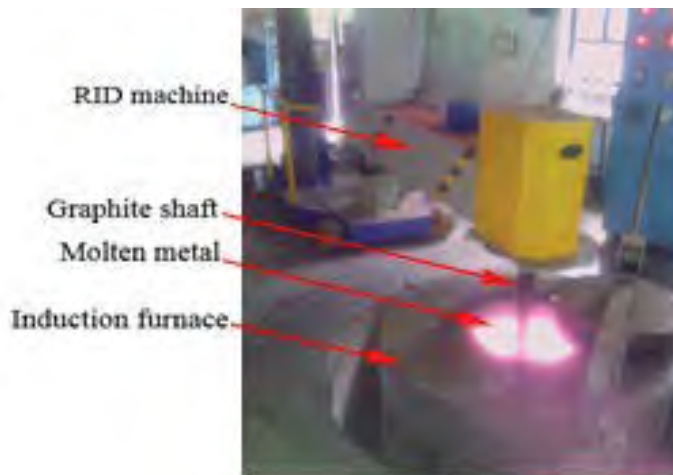


Figure 9.4: Degassing of the molten metal with RID machine

9.2.5 A390-5%Mg aluminium alloy formation

Commercially available A390 alloy was used as the raw material for the production of A390-5%Mg ingots. For the A390-5%Mg ingot preparation, 5 %W of pure magnesium (Mg) was added to the molten metal of A390 alloy at 750 °C, which is about 100 °C above A390 melting point temperature [12]. The ingot was processed in clay graphite crucibles and degassing of the molten metal to prevent hydrogen entrapment was done by adding hexachloroethane at 750 °C. The chemical composition of A390-5%Mg ingot as analysed by spark emission spectrometer is contained in Table 9.2.

Table 9.2: Elemental composition of A390 and A390-5%Mg

Alloy	Al	Si	Cu	Mg	Fe	Mn	Zn	Ti
A390	77.10	17.00	4.50	0.60	0.40	0.10	0.10	0.20
A390-5%Mg	74.03	16.20	4.30	4.80	0.37	0.06	0.07	0.17

The A390-5%Mg ingot was charged into the furnace with the addition of 1 Kg of pure Mg to account for the loss due to oxidation. The molten A390-5%Mg was poured at 750 °C into the Pelton turbine bucket mould that was preheated to 300 °C and spinning at a speed of 1200 rpm. The rotation continued for 5 minutes after pouring and Figure 9.5 shows the vertical centrifugal casting machine used.

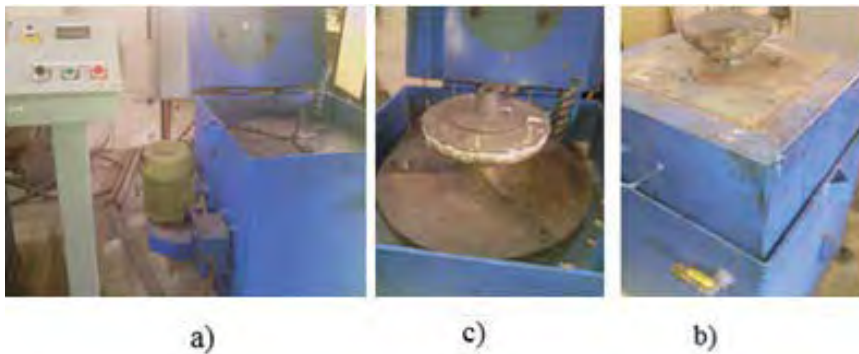


Figure 9.5: Vertical centrifugal casting machine: a) Unloaded centrifugal machine; b) Centrifugal machine with circular mould and; c) Centrifugal machine ready for pouring

The schematic diagram in Figure 9.6 depicts the arrangement of the buckets in the mould and the direction of rotation. The face of one of the buckets is turned away from the centre of rotation while the other faces the centre of rotation.

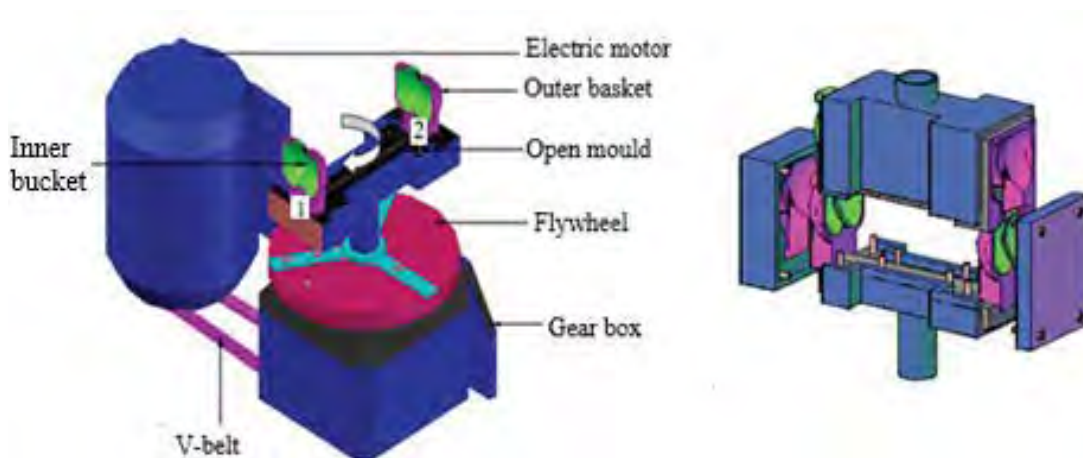


Figure 9.6: The arrangement of the buckets in the mould

Apart from the bucket mould, circular and rectangular moulds were also prepared. A390-5%Mg molten metal was poured into the circular mould at rotational speed of 1200 rpm while the rectangular mould was filled with A390-5%Mg alloy gravity casting. The moulds were pre-heated to 300 °C and the circular mould rotated for 5 minutes after pouring. The castings made are shown in Figure 9.7.

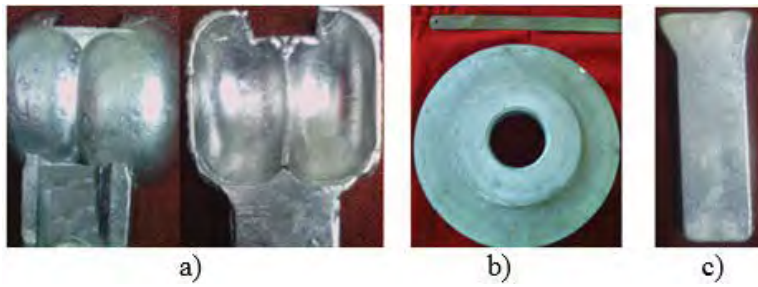


Figure 9.7: Castings from different casting techniques: a) Pelton Turbine bucket cast by centrifugal casting method; b) Cylindrical from circular casting mould cast by centrifugal casting method; c) Castings made by gravity casting method.

9.2.6 Electrochemical corrosion test

A CH Instrument 680 Amp Booster laboratory workstation was used to carry out electrochemical corrosion tests. The setup is shown in Figure 9.8 and consists of three standard electrodes in a Pyrex glass cell; a platinum counter electrode; saturated calomel electrode as a reference electrode; and working electrode (specimen). 3.5 % sodium chloride (NaCl) solution was used as the corrodent. Potentiodynamic current-potential curves were obtained from specimens' polarisation into cathode (-) and anode (+) as regards the open circuit potential (OCP) and scanned at 0.05 V/s. Electrochemical Impedance Spectroscopy (EIS) measurements at the calculated OCP in 1200 seconds were carried out at frequency range 0.01 Hz-100 kHz at a small amplitude AC signal (10 mV). Rectangular specimens of dimension 25 mm x 25 mm x 2 mm were prepared based on the standard metallographic process: polished with grit emery papers of the following grades 80, 100, 320, 400, 600 and 1000 consecutively and washed with distilled water [13]. This was followed by whirl cloth polishing with 6 μm , 3 μm and 1 μm SiC particle paste consecutively, washed in acetone and rinsed with distilled water.

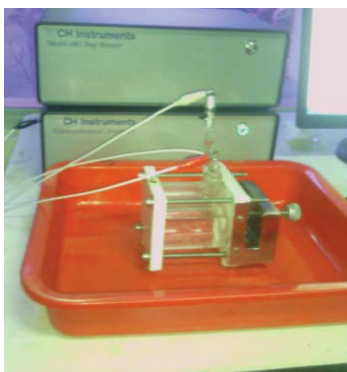


Figure 9.8: The setup of the electrochemical corrosion laboratory workstation (CH Instrument 680 Amp Booster)

9.2.7 Specimen preparation

The test samples were prepared from A390-5%Mg aluminium alloy. The bucket was sliced at the centre into two specimens, A and B (Figure 9.9) and then their surfaces were prepared for microstructure examination and hardness testing respectively.

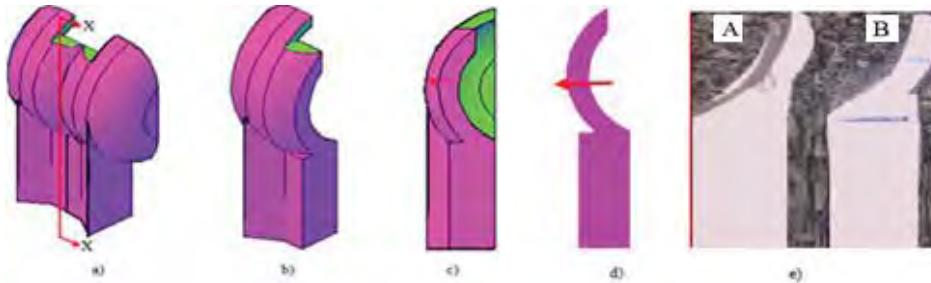


Figure 9.9: Preparing microstructural and hardness specimens

Three specimens (C, D and E) were cut from the cylindrical cast as shown in Figure 9.10. Specimen C and D were prepared for microstructure examination and hardness testing respectively.

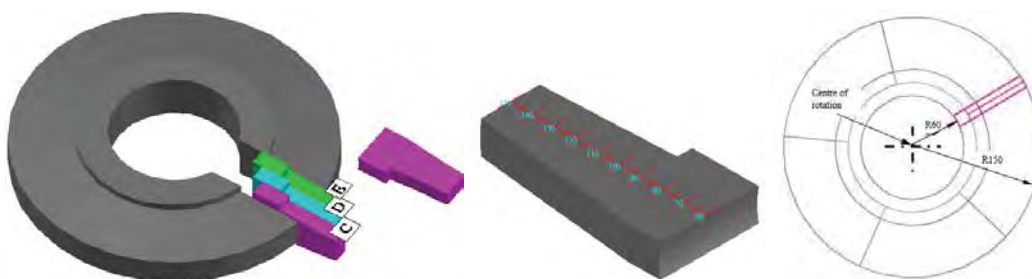


Figure 9.10: Schematic of how the specimens were cut from the cylindrical casting

The electrochemical corrosion test specimens, E₁, E₂ and E₃, were produced from specimen E as depicted in Figure 9.11. Specimens F and G were cut from the A390 cylindrical cast alloy in the same way as represented in Figure 9.10. The specimens were prepared for microstructure examination and hardness testing respectively. Specimens H and I were prepared from gravity casting of A390-5%Mg microstructure examination and hardness testing respectively.

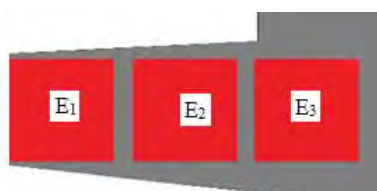


Figure 9.11: Specimens for electrochemical test

The specimens for the microstructural view were prepared by polishing the surface of the specimens with grit emery papers of 80, 100, 320, 400, 600 and 1000 grades consecutively and washing with distilled water. This was followed by whirl cloth polishing with 6 μm , 3 μm and 1 μm SiC particle paste consecutively, acetone washing and rinsing with distilled water.

9.2.8 Hardness test

A Tinius Olsen hardness test machine with 2.5 mm diameter indenter ball was used to measure the macro-hardness of the different specimens in terms of the Brinell Hardness Number (BHN) scale under a load of 62.5 Kgf for 20 seconds. The samples for hardness testing were polished with grit emery papers of 80, 100, 320, 400, 600 and 1000 grades consecutively and washed with distilled water. The offset of the bucket specimen surface prepared for hardness test and the points where the readings were taken is depicted in Figure 9.12.

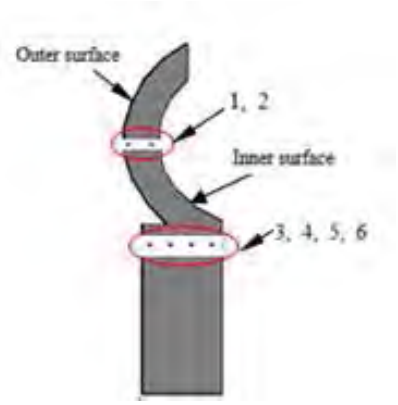


Figure 9.12: Bucket test samples

9.2.9 Heat treatment

Heat treatment was carried out on specimens B, D, G and I and were given the same heat treatment as represented in the diagram in Figure 9.13. A temperature of 495 $^{\circ}\text{C}$ was used for solutionizing and held for 8 hours followed by quenching with 60 $^{\circ}\text{C}$ hot water. Artificial ageing was done at 175 $^{\circ}\text{C}$ and held for 8 hours.

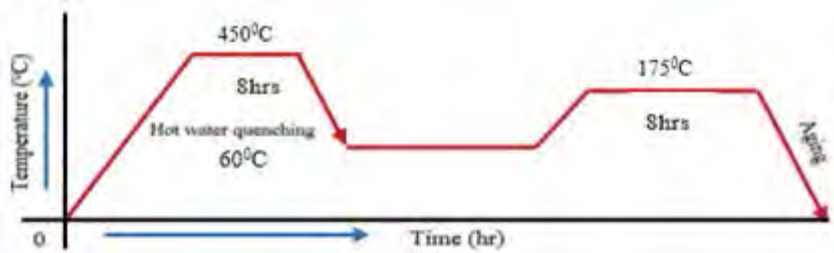


Figure 9.13: Schematic of T6-Heat Treatment profile of A390 and A390-5%Mg

9.3 Theoretical background

In the vertical centrifugal casting process, a particle moving in a molten metal is under the influence of four forces: gravity, F_G ; drag force (viscosity effect), F_D ; centrifugal force (spinning of the mould), F_C ; and Van der Waal forces repulsive force (solid-liquid interface movement), F_L .

The particle movement is controlled by the net resultant force F_{net} :

$$F_{net} = F_C - F_D - F_L \quad (9.1)$$

The force balance expression when fluid flow is laminar ($Re \leq 1$) (assumption) is:

$$4/3 * \pi * R^3 * \rho_p (d^2r/dt) = 4/3 * \pi * R^2 (\rho_p - \rho_m) \omega^2 * r - 6 * \pi * R * \mu (dr/dt) \quad (9.2)$$

Where R - particle radius; g - gravitational acceleration; μ - melt viscosity; $\Delta\rho = \rho_p - \rho_m$ - density difference and; ρ_p and ρ_m particle and molten metal densities respectively; ω - angular velocity and; r - particle position.

$$m_p \frac{d^2x}{dt^2} = |\rho_p - \rho_m| \frac{4}{3} \pi \left(\frac{D_p}{2} \right)^3 G g - 3\pi\mu D_p \frac{dx}{dt} \quad (9.3)$$

The direction of the movement of particles is due to centrifugal force, determined by the relative values of the densities; particles are segregated to the outer periphery of the cast if $\rho_p > \rho_m$ and vice versa.

The ratio of the centrifugal force to gravity, G is defined as:

$$G = \frac{4\pi^2 N^2}{g} r \quad (9.4)$$

Where dx/dt - velocity; d^2x/dt^2 - acceleration; m - mass; g - gravitational acceleration; D_p - particle diameter; r - circular mould diameter (m); N - velocity of mould rotation and; μ - viscosity (m^2/s).

The centripetal acceleration, a_p , of the reinforcement particle is derived from equations (3) and (4):

$$m_p \frac{d^2x}{dt^2} = |\rho_p - \rho_m| \frac{4}{3} \pi \left(\frac{D_p}{2} \right)^3 4\pi^2 N^2 r \quad (9.5)$$

$$a_p = \frac{|\rho_p - \rho_m|}{\rho_p} 4\pi^2 N^2 r \quad (9.6)$$

9.4 Result and discussion

9.4.1 Microstructure

The microstructural examination of the centrifugal casting of A390 was divided into three zones; the inner zone, Figure 9.14(a-b); middle zone, Figure 9.14(c-d); and outer zone (Figure 9.14(e-f)). It was observed that the highest volume of the distribution of fine Si particles of an average size of 5-15 μm was observed at the outer periphery and few at the mid zone. However, the formation of large flakes of α -Al dendrites and bigger Si particles of the average of 25 μm to 35 μm were seen in the inner zone.

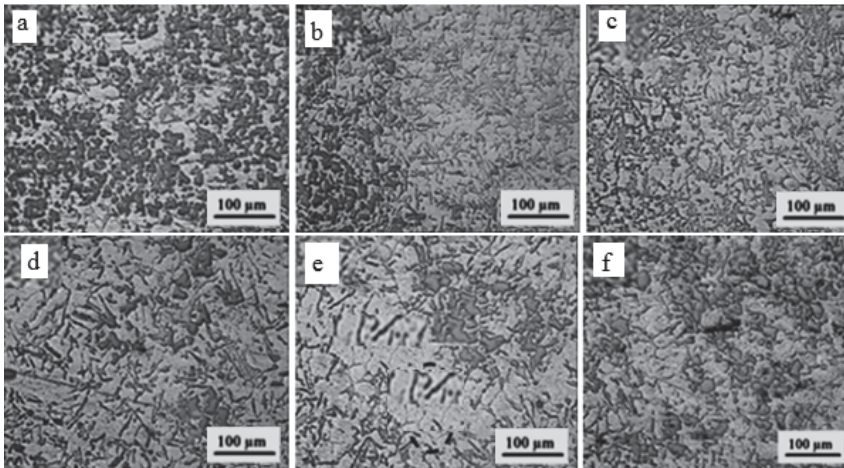


Figure 9.14: Micrographs of centrifugally cast aluminium A390 alloy, showing the trend of gradient

The micrographs of As-Cast A390-5%Mg alloys fabricated by gravity and centrifugal casting methods are shown in Figure 9.14. Figures 9.15(a) and 9.15(b-h) are the micrographs of A390-5%Mg alloys fabricated by gravity and centrifugal casting methods respectively. The micrographs in Figure 9.15(b-h) represent the gradient of the microstructure. As can be seen in the micrographs, there is a difference in the microstructure morphology between gravity cast and centrifugal cast alloys. In Figure 9.15(a), large flakes of silicon, coarse Mg_2Si , large dendritic cells, and large α -aluminium dendrites are seen. In the centrifugal casting alloy micrographs, a fibrous form of silicon is seen in the outer periphery (Figure 9.15(h)), followed by fine Si particles toward the inner surface. In the inner surface, there are a lot of coarse Mg_2Si surrounding Si and also standing individually, polygon primary silicon and large α -aluminium dendrites segregation.

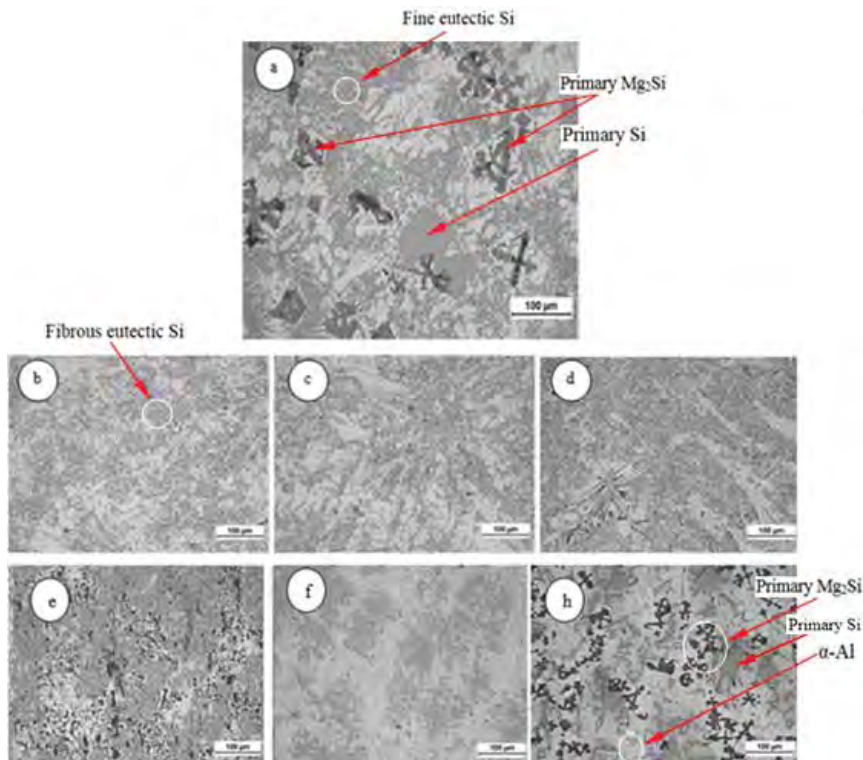


Figure 9.15: Optical micrographs of a) A390-5%Mg by gravity; (b-g) Gradient of A390-5%Mg by centrifugal casting, taken at 15 mm intervals with (g) and (b) at 65 mm and 145 mm from the centre rotation respectively

A similar gradient trend, as represented in Figure 9.16, was found in the bucket specimens. However, the gradient direction of the two specimens is in opposite directions. It was observed that bucket 1 has a fibrous silicon at the inner surface periphery and coarse Mg_2Si , and large α -aluminium dendrites at the outer surface. But for bucket 2, the reverse was the case (Figures 9.6, 9.7 and 9.9).

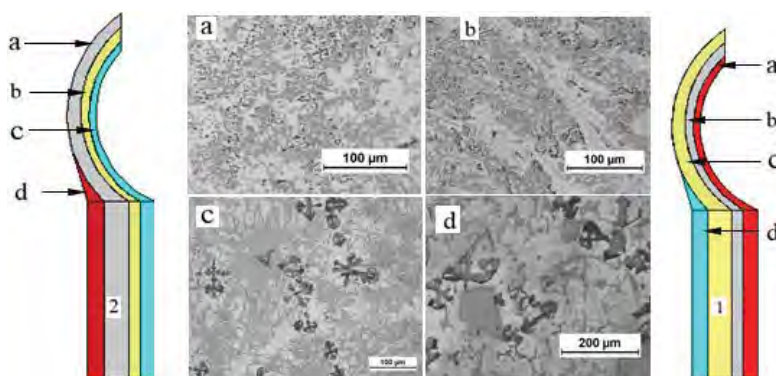


Figure 9.16: Optical micrograph showing the gradient pattern of A390-5%Mg bucket fabricated by the centrifugal cast process

The microstructure formation was affected in both the cylindrical cast and the bucket by the centrifugal force generated by the spinning of the mould. Some of the coarse Mg_2Si and large primary Si in the microstructure formed were modified and refined by the centrifugal casting

technique into fibrous and finer Si. Consequently, the mechanical properties of the alloy are improved by this modification and refinement [6, 14-16]. The inherent attributes of corrosion and wear resistance, light weight, the thermal and electrical conductivity of aluminium and its alloys and composites are resultant effects of microstructure modifications.

Fine Si particles are formed from the liquid by the melt rotation of Al-Si-based alloys during solidification. The cooling rate of Al-Si alloys has a strong effect on the microstructure; as such, rapid cooling causes transformation of plate morphology of eutectic silicon to fibre [17, 18]. Rapid solidification processing (RSP) during liquid to solid state transition results in grain size reduction, increased alloying elements solid solubility and segregation reduction. Furthermore, amorphous phases and metastable crystalline are formed at times. Rapid solidification is very effective in the production of nanocrystalline of Al-based alloys with Si, rare earth metal (RE), and late transition metal (Ni) (19). Centrifugal casting causes rapid cooling that facilitates the rate of solidification and consequently enhances the quality of casting.

The speed of rotation is a factor that affects the rate at which the microstructure of an alloy is modified and refined. Some studies have put the optimum speed of rotation in centrifugal casting operation between 1200 rpm to 1500 rpm [18, 20]. The microstructure of both the cylindrical and bucket cast was observed to show the following at the speed of 1200 rpm: changing of large primary Si into needle-shaped eutectic Si near the surface; long needle-shaped eutectic Si transformed into fine primary Si; and, the formation of fine grain.

The particles acceleration variation and solidifications model as related by equation (6), is represented in the graph in Figure 9.17. The graph shows that the particles of the Mg_2Si and Al-Si possess different acceleration at the same speed. This is due to the difference in their densities. The densities of the particles are: $Mg_2Si = 1.93 \times 10^3 \text{ Kg/m}^3$; $Si = 2.331 \times 10^3 \text{ Kg/m}^3$ and $Al-Si \text{ (matrix)} = 2.371 \times 10^3 \text{ Kg/m}^3$.

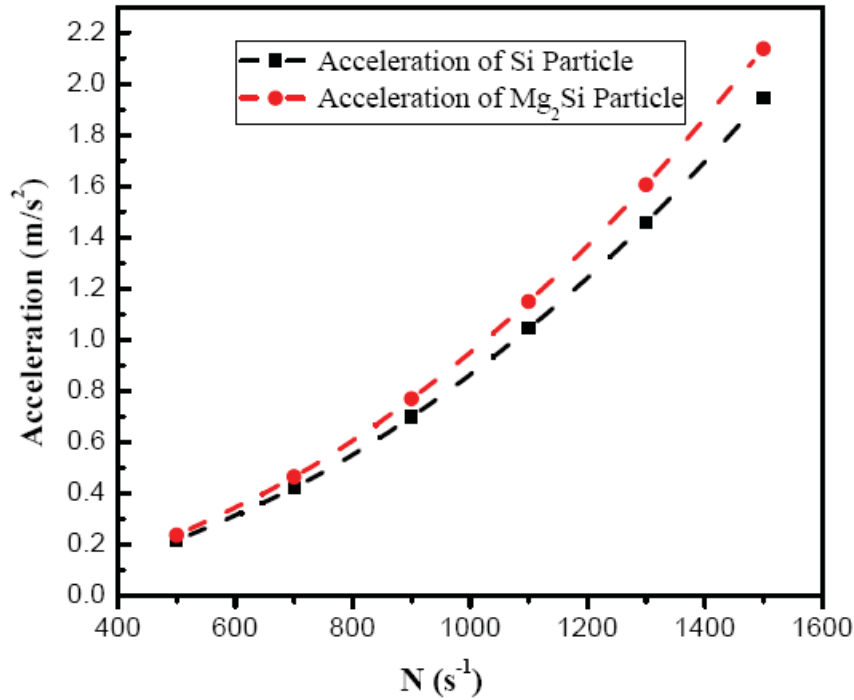


Figure 9.17: The particles acceleration and centrifugal-gravity ratio curve

9.4.2 Effect of centrifuge and heat treatment on hardness

The magnitude of the hardness varied between the inner region and the outer region of both the cylindrical cast and the bucket. A hardness of 150 BHN was observed at points 2 and 6, while the minimum, 110 BHN, was recorded at points 1 and 5 in the bucket specimen of A360-5Mg-T6. Figure 17 shows the hardness values along specimen D as-cast. The maximum and minimum BHN of as-cast were obtained at 140 mm (120 BHN) and 100 mm (87 BHN) from the axis of rotation respectively. A maximum hardness of 157 BHN was recorded at 70 mm and 145 BHN at 140 mm in a heat treated sample.

The microstructure formation at the maximum hardness point in as-cast A390-5%Mg is fine and fibrous silicon particles, while voids and α -Al dendrites are the predominant features of the minimum hardness point. The hardness magnitude at 140 mm from the centre of rotation is the resultant effect of coarse Mg_2Si and large primary Si refinement by the centrifuge. The high volume of aluminium insoluble hard Si precipitates at the inner zone and is responsible for the 118 BHN hardness recorded (Figure 9.18).

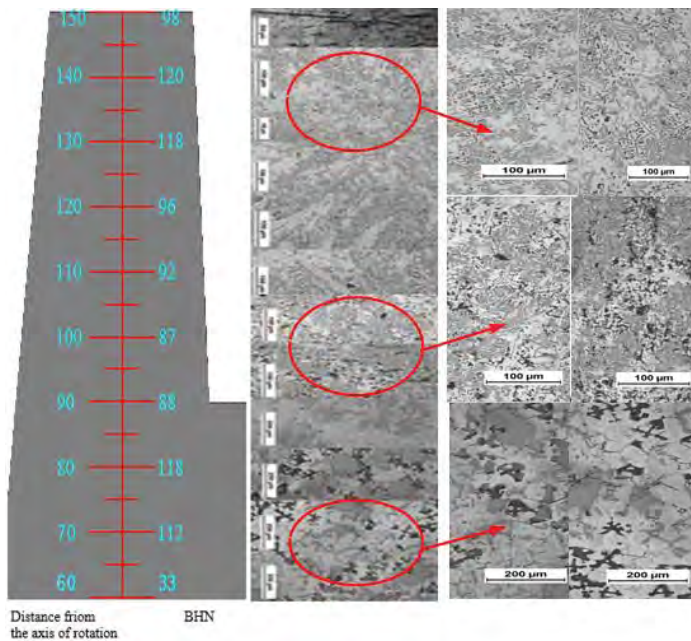


Figure 9.18: Hardness of A390-5%Mg as-cast by centrifugal casting in relation to the microstructure

A non-uniform morphology was seen in A360-T6, as shown in Figure 9.19(b), due to the formation of smaller Mg_2Si and primary Si particles, a fusion of Si and Mg_2Si particles, finer and needle-shaped eutectic Si after heat treatment. A hardness of 143 BHN was observed in A360-T6.

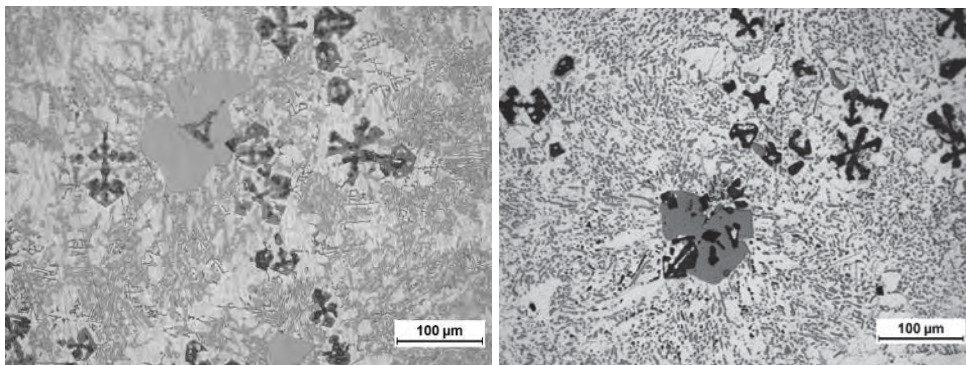


Figure 9.19: Optical micrographs of A390 and A390-6T as-cast by gravity casting a) A390 as-cast; b) A390-6T

A390 belongs to the heat treatable class of aluminium alloy (3xx series) and heat treatment studies have shown that the process enhances mechanical properties such as hardness and strength [21-23]. The increase in hardness that accompanies the T6 process is caused by the production of supersaturated solid solution during solutionizing and re-precipitation during ageing. The T6 heat treatment process executes homogeneity of the structure of as-cast intermetallic phases such as Al_2Cu and Mg_2Si dissolution and refinement of eutectic silicon morphology [24, 25]. The modification and refinement which occurs includes the

disintegration of the eutectic silicon branches and spheroidization of the separated branches [26-29]. The high hardness value observed at the inner region of A360-5%Mg-T6, represented in Figure 9.20 is due to the high volume of Mg₂Si precipitates that dissolved during solutionizing, and to the presence of a cluster of the refined eutectic Si in the region.

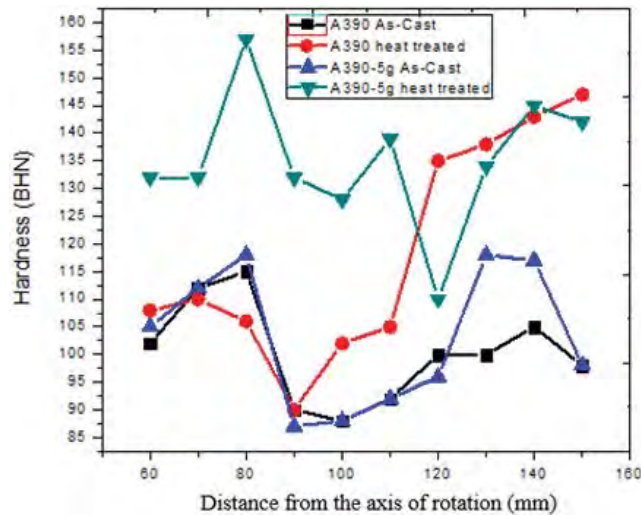


Figure 9.20: Graphs of hardness variation of A390 and A390-5%Mg fabricated by centrifugal casting technique of both as-cast and heat treated alloys

9.4.3 Electrochemical corrosion

The difference in corrosion behaviour of A390 and A390-5%Mg alloys in 3.5% NaCl solution is shown in Figure 9.21 and Table 9.3. The tafel (polarisation) curves in the Figure 20(a) indicate that less corrosion occurred in the A390-5%Mg alloy. The base alloy showed continuous pitting prospect while the alloy with 5%Mg showed higher resistance. Table 9.3 presents the A390 and A390-5%Mg alloys in 3.5% NaCl solution polarisation parameters. It was observed that the corrosion current (I_{corr}) of A390 alloy is higher than that of A390-5%Mg alloy. This means that A390 alloy will corrode more.

Table 9.3: A390 and A390-5%Mg alloys in 3.5 % NaCl solution polarisation parameters

Alloy	E_{corr} (V)	I_{corr} (A)	$A_{cathode}$	A_{anode}
A390	-0.886	2.98×10^{-4}	4.833	6.228
A390-5%Mg	-0.01	2.8×10^{-6}	9.169	4.484

In Figure 9.21(b) the inner (E_1), and the mid (E_2) regions show the highest and least resistance respectively. The A390-5%Mg alloy resistance arrangement as shown in Figure 9.21(b), is due to the large Mg₂Si precipitates at the surface of the A390-5%Mg alloy. This result is in accord with some of the previous studies. Several studies have shown that alloying aluminium with 3 % to 4 % magnesium enhances the corrosion resistance of aluminium and its alloys in

seawater. The high corrosion resistance of the Al-Mg system coupled with its mechanical and weldability properties, means that alloys of Al-Mg are widely applied in sea shipbuilding and other seawater related applications [30, 31].

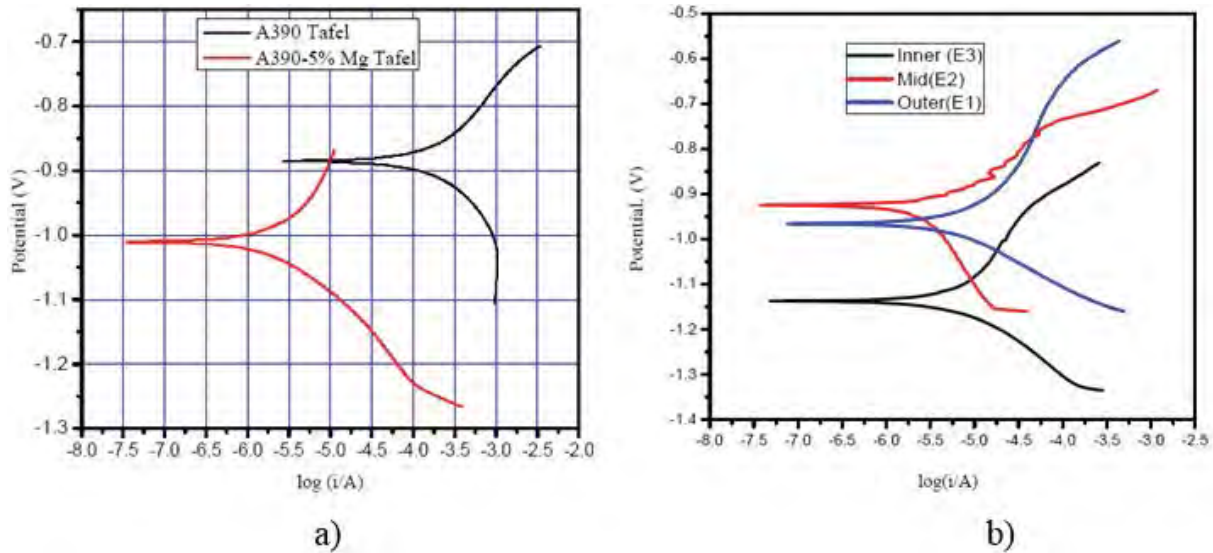


Figure 9.21: Tafel of a) A390 and A390-5%Mg; b) Specimens E₁, E₂, and E₃ (see also Figure 9.10)

9.5 Protective coating of Pelton bucket

For functional performance therefore, the surface of the bucket should be hardened and smoothed to withstand the silt erosion, cavitation and pressure from jet water. Using centrifugal casting processes and heat treatment has tremendously enhanced the surface hardness property and strength.

For better service performance, bucket surface coating with harder and tougher material is recommended. Coating the surface of a bucket with a ceramic material is effective and the use of Al₂O₃ implanted with Fe micrograins, and microarc oxidation (MAO) or plasma electrolytic oxidation (PEO) as coatings are recommended by this study.

9.6 Conclusion

This study observed that: it is possible to fabricate a complex shaped Pelton turbine bucket by means of a centrifugal casting process with the right permanent mould configuration; the mechanical properties of the bucket can be improved by 5 %Mg addition to A390 alloy using gravity casting and heat treatment; a hardness of 143 BHN was observed in A360-T6; large silicon flakes, large α -aluminium dendrites inter-dendrite arm spacing and large dendritic cells are formed by low solidification which are converted to small silicon flakes, small inter-

dendrite arm spacing and changed acicular silicon to fibrous silicon by centrifugal casting technique; and, the mechanical properties of the inner surface (the face that receives jet water) can be improved using a centrifugal casting technique and heat treatment. Improvement was also observed at the outer surface of the bucket due to large Si and Mg_2Si particles that were segregated in that region, and the electrochemical corrosion property of A390 alloy in 3.5 NaCl solution was enhanced by the addition of 5 %Mg to form A390-5%Mg alloy. However, due to the pattern of the microstructure influenced by the centrifuge, the inner zone of the circular cast shows the highest corrosion resistance.

Bibliography

- [1] S. K. Bohidar, R. Sharma and P. R.. Mishra, "Functionally graded materials: A critical review," *International Journal of Research (IJR)*, vol 1, pp. 289-301, 2014.
- [2] G. E. Knoppers, J. W. Gunnink, J. Van Den Hout, W. P. Van Vliet, "The reality of functionally graded material products," International Solid Freeform Fabrication Symposium; University of Texas at Austin, Texas 2004, pp. 38-43.
- [3] S. S. Wang, "Fracture mechanics for delamination problems in composite materials," *Journal of Composite Materials*, vol. 17, no. 3, pp. 210-223, 1983.
- [4] T. P. D. Rajan and B. C. Pai, "Formation of solidification microstructures in centrifugal cast functionally graded aluminium composites," *Transactions of The Indian Institute of Metals*, vol 62, no. 4-5, pp. 383-389, 2009.
- [5] A. Banerji, P. K. Rohatgi and W. Reif, "Research and development of transportation of composites,". In *Procedures of the European MRS Conference on Advanced Materials*, Strassburg, France 1985.
- [6] Y. B. Zuo, Z. Fan, Q. F. Zhu, L. Lei and J. Z. Cui, "Modification of a hypereutectic aluminium silicon alloy under the influence of intensive melt shearing." *Materials Science Forum*, vol. 765, pp. 140-144, 2013.
- [7] Y. Watanabe, H. Sato, T. Ogawa and I. S. Kim, "Density and hardness gradients of functionally graded material ring fabricated from Al-3 mass%Cu alloy by a centrifugal in-situ method," *Materials Transactions*, vol. 48, 2945-2952, 2007.
- [8] K. Patel, H. Patel and F. Patel, "Effect of mould rotation speed on hardness and sliding wear resistance of hypereutectic Al-Si alloy," *Indian Journal of Applied Research*, vol. 5, no. 1, pp. 78-81, 2015.
- [9] P. Adhikary, P. K. Roy and A. Mazumdar, "Selection of hydro-turbine blade material: application of fuzzy logic (MCDA)," *International Journal of Engineering Research and Applications*. vol. 3, no. 1, pp. 426-430, 2013.
- [10] SAAJ Steel Corporation, Die steel grade OHNS: SAAJ Steel Corporation; 2014 [cited 2016 23/03/2016]. Available from: http://saa Steele.com/?page_id=1055.

- [11] The New Zealand Digital Library Project. Micro Pelton turbines: components and design principles - bucket, New Zealand Digital Library Project; [cited 2016 06/03/2016]. Available from: <http://www.nzdl.org/cgi-bin/library.cgi>.
- [12] M. M. Rahvard, M. Tamizifar, S. M. A. Boutorabi and S.G. Shiri, "Characterization of the graded distribution of primary particles and wear behaviour in the A390 alloy ring with various Mg contents fabricated by centrifugal casting," *Materials and Design*, vol. 65, pp. 105-114, 2014.
- [13] R. D. Pruthviraj, P. V. Krupakara and H. P. Nagaswarupa, "Open circuit potential studies of ZA- 27/SiC metal matrix composites in acid chloride mediums," *Transactions of SAEST*, vol. 41, pp. 94-96, 2006.
- [14] O.V. Abramov, B.B. Straumal and W. Gust, "Hypereutectic Al-Si based alloys with a thixotropic microstructure produced by ultrasonic treatment," *Material and Design*, vol. 18, no. 4-6, 323-326, 1997.
- [15] C. Cui, A. Schulz, K. Schimanski and H. W. Zoch, "Spray forming of hypereutectic Al-Si alloys," *Journal of Material Process Technology*, Vol. 209, pp. 5220-5228, 2009.
- [16] D. Lu, Y. Jiang, G. Guan, R. Zhou, Z. Li and R. Zhou, "Refinement of primary Si in hypereutectic Al-Si alloy by electromagnetic stirring," *Journal of Material Processes Technology*, vol. 189, pp. 13-18, 2007.
- [17] N. V. Rafiei, N. Varahram and P. Davami, "Microstructure study of Al-20Si-5Fe alloys produced by melt-spinning process," *Metallurgy Material Engineering*, vol. 19, no. 1, pp. 85-94, 2013.
- [18] V. B. Patel, "Investigations on the properties of Al-Si alloy synthesized by centrifugal casting process," Doctor of Philosophy dissertation, Ganpat Uniiversiity, Kherva, India; 2014.
- [19] E. J. Abed, "Rapidly solidified of hyper eutectic aluminum-silicon alloys ribbons by using melt-spinning techniques," *International Journal of Current Engineering and Technology*, vol. 4, no. 3, pp. 1394-1398, 2014.
- [20] R. A. Shailesh, M. S. Tattimani and S. S. Rao, "Understanding melt flow behavior for Al-Si alloys processed through vertical centrifugal casting," *Materials and Manufacturing Processes*, vol. 30, no. 11, pp. 1305-1311, 2015.

- [21] S. Raghunandan, J. A. Hyder, T. P. D. Rajan, K. N. Prabhu and B. C. Pai, "Processing of Primary silicon and Mg₂Si reinforced hybrid functionally graded aluminum composites by centrifugal casting," *Materials Science Forum*, vol. 710 pp. 395-400, 2012.
- [22] A. M. A. Mohamed, F. H. Samuel and S. Alkahtani, "Influence of Mg and solution heat treatment on the occurrence of incipient melting in Al-Si-Cu-Mg cast alloys," *Materials Science and Engineering A*, vol. 543, pp. 22-34, 2012.
- [23] A. M. A. Mohamed, F.H. Samuel: "A review on the heat treatment of Al-Si-Cu/Mg casting alloys," *InTech*, Chapter 4, 2012.
- [24] J. Barresi, M. J. Kerr, H. Wang and M. J. Couper, "Effect of magnesium, iron, and cooling rate on mechanical properties of Al-7Si-Mg foundry alloys," *Transactions American Foundrymens' Society*, vol. 108, pp. 563-570, 2000.
- [25] J. Gauthier, P. Louchez and F. H. Samuel, "Heat treatment of 319.2 Al automotive alloy: Part 1, solution heat treatment," *Cast Metals*, vol. 8, no. 1, pp. 91-106, 1995.
- [26] D. V. Khera and R. S. Chadhawork, "Silt erosion. trouble for turbines," *International Water Power and Dam Construction*, vol. 53, no. 4, pp. 22-23, 2001.
- [27] W. S. Miller, L. Zhuang, J. Bottema, A. J. Wittebrood, P. De Smet, A. Haszler, *et al.*, "Recent Development in Aluminium Alloys for the Automotive Industry," *Material Science Engineering A*, vol. 280, pp. 37-49, 2000.
- [28] M. K. Padhy and R. P. Saini, "Effect of size and concentration of silt particles on erosion of Pelton turbine buckets," *Energy*, vol. 34, no. 10, pp. 1477-1483, 2009.
- [29] G. W. Birdsall, "Aluminium heat treatment," Reynolds Metal Company, Virginia, 1958.
- [30] F. I. Kvasov and I. N. Fridlyander, Eds., "Commercial Wrought, Sintered, and Casting Aluminum Alloys," Moscow: Metallurgiya, 1972.
- [31] H. H. Uhlig and R. W. Revie: *Corrosion and Corrosion Control: An Introduction to Corrosion Science and Engineering*, 4th ed. New York, NY: John Wiley & Sons, Inc., 2008.

CHAPTER 10: CONCLUSION AND FUTURE WORK

10.1 Conclusion

The aim of the study was to analyse and identify power issues, advance solutions and facilitate increase in the domestic production of hydropower components and systems. The objectives of the study were set to reflect the aim and to ensure that the set goals were achieved. Consequently, the study cuts across energy management, engineering design and manufacturing. These have been executed successfully in a number of publications and conferences papers presented in this thesis.

Chapter 2 deals with power issues and ways of lifting the present power situation in SSA and the chapter is divided into three parts. These parts observed that there is gross power inadequacy and erratic power supply in SSA. It noted that the majority of people without access to power in SSA live in the rural and remote areas. This has deterred economic growth, notwithstanding the enormous energy sources and other economic natural resources present in the region. This situation was attributed to many factors which include insufficient national and continental collective efforts, research results not being used appropriately, inadequate manufacturing infrastructure, over dependence on foreign technology, insufficient human capacity development and high cost of power projects in the region. The study identified SHP off grid schemes as being vital for rural, industrial estate and standalone electrification but that the region lacks the capacity. It was, however, proposed that many of these limitations can be resolved by domestic participation in the design and production of SHP components and their production technologies. The papers concluded that capacity development needs to occur in the design and manufacture of SHP components and systems.

The needed sensitisation and capacity enhancement in SHP design and manufacturing were tackled in Chapter 3. A simplified general hydro turbine design process was presented and a locally sourced A6061 aluminium alloy was considered as the blade material. The performance of the material as shown by the simulation results was satisfactory.

Further, the study found that bulk functionally graded materials production methods could be used to enhance the mechanical and corrosion properties of Pelton bucket. Various FGM fabrication techniques were studied and presented in Chapter 4. Chapter 5 presented centrifugal casting technique as a simple, and cost effective production process that can improve the mechanical properties of locally sourced aluminium based FGMs. Functionally

graded metal matrix composite by centrifugal casting technique mathematical correlation was studied in Chapter 6.

Chapter 7 presented a smart design procedure of civil works and mechanical design aspects of a SHP system. Design charts that will be useful in the selection and design of SHP were developed. A Pelton turbine bucket was designed for prototype purposes and locally sourced aluminium based material was considered as the bucket material.

Domestic development of SHP technologies was considered as a viable way of tackling rural electrification problems in SSA. Thus, the study developed a particular production technology of a prototype Pelton turbine bucket, involving the centrifugal casting method and heat treatment as showed by Chapters 8 and 9. The prototype buckets were successfully fabricated and characterised to investigate the effects of the manufacturing technique and other process parameters. The performance of A390, A390-5%Mg, A356 alloy, and A356-SiC_p composite that are locally sourced were satisfactory. The results show that: centrifugal casting method and heat treatment improved the mechanical properties of A356 alloy and A356-SiC_p composite; the anti-corrosion properties of A390 alloy in 3.5 NaCl solution were enhanced by the addition of 5 %Mg to form A390-5%Mg alloy; and, the mechanical properties of the inner surface of the bucket (the face that receives jet water) was improved using a centrifugal casting technique and heat treatment.

10.2 Future work

In the course of this research, a number of areas were noted, where worthwhile further investigative study and development are required. The number of iterations that could be made to enhance the performance of the SHP system is limitless and include the areas enumerated below.

10.2.1 Materials and manufacturing process

Much research is required regarding manufacturing methods to enhance mechanical properties of locally sourced materials for hydro turbine blade production, for instance, other FGMs fabrication methods such as squeeze and stirring casting methods. In terms of materials, other types of aluminium alloys and scrap such as automobile pistons need to be investigated for turbine blade or bucket fabrication.

10.2.2 Optimisation of domestic design and production

Study of the hydrodynamic and aerodynamic behaviour of blades or buckets fabricated from locally sourced material for hydro turbine optimisation is recommended.

APPENDIXES

439: Domestic turbine design, simulation and manufacturing for Sub-Saharan Africa energy sustainability

Ebhota WILLIAMS S.^{1*} AND Inambao, FREDDIE L.²

^{1, 2}Discipline of Mechanical Engineering, Howard College,
University of KwaZulu-Natal, Durban, South Africa

*Correspondence Author: willymoon2001@yahoo.com

The quest for options to the conventional energy sources especially to supply power to remote and rural locations in Sub-Africa has led to several power schemes. The identified options include solar, geothermal, wind and hydro and they belong to renewable energy. However, hydropower has been singled out as the best alternative renewable energy to increase access to power in the region. This study identified inadequate local contents in terms of manufacturing in the small hydropower system technologies in the region as the main hindrance in increasing the rate of power access in Sub-Saharan Africa. The study sees human and manufacturing infrastructure capacities building in small hydropower plant (SHP) technologies as a boost to local production of SHP parts and systems in the region.

For the purposes of design capacity building, a simplified design process was executed for low (3m) and high (60m) heads for Kaplan/Propeller and Pelton pico hydro turbines respectively. The design of a propeller turbine with a river hydrological data of flow rate (Q) 0.2m³/s and head (H_n) 3m using rotational speed (N) of 1500rpm. 6kW turbine power was developed from propeller blade of 0.166m tip diameter (Dt) with specific speed (Ns) of 294. In the case of Pelton turbine, given parameters of flow rate (0.02m³/s), net head (60m) and rotational speed (N) of 1500rpm were used to design a 8.2kW output power P_{to} of Pelton turbine with specific speed Ns of 26.16. Solidworks modeling and simulation software was used to evaluate the mechanical design of a Pelton bucket. The study concludes that adaptive design and domestic manufacturing are tools for sustainable power development and recommends that a regional joint funding of research on appropriate SHP technologies should be established.

Key words: Power, Design, Turbine, Pelton, Propeller

1. INTRODUCTION

The power situation in Sub-Saharan Africa is in a pathetic state despite several remedial interventions. The problems and challenges that trail the power sector in the region seem as fresh as if they were identified in two decades ago and deepened in some areas. Truly, this is heartbreaking considering the resources and efforts that have been put to fix it. IRENA (2012) reported that the average rate of electrification in Sub-Saharan Africa is about 35%. It was added that the situation is worse in the rural areas and this was put at below 20%. Further, over 50% of the population in 41 countries in the region has no opportunity to electricity (IRENA, 2012). Some of the factors responsible for this ugly situation are under developed manufacturing infrastructure, over reliance on foreign power technologies, exorbitant cost of power projects and under developed human capacity in power sector.

The search for ways of increasing access to power and alternatives to the conventional energy source (fossil fuel) to supply power to remote and rural areas in the region is massive. This has led to several power schemes. The identified options include solar, geothermal, wind and hydro and they are generally called renewable energies. However, hydropower has been singled out as the best alternative renewable energy with the potential of increasing access to power in the region. This study presents increase in local content in the design and manufacturing of small hydropower system technologies as a potential step to power problems in the region.

2. PRINCIPLE OF OPERATION OF A HYDRO TURBINE

Hydro turbine plants are rotating machines that transform the mechanical energy in flowing water into torque to turn the generator for the purpose of electricity production. Turbine can be categorised into two types, impulse turbines and reaction turbines (Barelli, Liucci, Ottaviano, & Valigi, 2013; Bilal, 2013; Loice & Ignatio, 2013). This classification depends on the water energy transfer method.

For impulse turbines, water is projected from the nozzle as jet and strikes on the buckets that are arranged on the circular edge of the runner. Though, the runner is enclosed in a casing, it is not very important. The buckets are made up of double hemispherical cups. The nozzle is the end of penstock while the buckets discharge used water on the tailrace. A schematic diagram of Pelton turbine is shown in Figure 1.

In reaction turbine, the runner or spinning wheel (blade) is completely immersed in the flow and they use water pressure and kinetic energy of the flow. They are appropriate for low to medium head applications. The two main types of reaction turbine are the propeller (with Kaplan variant) and Francis turbines.

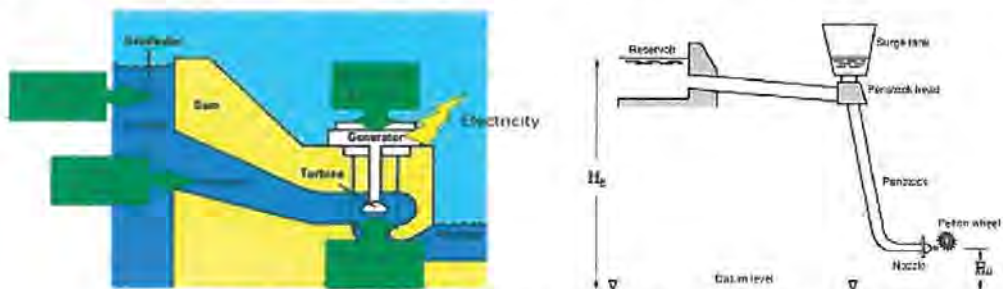


Figure 1: Schematic diagram of a hydro turbine system (Shesha, 2014)

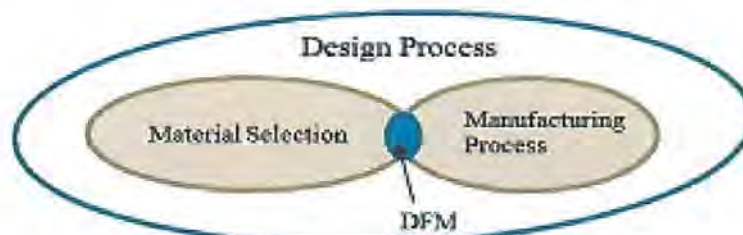
3. HYDRO TURBINE MAIN COMPONENTS

The hydro turbine is composed of the following main components as shown in Figure 1: **the Dam/Weir** – is a wall across the river or flow channel to store water. The reservoir created by the dam/weir is termed **Headrace**; **the Penstock** – This is the pipe that connects the headrace to the turbine runner; **the Runner** – the part of the layout that converts the energy of the flowing water into torque that drives the generator via shaft is called runner. The runner of a turbine has the wheel and buckets or cups for Pelton turbine; blade and hub for Kaplan, Turgo and Francis turbines. The **Shaft** – the part that connects the blade and the generator; **the generator** – this is the device that receives the mechanical energy through the shaft and

converts this energy into electrical energy. *Tailrace* – the used water flow out of the turbine through a channel called tailrace.

4. HYDRO TURBINE DESIGN AND MANUFACTURING PROCEDURES

There is strong correlation between material selection and manufacturing process. They could be said to be elements of the universal set called *Design Process*. Figure 2 represents the relation that exists between material selection and manufacturing process. For successful product design, the design process should provide an interphase between material selection and manufacturing process. This interphase is subjected to material and manufacturing facility availability. The manufacturing system in Sub Saharan Africa is not as advanced and adequate compared to what is obtainable in Europe and America even in Asia. However, good hydro turbine products can still come out of the region if material and manufacturing inadequacies are factored into the design process early.



DFM – Design for manufacturing

Figure 2: Correlation between material selection and manufacturing process.

A simplified hydro turbine production procedure can be categorised into twelve sequential steps as shown in Figure 3.

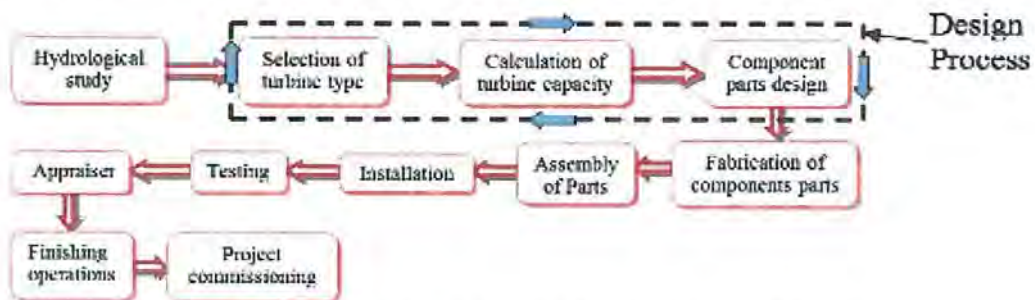


Figure 3: A Production layout Model of a Pico Hydro Turbine System

5. SELECTION OF TURBINE AND DESIGN OF TURBINE

There are two factors that determine the kind of turbine to be used. These factors are products of hydrological study of the hydro potential like river or water falls. The parameters are head (H) and the volumetric discharge (Q) of the river (Figure 4 refers).

The type of turbine to be used according to head classification; the head is classified into low (>10m), medium (10-50m) and high head (above 50m). Table 1 shows type of turbines and the various head domains where they are applied.

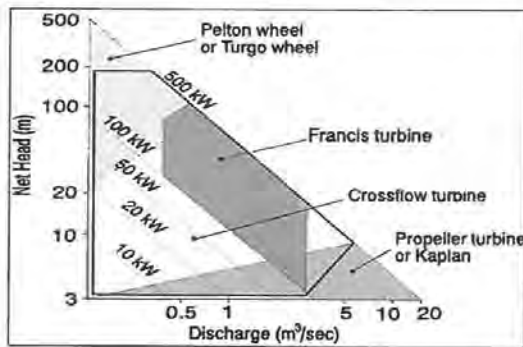


Figure 4: Head-flow Range of Small Hydro Turbines (Paish, 2002)

Table 1: Types of Hydro Turbine and their Applications (John, 2011; Shesha, 2014)

Turbine	Head Classification		
	High (>50m)	Medium (10-50m)	Low (<10m)
Impulse	Pelton, Turgo, Multi-jet Pelton	Crossflow, Pelton, Turgo, Multi-jet Pelton	Crossflow
Reaction		Francis (spiral case)	Francis (open-flume), Propeller, Kaplan, Darius

5.1 The Kaplan/Propeller Turbine

The Kaplan or propeller turbines are very appropriate for low head and large discharge operations. The Kaplan is an adjustable runner blade with high, almost constant efficiency over a wide range of load. The range of Kaplan turbine applications has been greatly improved, which has favoured the improvement of numerous undeveloped hydro sources previously discarded for economic or environmental reasons. The Kaplan Turbine generation efficiency is sometimes over 90% at low heads and high flows (Will, 2010).

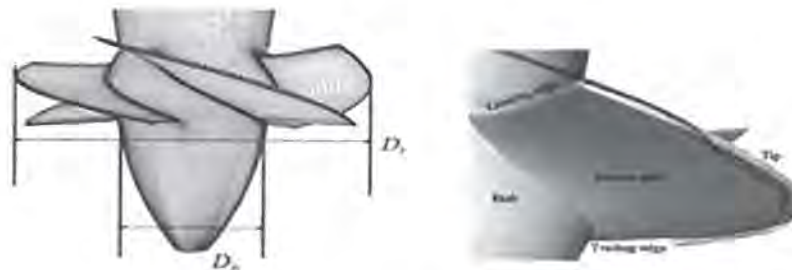


Figure 5: Kaplan/Propeller runner blade parameters and parts

5.2 The Pelton Turbine: Main Elements of a Pelton Turbine System

This turbine is typically used in small-scale micro-hydro systems (with power of up to about 100kW) and a head ranging from 10m to 200m. It consists of a wheel (or runner) with a number of buckets attached around its edge, which are shaped like two cups joined together with a sharp ridge between them as represents by Figure 6. In addition, a notch is cut out of the bucket at the outside end of the ridge. Water is directed to the turbine through a pipe and nozzle to this ridge. Its shape allows for the production of a lot of power from such a small unit and it is easy to manufacture.

As the water strikes at the symmetrical line it then distribute into the two halves of the bucket while some water are reflected back to the nozzle. The angle of jet deflection theoretically for a perfect hemispherical

bucket is 180° . This is not possible to obtain practically rather the angular deflection of 165° is used in practice (Bilal, 2013).

The main parts of Pelton turbine are penstock, spear, nozzle, wheel and buckets, shaft, generator, valves and powerhouse, Figure 7 refers. Water flows from the headrace through the penstock to runner. The penstock has a nozzle at its exit before the runner.

The flow rate of the water jet from the nozzle can be control with the use of spear. This spear helps to adjust the flow rate to balance the change caused by site conditions, see spear in Figure 6.

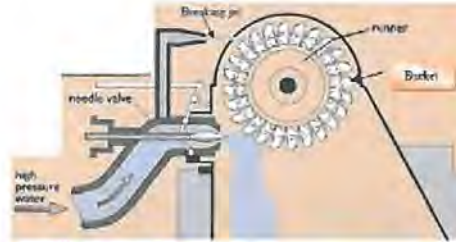


Figure 6: Pelton turbine arrangement

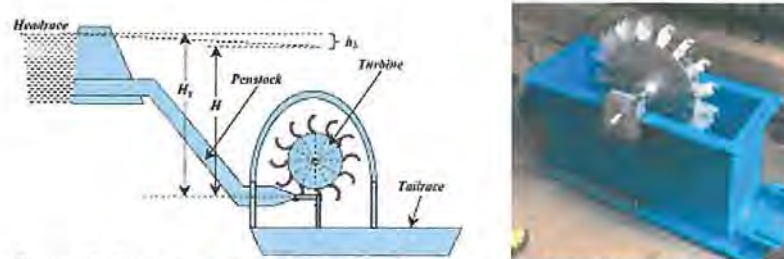


Figure 7: Shows a general layout of a Pelton hydro turbine plant (Shesha, 2014)

5.3 Pelton Design Parameters

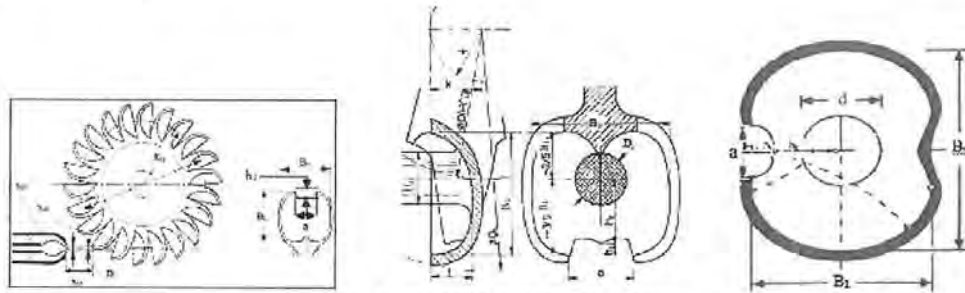


Figure 9: Runner and bucket parameters

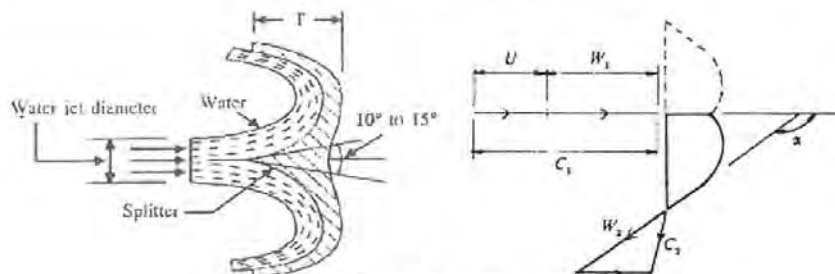


Figure 10: Turbine Velocity diagrams

5.4 Propeller Turbine Design for Low Head

Table 2: Nominal conditions for Kaplan/Propeller turbine design (refer to Figures 5) (Timo, 2007).

Given parameters: Q = 0.2m³/s; H _n = 3m; ρ = 1000; K _u = 1.7; N = 400rpm and; η = 0.8				
S/N	Step	Relevant Equations	Input numerical value input	Answer
	Turbine capacity, P.	$P = \rho * g * Q * H_n$	$P = 1000 * 9.81 * 0.2 * 3$	6kW
	Specific speed, N _s	$N_s = \frac{N * \sqrt{Q}}{H_n^{0.75}}$	$N_s = \frac{1500 * \sqrt{0.2}}{3^{0.75}}$	294
	Velocity, u	$u = K_{ug} \sqrt{2gH_n}$	$u = 1.7 * \sqrt{2 * 9.81 * 3}$	13.04m/s
	The angular velocity of the turbine runner, rad/s	$\omega = \frac{2\pi N}{60}$	$\omega = \frac{2 * \pi * 1500}{60}$	157rad/s
	The blade tip radius, r _t	$r_t = \frac{K_{ug} \sqrt{2gH_n}}{\omega}$	$r_t = \frac{1.7 * \sqrt{2 * 9.81 * 3}}{157}$	0.083m
	The blade tip diameter, D _t	D _t = 2r _t	D _t = 2*0.083	0.166m
	The hub diameter, D _h	$\frac{D_h}{D_t} = 0.35$	D _h = 0.35*0.166	0.058m
	Cross sectional area, A	$A = \frac{\pi}{4} (D_t^2 - D_h^2)$	$A = \frac{\pi}{4} * (0.166^2 - 0.058^2)$	0.019m²
	Axial velocity [m/s]	$V_{axial} = \frac{4Q}{\pi (D_t^2 - D_h^2)}$	$V_{axial} = \frac{4 * 0.2}{\pi * (0.166^2 - 0.058^2)}$	10.53m/s
	Flow coefficient, Φ:	$\Phi = \frac{Q}{ND_t^3}$	$\Phi = \frac{0.2}{1000 * 0.166^3}$	0.044
	Power coefficient, Γ:	$\Gamma = \frac{P}{\rho N^3 D_t^5}$	$\Gamma = \frac{6}{10^3 * 1500^3 * 0.166^5}$	1.4*10 ⁻⁶
	Energy coefficient, Ψ:	$\Psi = \frac{gH}{N^2 D_t^2}$	$\Psi = \frac{9.81 * 3}{1500^2 * 0.166^2}$	4.7*10 ⁻⁴

Where A - area; Q - flow rate and; r_t - blade radius; r_h - hub radius; D_t - blade diameter and; D_h - hub diameter; K_{ug}, the tip-to-head velocity ratio (D_t/D); ρ - density of water (kg/m³); g - acceleration due to gravity (9.81m/s²); H_n - net head (m) and; η_t - total efficiency.

5.4 Pelton Design for High Head Design and Simulation of Bucket

Table 3: Nominal Conditions for Pelton Turbine Design (refer to Figure 9 and 10) (Anders & Owen, n.d.; Obretenov, 2006; Shesha, 2014; Will, 2010).

Given quantities: Q = 0.015m³/s; H _n = 60m; C _n = 0.98; ρ = 103Kg/m³; x = 0.46; n _j = 1; L _{pt} = 100m; ψ = 0.98 and; θ = 165°. The generator is rated at 120 watts, and the rotation (N) is 1500 RPM.				
S/N	Parameters	Relevant Equations	Input numerical value input	Answer
	The input power to the turbine, P _t	$P_t = \rho * g * C_n^2 * H_n * Q$	$P_t = 10^3 * 9.81 * 0.98^2 * 60 * 0.015$	8.48kW
	Specific speed (N _s)	$N_s = \frac{N * \sqrt{P_t}}{H_n^4}$	$N_s = \frac{1500 * \sqrt{8.48}}{60^4}$	26.16
	Jet velocity, V _j (m/s)	$V_j = C_n * \sqrt{2 * g * H_n}$	$V_j = 0.98 * \sqrt{2 * 9.81 * 60}$	33.62m/s
	Jet/nozzle diameter, D _j	$D_j = \sqrt{\frac{4 * Q}{\pi * n_j * V_j}}$	$D_j = \sqrt{\frac{4 * 0.015}{\pi * 1 * 33.62}}$	0.024m


Tangential velocity of the runner, V_r	$V_r = x * V_j$	$V_r = 0.46 * 33.62$	15.47m/s
Runner diameter D_r , (m)	$D_r = \frac{60 * V_r}{\pi * N}$	$D_r = \frac{60 * 15.47}{\pi * 1500}$	0.20m
Jet/nozzle cross sectional area, A_j	$A_j = \frac{\pi * D_j^2}{4}$	$A_j = \frac{\pi * 0.024^2}{4}$	$4.5 * 10^{-4}$
Nozzle flow rate, Q_n (m ³ /s)	$Q_n = V_j * A_j$	$Q_n = 33.62 * 4.5 * 10^{-4}$	0.015m ³ /s
Distance between bucket and nozzle, x_{nb} (m)	$x_{nb} = 0.625 D_r$	$x_{nb} = 0.625 * 0.20$	0.125m
Radius of bucket center of mass to runner center R_{br} (m)	$R_{br} = 0.47 D_r$	$R_{br} = 0.47 * 0.20$	0.094m
Bucket axial width, B_w (m)	$B_w = 3.4 D_r$	$B_w = 3.4 * 0.024$	0.082m
Bucket radial length, B_l (m)	$B_l = 3 D_r$	$B_l = 3 * 0.024$	0.072m
Bucket depth, B_d (m)	$B_d = 1.2 D_r$	$B_d = 1.2 * 0.024$	0.029m
Cavity Length, h_1 , (m)	$h_1 = (0.35) D_r$	$h_1 = (0.35) * 0.024$	0.008m
Length to Impact Point, h_2 (m)	$h_2 = (1.5) D_r$	$h_2 = (1.5) * 0.024$	0.036m
Offset of Bucket, k (m)	$k = (0.17) D_r$	$k = (0.17) * 0.024$	0.004m
Cavity Width, a (m)	$a = (1.2) D_r$	$a = (1.2) * 0.024$	0.029m
Number of bucket n_b	$n_b = 15 + \frac{D_r}{2 D_l}$	$n_b = 15 + \frac{0.20}{2 * 0.024}$	19
Length of bucket moment arm, L_{ab} (m)	$L_{ab} = 0.195 D_r$	$L_{ab} = 0.195 * 0.20$	0.039m
Volume of bucket, V_b (m ³)	$V_b = 0.0063 * D_r^3$	$V_b = 0.0063 * 0.20^3$	$5.04 * 10^{-5} \text{m}^3$
The output power to the turbine, P_{to} (kW)	$P_{to} = \rho * Q * V_r * \left[\frac{(V_j - V_r) * a}{(1 + \psi * \cos(\phi))} \right]$	$P_{to} = 1000 * 0.015 * 15.47 * \left[\frac{(33.62 - 15.47) * a}{(1 + 0.98 * \cos(15))} \right]$	8.20kW
Turbine hydraulic efficiency, η_{th}	$\eta_{th} = \frac{P_{to}}{P_u} * 100$	$\eta_{th} = \frac{8.20}{8.48} * 100$	97%
Mass of a bucket (Kg)	$M_b = \rho_m * V_b$ $\rho_m =$	$M_b = \rho_m * V_b$	
The torque produced by the turbine, T_i (N-m)	$T_i = \frac{P_{to}}{\omega} = Q * D_r * (V_j - V_r)$	$T_i = 0.015 * 0.2 * (33.62 - 15.47)$	0.054N-m
The deflector required force, F_d :	$F_d = \rho * Q * V_j$	$F_d = 1000 * 0.02 * 33.62$	672.4N
Force acting on the runner	$F_{a1} = 2 * \rho * Q_n * (V_j - V_r)$	$F_{a1} = 2 * 1000 * 0.015 * (33.62 - 15.18)$	555.2N

Where C_n – nozzle discharge coefficient (0.98); N – runner speed (rpm); x – ratio of V_r to V_j ; Q - flow rate; g - acceleration due to gravity (9.81m/s²); H_n - net head (m); ρ - density of water (kg/m³)

6. MATERIAL SELECTION FOR PELTON BUCKET

Material selection is a very important part of design and manufacturing. One of the variables for design process iteration is material and it influences on manufacturing process. In this study, the selection of material for the bucket was determined by availability, functional requirements, cost and manufacturing facility available. Aluminium alloy (6061-T6) was selected because aluminium is readily available in Sub-Saharan Africa and it can easily be worked upon. Table 4 shows the material properties


Table 4: Material Properties

Model Reference	Volumetric Properties	
	Name: 6061-T6 Aluminum Alloy	Mass: 0.249492 kg
	Model type: Linear Elastic Isotropic	Volume: 9.24044e-005 m ³
	Yield strength: 2.75e+008 N/m ²	Density: 2700 kg/m ³
	Tensile strength: 3.1e+008 N/m ²	Weight: 2.44502 N
	Elastic modulus: 6.9e+010 N/m ²	Shear modulus: 2.6e+010 N/m ²
	Poisson's ratio: 0.33	Thermal expansion coefficient: 2.4e-005 /Kelvin

6.1 Evaluation of 6061-T6 Aluminium Alloy: Results of Mechanical Simulation of Pelton Bucket

The necessary design parameters in table 3 were used in the simulation to validate the stress and fatigue of the part (bucket). The results of the simulation are shown in Tables 5 and 6 and diagrams 12 and 13.

Table 5: Mesh Information

	Mesh type	Solid Mesh	Total Nodes	14895
	Mesher Used:	Standard mesh	Total Elements	8568
	Total Nodes	14895	Maximum Aspect Ratio	19.602
	Total Elements	8568	% of elements with Aspect Ratio < 3	97.5
	Jacobian points	4 Points	% of elements with Aspect Ratio > 10	0.0817
	Element Size	4.52077 mm	% of distorted elements (Jacobian)	0
	Tolerance	0.226039 mm	Time to complete mesh(hh:mm:ss):	00:00:07
	Mesh Quality	High		

The static analysis (von Mises) shows that the highest stress (1.95904e+008 N/m²) as a result of the load is located at node 723 as indicated in Table 6 and Figure 12. This value is less than the material's yield stress of 2.75e+008 N/m² as presented in Table 4.

The fatigue distribution along the longitudinal section is shown in Figure 13. The highest fatigue value was recorded at nodal 723 as shown by 13.

The minimum Factor of Safety (FOS) is value at 1.404 and this value was recorded at nodal point 723 as show in Figure 14. However, the FOS is >1. For solidworks software, the FOS benchmark is 1.4. the value of FOS (1.404) recorded from the simulation validates the design good.

7. CONCLUSION

The manufacturing infrastructure in Sub-Saharan Africa is inadequate to support energy sustainability. As a result, the region depends on foreign technology massively and this makes power projects cost very high. This has left the region's socio-economic situation pitiable. In order to increase access to electricity in the region, it is therefore pertinent to building capacity in power technology. The design process should focus on local contents in terms material selection and manufacturing facility. This study recommends capacity building in small hydropower (SHP) technology, establishment of regional energy research institutions, transformation of research findings into real products, and adopt China's energy development approach of massive use of micro hydro turbines.

8. ACKNOWLEDGEMENT

The authors hereby acknowledge the Centre for Engineering Postgraduate Studies (CEPS)/HVDC/Smart Grid Centre of the University of KwaZulu-Natal.

9. REFERENCES

- ANDERS, A., & Owen, S. (n.d.). *Kaplan Turbine From Remote HydroLight* (pp. 49). Retrieved from www.remotehydrolight.com
- BARELLI, L., Liucci, L., Ottaviano, A., & Valigi, D. (2013). Mini-Hydro: A Design Approach in Case of Torrential Rivers. *Energy*, 58, 695-706. doi: <http://dx.doi.org/10.1016/j.energy.2013.06.038>
- BILAL, A. N. (2013). Design of High Efficiency Pelton Turbine for Microhydropower Plant. *International Journal of Electrical Engineering and Technology (IJEET)*, 4(1), 171-183.
- IRENA. (2012). Prospects for the African Power Sector. United Arab Emirates.
- JOHN, F. C. (2011). Turbines. Retrieved 18/05/2015, 2015, from <http://www.jfccivilengineer.com/turbines.htm>
- LOICE, G., & Ignatio, M. (2013). Efficiency improvement of Pelton Wheel and Crossflow Turbines in Micro-Hydro Power Plants: Case Study. *International Journal of Engineering and Computer Science*, 2(2), 416-432.
- OBRETENOV, V. S. (2006). Modernization of a Pelton Water Turbine. *Пробл. Машиностроения*, 4, 1-5.
- PAISH, O. (2002). Small Hydro Power: Technology and Current Status. *Renewable and Sustainable Energy Reviews*, 6 537-556.
- SHESHA, P. M. N. (2014). Hydraulics and Hydraulic Machines. *VTU Learning*, 1-22. http://elearning.vtu.ac.in/P6/enotes/CV44/Pel_Whe-MNSP.pdf
- TIMO, F. (2007). Design of the Runner of a Kaplan Turbine for Small Hydroelectric Power Plants. (Master), Tampere University of Applied Sciences.
- WILL, S. (2010). Corazón del Bosque Hydroelectric Scheme: Engineering Design Document. In V. M. 2010 (Ed.), (Vol. 1, pp. 37). Guatemala: Appropriate Infrastructure Development Group (AIDG).

Examining the Effects of Production Method on Aluminium A356 Alloy and A356-10%SiC_p Composite for Hydro Turbine Bucket Application

Williams S. Ebhota, Freddie L. Inambao

Abstract—This study investigates the use of centrifugal casting method to fabricate functionally graded aluminium A356 Alloy and A356-10%SiC_p composite for hydro turbine bucket application. The study includes the design and fabrication of a permanent mould. The mould was put into use and the buckets of A356 Alloy and A356-10%SiC_p composite were cast, cut and machined into specimens. Some specimens were given T6 heat treatment and the specimens were prepared for different examinations accordingly. The SiC_p particles were found to be more at inner periphery of the bucket. The maximum hardness of As-Cast A356 and A356-10%SiC_p composite was recorded at the inner periphery to be 60 BRN and 95BRN, respectively. And these values were appreciated to 98BRN and 122BRN for A356 alloy and A356-10%SiC_p composite, respectively. It was observed that the ultimate tensile stress and yield tensile stress prediction curves show the same trend.

Keywords—A356 alloy, A356-10%SiC_p composite, centrifugal casting, pelton bucket, turbine blade.

I. INTRODUCTION

In this study, the focus is on property enhancement of A356 aluminium alloy and A356-10%SiC_p composite, through manufacturing and heat treatment techniques for Pelton bucket application. The search for locally sourced materials for Small Hydropower (SHP) turbine components and systems production and their manufacturing technologies is very critical to energy sustainability in Sub-Saharan Africa (SSA). SHP technology domestication is the key to the perennial power problem in the region.

Capacities for turbine components and system design, material and manufacture should be enhanced through regional joint efforts, academic research, and an exchange programme with developed countries, etc. [1], [2]. The capacity building should be geared to increasing local participation and technology domestication in the region. SSA with a lot of SHP potentials as presented in Table I, needs to explore merits of switch-mode power supply (SMPS) for greater access to power [3].

A theoretical micro-hydroelectric plant design for off grid applications was carried out to produce a green power for remote farms or cottage.

Williams S. Ebhota, PhD candidate, and Freddie Inambao, Associate professor, are with the University of KwaZulu-Natal, Durban, South Africa (phone: +27633840252; e-mail: willymoon2001@yahoo.com, inambao@ukzn.ac.za).

TABLE I

Regions in SSA	SHP POTENTIAL IN SSA [3]		
	Available SHP potential (MW)	Installed capacity (MW)	Installed capacity (%)
Eastern Africa	6,262	209	3.3
Middle Africa	328	76	23.1
South Africa	384.5	43	11.2
West Africa	742.5	82	11.1

II. REVIEW

Loice and Ignatio investigated the effects of material, surface texture and fabrication methods on the efficiency of hydropower plant projects within an acceptable cost range. In their project, more electricity was generated at a reduced cost per unit kW. The study concluded that manufacturing of more efficient financially viable Pelton turbines for the micro hydro system (MHS) is possible [4]. A theoretical micro-hydroelectric plant design for off-grid applications was carried out to produce green power for remote farms or cottage. A prototype of the system was built to test the design [5].

A study on the modelling and validation of results empirically, using locally available materials in Kenya was carried out [6]. In the study, stress reduction of 14.2% was achieved by modifying the profile of the Pelton bucket. A recycled A356 aluminium alloy was found to withstand the stress of 150 MPa, produced by the generated 5 kW of power [6]. A Pico Pelton turbine was designed and manufactured using chopped glass fibres reinforced epoxy matrix composite as the bucket material [7]. A 50,000 litre capacity storage tank in a 10 storey tower was used as a water source to operate the turbine. In the study, 1.5 kW was generated out of the 2.793 kW that it was theoretically designed for. In the design study of Nava and Siva, CATIA V5 design and modelling software were used to design an optimised Pelton turbine considering three materials in the analysis [8]. Efficiency and stress in relation to the number of buckets were studied in the work. In the three bucket materials selected (steel, cast iron and fibreglass reinforced plastic matrix), the study concluded that fibreglass reinforced plastic matrix shows exceptional performance compared to cast iron.

It is obvious that a lot of theoretical hydro turbine design works have been studied. However, only little is known when it comes to aluminium alloys and their composites for the fabrication of a Pelton turbine bucket. Considering the present

application of aluminium alloys and their composites, hypothetically, this study sees this group of materials versatile in Pelton turbine bucket application.

A. Application of A356 Alloy and A356-SiCp Composite Suitability for a Pelton Turbine Bucket

Previous studies of hydro turbine plants revealed that silt erosion affects the underwater components which include turbine blade greatly [3]. In some cases, water is stored in a reservoir or in a settling basin to be used when the need arises. Over a period of time, sediment with silt and hard abrasive sand as the components, settle in the reservoirs or basins. This problem must be taken care of with the use of sediment settling systems in power plants. However, a lot of unsettled sediment passes through turbines every year and turbine parts are exposed to severe erosion. This sediment should be prevented from passing through the turbine by incorporating the sediment settling systems in the power plant. However, there are still possibilities of unsettled sediment passing through the turbine and this occurrence causes serious erosion to the nozzle system and the turbine blade/bucket.

B. Functionally Graded Manufacturing Technique: Centrifugal Casting Technique

The centrifugal casting technique was chosen due to its mechanical and microstructural enhancing advantages. The process aids microstructure gradient and hardness in alloys even without reinforcement, and therefore, gives the material a better wear and corrosion resistance [9]. The mechanical properties of aluminium-silicon alloys are often improved by casting technology [10]. Quite often, hypoeutectic and near eutectic Al-Si alloys are applied when corrosion resistance and good castability are needed with a small amount of Mg and Cu for heat treatment enhancement. It has been revealed that centrifugal casting can increase: rupture strain by 160% and

rupture strength by 35%; young modulus by 18% and; fatigue life by 1.5% [11].

III. METHODOLOGY OF THE STUDY

The study is methodically divided into three: fabrication of the Pelton turbine bucket permanent mould; centrifugal casting of the bucket; and, characterisation of the Pelton turbine bucket materials.

A. Fabrication of Pelton Turbine Bucket

The fabrication of the Pelton turbine bucket has two stages: Production of permanent mould; and, centrifugal casting of the Pelton bucket. The 3D model of the bucket is shown in Fig. 1. In this study, the bucket was designed for a capacity of 18.45kW turbine power.

1) Production of Mould

The mould was designed with Solidworks software where the IGES files of the mould components were generated. The parts of the mould were machined according to the specifications in Initial Graphics Exchange Specification (IGES) files. The CAD of the mould as designed and produced are shown in Figs. 2 (a) and (b), respectively.

2) Mould Material

Oil Hardening Non-Shrinking Die Steel (OHNS) was used as the mould material and the components were heated treated before they were put to use. The chemical composition is shown in Table II. OHNS steel is a reliable material for gauging, blanking and cutting tools, as well as for hardness and elevated temperature applications [12]. A hardening temperature of 800 °C was used and a hardness of about 432 BHN of a 3,000 kgf standard force was recorded. The fabricated Pelton bucket mould components are presented in Fig. 3.

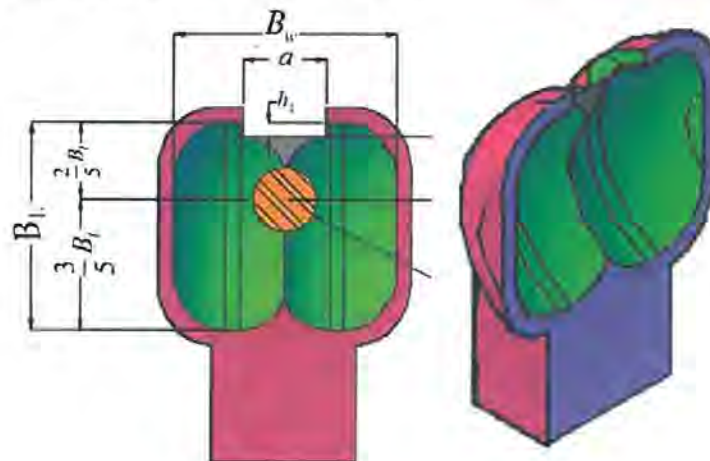
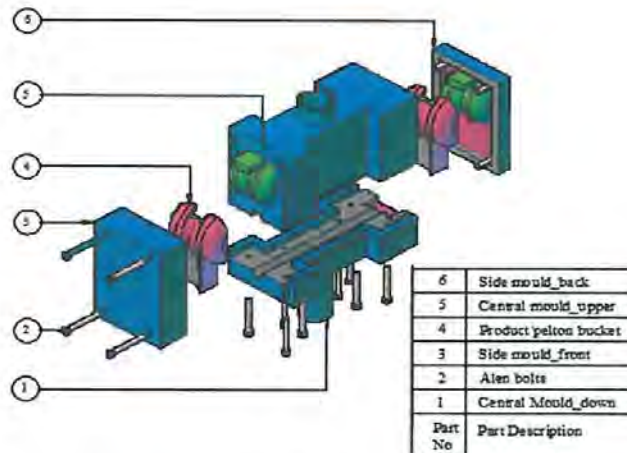
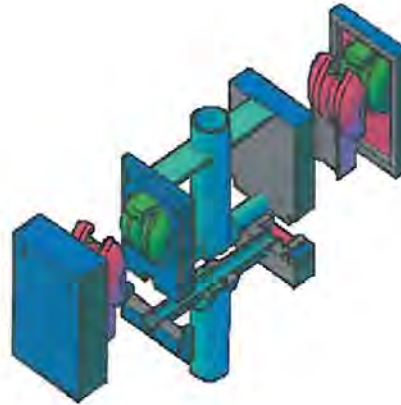


Fig. 1 The design parameters of a bucket



(a)



(b)

Fig. 2 (a) Exploded diagram of the Pelton bucket mould as designed, (b) Exploded diagram of the Pelton bucket mould as fabricated

TABLE II
CHEMICAL COMPOSITION OF THE OHNS MATERIAL USED FOR THE PELTON BUCKET MOULD

Element	C	Mn	Cr	W	V
%	0.95	1.1	0.6	0.6	0.2

B. Centrifugal Casting of Pelton Bucket

The chemical composition of A356 used is shown in Table III.

TABLE III
A356 ALLOY CHEMICAL COMPOSITION

Elements	Cu	Mg	Mn	Si	Fe	Ti	Zn	Al
%	0.25	0.30	0.35	7.5	0.35	0.05	0.10	91.10

1) Casting of A356 Alloy

Clay graphite crucible was used to process A356 alloy. Hexachloroethane was applied at 720 °C for degassing of the molten metal to prevent hydrogen entrapment. The molten

metal was superheated to (750 °C), which is above its liquidus temperature before pouring it into a spinning mould and a stationary rectangular mould for gravity casting. The Pelton bucket permanent mould was preheated to 300 °C and rotated at 1,500 rpm during pouring and solidification. The rotation was stopped five minutes after pouring.

2) Casting of A356-10%SiC_p Composite

The same melting conditions for the A356 alloy, as stated above, were followed for the casting of the A356-10%SiC_p composite. The 25 μm SiC particle was preheated to 600 °C before inserting it into the A356 molten. The mixture was stirred with an electric motor driven impeller at a speed of 300 rpm. The particle feed rate to the molten metal is about 1 gm/s and the stirring continues for 15 minutes after the particles addition.



Fig. 3 The fabricated Pelton bucket mould components

In the mould configuration, it is designed to produce two castings in one operation. The arrangement is such that the faces are in the same direction as depicted in Fig. 4.

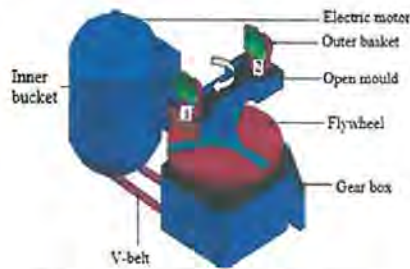


Fig. 4 Centrifugal casting machine with an opened mould in which the buckets are facing the same direction

C. Characterisation of Cast Bucket: Preparation of Test Specimen.

1) Microstructure Examination

The cast bucket of both materials under investigation was sliced at the middle, see Fig. 5 (a), into two parts and both halves were prepared for microstructural examination and hardness test. The samples for the microstructural view were polished using the following grits of polishing paper consecutively: 80, 100, 220, 400, 600 and 1,000. The paper polishing was followed by cloth polishing with 6 μm , 3 μm and 1 μm SiC_p particle paste. The polished sample was subjected to Leica optical microscopy for transverse viewing, as shown by the arrow in Fig. 5 (b).

2) Hardness Test

The second half of the sample was prepared for the Brinell hardness test and was only subjected to paper polishing grades of 80, 100, 220, 400, 600 and 1,000. The prepared sample for the hardness test is shown in Fig. 5. The polished sample was

subjected to 62.5 kgf load of the Tinus Olsen hardness testing machine transversely, as shown by the dots in Fig. 5 (b).

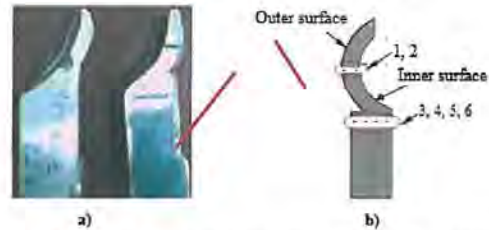


Fig. 5 (a) Samples for microstructural examination and for hardness test; (b) offset of the test sample's face

D. Heat Treatment

Solution heat treatment (T6) is the most widely used for the improvement of the combination of strength and ductility. The sample of A356 alloy was treated according to the T6 standard heat treatment of A356 alloy for hardness, strength and ductility enhancement. The specimen was heated to 540 $^{\circ}\text{C}$ and held for four hours and quenching in water of 65 $^{\circ}\text{C}$ temperature according to earlier studies [13], [14]. Artificial ageing was carried out at 165 $^{\circ}\text{C}$ for six hours and the process profile is shown in Fig. 6. The A356-10% SiC_p composite specimen was heated to 520 $^{\circ}\text{C}$, held for eight hours and quenching in water at a temperature of 80 $^{\circ}\text{C}$. The artificial ageing was done at 160 $^{\circ}\text{C}$ and held for 20 hours [15].

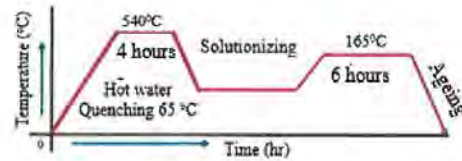


Fig. 6 Schematic of T6 Heat Treatment of A356 Alloy at 160 $^{\circ}\text{C}$

The heat treatment process for A356-10% SiC_p is represented in Fig 7. Quenching was done according to B-917 ASTM standard, where the cooling was from 400 $^{\circ}\text{C}$ to 260 $^{\circ}\text{C}$ and the quenching delay time was less than 10 seconds. These precautionary steps ensure that there was no formation of a premature precipitate.

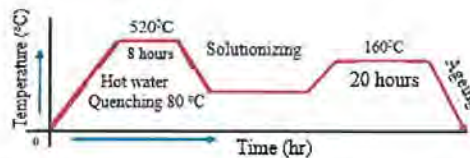


Fig. 7 Schematic of T6 Heat Treatment of A356-10% SiC_p composite profile

IV. RESULTS AND DISCUSSION

A. Casting of Pelton Bucket by Centrifugal Process

The defect caused by the centrifugal force on the cast bucket was a major challenge and the defect is shown Fig. 8 (a). In the study, several attempts were made by changing the process variables before a good cast was made. In centrifugal casting, there is the tendency of the surface of the cast, towards the centre of rotation, to form a parabola of revolution as depicted in the schematic in Fig. 8 (b).



Fig. 8 (a) A defected cast caused by centrifuge; (b) schematic of effect of centrifuge

The curve formed is a function of these parameters: the rotational speed; the cast geometry; and, the pouring and

mould temperatures. In this work, the defect was corrected significantly by geometry and Fig. 9 shows the defect free Pelton bucket cast.



Fig. 9 The defect-free Pelton bucket cast

B. Microstructural Examination

The micrographs of buckets 1 and 2 in Fig. 10, shows the same gradient trend for both alloy and composite, but the trend in bucket 2 was in the opposite direction of bucket 1. For the purpose of bucket performance during operation, especially for wear resistance, bucket 1 in Fig. 10 is preferred. Figs. 10 and 11 show the pattern of the gradient in bucket 1 for the alloy and composite, respectively.



Fig. 10 The micrograph the gradient of cast bucket 1 of A356 alloy

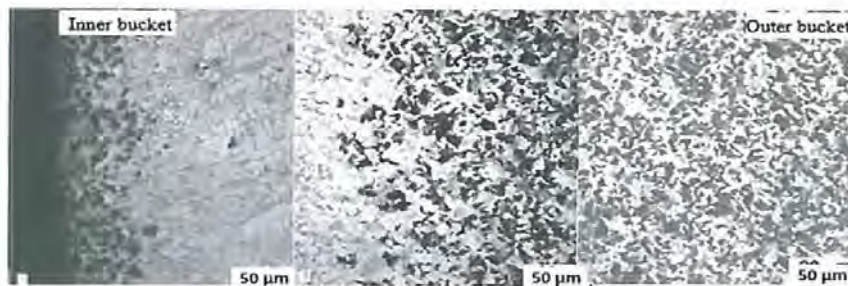


Fig. 11 The micrograph the gradient of cast bucket 1 of A356-10%SiCp composite

C. Effect of T6 Heat Treatment and Centrifugal Casting Technique on Hardness

A356 alloy, which has Al-7.5%Si-0.3Mg is widely used in engineering industries including automotive, aerospace and military applications for high strength parts. It offers a good combination of mechanical properties such as castability,

strength, corrosion resistance and pressure tightness in both the permanent mould and sand cast condition. Despite these attributes, in most cases, A356 alloy is not used as cast, as the presence of eutectic silicon causes it to perform below optimal value. Generally, the mechanical properties of aluminium alloys and composites are reduced by coarse grain, cavities

International Science Index, Materials and Metallurgical Engineering Vol: 10, No: 10, 2016 waset.org/Publication/10005595

and needle shape eutectic silicon. Modification and refinement improves the mechanical properties such as tensile strength, impact strength, wear resistance and hardness significantly [16], [17]. Very fast solidification rate, heat and chemical treatments are the three basic methods of enhancing the properties. In chemical treatment, a small amount of sodium is added to the melt and this changes the eutectic silicon phase morphology from coarse acicular to fine fibrous. This process enhances the mechanical properties of aluminium alloys [18]-[20].

3) Centrifugal Casting

The large dendritic cells, large flakes of silicon and large inter-dendrite arm spacing of α -aluminium dendrites that are produced by a low solidification rate, need to be reduced. While a high solidification rate gives small dendritic cells, small inter-dendrite arm spacing and small flakes of silicon and morphologically changed from acicular to fibrous [21]. Centrifugal casting affects the rate of solidification and consequently enhances the quality of casting.

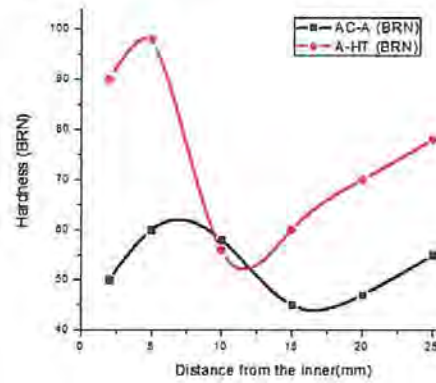
The rate at which centrifuge affects the microstructure of an alloy depends on the speed. Studies have shown that the optimum centrifugal is between 1,200-1,500 rpm [21], [22]. At a speed of 1,500 rpm, the microstructure of the bucket experiences the following: the transformation of large primary silicon into needle-shaped eutectic silicon in the inner; long needle-shaped eutectic silicon is converted into fine primary silicon at the outer; and, there is the formation of fine grain. The transformations and the high rate of solidification enhanced the hardness value of both A356 alloy and A356-10%SiC_p composite. The maximum hardness of 60BRN was recorded at 5 mm from the surface of the inner part of the bucket and 55 BRN was recorded in the outer region.

4) Heat Treatment

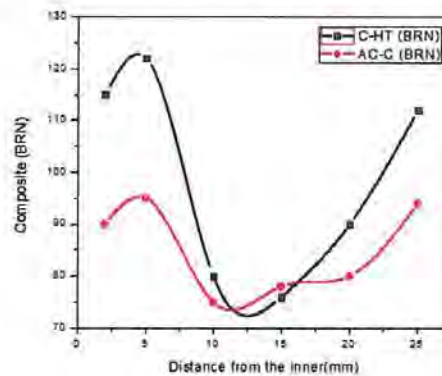
The heat treatment of A356 can be classified into three, based on soaking temperatures: Soaking at a high temperature of 560 °C [13], [14]; soaking temperature slightly below the eutectic temperature at 540 °C [23]-[25]; and, the soaking temperature at 500 °C. Quite often, hypoeutectic and near eutectic Al-Si alloys are applied when corrosion resistance and good castability are needed and with a small quantity of Mg and Cu for heat treatment enhancement. In certain heat treatment conditions, as in the case of the T6 treatment of A356, precipitation of Mg₂Si and that of silicon occur [18].

The hardness of both the alloy and composite samples increased appreciably after the heat treatment. Maximum hardness (98 and 122 BRN for the alloy and composite, respectively) was recorded at about 5 mm from the inner face in both samples. Lesser hardness values were recorded at about 2 mm from the inner surface in all the samples. This is due to the rapid solidification at the inner surface periphery, facilitated by cooling caused by mould rotation. The hardness increase recorded is due to supersaturate solid solution production that occurred during the soaking of A356 alloy at 540 °C for four hours. This process causes the dissolution of hardening elements (Mg₂Si) in the matrix into globular

primary α -Al, spheroidisation of eutectic silicon and casting homogenisation [3]. Fig. 12 shows the hardness trends in the samples.



(a)



(b)

Fig. 12 Brinell micro-hardness plot for a) A356 alloy as-cast and heat treated; and, b) A356-10%SiC_p as-cast and heat treated where AC = as-cast A356 alloy; A-HT = A356 alloy heat treated; AC-C = As-cast A356-10%SiC composite; C-HT = A356-10%SiC composite heat treated.

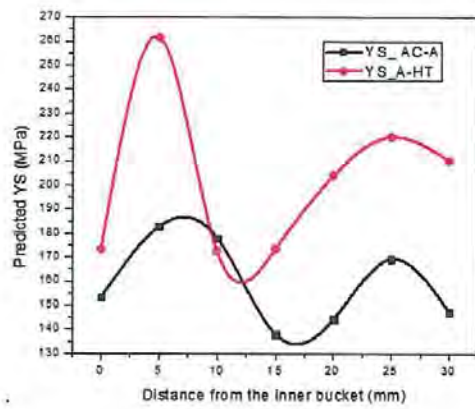
The dissolution of Mg₂Si, Spheroidisation and homogenisation of eutectic silicon in A356 happens within five minutes of soaking at 540 °C.

5) Yield Strength (YS) and Ultimate Tensile Strength (UTS) Predictions

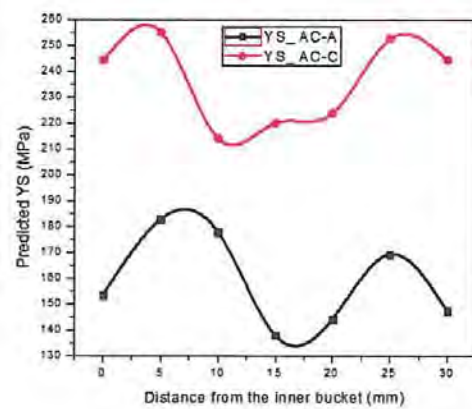
The strength of A356-T6 and A356-SiC-T6 can be predicted using an equation in a previous work [26]:

$$YS = 3.03 \times VHN \times (0.055)^n \quad (1)$$

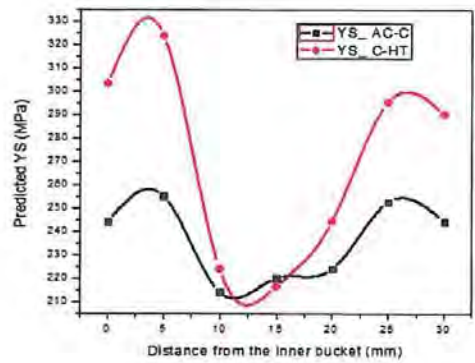
where YS - yield strength, VHN - Vickers hardness number, and n - strain hardening exponent (0.091). The YS and UTS prediction curves for the samples are shown in Figs. 13-15.



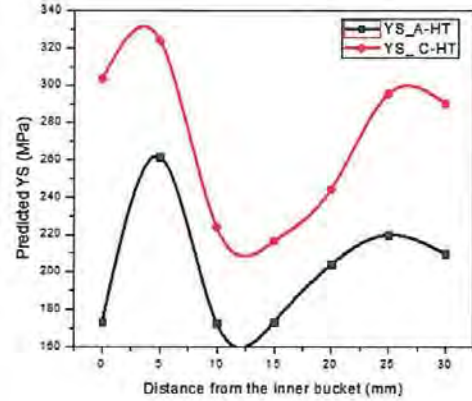
(a)



(a)



(b)



(b)

Fig. 13 Yield strength prediction of a) A356 as cast (YS_AC-A) and heat treated (YS_AC-HT) and b) A356-SiC_p as cast (YS_A-C) and heat treated (YS_C-HT)

Fig. 14 Yield strength prediction of a) A356 as cast (YS_AC-A) and A356-SiC_p as cast (YS_A-C) and b) A356 heat treated (YS_A-HT) and A356-SiC_p heat treated (YS_C-HT)

Again, the YS-UTS ratio can be predicted in terms of n , using (2) and (3):

$$YS_{0.2\%}/UTS = \frac{[(0.002)^n (exp n)]}{(n)^n} \quad (2)$$

$$UTS = \frac{YS_{0.2\%} n^n}{[(0.002)^n (exp n)]} \quad (3)$$

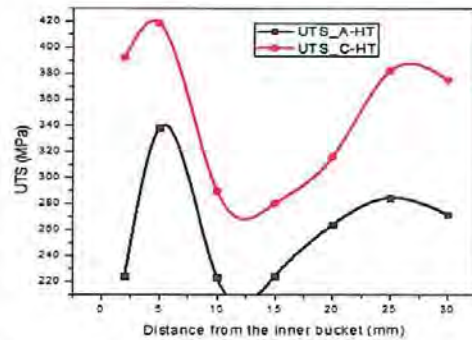


Fig. 15 UTS prediction of heat treated a) A356 (UTS_A-HT) and A356-SiC_p (UTS_C-HT)

From Figs. 13-15, it was observed that the YS and UTS, appreciated greatly across the surface for both A356 alloy and A356-SiC_p composites after heat treatment.

V. PROTECTIVE COATING OF PELTON BUCKET

Despite the wear and corrosion resistance of the A356 alloy and A356-SiC_p composite, they are still very much susceptible to seawater corrosion and silt erosion over time. For better operation performance and lifespan, coating the bucket's inner surface with tougher and hardened material is recommended. Coating the turbine with ceramic is common and effective due to the provision of the following protective service to the turbine surface: Wear and corrosion protection, impingement protection, silt erosion protection and surface hardness improvement. This study recommends a ceramic coating of Al₂O₃ implanted Fe micrograins, and microarc oxidation (MAO) or plasma electrolytic oxidation (PEO).

VI. CONCLUSION

This study concludes that:

- i. To genuinely turn around the perennial power issues in SSA, power should be generated from the abundant small hydro potentials with the application of indigenous technology and materials.
- ii. Use of centrifugal casting method and heat treatment improved the mechanical properties of the A356 alloy and A356-SiC_p composite, making them more suitable for Pelton bucket application.
- iii. Heat treated A356 alloy and A356-SiC_p composite, will be suitable for turbine materials for a water storage turbine system. This is due to the minimal percentage of silt in the stored water and the enhanced corrosion and wear resistance properties of the materials.
- iv. To further improve the life span of the bucket, hard surface coating should be applied

ACKNOWLEDGEMENTS

The authors hereby acknowledge the Centre for Engineering Postgraduate Studies, management and staff of the University of KwaZulu-Natal.

REFERENCES

- [1] W. S. Ebhota, A. C. Eloka-Eboka, and F. L. Inambao, "Energy sustainability through domestication of energy technologies in third world countries in Africa," in *Industrial and Commercial Use of Energy (ICUE), 2014 International Conference on the "Energy efficiency in buildings"*, 2014, pp. 1-7.
- [2] W. S. Ebhota & F. L. Inambao (2016) Electricity insufficiency in Africa: A product of inadequate manufacturing capacity, *African Journal of Science, Technology, Innovation and Development*, vol. 8, pp. 197-204.
- [3] H. Liu, D. Masera, and L. Esser, "World Hydropower Development Report 2013," United Nation Industrial Development Organisation (UNIDO) and International Centre on Small Hydropower (ICSHIP), 2013.
- [4] G. Loice and M. Ignatio, "Efficiency Improvement of Pelton Wheel and Crossflow Turbines in Micro-Hydro Power Plants: Case Study," *International Journal of Engineering and Computer Science* vol. 2, pp. 416-432, 2013.
- [5] B. William, S. Vasu, and S. Manjot, "Green Mechatronics Project Pelton Wheel Driven Micro-Hydro Plant," Mechanical Engineering University of Ottawa, 2010.
- [6] R. N. Mbiui, S. M. Maranga, and H. Ndiritu, "Performance of Aluminium A356 Alloy Based Buckets Towards Bending Forces on Pelton Turbines," in *Sustainable Research and Innovation (SRI) Conference*, Nairobi, Kenya, 2015, pp. 134-138.
- [7] J. A. K. M. Khabirul, B. Sahnewaz, and A. C. Farooque, "Advanced Composite Pelton Wheel Design and Study its Performance for Pico/Micro Hydro Power Plant Application," *International Journal of Engineering and Innovative Technology (IJEIT)*, vol. 2, pp. 126-132, 2013.
- [8] N. I. R. Nava and T. S. Prasad, "Design and Static Analysis of Pelton Turbine Bucket," *International Journal of Science Technology and Management*, vol. 4, pp. 19-25, 2015.
- [9] A. C. Vieira, P. D. Sequeira, J. R. Gomes, and L. A. Rocha, "Dry Sliding Wear of Al Alloy/SiC_p Functionally Graded Composites: Influence of Processing Conditions," *Wear* vol. 267 pp. 585-592, 2009.
- [10] *Casting Metal handbook*, 9th ed. vol. 15: ASM International, 1997.
- [11] G. Chirita, I. Stefanescu, D. Cruz, D. Soares, and F. S. Silva, "Sensitivity of Different Al-Si Alloys to Centrifugal Casting Effect," *Materials and Design* vol. 31 pp. 2867-2877, 2010.
- [12] SAAJ (2014, 23/03/2016). *Die Steel Grade OHNS*. Available: http://saajsteel.com/?page_id=1055.
- [13] D. L. Zhang, L. Zheng, and D. H. StJohn, "Effect of Solution Treatment Temperature on Tensile Properties of Al-7Si-0.3 (wt-%) Alloy," *Materials Science and Technology*, vol. 14, pp. 619-625, 1998.
- [14] S. Shivkumar, S. Ricci, B. Steenhoff, and D. Apelian, "An Experimental Study to Optimize the Heat Treatment of A356 alloy," *American Foundry Society Transaction*, vol. 97, pp. 791-810, 1989.
- [15] M. Drouzy, S. Jacob, and M. Richard, "Interpretation of Tensile Results by Means of Quality Index and Probable Yield Strength," *AFS International Cast Metals Research Journal*, vol. 5, pp. 43-50, 1980.
- [16] K. G. Basavakumar, P. G. Mukunda, and M. Chakraborty, "Impact Toughness in Al-12Si and Al-12Si-3Cu Cast Alloys- Part - I. Effect of Process Variables and Microstructure," *International Journal of Impact Engineering*, vol. 25, pp. 199-205, 2008.
- [17] T. M. Chandrashekharaiah and S. A. Kori, "Effect of Grain Refinement and Modification on the Dry Sliding Wear Behaviour of Eutectic Al-Si Alloys," *Tribology International*, vol. 42, pp. 59-65, 2009.
- [18] F. H. P. Juan, "Heat Treatment and Precipitation in A356 Aluminum Alloy," Doctor of Philosophy, Mining, Metals and Materials Engineering, McGill University, Montreal, Canada, 2003.
- [19] L. Heusler and W. Schneider, "Recent Investigations of Influence of P on Na and Sr Modification of Al-Si Alloys," *American Foundry Society Transaction*, vol. 97, pp. 915-921, 1997.
- [20] B. C. a. J. E. Gruzleski, "Mechanical Properties of A356.0 Alloys Modified with Pure Strontium," *American Foundry Society Transaction*, pp. 453-464, 1982.
- [21] B. P. Vikramkumar, "Investigations on the Properties of Al-Si Alloy Synthesized by Centrifugal Casting Process," Metallurgical Engineering, Ganpat University, Kherva, India, 2014.
- [22] A. S. Rao, S. T. Mahantesh, and S. R. Shrikantha, "Understanding Melt Flow Behavior for Al-Si Alloys Processed Through Vertical Centrifugal Casting," *Materials and Manufacturing Processes*, vol. 30, pp. 1305-1311, 2015.
- [23] M. Ishak, A. Amir, and A. Hadi, "Effect of Solution Treatment Temperature on Microstructure and Mechanical Properties of A356 Alloy," presented at the International Conference on Mechanical Engineering Research (ICMER2013), Bukit Gambang Resort City, Kuantan, Pahang, Malaysia, 2013.
- [24] B. A. Dewhirst, "Optimisation of the Heat Treatment of Semi-Solid Processed A356 Aluminum Alloy," Masters Worcester Polytechnic Institute, 2005.
- [25] M. Rosso and G. M. Actis, "Optimisation of Heat Treatment Cycles for Automotive Parts Produced by Rheocasting Process," *Solid State Phenom.*, vol. 116-117, pp. 505-8, 2006.
- [26] M. K. Padhy and R. P. Saini, "Effect of Size and Concentration of Silt Particles on Erosion of Pelton Turbine Buckets," *Energy* vol. 34, pp. 1477-1483, 2009.



Ebhota Williams S. received Bachelor of Engineering degree from Ambrose Alli University, Ekpoma, Nigeria and Master of Engineering degree in Mechanical Engineering from Nnamdi Azikiwe, University, Awka, Nigeria. He is specialised in Design, Material, Manufacturing, and Energy Studies. He has worked as a

research and production engineer from 2002 to 2014 in National Engineering Design Development Institute, Nnewi, Nigeria. Presently, he is a doctoral candidate in the Discipline of Mechanical Engineering, Howard College, University of KwaZulu-Natal, Durban, South Africa.



Freddie L. Inambao holds a Master of Science (M. Sc) and Ph. D in Mechanical Engineering with specialisation in Thermodynamics and Internal Combustion Engines from Volgograd Polytechnic Institute, Russia. He has lectured at several universities in Southern Africa including the University of Zambia, University of Botswana, the University of Durban-Westville (before the merger with the University of Natal) and currently a

Senior Lecturer in the Discipline of Mechanical Engineering of the University of KwaZulu-Natal, Howard College, Durban, South Africa.

Appendix 3

Civil works design;

```
Q = 0.0:0.02:1; % Design discharge (m^3/s)
V = 1.4; % Channel/canal Velocity (m/s)
A = Q/V; % Cross sectional area of the canal
b = 0.30; % width
h = A/b;% Depth
plot(A,Q) % rating curve
% grid on
% axis on
% Xlabel('Canal sectional area m^2')
% Ylabel('Canal discharge m^3/s')

% Intake
hr = 0.7; % Normal river water level (m)
hh = 0.4; % headrace level (m)
g = 9.81; % gravity acceleration
Cint = 0.6; % discharge coefficient for roughly finished masonry
Qint = A*Cint*(2*g*(hr-hh)).^0.5; % Intake discharge
% plot(A,Qint);
% grid on
% axis on
% Xlabel('Intake sectional area m^2')
% Ylabel('Intake discharge m^3/s')

% Weir
C1 = 1.84;
for i=1:length(h)
    Qwr(i) = C1*(b-0.2*h(i))*h(i).^1.5; % rectangular notch
end
% plot(h,Qwr);
% grid on
% axis on

C2 = 0.60;
tan45 = 1;
for i=1:length(h)
    Qwv = C2*(8/15)*(2*9.81).^0.5*tan45*(h/2).^1.5; % V notch
end
% plot(h,Qwv);
% grid on
% axis on

C3 = 1.86;
for i=1:length(h)
    Qwc = C3*b*h.^1.5; % Cipolletti notch
end
% plot(h,Qwc);
% grid on
% axis on

% plot(h,Qwc,'r',h,Qwv,'b')
% Xlabel('weird depth (m)')
% Ylabel('Cipolletti & Vee notch discharge (m^3/s)')
% grid on
```

```

% axis on

% Headrace canal
Qch = 0.0:0.02:1; % Design discharge (m^3/s)
Vch = 1.4; % Channel/canal Velocity (m/s)
Ach = Qch/Vch; % Cross sectional area of the canal
bch = 0.30; % width
hch = Ach/bch;% Depth
Pw = bch+2*hch;
for i = 1:length(Ach)
Rch(i) = Ach(i)/Pw(i); % hydraulic radius
end
% plot(Pw,Ach)
% grid on
% axis on
% Xlabel('wet perimeter (m)')
% Ylabel('Cross sectional area of the canal (m^2)')

nch = 0.014; % manning roughness value
k = 0.85;
Cc = (1/nch)*Rch.^0.1667; % roughness coefficient
% for ii = 1:length(Rch)
% Sch = ((Qch*nch)/(Ach*Rch.^0.667)).^2;
% end

for i=1:length(Ach)
Sch(i) = (Qch(i)*nch)/((Ach(i)*Rch(i).^0.667)).^2; % side slope
end

for ii=1:length(Sch)
Vchc(ii) = (Cc(ii)*Rch(ii)*Sch(ii)).^0.5; % Velocity by Chezy equation
end
% plot(Sch,Rch)
%grid on
% axis on

Cw = 135; % assumed Hazen-Williams roughness coefficient
for ii=1:length(Sch)
Vchw(ii) = k*Cw*Sch(ii)*Rch(ii).^0.64; % Velocity by Hazen-Williams
equation
end

for ii=1:length(Sch)
Vchm(ii) = ((Rch(ii).^0.667)*(Sch(ii).^0.5))/nch; % Velocity by Manning
equation
end
% plot(Vchw,Qch,'b',Vchm,Qch,'g')
% grid on
% axis on
% Xlabel('Hazen & Manning velocity relations (m/s)')
% Ylabel('Canal discharge (m^3/s)')

% Settling basing

Tsilt = 43200;
bch = 0.30;
W = 5*bch; % width

```



```

Vvert = 0.03; % fall velocity
Lset = (2*Qch)/(W*Vvert); %settling basin length
Csilt = 0.5; % silt concentration of incoming flow
psilt = 2600; % silt density
Pfactor = 0.5; % p factor
Sload = Qch*Tsilt*Csilt; % Silt load Sload (kg)
Vlsilt = Sload/(psilt*Pfactor); % Volume of the silt in basin

% plot(Lset,Vlsilt)
% grid on
% axis on
% Xlabel('settling basin length (m)')
% Ylabel('Volume of the silt in basin (m^3)')

% Penstock

Vp = 3.5; % penstock velocity (m^3/s)
Lp = 20; % gross head (m)
np = 0.011;
Hg = 50:4:250; % penstock length
f = 0.0014; % friction factor in Darcy Weisbach and ASCE relation
SF = 10; % safety factor
Q = 0.0:0.02:1;
Dp = ((4*Q)/(3.14*Vp)).^0.5; % theoretical relation of penstock internal
diameter (m)
Dpmm = Dp*1000; % penstock internal diameter (mm)
Ap = Q/Vp; % penstock cross sectional area (m^2)
for q=1:length(Q)
    hl = ((10.29*np.^2*Q(q).^2)/Dp(q).^5.33)*Lp; % major head loss
end
for ij=1:length(Hg)
    hlp(ij) = [hl/Hg(ij)]*100; % percentage head loss
end
Kent = 0.2; % Loss of head through entrance
Kben = 0.34; % Loss of head through bend
Kcon = 0; % Loss of head through contraction
Kval = 0.04; % Loss of head through valves
hlm = (Vp.^2/(2*g))*(Kent+Kben+Kcon+Kval); % minor head loss

Hn = Hg-hl-hlm; % net head (m)
for ij=1:length(Hg)
    neff(ij) = (Hn(ij)/Hg(ij))*100; % penstock efficiency
end
% plot(Hg,neff)

tp1 = ((Dpmm+508)/400)+1.2; % penstock thickness (mm)
E = 206*10.^9; % Young modulus of the penstck material (N/m^2)
Ew = 2.1*10.^9; % bulk modulus of water (N/m^2)
p = 0.000617800; % Working pressure (kN/mm^2)
Tst = 0.400; % Tensile strength (kN/mm^2)
tc = 3; % corrosion allowance
tp2 = ((p*Dpmm)/(2*Tst))+tc; % minimum thickness based on hoop-stress
relation
for j=1:length(Dpmm)
    check1(j) = Dpmm(j)/tp2(j); % Dp/tp>20
end
tp = tp1+3; % extra 3mm is added for impact of pipe handling in
transportation, laying, deformation, etc
tpd = tp2+3;

```

```

% plot(tp,Q,'r',tpd,Q,'b')
% grid on
% axis on
% Xlabel('penstock thickness (mm)')
% Ylabel('Penstock discharge (m^3)')

for ij=1:length(Hg)
check2 = Hg/Lp; % Surge tank is needed if Hg/Lp>5
end

% Empirical calculation of penstock diameter Dp

Dpw = 0.7*Q.^0.5; % Warnick et al relation
Dpf = (1.127*Q.^0.45)/Hg.^0.17; % Fahlbusch relation for Q>0.56
for q=1:length(Q)
Dpu(q) = ((1.517*Q(q).^0.5)/Hg(q).^0.25); % USBR relation for Q>0.56
end

Dpl = (0.05*(Q.^0.143)).^0.143; % Ludin-Bundschu relation when Hg<100m
% for t=length(Q)
% Dpm = 2.69*((np.^2)*(Q(t).^2)*(Lp/Hg(t)).^0.1875)
% end
% % plot(Q,Dp,'r',Q,Dpw,'b',Q,Dpu,'g')
% % grid on
% % axis on
% Xlabel('Penstock flow rate (m^3/s)')
% Ylabel('penstock internal diameter (m)')
%
% penstock air vent
Es = 201*10.^9; % Young's modulus of mild steel for the penstock (N/m^2)
Epsc = 2.75*10.^9;
f = 0.0014; % dimensionless friction factor for pipe material
F = 5; % safety factor for exposed pipe
dvth = Q.^0.5*[(F/E)*(Dp/(tp*f)).^3]; % penstock air vent diameter from
theoretical
dvw = Q.^0.5*[(F/E)*(Dpw/(tp*f)).^3]; % penstock air vent diameter from
Warnick et al relation
dvu = Q.^0.5*[(F/E)*(Dpu/(tp*f)).^3]; % penstock air vent diameter from
USBR relation

% plot(Q,dvth,'r',Q,dvw,'b',Q,dvu,'g')
% grid on
% axis on
% Xlabel('Penstock flow rate (m^3/s)')
% Ylabel('penstock vent diameter (m)')

```

```

% plot(Dp,dvent,'b')
% grid on
% axis on
K = 2.1*10.^9; % bulk modulus of water (N/m^2)

for r=1:length(tpd)
Vws(r) = [(K*10.^-3)/(1+K*Dp(r)/(Es*tpd(r)))].^0.5;
end

for r=1:length(tpd)
Vwpvc(r) = [(K*10.^-3)/(1+K*Dp(r)/(Epvc*tpd(r)))].^0.5;
end

% plot(Dp,Vws,'b',Dp,Vwpvc,'r')

% Turbine Design

% Q = 0.033 m3/s;
% Hn = 60 m;
% g = 9.81 m/s2;
% Cn = 0.97;
% ku = 0.46;
% den = 103 Kg/m3;
% x = 0.46;
% nz =2;
% N = 1500 RPM;
% nt = 95%

```

Appendix 4;

Turbine design;

```
g = 9.81; % gravity (m/s2)
Vp = 3.5; % penstock velocity (m^3/s)
Lp = 20; % gross head (m)
np = 0.011;
Hg = 50:4:250; % penstock length
f = 0.0014; % friction factor in Darcy Weisbach and ASCE relation
SF = 10; % safety factor
Q = 0.0:0.02:1;
% Dp = ((4*Q)/(3.14*Vp)).^0.5; % penstock internal diameter (m)
C = 1.273; % constants
Dp = ((C*Q)/Vp).^0.5;
Dpmm = Dp*1000; % penstock internal diameter (mm)
Ap = Q/Vp; % penstock cross sectional area (m^2)
for q=1:length(Q)
    hl = ((10.29*np.^2*Q(q).^2)/Dp(q).^5.33)*Lp; % major head loss
end
for ij=1:length(Hg)
    hlp(ij) = [hl/Hg(ij)]*100; % percentage head loss
end
Kent = 0.2; % Loss of head through entrance
Kben = 0.34; % Loss of head through bend
Kcon = 0; % Loss of head through contraction
Kval = 0.04; % Loss of head through valves
hlm = (Vp.^2/(2*g))*(Kent+Kben+Kcon+Kval); % minor head loss
Hn = Hg-hl-hlm; % net head (m)

% Turbine Design

Cn = 0.97;
ku = 0.46;
den = 10.^3; % water density Kg/m3;
x = 0.46;
nz = 2;
N = 1500; % generator rotation (rpm)
nt = 0.83; %
for q=1:length(Q)
    Pti(q) = (den*g*nt*Hn(q)*Q(q))/1000; % The input power to the turbine, Pti
    (kW)
end
% % Q = 0.0:0.02:1;
% % plot(Q,Pti);
% % grid on
% % axis on
% % Xlabel('Flow rate (m^3/s)')
% % Ylabel('Turbine power (kW)')

% plot(Hn,Pti)
% grid on
% axis on
% Xlabel('Net head (m^3/s)')
% Ylabel('Turbine power (kW)')

for i=1:length(Pti)
    Ns(i) = (N*(Pti(i)).^0.5)/Hn(i).^1.25; % Specific speed (Ns)
end
Vj = Cn*(2*g*Hn).^0.5; % Jet velocity, Vj (m/s)
```

```

for q=1:length(Q)
Dj(q) = ((4*Q(q))/(pi*nz*Vj(q))).^0.5; % Jet/nozzle diameter, Dj
end
N1 = 1200;% generator rotation (rpm)
N2 = 1000; % generator rotation (rpm)
N3 = 800; % generator rotation (rpm)
N4 = 600; % generator rotation (rpm)
N5 = 400; % generator rotation (rpm)
Vtr = x*Vj; % Tangential velocity of the runner, Vtr
Dr = (60*Vtr)/(pi*N); % Runner diameter Dr, (m)
Dr1 = (60*Vtr)/(pi*N1);
Dr2 = (60*Vtr)/(pi*N2);
Dr3 = (60*Vtr)/(pi*N3);
Dr4 = (60*Vtr)/(pi*N4);
Dr5 = (60*Vtr)/(pi*N5);

%
plot(Dr,Vtr,'r',Dr1,Vtr,'b',Dr2,Vtr,'g',Dr3,Vtr,'y',Dr4,Vtr,'c',Dr5,Vtr,'m'
)
% grid on
% axis on
% Xlabel('Runner diameter (m)')
% Ylabel('Tangential velocity of the runner(m/s)')

% plot(Dj,Q)
% grid on
% axis on
% Xlabel('Jet diameter(m)')
% Ylabel('Flow rate(m^3/s)')

Aj = (pi*Dj.^2)/4; % nozzle cross sectional area, Aj
for ij=1:length(Vj)
Qn(ij) = Vj(ij)*Aj(ij); % Nozzle flow rate, Qn (m3/s)
end

Xnb = 0.625*Dr; % Distance between bucket and nozzle, Xnb (m)
Rbr = 0.47*Dr; % Radius of bucket centre of mass to runner centre Rbr (m)
Bw = 3.2*Dj; % Bucket axial width, Bw (m)
Bl = 3*Dj; % Bucket radial length, Bl (m)
Bd = 1.2*Dj; % Bucket depth, Bd(m)
h1 = 0.35*Dj; % Cavity Length, h1 (m)
h2 = 1.5*Dj; % Length to Impact Point, h2 (m)
k = 0.17*Dj; % Offset of Bucket(m)
a = 1.2*Dj; % Cavity Width (m)
Lab = 0.195*Dr; % Length of bucket moment arm(m)

for j=1:length(Dj)
nz(j) = 15+(Dr(j)/(2*Dj(j))); % number of nozzle
end
% plot(Dj,Bw,Dj,Bd,Dj,Bl,Dj,h1,Dj,h2)
% grid on
% axis on
% legend('Bw','Bd','Bl','h1','h2')
% Xlabel('Jet diameter (m)')
% Ylabel('Bucket dimension parameters(m)')

for i=1:length(Pti)
Ns(i) = (N*Pti(i).^0.5)/(Hn(i).^1.25);
Ns1(i) = (N1*Pti(i).^0.5)/(Hn(i).^1.25);
Ns2(i) = (N2*Pti(i).^0.5)/(Hn(i).^1.25);

```

```

Ns3(i) = (N3*Pti(i).^0.5)/(Hn(i).^1.25);
Ns4(i) = (N4*Pti(i).^0.5)/(Hn(i).^1.25);
Ns5(i) = (N5*Pti(i).^0.5)/(Hn(i).^1.25);
end
% plot(Q,Ns,'r',Q,Ns1,'b',Q,Ns2,'g',Q,Ns3,'y',Q,Ns4,'c',Q,Ns5,'m')
% grid on
% axis on
% Xlabel('Operational flow rate(m^3/s)')
% Ylabel('Specific speed (Ns)Specific speed (Ns)')

Hn1 = 30; % net head (m)
Hn2 = 50;
Hn3 = 70;
Hn4 = 90;
Hn5 = 110;
Hn6 = 130;
for i=1:length(Pti)
nt1(i) = (100*Pti(i))/(den*g*Hn1*Q(i));
nt2(i) = (100*Pti(i))/(den*g*Hn2*Q(i));
nt3(i) = (100*Pti(i))/(den*g*Hn3*Q(i));
nt4(i) = (100*Pti(i))/(den*g*Hn4*Q(i));
nt5(i) = (100*Pti(i))/(den*g*Hn5*5*Q(i));
nt6(i) = (100*Pti(i))/(den*g*Hn6*Q(i));
end
% plot(Pti,nt1,Pti,nt2,Pti,nt3,Pti,nt4,Pti,nt5,Pti,nt6)
% grid on
% axis on
% Xlabel('Turbine power(kW)')
% Ylabel('Turbine efficiency')

for q=1:length(Q)
    F(q)= 2*den*Q(q)*(Vj(q)-Vtr(q)); % Absolute reaction force acting on the
Pelton runner
end

for ii=1:length(Dr)
    Tr(ii) = (Dr(ii)*F(ii))/2; % The torque on the runner is Tr
end
% plot(Tr,F)
% grid on
% axis on
% Xlabel('The torque on the runner(N-m)')
% Ylabel('reaction force acting on the Pelton runner (N)')

% Shaft
N1 = 1500; % generator rotation (rpm)
N2 = 1200; % generator rotation (rpm)
N3 = 1000; % generator rotation (rpm)
N4 = 800; % generator rotation (rpm)
N5 = 600; % generator rotation (rpm)
N6 = 400; % generator rotation (rpm)

Ds1 = 105*(Pti/N1).^0.38;
Ds2 = 105*(Pti/N2).^0.38;
Ds3 = 105*(Pti/N3).^0.38;
Ds4 = 105*(Pti/N4).^0.38;
Ds5 = 105*(Pti/N5).^0.38;

```



```
Ds5 = 105*(Pti/N6).^0.38;  
  
plot(Ds1,Pti,Ds2,Pti,Ds3,Pti,Ds4,Pti,Ds5,Pti)  
grid on  
axis on  
Xlabel('Shaft diameter (mm)')  
Ylabel('Turbine power (kW)')  
  
% plot(Ds1,Pti,'r',Ds5,Pti,'b')
```